National Institute of Materials Physics

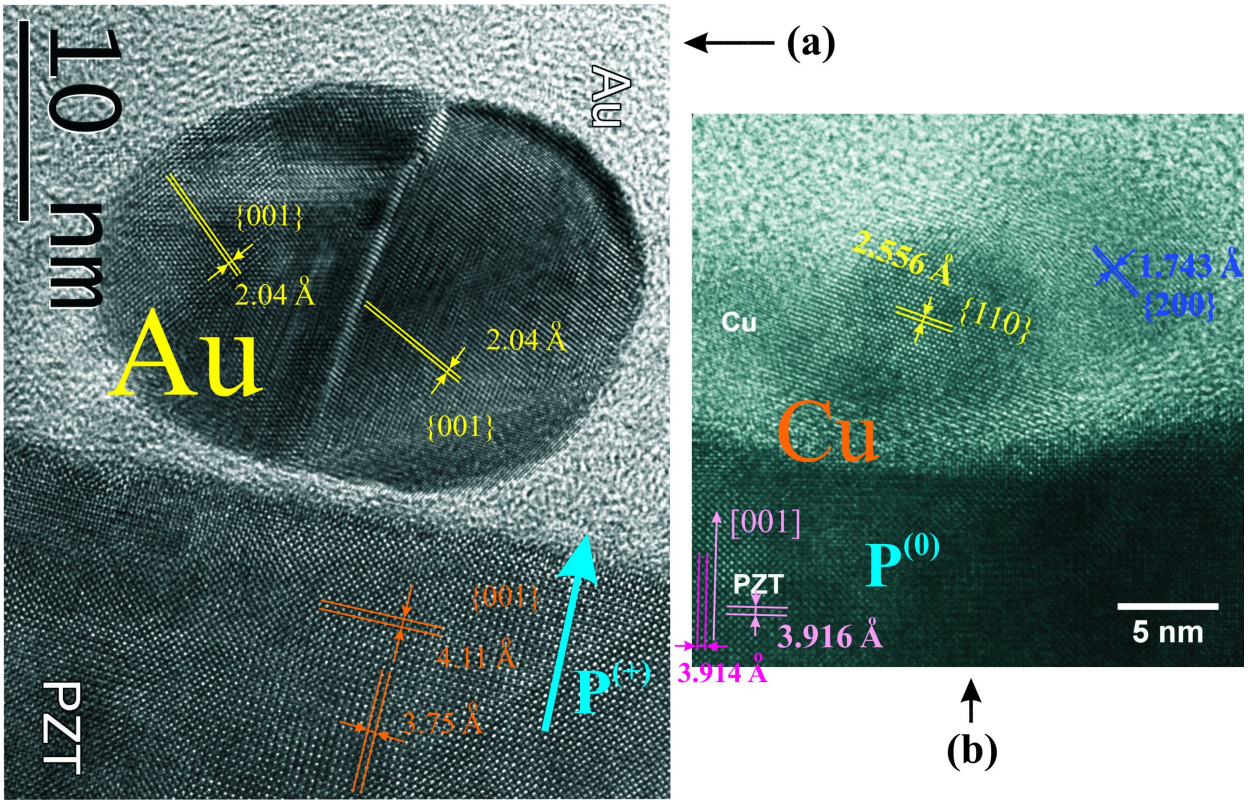

Annual Report

2014

National Institute of Materials Physics

(Institutul Național de Cercetare-Dezvoltare pentru Fizica Materialelor)

National Institute of Materials Physics

(Institutul Național de Cercetare-Dezvoltare pentru Fizica Materialelor)

DIRECTORATE

Director: Dr. Ionut Enculescu

Scientific Director: Dr. Florin Vasiliu

ADDRESS

P.O. BOX MG – 7
Bucharest – Magurele / ROMANIA
Tel. (+4) 021 369 01 85
Fax (+4) 021 369 01 77

E-Mail

I. Enculescu: encu@infim.ro
F. Vasiliu: fvasiliu@infim.ro

WWW

http: // www.infim.ro

Contents

Cover image: *HRTEM images of (a) a typical Au insulated nanoparticle and (b) Cu coalescing nanoparticles deposited on PZT.*
L.E. Ştoflea, N.G. Apostol, L. Trupină, C.M. Teodorescu, J. Mater. Chem. A 2, 14386-14392 (2014).

PREFACE

It is a special pleasure to bring you this 19th edition of the NIMP Annual Report. We hope to reflect in a comprehensive manner the main achievements of our researchers during the past year.

To begin with some special and notable events , happened in 2014, must emphasized, such as: the launching of a new infrastructure project POS-CCE "Research Innovation and Technology Center for New Materials", RITecC, organization of the prestigious XIV ELECTROCERAMICS Conference and the seminary given by the Nobel Prize winner, Prof. Albert Fert.

This scientific report documents the results of our applied and basic research and serves as a record of the increased level of scientific and technological outputs of NIMP during 2014. The results of our research show again a number of highlights and some of them are presented in the "Selected Results".

In the year 2014, National Institute for Materials Physics (NIMP) has published 171 papers in ISI journals which correspond to a cummulated impact factor of 409 which has an increase of 15% as compared to the previous year. The cummulated impact factors associated to the papers published by NIMP researchers in the period 2010-2014 show a constant increase, proving a consolidated research performance of our activity.

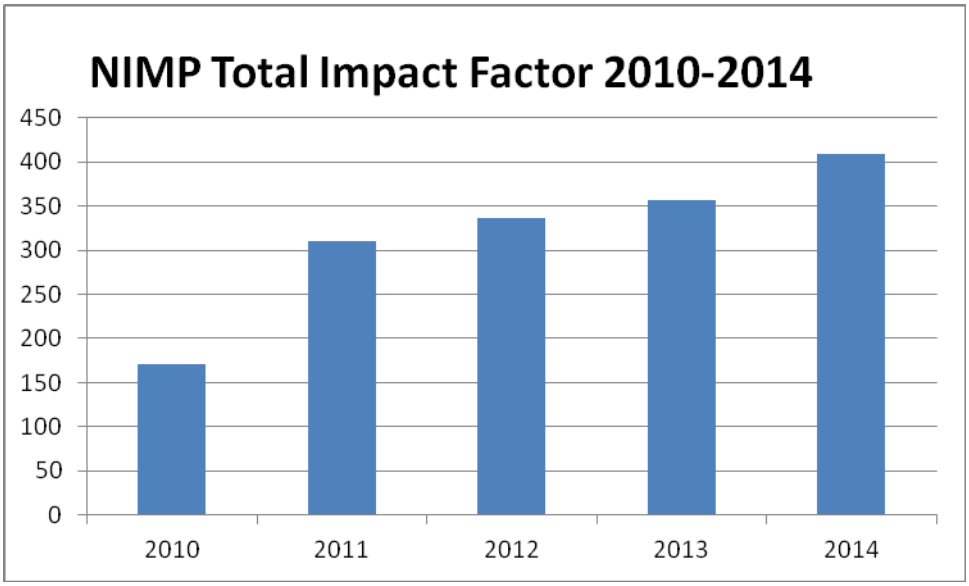

Fig.1- Cummulated impact factors of NIMP papers published in 2010-2014

In Fig. 2, a impact factor distribution for papers published by NIMP researchers between 2009 -2014 is shown. As compared to the years 2010, 2011, we have in the last two years a doubling of papers published in journals with FI > 3 can be observed . Moreover, it is registered a constant increase of the number of papers published in top journals with FI > 5. An impressive growth of about 40% has been observed also in the case of papers published in journals with impact factors between 2 and 3.

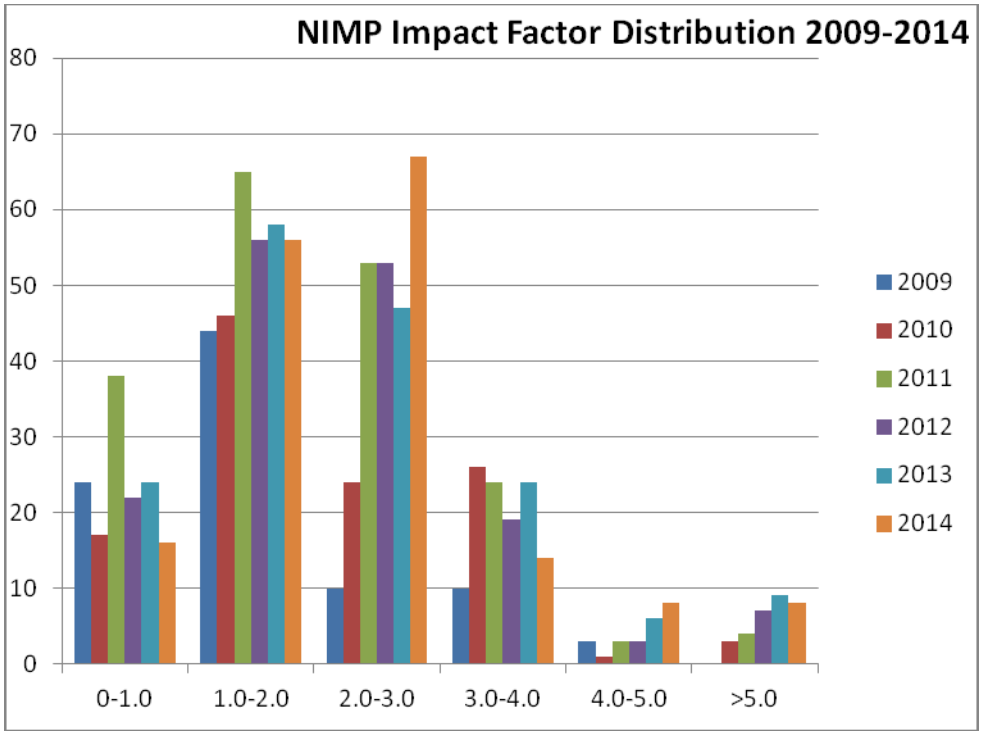

Fig. 2-NIMP Impact Factor distribution of the papers published in the period 2009-2014

The number of citations in ISI journals in 2014 reached about 2760 (Web of Science, for papers published in the period 1989-2014) and about 9400 (Scopus , for papers published in the period 1996-2013).

In the framework of various international conferences and congresses , our researchers have presented in 2014 a number of 231 scientific communications, representing an increase of about 37% as compared to 2013.

In 2013 three patents have been obtained and ten patent requests have been registered. Eight new products and eighteen material technologies have been elaborated on the basis of current intitute research whereas 11 services have been offerred by contracts with economical agents.

The 24th RD50 Workshop has been held in Bucharest, Romania, on June 11 - 13, 2014. RD50-Radiation hard semiconductor devices for very high luminosity colliders is an international collaboration lead by CERN having as major goal the development of radiation hard semiconductor detectors for very high luminosity colliders, particularly to face the requirements of a possible upgrade scenario of the LHC (Large Hadrons Collider) at CERN, Geneva, Switzerland. The workshop was organized in Romania for the first time and was attended by 50 researchers representing the research institutions involved in RD50. Latest achievements in the field of Si radiation detectors were presented, with a special emphasis on defect engineering to enhance the detection characteristics.

The fourteenth edition of ELECTROCERAMICS conference has been held in Bucharest, Romania, June 16th – 20th, 2014, NIMP being awarded as the organizer of this very important international event .

The conference program has covered a broad range of scientific interest, such as fundamental, theoretical, modeling & simulation studies, innovative processing, advanced characterisation, properties and applications in several fields of electroceramics materials like dielectrics, ferroelectrics and multiferroics, as well as ionic, mixed and electronic conduction structures, in the state from bulk to ultrathin films and nanostructures.

Two other events satellite have been organized during the same period:

- COST MP0904 Action Showcase "Ferroelectric and multiferroic electroceramics: trends and perspectives"
- Brokerage"From Projects Ideas to Projects Developments" organized in the framework of the NMP TeAM2 project

At this conference have participated over 300 researchers from all the world and 2 plenary contributions, 46 invited lectures, 166 oral contributions and 112 poster presentations.

Among the invited academics which has offerred plenary or invited lectures ,an important number of researchers had a world reputation : Jim Scott (University of Cambridge, United Kingdom), Harry Tuller (MIT Department of Materials Science and Engineering, USA), Manuel Bibes (Unité Mixte de Physique CNRS/Thales, France) , Nava Setter (EPFL, Switzerland), Vincenzo Buscaglia (Institute of Energetics & Interphases IENI- CNR Genoa, Italy), Dragan Damjanovici (EPFL, Lausanne, Switzerland), Dietrich Hesse (Max Planck Institute for Microstructure Physics, Halle, Germany), Barbara Malic (Jozef Stefan Institute, Ljubljana, Slovenia), Susan Trolier McKinstry (Penn State University, USA), Hiromi Nakano (Toyohashi University of Technology, Japan), Alain Pignolet (Institut National de la Recherche Scientifique – Centre Énergie, Matériaux et Télécommunications, Québec, Canada) and others.

Professor Jim Scott during his plenary presentation at Conference ELECTROCERAMICS XIV

Professor Albert FERT, Nobel Prize laureate for Physics in 2007, has visited the National Institute of Materials Physics (NIMP) between 1st and 3rd of October 2014. Professor FERT has won the Nobel Prize, together with Professor Peter Grunberg, for the discovery of the Giant magnetoresistance. At present he is Scientific Director of a joint laboratory of CNRS and company Thales, Emeritus Professor at University Paris-Sud and member of the French Academy of Sciences. Professor FERT is the first Nobel Prize laureate to visit a research institution from Romania. This is again a confirmation of the level of excellence in research reached by NIMP which, by infrastructure, quality of the human resources and of the research results, become competitive with top research institutes from Europe and from the world.

The Nobel Prize Laureate, Professor ALBERT FERT, during the seminary held at National Institute of Materials Physics

On 5th of September 2014, NIMP hosted the launching conference for the project "Research Innovation and Technology Center for New Materials", RITecC.The POS-CCE project is co-financed by the Sectoral Operational Programme "Increase of Economic Competitiveness" "Investments for your future". The event gathered over 30 guests, including officials of the National Ministry of Education and of the Implementation Organism, representatives of firms and of the local authorities, directors and researchers from the same field institutes and universities, as well as mass-media.
NIMP's General Director, Dr. Ionut Enculescu, presented the development vision of the institution underlining the convergency of the new project with the NIMP development strategies. As a final part, the guests visited the institute laboratories and relevant facilities.

Research work was dedicated to a high number of projects such as: 3 CORE projects, 3 projects UEFISCDI Module III, 17 IDEAS-PCE projects, 10 HUMAN RESOURCES projects, 1 IDEAS-PCCE projects as coordinator, 3 IFA-CEA projects, 4 EURATOM projects, 6 ROSA projects, 11 PARTNERSHIP projects as coordinator and other 20 as partner.

NIMP continued to develop new international collaborations with research institutions from whole word. In 2014 NIMP has continued 2 FP7 projects, 2 projects Romanian Swiss Research Program RSRP, 3 projects with Commissariat de l' Energie Atomique (CEA), 1 SEE project with Norway, 1 project with Agence Nationale de Recherche (ANR), other 8 European-funded projects, 5 inter-governmental agreements and 24 bilateral cooperation with foreign institutes or universities.

After a very good and fruitful year 2014, we hope to continue also in the year 2015 excellent results in scientific research and to finish successfully the new POS-CCE RITecC project which is a real challenge for NIMP research team.

Dr. Ionut Enculescu

General Director

Laboratories

10. Laboratory of Multifunctional Materials and Structures

Currently the laboratory is divided in two research groups:

- The group of functional nanostructures: works on preparation and characterization of different nano-objects (nanotubes, nanowires, nanorods, etc.) with potential of applications in micro-, nano- and opto-electronics (field effect transistors, organic and hybrid LED and photovoltaic cells, photodiodes, etc.), sensors (with focus on bio-sensors), renewable energy sources.
- The group of complex heterostructures and perovskite oxides: works on preparation and characterization of oxide materials with dielectric, ferroelectric, multiferoic, semiconductor properties with potential of applications in micro- and nano-electronics (non-volatile memories, transparent electronics), telecommunications and security (microwave devices), sensors (pyroelectric, photoconductive cells), solar cells (based on photovoltaic effect in ferroelectrics or other perovskite materials).

The human resources is formed by 4 CS1 (equivalent professor), 4 CS2 (equivalent assistant professor), 10 CS3 (equivalent lectureship), 7 CS (junior researchers), 12 ACS (equivalent assistant junior researcher), 2 sub-engineers, 5 technicians and 2 workers. The infrastructure comprises modern equipments for preparation and characterization such as: PLD workstation; RF sputtering; SEM; micro-fluorescence microscope; cryostations with vertical and horizontal magnetic fields; network analyzers up to 325 GHz; THz spectrometer; elipsometer; magnetic dichroism, etc.

20. Laboratory of Magnetism and Superconductivity

The laboratory is devoted to research in the field of materials with magnetic or superconducting properties and related electronic phenomena. The research process covers all the steps from preparation (powder, bulk, ribbons, thin films or nanostructures), going through basic physical characterizations, and ending with in-depth analysis of the magnetic dependent and superconducting properties.

The our research is especially focused on nanostructure study, in the case of magnetic: magnetic nanoparticle systems and multilayers, materials for colossal magnetoresistance (CMR), gigant magnetoresistance (GMR) and tunelling magnetoresistance (TMR), soft and hard magnetic materials, and in the case of superconducting: high Tc superconducting thin films including nanometric inclusions as pinning centers, new superconducting materials for electronic applications, new multifunctional (magneto-elastic, magneto-caloric, magneto-strictive) alloys for magnetic sensors, actuators and refrigerators

A special research field, strongly oriented to applications, is related on study and preparation of materials for extreme conditions. For example, various materials for nuclear fusion or fission and for aerospace applications are currently investigated.

The magnetic and superconducting structures are prepared by various technologies, like spark plasma & hot press sintering, microwave sintering. melt spinning, RF and DC sputtering system for magnetic multilayer deposition, etc. The structural and morphological characteri zation of the samples including magnetic, thermodynamic and transport properties are studied by thermogravimetric (DSC/DTA) measurement system, Vibrating Sample Magnetometry (VSM), Physical Properties and Magnetic Properties Measurement systems (PPMS, MPMS-SQUID), Mossbauer spectroscopies with various accessories for measurements in a temperature range of 4.5 K – 1000 K and in applied fields, for the detection of gamma radiation/X-rays/conversion electrons at as well as liquid He production unit (18 l /24 h).

Spark Plasma Sintering

30. Laboratory of Nanoscale Condensed Matter

The three groups of Laboratory 30 develop complex experimental studies of surfaces, interfaces, thin films and amorphous Ge and Si-based nanostructures as well as theoretical research concerning the modelling of mesoscopic systems.Various nanostructured materials (for ex. nanostructures and nanocomposites, magnetic thin films, hard layers) are prepared by advanced methods.

Experimental investigation topics are related to the properties and processes specific to low dimensional systems, being also supported by modelling about composition and structure, electric transport and phototransport, magnetic properties and surface/interface processes, trapping phenomena. Theoretical studies are focused especially on stationary and/or time dependent electron transport in strongly confined mesoscopic systems, spin dynamics and quantum interference effects.

The group of surface physics and X-ray spectroscopy utilizes and maintains a special "cluster" for in-situ surface study, having as central unit a MBE (Molecular Beam Epitaxy) deposition chamber. This "cluster" works in real ultrahigh vacuum (UHV, 10-10 to 10-11 mbar) and provides the following characterization procedures: RHEED (Reflection High Energy Electron Diffraction); LEED (Low Energy Electron Diffraction); XPS (X-Ray Photoelectron Spectroscopy); SARPES (Spin Angular Resonant Photoelectron Spectroscopy); STM (Scanning Tunnelling Microscopy). A microscope devoted to Low-Energy Electron Microscopy- Photoelectron Electron Microscopy (LEEM-PEEM) is also associated to this "cluster". Other equipments are: a complex equipment of RF sputtering deposition, incorporating attachments of Auger spectroscopy and LEEM; a Hall effect measurements system; a setup for electrical and photoelectric measurements.

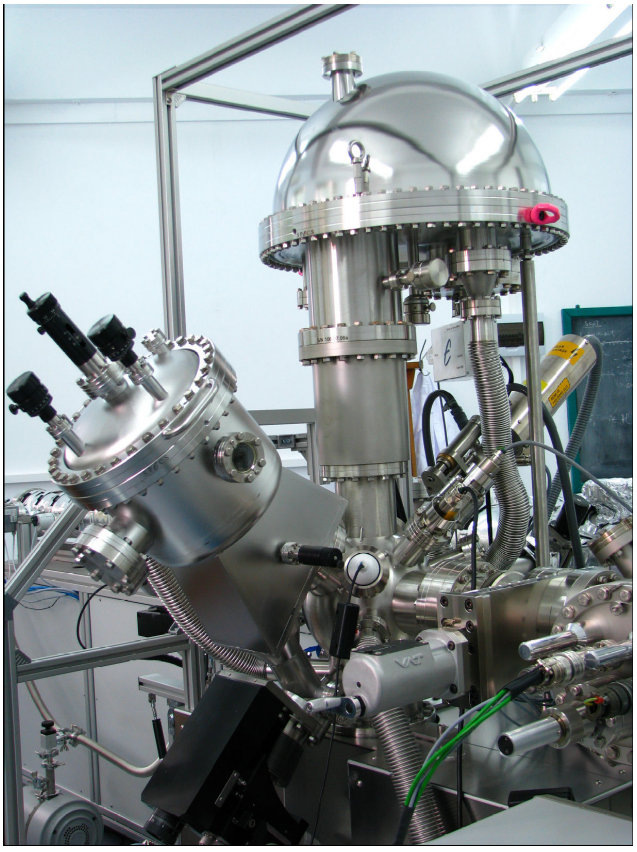

Complex system of multimethod surface analysis by XPS, AES and STM

40. Laboratory of Optical Process in Nanostructured Materials

This laboratory is focused on the study and characterization by optical methods of the nanocomposites and nanostructured materials. Other research topics are related to the preparation and characterization of semiconducting nanometric structures, electrochemical synthesis of polymers with special properties as well as the synthesis and characterization of chalcogenide glasses. The main equipments used for optical characterization of investigated materials are: UV – Vis -NIR and FTIR absorbtion spectrophotometer, FTIR imaging microscope , FTRaman equipped with a YAG: Nd laser, confocal Raman spectrophotometer equipped with Ar and Kr lasers, Scanning Near-Field Optical Microscope (SNOM) coupled with AtomicForce Microscope (AFM),experimental setups for photoluminescence in VIS and NIR range and thermoluminescence, experimental setup for photoconductivity studies and solar simulator.

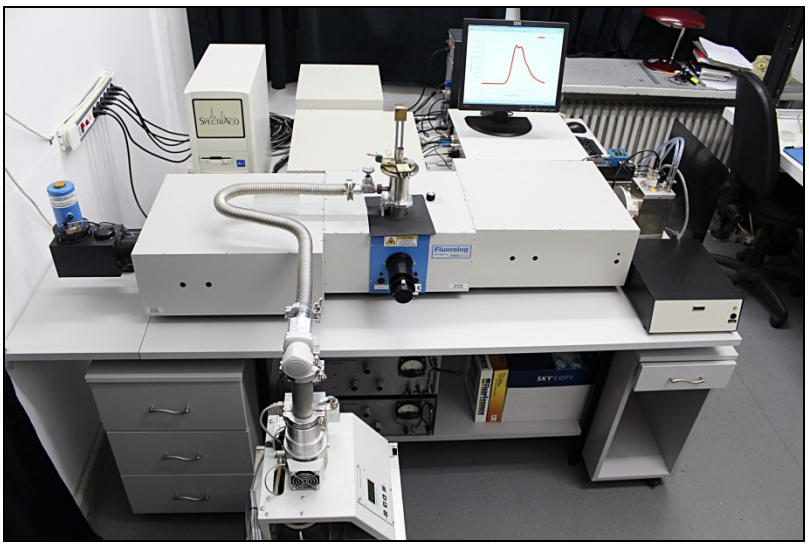

Fluorolog-3, model FL3-22, Horiba Jobin Yvon

Other equipments used for characterization and/or preparation of materials are: broadband dielectric spectroscopy system, drop shape analysis for estimation of contact angle, the film evaporation system for organic materials research, Langmuir–Blodgett film deposition systems and potentiostats/galvanostats for the synthesis of composite materials and their testing as electrode materials in battery and supercapacitors.

50. Laboratory of Atomic Structures and Defects in Advanced Materials

This laboratory is mainly committed to structural investigations by advanced characterization methods such as analytical transmission electron microscopy (TEM) and scanning electron microscopy (SEM), electron paramagnetic resonance (EPR), Mössbauer spectroscopy, evaluation of physical properties in controlled environments (gas sensors, photocatalysis). The research activity includes, also, synthesis of nanostructured materials by the hydrothermal or co-precipitation methods.

Among the important research equipments we mention: a high resolution analytical electron microscope; aconventional transmission electron microscopy which allows working in the temperature range 77-1300 K ; preparation equipments of TEM/SEM specimens; a SEM-FIB dual analytical system, five EPR spectrometers operating in several microwave bands and working modes in continous wave or in pulsed regime, down to liquid He temperature; He liquefaction station; three Mössbauer spectrometers in the temperature range 4-1000 K ; XRD diffractometers for powders and thin films; specialized equipments for hydrothermal and co-precipitation synthesis.

The high resolution electron microscope is provided with probe Cs corrector of the spherical aberration and EDS and EELS microanalytical facilities, allowing the obtaining of a spatial resolution under 1 A and atomic elemental mapping. The SEM-FIB dual system which has been installed in a cleanroom is used for morphostructural and microanalytical investigations (SEM, EDS, EBSD) and for the processing of advanced materials at micro and nanometric scale by means of ion beams and nanomanipulators. Electron microscopy and RES spectroscopy facilities are included in the european network of research infrastructures C-ERIC (http://www.c-eric.eu/).

a. High resolution analytical transmission electron microscope (0.08 nm in mode STEM HAADF);

b. Analytical SEM-FIB dual system;

c. RES spectrometer in X band (9.7 GHz) in pulsed regime with accessories ENDOR;

d. Mossbauer spectrometer with cryostate for high magnetic fields (7 T) and cryogenic temperatures

e. Setup for electrical measurements in controlled atmosphere gas mixing station.

The research activity of the scientists working in this laboratory is focused on the physical properties of advanced materials (structure, optical, electrical properties), resulting either as size effects (nanostructures, thin films) or by structural defect engineering. The scientific concerns are mainly directed towards the discovery, investigation and manipulation of physical properties at nanometric and atomic scale for the development and characterization of new materials (dielectrics, semiconductors, alloys, ceramics) to be used in various applications (semiconductor technology, gas sensing, radiation detectors, telecommunications, aerospace technologies).

Personnel

List of Personnel

Lab. 10 – Laboratory of Multifunctional Materials and Structures

HEAD: Dr. Lucian PINTILIE
E-mail: pintilie@infim.ro
Tel : (+4) 021 369 01 85
Fax: (+4) 021 369 01 77

1. Dr. Gabriel BANCIU	senior researcher I
2. Dr. Cornel MICLEA	senior researcher I
3. Dr. Ioana PINTILIE	senior researcher I
4. Dr. Daniela PREDOI	senior researcher I
5. Dr. Marin CERNEA	senior researcher II
6. Dr. Monica ENCULESCU	senior researcher II
7. Dr. Corneliu Florin MICLEA	senior researcher II
8. Dr. Silviu POLOSAN	senior researcher II
9. Dr. Luminita AMARANDE	senior researcher III
10. Dr. Lucian Dragos FILIP	senior researcher III
11. Dr. Aurelian GALCA	senior researcher III
12. Dr. Luminita HRIB	senior researcher III
13. Dr. Alin IUGA	senior researcher III
14. Dr. Elena MATEI	senior researcher III
15. Dr. Liviu NEDELCU	senior researcher III
16. Dr. Iuliana PASUK	senior researcher III
17. Dr. Nicoleta PREDA	senior researcher III
18. Dr. George STAN	senior researcher III
19. Dr. Viorica STANCU	senior researcher III
20. Dr. Lucian TRUPINA	senior researcher III
21. Georgia BONI	researcher
22. Cristina BESLEAGA STAN	researcher
23. Dr. Cristina BUSUIOC	researcher
24. Dr. Cristina CHIRILA	researcher
25. Dr. Marius CIOANGHER	researcher
26. Dr. Carmen CIOBANU	researcher
27. Mihaela BOTEA	assistant researcher
28. Constantin CIOBOTARU	assistant researcher
29. Corina CIOBOTARU	assistant researcher
30. Andreea COSTAS	assistant researcher
31. Constantin DUTU	assistant researcher
32. Alexandru EVANGHELIDES	assistant researcher
33. Camelia FLORICA	assistant researcher
34. Irina GHITA	assistant researcher
35. Simona ICONARU	assistant researcher

36. Mihaela OANCEA	assistant researcher
37. Claudiu POPA	assistant researcher
38. Cristina POPA	assistant researcher
39. Roxana RADU	assistant researcher
40. Andrei Gabriel TOMULESCU	assistant researcher
41. Liliana TRANCA	assistant researcher
42. Alexandru GAVRILA	engineer
43. Vasilica TOMA	engineer

Lab. 20 – Laboratory of Magnetism and Superconductivity

HEAD: Dr. Victor Eugen KUNCSER
E-mail: kuncser@infim.ro
Tel.: (+4) 021 369 01 85
Fax: (+4) 021 369 01 77

1. Dr. Gheorghe Virgil ALDICA	senior researcher I
2. Dr. Petre BADICA	senior researcher I
3. Dr. Ovidiu CRISAN	senior researcher I
4. Dr. George FILOTI	senior researcher I (associate collaborator)
5. Dr. Andrei GALATANU	senior researcher I
6. Dr. Lucica MIU	senior researcher I
7. Dr. Neculai PLUGARU	senior researcher I
8. Dr. Viorel Constantin SANDU	senior researcher I
9. Dr. Mihaela VALEANU	senior researcher I
10. Dr. Alina CRISAN	senior researcher III
11. Dr. Valentina MIHALACHE	senior researcher III
12. Dr. Petru PALADE	senior researcher III
13. Dr.Gabriel SCHINTEIE	senior researcher III
14. Ancuta BARSAN	researcher
15. Dr. Ion IVAN	researcher
16. Dr. Carmen PLAPCIANU	researcher
17. Dr. Bogdan POPESCU	researcher
18. Dr. Mihaela SOFRONIE	researcher
19. Dr. Felicia TOLEA	researcher
20. Dr. Maria-Cristina BARTHA	researcher
21. Mihai Burdusel	assistant researcher
22. Cezar-Catalin COMANESCU	assistant researcher
23. Magda GALATANU	assistant researcher
24. Simona Gabriela GRECULEASA	assistant researcher
25. Marilena Alina IONESCU	assistant researcher
26. Aurel LECA	engineer
27. Dr. Adrian Ioan CRISAN[1]	senior researcher I
28. Dr. Adrian JIANU[2]	senior researcher I
29. Dr. Marilena TOMUT[3]	senior researcher III

[1] Univ. Birmingham, Dept. Met & Mat., Birmingham, England.
[2] Institute for Pulsed Power and Microwave Technology, Forschungszentrum Karlsruhe.
[3] GSI / KP2 Nuclear Structure and Nuclear Chemistry, Darmstadt.

Lab. 30 – Laboratory of Nanoscale Condensed Matter

HEAD: Dr. Valeriu MOLDOVEANU
E-mail: valim@infim.ro
Tel.: (+4) 021 369 01 85
Fax: (+4) 021 369 01 77

1.	Dr. Alexandru Emil ALDEA	senior researcher I
2.	Dr. Magdalena Lidia CIUREA	senior researcher I
3.	Dr. Paul GARTNER	senior researcher I
4.	Dr. Sorina LAZANU	senior researcher I
5.	Dr. Dan MACOVEI	senior researcher I
6.	Dr. Nicolae POPA	senior researcher I
7.	Dr. Cristian-Mihail TEODORESCU	senior researcher I
8.	Dr. Gheorghe IORDACHE	senior researcher II
9.	Dr.Nicoleta APOSTOL	senior researcher III
10.	Dr. Maria-Ruxandra COSTESCU	senior researcher III
11.	Dr.Ion Viorel DINU	senior researcher III
12.	Dr. Rodica GHITA	senior researcher III
13.	Dr. Marius Adrian HUSANU	senior researcher III
14.	Dr. Ana Maria LEPADATU	senior researcher III
15.	Dr. Stefan NEATU	senior researcher III
16.	Dr. Constantin Catalin NEGRILA	senior researcher III
17.	Dr. Marian NITA	senior researcher III
18.	Dr. Ionel STAVARACHE	senior researcher III
19.	Dr. Mihaela STEGARESCU	senior researcher III
20.	Dr. Mugurel TOLEA	senior researcher III
21.	George-Adrian LUNGU	researcher
22.	Dr. Dana Georgeta POPESCU	researcher
23.	Adrian SLAV	researcher
24.	Laura Elena ABRAMIUC	assistant researcher
25.	Amelia Elena BOCARNEA	assistant researcher
26.	Radu DRAGOMIR	assistant researcher
27.	Bogdan OSTAHIE	assistant researcher
28.	Catalin PALADE	assistant researcher
29.	Nicoleta RADUTOIU	assistant researcher
30.	Liviu Cristian TANASE	assistant researcher
31.	Ioana Cristina BUCUR	engineer
32.	Cristian TACHE	engineer
33.	Dr. Nicolae BARSAN[1]	senior researcher I
34.	Dr. Andrei MANOLESCU[2]	senior researcher I
35.	Dr. Paul RACEC[3]	senior researcher III
36.	Dr. Toma STOICA[4]	senior researcher I

[1] Institute of Physical and Theoretical Chemistry, University of Tübingen
[2] School of Science and Engineering, Reykjavik, Iceland
[3] Institut fur Theoretische Physik, Universitat Bremen, Germany
[4] Forschungszentrum Julich, Peter Grunberg Institut, Julich, Germany

Lab. 40 – Laboratory of Optical Processes in Nanostructured Materials

HEAD: Dr. Mihaela BAIBARAC
E-mail: barac@infim.ro
Tel.: (+4) 021 369 01 77
Fax: (+4) 021 369 01 77

1.	Dr. Ioan BALTOG	senior researcher I
2.	Dr. Ligia FRUNZA	senior researcher I
3.	Dr. Stefan FRUNZA	senior researcher I
4.	Dr. Mihai POPESCU	senior researcher I
5.	Dr. Mihai SECU	senior researcher I
6.	Dr. Marian SIMA	senior researcher II
7.	Dr. Anca STANCULESCU	senior researcher II
8.	Dr. Adam LORINCZI	senior researcher III
9.	Lucian MIHUT	senior researcher III
10.	Dr. Corina SECU	senior researcher III
11.	Dr. Marcela SOCOL	senior researcher III
12.	Dr. Alin VELEA	senior researcher III
13.	Timucin VELULA	senior researcher III
14.	Dr. Irina Ionela ZGURA	senior researcher III
15.	Dr. Florin COTOROBAI	physicist
16.	Paul Constantin GANEA	researcher
17.	Dr. Florentina NEATU	researcher
18.	Dr. Oana RASOGA	researcher
19.	Dr. Florinel SAVA	researcher
20.	Dr. Mariana SIMA	researcher
21.	Carmen BREAZU	assistant researcher
22.	Monica DAESCU	assistant researcher
23.	Ioana DUMITRESCU	assistant researcher
24.	Mirela ILIE	assistant researcher
25.	Adelina MATEA	assistant researcher
26.	Andreea NILA	assistant researcher
27.	Daniel-Iosif SIMANDAN	assistant researcher
28.	Ion SMARANDA	assistant researcher
29.	Malvina STROE	assistant researcher

Lab. 50 – Laboratory of Atomic Structures and Defects in Advanced Materials

HEAD: Dr. Corneliu GHICA
E-mail: cghica@infim.ro
Tel.: (+4) 021 369 01 85
Fax: (+4) 021 369 01 77

1. Dr. Ion BIBICU	senior researcher I
2. Dr. Lucian DIAMANDESCU	senior researcher I
3. Dr. Nicoleta Maria GRECU	senior researcher I
4. Dr. Leona Cristina NISTOR	senior researcher I
5. Dr. Sergiu Vasile NISTOR	senior researcher I
6. Dr. Corneliu SARBU	senior researcher I
7. Dr. Valentin Serban TEODORESCU	senior researcher I
8. Dr. Marcel FEDER	senior researcher II
9. Dr. Adelina STANOIU	senior researcher II
10. Dr. Mariana STEFAN	senior researcher II
11. Dr. Alina BANUTA	senior researcher III
12. Dr. Daniela GHICA	senior researcher III
13. Dr. Mihai VLAICU	senior researcher III
14. Dr. Cristian Eugen SIMION	researcher
15. Alexandra Camelia JOITA	assistant researcher
16. Andrei Cristian KUNCSER	assistant researcher
17. Dr. Valentin Adrian MARALOIU	assistant researcher
18. Dr. Ionel Florinel MERCIONIU	assistant researcher
19. Raluca NEGREA	assistant researcher
20. Andreea Alexandra NILA	assistant researcher
21. Dr. Traian POPESCU	assistant researcher
22. Anda STANCIU	assistant researcher
23. Ioana VLAICU	assistant researcher
24. Stefan BULAT	engineer
25. Gheorghe STERIAN	assistant engineer
26. Dr. Manuela STIR[1]	assistant researcher

[1] EMPA Materials Research and Technology, Thun, Switzerland

MAAS Laboratory for X-Ray Photoelectron Spectroscopy (XPS) Analysis

1. Dr. Mihail Florin LAZARESCU	senior researcher I
2. Dr. Stefan Adrian MANEA	senior researcher I
3. Dr. Constantin LOGOFATU	senior researcher III
4. Dr. Costel COTIRLAN-SIMIONUC	assistant researcher
5. Dr. Florica FRUMOSU	assistant researcher

Visiting Guests

Workshop RD50
Organizer INCDFM
Chair: Pintilie I
11-13 June 2014, Novotel hotel, Bucharest, Romania
https://indico.cern.ch/event/307015/other-view?view=standard#
about 80 participants from abroad and Romania

Conference Electroceramics XIV
Main Organizer INCDFM
Chair: Pintilie L
15-19 June 2014, Intercontinental hotel, Bucharest, Romania
http://www.electroceramics14.com/
about 300 participants all over the world

Prof. Peter Hänggi, University of Augsburg, Germany
The Ring of Brownian motion: The good, the bad and some simply silly
07.07.2014

Prof. Albert Fert, Nobel Prize laureate (Physics, 2007)
CNRS, THALES group, Palaiseau, France
SPIN-ORBITRONICS, A NEW DIRECTION FOR SPINTRONICS
02.11.2014

Prof. Stefano Bellucci, NEXT Nanotechnology Laboratory, INFN-Laboratori Nazionali Frascati, Frascati, Italy
Research highlights in nanoscience and technology at Frascati Laboratories
16.11.2014

Dr. Matthias GIROD, Elettra Sincrotrone, Trieste (Italy)
A unique opportunity for multi-technique research projects
28.11.2014

Prof. Kazuo WATANABE, High Field Laboratory for Superconducting Materials (HFLSM), Tohoku University Japan
New High Magnetic Field Facilities in the World
28.11.2014

Prof. Bengt G. Svensson, University of Oslo, Department of Physics, Physical Electronics, Oslo, Norway
Functional Oxides for Energy Technology
31.11.2014

Prof. Annie Powell, Institute of Inorganic Chemistry and Institute of Nanotechnology, Karlsruhe Institute of Technology
Incorporating highly anisotropic metal ions into coordination clusters in the quest for improved Single Molecule Magnets
04.12.2014

Working stages and Guest visitors

Dr. Tomas CEPONIS
Institute of Applied Physics, University of Vilnius, Lithuania
Training in EPR techniques at cryogenic temperatures in the Center for advanced ESR techniques-CetRESav from lab. 50
Working stage (17.03 – 17.04.2014) in Laboratory 50 (RES spectroscopy group, invited by Dr. S. V. Nistor)

Dr. Margit FABIAN
Centre for Energy Research - Hungarian Academy of Sciences, Budapesta, Ungaria
NMR and HTEM structure characterization of new borosilicate and boromolybdate glasses
Working stage (21.10 – 24.10.2014) in the frame of C-ERIC consortium in Laboratory 50 (Electron Microscopy group, invited by Dr. C. Ghica)

Dr. Udo Gommel
Fraunhofer-Institut für Produktionstechnik und Automatisierung IPA, Sttutgart, Germania
Guest visitor (December 16, 2014), lecture about the technologies for clean rooms

Ph. D. Theses

Cristina Besleaga Stan
Wide band semiconductors with application in transparent electronics
February 2014

Iosif Daniel Simandan
Complex Langmuir-Blodgett multilayers and applications in sensorics
March 2014

Iulia Corina Ciobotaru
Semiconducting organic materials for photonics applications
March 2014

Traian Popescu
Properties of TiO_2 based oxidic nanomaterials and their biologic interactions
March 2014

Ioana-Dorina Vlaicu
Complex combinations of some 3d transitional metals with azol ligands, as materials with biologic activity
March 2014

George-Adrian Lungu
Contributions to study of the structural and magnetic properties of some thin films
June 2014

Constantin Claudiu Ciobotaru
Polymeric nanocomposites based on carbonic structures
July 2014

Camelia – Florina Florica
Electronic and optoelectronic devices based on nanowires
November 2014

Awards

- ***Besleaga C*: Best Poster award, 10th International Conference on Physics of Advanced Materials, Iasi, Romania,** 22 - 28 September 2014, for the contribution "*Advanced characterization of amorphous oxide semiconductor thin films by x-ray reflectivity and thermal stimulated current spectroscopy*"
- ***Negrea R F*: Prize Best Student Poster la Europhysical Conference on Defects in Insulating Materials (Eurodim 2014),** Canterbury, UK, 13-19 July 2014 for the contribution *„Atomic scale STEM and EELS characterization of $BaTiO_3/SrRuO_3/SrTiO_3$ ferroelectric heterostructure"*
- ***Palade C*: Best Paper Award** for the contribution "*Conduction mechanism versus annealing in SiO_2 films with Ge nanoparticles*" (authors: C Palade, AM Lepadatu, I Stavarache, VS Teodorescu and ML Ciurea), awarded in October 2014 at **CAS 2014**
- ***Palade C*: Best Paper Award at CAS 2014** in Session Nanoscience and Materials - Student Papers for the contribution *"Trapping centers in havy ion irradiated silicon",* (authors: C Palade, S Lazanu and ML Ciurea)
- ***Trinca LM*: Best Poster award, Electroceramics XIV, Bucharest, Romania**, 16–20 June 2014, for the contribution "*ZnO - based homo and hetero - structures: assembling and characterization*"
- ***Apostol N.*** **Romanian Academy Prize „Radu Grigorovici**"-2012 for the group of papers entitled *Fenomene de suprafață și de interfață evidențiate prin spectroscopii de electroni XPS/Auger și alte tehnici de caracterizare a suprafețelor și interfețelor*, awarded in December 2014.
- ***Predoi D*: Romanian Academy Prize „Radu Grigorovici"**-2012 for the group of papers entitled: « *Materiale biocompatibile: preparare și caracterizare* » awarded in December 2014.

Awards at International Fairs and Exhibitions

XII International Inventics Salon PRO INVENT, Cluj-Napoca, 18-22 martie 2014

- **Cotarlan Simioniuc Costel, Lazarescu Mihail Florin: Detection system based on nanostructured surfaces for biosensors and imagistics with resolution below diffraction limit**
  Patent request A/00244/25.03.2013
  DIPLOME OF EXCELLENCE and GOLD MEDAL
- E. Andronescu, **R. Ghita, C.D. Ghitulica, S.L. Iconaru, D. Predoi,** R. Trusca, **F. Ungureanu: Synthesis of supermagnetic iron oxides in polysaccharides**
  Patent RO 128484-A2, 2013
  DIPLOME OF EXCELLENCE and GOLD MEDAL
- **Alexandru Evanghelidis, Cristina Busuioc, Nicoleta Preda, Elena Matei, Monica Encluescu, Camelia Florica, Andreea Costas, Mihaela Oancea, Ionut Enculescu: Procedure of obtaining of ZnO submicronic fibers by electrospinning, using polymetacrilate solutions**
  DIPLOME OF EXCELLENCE and GOLD MEDAL

- **Alexandru Evanghelidis, Cristina Busuioc, Nicoleta Preda, Elena Matei, Monica Enculescu, Camelia Florica, Andreea Costas, Mihaela Oancea, Ionut Enculescu:** ELECTROSPINNING
  DIPLOME OF EXCELLENCE – for promotion of creativity
- **M.G. Banciu, L. Nedelcu: Microstrip filter on ZsT substrates**
  DIPLOME OF EXCELLENCE and GOLD MEDAL
- **Andrei Galatanu, Bogdan Popescu, Magdalena Galatanu, Monica Enculescu, Mihai Cioca: Electrical field assisted brazing technology for refractory metals**
  PRIZE I, awarded by Polytechnica University Bucharest

European Exhibition of Creativity and Innovation EUROINVENT, IASI 22-24 MAI,2014

- **Andrei Galatanu, Petre Palade, Bogdan Popescu, Magdalena Galatanu, Monica Enculescu, Cornel Sarbu:** Development of high heat flux materials and technologies for fusion reactors
  GOLD MEDAL
- **Mihaela Valeanu, Victor Kuncser, Felicia Tolea, Mihaela Sofronie, Neculai Plugaru**: Magneto-caloric and magneto-resistance effects in Heussler type Feromagnetic shape Memory Alloys
  SILVER MEDAL
- **Stefan Frunza, Traian Beica, Ionela Zgura, Ligia Frunza, Alexandrina Nuta, Ana Alexandra Sorescu, Corneliu Nicolae, Zaharia Ionica Bunea**: Device and method for detection of the viral antigen-specific antibody interactions by determining the contact angle
  SILVER MEDAL
- **Ionut Enculescu, Alexandru Evanghelidis, Cristina Busuioc, Nicoleta Preda, Elena Matei, Monica Enculescu, Camelia Florica, Andreea Costas, Mihaela Oancea, Alexandru Gavrila, Mihai Cioca, Liviu Culea**: 'INFIM SPIN 1.0'
  GOLD MEDAL
- **I. Enculescu, A. Evanghelidis, C. Busuioc, N. Preda, E. Matei, M. Enculescu, C. Florica, A. Costas, M. Oancea, A. Gavrila, M. Cioca, L. Culea:** 'INFIM SPIN 1.0'
  PRIZE FOR THE BEST DESIGN
- **A. Evanghelidis, C. Busuioc, N. Preda, E. Matei, M. Enculescu, C. Florica, A. Costas, M. Oancea, I. Enculescu:** Electrospining INCDFM
  DIPLOME OF EXCELLENCE – for promotion of creativity
- **Stefan Frunza, Traian Beica, Ionela Zgura, Ligia Frunza, Alexandrina Nuta, Ana Alexandra Sorescu, Corneliu Nicolae, Zaharia Ionica Bunea:** Device and method for detection of the viral antigen-specific antibody interactions by determining the contact angle
  DIPLOME OF EXCELLENCE, awarded by University Valahia Targoviste - Research Center for Mechanical Microsystems

Honorary Membership

NIMP is honorary membership in various prestigious professional societies and associations, such as:

- **American Chemical Society**
- **German Physical Society**
- **European Society of Applied Superconductivity**
- **Japanese Applied Physics Society (former)**
- **Cryogenic Society of Japan (former)**
- **Alumni JSPS, Romania (founding member)**

3 NIMP distinguished researchers are **Editor-in-chief or Co-Editor for 8 ISI journals**. Finally, 16 researchers are members in **Editorial Board and Advisory Board for 11 ISI journals (6 edited in Romania)**.

Also, NIMP is present in following databases:

- **MyNet Research** Empowering Collaboration (www.mynetresearch.com) – international resource for innovation centers in Eastern Europe and Central Asia. The top five Romanian institutions in terms of research productivity are:
  - Univ Bucharest
  - Univ Babes Bolyai
  - Romanian Acad
  - Inst Atom Phys
  - Natl Inst Mat Phys
- The **CEEC IST NET** portal (www.eu-istcommunity.net) – is a support instrument for partners search and consortia creation in the field of research and innovation concerning the information society technologies
- **Europartners Search** (www.europartnersearch.net)
- **Resource Guide to Nanotechnology and Nanomaterials Services** (**NanoPerspective**)
  This guide includes a list of more 1000 organizations active in the field of Nanotehnology and Nanomaterials.
  - http://wikimapia.org/19116027/INCDFM-National-RD-Institute-of-Materials-Physics-NIMP
  - http://cercetare.ccib.ro/intranetHTML/infoFILES/infoHTML/File/2012_03_22_prezentareINCDFM.pdf
  - http://www.ancs.ro/ro/articol/1325/de-cercetare-incd-institute-nationale-de-cercetare-dezvoltare-incd-in-coordonarea-ancs-institutul-national-de-cercetare-dezvoltare-pentru-fizica-materialelor-incdfm-bucuresti
  - http://www.infocercetare.ro/ro/Listeaza-Institutie/Ilfov-84_Localitate_Magurele-86_Institutie_INCD-pentru-Fizica-Materialelor-INCDFM-253

INCDFM is membership of C-ERIC (Central European Research Infrastructure Consortium) **Consortium** (*http://www.ceric-eric.eu/*). C-ERIC is a distributed research facility, set up as an ERIC, by ***Austria***, ***Czech Republic***, ***Italy***, ***Romania***, ***Croatia, Polonia***, ***Slovenia***, ***Serbia***, and ***Hungary*** and open to other interested countries.

The specific scope of this ERIC concerns the offer as an integrated service to external researchers of the access to *synchrotron light and other microscopic probes for analytical and modification*

techniques notably for materials preparation and characterization, structural investigations and imaging in Life Sciences, Nanoscience and Nanotechnology, Cultural Heritage, Environment and Materials Sciences and to their various technological and industrial outcomes ranging from energy to biomedical and of interest to most manufacturing industries.

CERIC's mission is to bring the integrated service to world-level quality thus contributing to the attractiveness of the European Research Area and stimulating a beneficial impact on the scientific and economic development of the entire region, also helping to introduce a strong interchange between scientists and technicians and attraction of scientists from other regions.

Membership in Other International Organizations

Badica Petre: member of American Chemical Society and German Physical Society
Banciu Marian Gabriel: member of IEEE: Microwave Theory and Techniques Society, Antennas and Propagation Society
Bibicu Ion: member of European Physical Society
- member of Academy of Technical Sciences from Romania
Ciurea Magdalena Lidia: member of European Physical Society
Crisan Ovidiu: member of Institute of Nanotechnology, UK
Diamandescu Lucian: member of "American Nano Science"
- Romanian Representative in International Board on the Applications of Mössbauer Effect - IBAME (2011-2017)
- member in Editorial Board of "ISRN Nanomaterials" (SUA)
Frunza Ligia: member of American Chemical Society and of Romanian Society of Catalysis
Ghica Corneliu: member of European Materials Research Society
Ghica Daniela: member of European Materials Research Society
Grecu Maria Nicoleta: member of AMPERE Group
Maraloiu Valentin Adrian: member of Société Française des Microscopies
Nistor Sergiu Vasile: member of American Physical Society
Pintilie Lucian: member of European Physical Society
Popescu Mihai: member of NACNOG (North Atlantic Consortium on Non-Oxide Glasses, 19 countries from Europe, Canada and USA)
- member of VIP (Virtual Institute of Physics): http://www.infim.ro/~inst
Predoi Daniela: member of Romanian Society of Catalysis
Sandu Viorel: member of American Physical Society and Material Research Society Singapore
Sarbu Corneliu: member of Microscopical Society of America
Socol Marcela: member of International Organization on Crystal Growth
Stanculescu Anca: member of International Organization on Crystal Growth
- member of SPIE

Publications and Presentations

BOOKS

Cernea M, Vasile BS, Trusca R, Andronescu E, **Ceramici piezoelectrice pe baza de $Bi_{0.5}Na_{0.5}TiO_3$** , Ed. Polytechnic-Press, Bucharest, 2014. ISBN: 978-606-515-562-6

Kuncser V, Miu L (Eds.), Size Effects in Nanostructures. Basics and Applications, Springer-Verlag Berlin Heidelberg 2014. ISBN 978-3-662-44478-8

BOOK CHAPTERS

- **M. Stefan, S.V. Nistor, D. Ghica,** Chapter 1 *ZnS and ZnO Semiconductor Nanoparticles Doped with Mn2+ Ions. Size Effects Investigated by EPR Spectroscopy*, pp. 3-28, in the book **Size Effects in Nanostructures: Basics and Applications,** Springer Series in Materials Science 205, Editors: V. Kuncser, L. Miu, Springer (2014).
- **M. Popescu, F. Sava, A. Velea**, Chapter 2. *Self-organization and size effects in amorphous silicon*, pp. 29-45, in the book **Size Effects in Nanostructures: Basics and Applications,** Springer Series in Materials Science 205, Editors: V. Kuncser, L. Miu, Springer (2014).
- **M.L. Ciurea, V.S. Teodorescu, I. Stavarache, A.M. Lepadatu,** Chapter 3 *GeSiO Based Nanostructures: Electrical Behaviour Related to Morphology and Preparation Method*, pp. 47-76, in **Size Effects in Nanostructures: Basics and Applications**, Springer Series in Materials Science 205, Editors: V. Kuncser, L. Miu, Springer (2014).
- **Pintilie I, Pintilie L, Filip LD, Nistor LC, Ghica C,** Chapter 4: *Oxide Thin Films and Nano-heterostructures for Microelectronics (MOS Structures, Ferroelectric Materials and Multiferroic Heterostructures)*, pp 77-108, in: **Size Effects in Nanostructures: Basics and Applications**, Springer Series in Materials Science vol. 205, Editors: V. Kuncser, L. Miu, Springer (2014).
- **N. Preda, M. Enculescu, I. Zgura, M. Socol, C. Florica, A. Evanghelidis, E. Matei, I. Enculescu,** Chapter 5 *Zinc Oxide and Polysaccharides: Promising Candidates for Functional Nanomaterials,* pp. 109-136 in: **Size Effects in Nanostructures: Basics and Applications**, Springer Series in Materials Science vol. 205, Editors: V. Kuncser, L. Miu, Springer (2014).
- **E. Matei, M. Enculescu, N. Preda, C. Florica, A. Costas, C. Busuioc**, M.E. Toimil Molares, **V. Kuncser, I. Enculescu,** Chapter 6 *Metallic Nanowires and Nanotubes Prepared by Template Replication*, pp.137-168 in: **Size Effects in Nanostructures: Basics and Applications**, Springer Series in Materials Science vol. 205, Editors: V. Kuncser, L. Miu, Springer (2014).
- **V. Kuncser, P. Palade, A. Kuncser, S. Greculeasa, G. Schinteie**, Chapter 7 *Engineering Magnetic Properties of Nanostructures via Size Effects and Interphase Interactions* pp.169-238 in: **Size Effects in Nanostructures: Basics and Applications**, Springer Series in Materials Science vol. 205, Editors: V. Kuncser, L. Miu, Springer (2014).
- **N. G. Apostol, C. M. Teodorescu**, Chapter 8*: Reactivity and magnetism at metal-semiconductor interfaces*, pp. 239-291 , in **Size Effects in Nanostructures: Basics and Applications**, Springer Series in Materials Science vol. 205, Editors: V. Kuncser, L. Miu, Springer (2014).

- **L. Miu, P. Mele, I. Ivan, A.M. Ionescu, A. Crisan, P. Badica** , D. Miu, Chapter 9: *Magnetization Relaxation in Superconducting $YBa_2Cu_3O_7$ Films with Embedded Nanorods and Nanoparticles*, pp. 293-337 in **Size Effects in Nanostructures: Basics and Applications**, Springer Series in Materials Science vol. 205, Editors: V. Kuncser, L. Miu, Springer (2014).
- **N. G. Apostol, C. M. Teodorescu**, Chapter 7*: Band bending at metal-semiconductor interfaces, ferroelectric surfaces and metal-ferroelectric interfaces investigated by photoelectron spectroscopy*, in **Surface Science Characterization Techniques for Nanomaterials**, Springer Series on Characterization Tools for Nanoscience & Nanotechnology, Vol. 4, C. Kumar (Ed.), Springer, Berlin, *in press* http://www.springer.com/chemistry/book/978-3-662-44550-1 (2015) ISBN: 978-3-662-44550-1.
- **Cernea M**, Vasile BS, Trusca R, Andronescu E*,* **Ceramici piezoelectrice pe baza de $Bi_{0.5}Na_{0.5}TiO_3$**, Ed. Polytechnic-Press, Bucharest, 2014. ISBN: 978-606-515-562-6
- S. Comorosan, **S. Polosan**, M. Apostol, I. Popescu, I. Farcasanu, L.Paslaru, E. Ionescu, Chapter: *Effects Induced in Complex Biological Systems by High Density Green Photons* in the book: **Localized Excitations in Nonlinear Complex Systems, Nonlinear Systems and Complexity**, volume 7, pp. 419-428, ISBN : 978-3-319-02056-3, 2014, Springer International Publishing.
- **G. A. Lungu, N. G. Apostol, C. M. Teodorescu**, Chapter 4*: Basic concepts in ferromagnetism of diluted magnetic semiconductors. The case of manganese embedded in Ge(001)*, in **Nanomagnetism**, J. M. Gonzalez Estevez (Ed.), One Central Press, Manchester, pp. 74-110 (2014), ISBN: 978-1-910086-05-6.
- **Teodorescu V S,** M-G.Blanchin**,** *TEM study of the sol-gel oxide thin films* in **Microscopy: advances in scientific research and education**, Ed. A.Mendez-Vilas, Microscopy Book Series, number 6 vol 2, Formatex 2014. ISBN: 978-84-942134-4-1

Papers in ISI Ranked Journals (with Impact Factor)

1. Acsente, T; **Negrea, RF**; Lazea-Stoyanova, A; **Nistor, LC**; Dinescu, G;
   Microstructure of the a-C:H/W layers deposited by plasma assisted sequential deposition method
   DIGEST JOURNAL OF NANOMATERIALS AND BIOSTRUCTURES, (2014), 9, pp. 443-450, **1.123**, **0.209**

2. **Aldica, G**; **Burdusel, M**; **Badica, P**;
   Trapped magnetic field in a (NdFeB)-(MgB_2) pair-type bulk magnet
   PHYSICA C-SUPERCONDUCTIVITY AND ITS APPLICATIONS, (2014), 505, pp. 18-23, **1.11**, **0.293**

3. **Aldica, G**; Popa, S; **Enculescu, M**; Batalu, D; **Miu, L**; Ferbinteanu, M; **Badica, P**;
   Addition of Ho_2O_3 of different types to MgB2 in the ex-situ Spark Plasma Sintering: Simultaneous control of the critical current density at low and high magnetic fields
   MATERIALS CHEMISTRY AND PHYSICS, (2014), 146, pp. 313-323, **2.129**, **0.546**

4. Alexandru, H. V., Mindru, C., Bacşei, R., **Ganea, C.-P.**
   Estimation of essential dielectric parameters in ferroelectric state of TGS crystal
   JOURNAL OF OPTOELECTRONICS AND ADVANCED MATERIALS, (2014) 16, pp. 457-462, **0.563**, **0. 111**

5. **Amarande, L**;
   Evaluation of the complex material constants of piezoelectric ceramics in the thickness vibration mode
   JOURNAL OF THE EUROPEAN CERAMIC SOCIETY, (2014), 34, pp. 1547-1552, **2.307**, **0.699**

6. **Amarande, L**; **Miclea, C**; **Cioangher, M**; Grecu, MN; **Pasuk, I**; **Negrea, RF**;
   Influence of co-dopants average valence on microstructural and electromechanical properties of lead titanate ceramics
   JOURNAL OF THE EUROPEAN CERAMIC SOCIETY, (2014), 34, pp. 1191-1200, **2.307**, **0.699**

7. Anastasescu, M; **Teodorescu, VS**; Buiu, O; Osiceanu, P; Calderon-Moreno, JM; Predoana, L; Preda, S; Nicolescu, M; Marin, A; Serban, B; Mihaila, M; Stoica, M; Zaharescu, M; Gartner, M;
   Substrate impact on optical and microstructural properties of TiO2-PEG sol-gel films
   CERAMICS INTERNATIONAL, (2014), 40, pp. 11803-11811, **2.086**, **0.439**

8. Avadanei, OG; **Banciu, MG**; **Nedelcu, L**;
   Higher-Order Modes in High-Permittivity Cylindrical Dielectric Resonator Antenna Excited by an Off-Centered Rectangular Slot
   IEEE ANTENNAS AND WIRELESS PROPAGATION LETTERS, (2014), 13, pp. 1585-1588, **1.948**, **0.776**

9. Axente, E; Socol, G; Beldjilali, SA; Mercadier, L; Luculescu, CR; **Trinca, LM**; **Galca, AC**; Pantelica, D; Ionescu, P; Becherescu, N; Hermann, J; Craciun, V;
   Quantitative analysis of amorphous indium zinc oxide thin films synthesized by Combinatorial Pulsed Laser Deposition
   APPLIED PHYSICS A-MATERIALS SCIENCE & PROCESSING, (2014), 117, pp. 229-236, **1.694**, **0.484**

10. Badea, M; **Vlaicu, ID**; Olar, R; Constand, M; Bleotu, C; Chifiriuc, MC; Marutescu, L; Lazar, V; Grecu, MN; Marinescu, D;
Thermal behaviour and characterisation of new biologically active Cu(II) complexes with benzimidazole as main ligand
JOURNAL OF THERMAL ANALYSIS AND CALORIMETRY, (2014), 118, pp. 1119-1133, **2.206**, **0.262**

11. **Badica, P**; **Aldica, G**; **Burdusel, M**; Popa, S; **Negrea, RF**; **Enculescu, M**; **Pasuk, I**; **Miu, L**;
Significant enhancement of the critical current density for cubic BN addition into ex situ spark plasma sintered MgB2
SUPERCONDUCTOR SCIENCE & TECHNOLOGY, (2014), 27, pp. -, **2.796**, **0.849**

12. **Badica, P**; Aldica, GV; **Burdusel, M**; Borodianska, H; Sakka, Y; Vasylkiv, O;
Challenges of nanostructuring and functional properties for selected bulk materials obtained by reactive spark plasma sintering
JAPANESE JOURNAL OF APPLIED PHYSICS, (2014), 53, pp. -, **1.057**, **0.227**

13. **Badica, P**; Borodianska, H; Xie, SM; Zhao, T; Demirskyi, D; Li, PF; Tok, AIY; Sakka, Y; Vasylkiv, O;
Toughness control of boron carbide obtained by spark plasma sintering in nitrogen atmosphere
CERAMICS INTERNATIONAL, (2014), 40, pp. 3053-3061, **2.086**, **0.439**

14. **Badica, P**; Grasso, S; Borodianska, H; Xie, SS; Li, PF; Tatarko, P; Reece, MJ; Sakka, Y; Vasylkiv, O;
Tough and dense boron carbide obtained by high-pressure (300 MPa) and low-temperature (1600 degrees C) spark plasma sintering
JOURNAL OF THE CERAMIC SOCIETY OF JAPAN, (2014), 122, pp. 271-275, **0.846**, **0.21**

15. **Baibarac, M**; **Baltog, I**; **Mihut, L**; Lefrant, S;
New features in the anti-Stokes and Stokes Raman spectra of single-walled carbon nanotubes that are highly separated into their semiconducting and metallic nanotube components
JOURNAL OF RAMAN SPECTROSCOPY, (2014), 45, pp. 323-331, **2.519**, **0.571**

16. **Baibarac, M**; **Baltog, I**; **Mihut, L**; **Matea, A**; Lefrant, S;
Nonlinear features of surface-enhanced Raman scattering revealed under non-resonant and resonant optical excitation
JOURNAL OF OPTICS, (2014), 16, pp. -, **2.01**, **0.7**

17. **Baibarac, M**; **Baltog, I**; **Smaranda, I**; Scocioreanu, M; Mevellec, JY; Lefrant, S;
Abnormal anti-Stokes Raman scattering and surface-enhanced infrared absorption spectroscopy studies of carbon nanotubes electrochemically functionalized with poly(2, 2 '-bithiophene-co-pyrene)
APPLIED SURFACE SCIENCE, (2014), 309, pp. 11-21, **2.538**, **0.55**

18. **Baibarac, M**; **Baltog, I**; Srnaranda, I; **Ilie, M**; Scocioreanu, M; Mevellec, JY; Lefrant, S;
Spectroelectrochemical properties of the poly[(2, 5-bisoctyloxy)-1, 4-phenylenevinylene]/single-walled carbon nanotube composite
SYNTHETIC METALS, (2014), 195, pp. 276-285, **2.222**, **0.44**

19. **Baibarac, M**; **Sima, M**; **Matei, E**; **Pasuk, I**; **Mihut, L**;
Synthesis and Raman scattering of multiferroic Fe-Pb(Zr0. 2Ti0. 8)O-3 core-shell wire arrays
PHYSICA STATUS SOLIDI A-APPLICATIONS AND MATERIALS SCIENCE, (2014), 211, pp. 200-205, **1.525**, **0.469**

20. Banik, I., **Popescu, M.**
Photoluminescence quenching in disordered semiconductors from point of view of the barrier-cluster-heating model
JOURNAL OF OPTOELECTRONICS AND ADVANCED MATERIALS, (2014), 16, pp. 1275-1284, **0.563**, **0. 111**

21. Baschir, L; Fagadar-Cosma, E; Creanga, I; Palade, A; Lascu, A; Birdeanu, M; Savastru, D; Savu, V; Antohe, S; **Velea, A**; Fagadar-Cosma, G; **Popescu, M**; **Simandan, ID**;
UV sensing effect in Langmuir-Blodgett complex films containing a novel synthesized Fe(III) porphyrin
DIGEST JOURNAL OF NANOMATERIALS AND BIOSTRUCTURES, (2014), 9, pp. 847-857, **1.123**, **0.209**

22. Batalu, D; **Aldica, G**; Popa, S; **Miu, L**; **Enculescu, M**; **Negrea, RF**; **Pasuk, I**; **Badica, P**;
High magnetic field enhancement of the critical current density by Ge, GeO_2 and $Ge_2C_6H_{10}O_7$ additions to MgB2
SCRIPTA MATERIALIA, (2014), 82, pp. 61-64, **2.968**, **1.172**

23. Batalu, D; Stanciuc, AM; Moldovan, L; **Aldica, G**; **Badica, P**;
Evaluation of pristine and Eu_2O_3-added MgB_2 ceramics for medical applications: hardness, corrosion resistance, cytotoxicity and antibacterial activity
MATERIALS SCIENCE & ENGINEERING C-MATERIALS FOR BIOLOGICAL APPLICATIONS, (2014), 42, pp. 350-361, **2.736**, **0.596**

24. **Besleaga, C**; **Galca, AC**; **Miclea, CF**; **Mercioniu, I**; **Enculescu, M**; **Stan, GE**; Mateescu, AO; Dumitru, V; Costea, S;
Physical properties of $Al_xIn_{1-x}N$ thin film alloys sputtered at low temperature
JOURNAL OF APPLIED PHYSICS, (2014), 116, pp. -, **2.185**, **0.724**

25. **Besleaga, C**; Ion, L; Antohe, S;
Azo thin films synthesized by RF-magnetron sputtering: the role of deposition power
ROMANIAN REPORTS IN PHYSICS, (2014), 66, pp. 993-1001, **1.137**, **0.133**

26. **Bibicu, I**; Constantinescu, S; **Diamandescu, L**; Voiculescu, AM; Cotoi, E;
Mossbauer spectroscopy study on YVO4:Eu luminescent material
ROMANIAN REPORTS IN PHYSICS, (2014), 66, pp. 1012-1017, **1.137**, **0.133**

27. **Birsan, A**;
Electronic structure and magnetism of new scandium-based full Heusler compounds: Sc(2)CoZ (Z = Si, Ge, Sn)
JOURNAL OF ALLOYS AND COMPOUNDS, (2014), 598, pp. 230-235, **2.726**, **0.534**

28. **Birsan, A**;
Magnetism in the new full-Heusler compound, Zr2CoAl: A first-principles study
CURRENT APPLIED PHYSICS, (2014), 14, pp. 1434-1436, **2.026**, **0.471**

29. Bisri, SZ; Degoli, E; Spallanzani, N; Krishnan, G; Kooi, BJ; **Ghica, C**; Yarema, M; Heiss, W; Pulci, O; Ossicini, S; Loi, MA;
Determination of the electronic energy levels of colloidal nanocrystals using field-effect transistors and ab-initio calculations
ADVANCED MATERIALS, (2014), 26, pp. 5639-+, **15.409**, **4.266**

30. Bucur, C; Badea, M; Chifiriuc, MC; Bleotu, C; Iorgulescu, EE; Badea, IA; **Grecu, MN**; Lazar, V; Patriciu, OI; Marinescu, D; Olar, R;
Studies on thermal, spectral, magnetic and biological properties of new Ni(II), Cu(II) and Zn(II) complexes with a bismacrocyclic ligand bearing an aromatic linker
JOURNAL OF THERMAL ANALYSIS AND CALORIMETRY, (2014), 115, pp. 2179-2189, **2.206**, **0.262**

31. **Busuioc, C**; **Evanghelidis, A**; **Florica, C**; **Enculescu, I**;
Influence of preparation steps on the properties of electrospun ZnO fibers
DIGEST JOURNAL OF NANOMATERIALS AND BIOSTRUCTURES, (2014), 9, pp. 1569-1578, **1.123**, **0.209**

32. **Busuioc, C**; Jinga, SI;
Preparation and characterization of LixZn2-xVxSi1-xO4 ceramics
CERAMICS INTERNATIONAL, (2014), 40, pp. 5931-5936, **2.086**, **0.439**

33. **Cernea, M**; **Trupina, L**; Vasile, B; **Bartha, C**; **Radu, R**; **Chirila, C**; Teodorescu, A;
BiFeO3 doped-BNT-BT0. 08 piezoelectric and magnetic nanowires, derived from sol-gel precursor
JOURNAL OF NANOPARTICLE RESEARCH, (2014), 16, pp. -, **2.278**, **0.647**

34. **Cernea, M**; Vasile, BS; Boni, A; **Iuga, A**;
Synthesis, structural characterization and dielectric properties of Nb doped BaTiO3/SiO2 core-shell heterostructure
JOURNAL OF ALLOYS AND COMPOUNDS, (2014), 587, pp. 553-559, **2.726**, **0.534**

35. **Cernea, M**; **Vasiliu, F**; **Bartha, C**; **Plapcianu, C**; **Mercioniu, I**;
Characterization of ferromagnetic double perovskite Sr2FeMoO6 prepared by various methods
CERAMICS INTERNATIONAL, (2014), 40, pp. 11601-11609, **2.086**, **0.439**

36. Chirita, P; Badica, CE; Constantin, CA; Birsa, LM; **Matei, E**; **Baibarac, M**;
Influence of 2, 2 '-bipyridine on oxidative dissolution of iron monosulfide
SURFACE AND INTERFACE ANALYSIS, (2014), 46, pp. 842-846, **1.393**, **0.371**

37. Chirila, R; **Dinu, IV**; **Moldoveanu, V**; Moca, CP;
Transport in a hybrid normal metal/topological superconductor Kondo model
PHYSICAL REVIEW B, (2014), 90, pp. -, **3.664**, **1.342**

38. **Ciobanu, CS**; **Iconaru, SL**; **Popa, CL**; Costescu, A; Motelica-Heino, M; **Predoi, D**;
Porous methyltrimethoxysilane coated nanoscale-hydroxyapatite for removing lead ions from aqueous solutions
JOURNAL OF NANOMATERIALS, (2014),, pp. -, **1.611**, **0.37**

39. **Ciobanu, CS**; **Popa, CL**; **Predoi, D**;
Sm:HAp nanopowders present antibacterial activity against Enterococcus faecalis
JOURNAL OF NANOMATERIALS, (2014),, pp. -, **1.611**, **0.37**

40. **Ciobotaru, CC**; Damian, CM; **Matei, E**; Iovu, H;
Covalent functionalization of graphene oxide with cisplatin
MATERIALE PLASTICE, (2014), 51, pp. 75-80, **0.463**, **0.045**

41. **Ciobotaru, CC**; Damian, CM; **Polosan, S**; **Matei, E**; Iovu, H;
Covalent functionalization of single walled carbon nanotubes with doxorubicin for controlled drug delivery systems
DIGEST JOURNAL OF NANOMATERIALS AND BIOSTRUCTURES, (2014), 9, pp. 413-422, **1.123**, **0.209**

42. **Ciobotaru, CC**; Damian, CM; **Polosan, S**; Prodana, M; Iovu, H;
Drug delivery study of single-wall carbon nanotubes covalent functionalized with cisplatin
DIGEST JOURNAL OF NANOMATERIALS AND BIOSTRUCTURES, (2014), 9, pp. 859-868, **1.123**, **0.209**

43. **Ciobotaru, IC**; **Matei, E**; **Ciobotaru, CC**; **Polosan, S**;
Embedding of IrQ(ppy)(2) organometallic compounds in polypyrrole conducting polymer for OLED's applications
SYNTHETIC METALS, (2014), 198, pp. 323-328, **2.222**, **0.44**

44. **Ciobotaru, IC**; **Polosan, S**; **Ciobotaru, CC**;
Dual emitter IrQ(ppy)(2) for OLED applications: Synthesis and spectroscopic analysis
JOURNAL OF LUMINESCENCE, (2014), 145, pp. 259-262, **2.367**, **0.459**

45. **Ciobotaru, IC**; **Polosan, S**; **Ciobotaru, CC**;
Dual emitter IrQ(ppy)(2) for OLED applications: Synthesis and spectroscopic analysis
JOURNAL OF LUMINESCENCE, (2014), 145, pp. 259 -262, **2.367**, **0.459**

46. **Ciurea, ML**; **Lazanu, S**; **Slav, A**; **Palade, C**;
Strain-induced modification of trap parameters due to the stopped ions in Bi-irradiated Si
EPL, (2014), 108, pp. -, **2.269**, **1.004**

47. **Ciurea, ML**; **Stavarache, I**; **Lepadatu, AM**; **Pasuk, I**; **Teodorescu, VS**;
Electrical properties related to the structure of GeSi nanostructured films
PHYSICA STATUS SOLIDI B-BASIC SOLID STATE PHYSICS, (2014), 251, pp. 1340-1346, **1.605**, **0.505**

48. **Comanescu, C**;
Synthesis and characterization of novel mesocomposites Co3O4 and CuO@OMS (ordered mesoporous silica) as active catalysts for hydrocarbon oxidation
JOURNAL OF NANOPARTICLE RESEARCH, (2014), 16, pp. -, **2.278**, **0.647**

49. Cornean, HD; **Moldoveanu, V**; Pillet, CA;
On the steady state correlation functions of open interacting systems
COMMUNICATIONS IN MATHEMATICAL PHYSICS, (2014), 331, pp. 261-295, **1.901**, **1.862**

50. **Cotirlan-Simioniuc, C**; **Ghita, RV**; **Negrila, CC**; **Logofatu, C**;
The evanescent-wave cavity ring-down spectroscopy technique applied to the investigation of thermally grown oxides on Si(100)
APPLIED PHYSICS A-MATERIALS SCIENCE & PROCESSING, (2014), 117, pp. 1359-1365, **1.694**, **0.484**

51. Craciun, F; Dimitriu, E; Grigoras, M; Lupu, N; Vasile, BS; **Cernea, M**;
The emergence of magnetic properties in (Pb0. 845Sm0. 08Fe0. 035)(Ti0. 98Mn0. 02)O-3 and (Pb0. 88Nd0. 08)(Ti0. 98Mn0. 02)O-3 perovskite ceramics
JOURNAL OF APPLIED PHYSICS, (2014), 116, pp. -, **2.185**, **0.724**

52. **Crisan, A**; Dang, VS; Yearwood, G; Mikheenko, P; Huhtinen, H; Paturi, P;
Investigation of the bulk pinning force in YBCO superconducting films with nano-engineered pinning centres
PHYSICA C-SUPERCONDUCTIVITY AND ITS APPLICATIONS, (2014), 503, pp. 89-93, **1.11**, **0.293**

53. **Crisan, A. D.** , Bednarcik, J. , Michalik, Š. , Crisan, O.
In situ monitoring of disorder-order A1-$L1_0$ FePt phase transformation in nanocomposite FePt-based alloys
JOURNAL OF ALLOYS AND COMPOUNDS, (2014) 615, pp. S188-S191, **2.726**, **0.534**

54. **Crisan, AD**; **Vasiliu, F**; **Mercioniu, I**; **Crisan, O**;
Role of Ag addition in L1(0) ordering of FePt-based nanocomposite magnets
PHILOSOPHICAL MAGAZINE, (2014), 94, pp. 174-189, **1.427**, **0.696**

55. Daviosdottir, S; Shabadi, R; **Galca, AC**; Andersen, IHI; Dirscherl, K; Ambat, R;
Investigation of DC magnetron-sputtered TiO2 coatings: Effect of coating thickness, structure, and morphology on photocatalytic activity
APPLIED SURFACE SCIENCE, (2014), 313, pp. 677-686, **2.538**, **0.55**

56. **Diamandescu, L**; Tarabasanu-Mihaila, D; **Feder, M**; **Enculescu, M**; **Teodorescu, VS**; Constantinescu, S; **Popescu, T**; **Bartha, C**; Pap, Z;
Indium-tin nanoscaled oxides synthesized under hydrothermal supercritical and postannealing pathway: Phase dynamics and characterization
MATERIALS CHEMISTRY AND PHYSICS, (2014), 143, pp. 1540-1549, **2.129**, **0.546**

57. Dinh, TM; Achour, A; Vizireanu, S; Dinescu, G; **Nistor, L**; Armstrong, K; Guay, D; Pech, D;
Hydrous RuO2/carbon nanowalls hierarchical structures for all-solid-state ultrahigh-energy-density micro-supercapacitors
NANO ENERGY, (2014), 10, pp. 288-294, **10.211**, **2.38**

58. Dumbrava, A; Olar, R; Badea, M; **Grecu, MN**; Patrascu, F; Marutescu, L; Stanica, N;
Synthesis and characterisation of Ni(II), Cu(II), and Zn(II) complexes with an acyclic Mannich base functionalised with thioglycolate moiety
JOURNAL OF THERMAL ANALYSIS AND CALORIMETRY, (2014), 115, pp. 2447-2455, **2.206**, **0.262**

59. Dumitru, CS; **Sima, M**; Cojocaru, A;
Electrochemical studies on the growth process of the zinc oxide films from nitrate solutions
REVISTA DE CHIMIE, (2014), 65, pp. 835-839, **0.677**, **0.056**

60. Duta, L; **Popa, AC**; Miculescu, F; Mihailescu, IN;
Ultra high molecular weight polyethylene acetabular cups functionalized with bioactive glass coatings synthesized by pulsed laser deposition
ROMANIAN REPORTS IN PHYSICS, (2014), 66, pp. 788-800, **1.137**, **0.133**

61. Duta, L; Popescu, C; Popescu, A; Motoc, M; **Logofatu, C**; Enesca, A; Duta, A; Gyorgy, E;
Nitrogen-doped and gold-loaded TiO2 photocatalysts synthesized by sequential reactive pulsed laser deposition
APPLIED PHYSICS A-MATERIALS SCIENCE & PROCESSING, (2014), 117, pp. 97-101, **1.694**, **0.484**

62. **Enculescu, M**; **Evanghelidis, A**; **Enculescu, I**;
Influence of morphology on the emissive properties of dye-doped PVP nanofibers produced by electrospinning
JOURNAL OF PHYSICS AND CHEMISTRY OF SOLIDS, (2014), 75, pp. 1365-1371, **1.594**, **0.405**

63. Erakovic, S; Jankovic, A; Ristoscu, C; Duta, L; Serban, N; Visan, A; Mihailescu, IN; **Stan, GE**; **Socol, M**; Iordache, O; **Dumitrescu, I**; Luculescu, CR; Janackovic, D; Miskovic-Stankovic, V;
Antifungal activity of Ag:hydroxyapatite thin films synthesized by pulsed laser deposition on Ti and Ti modified by TiO2 nanotubes substrates
APPLIED SURFACE SCIENCE, (2014), 293, pp. 37-45, **2.538**, **0.55**

64. Fagadar-Cosma, G; Taranu, BO; Birdeanu, M; **Popescu, M**; Fagadar-Cosma, E;
Influence of 5, 10, 15, 20-tetrakis (4-pyridyl)-21H, 23H-porphyrin on the corrosion of steel in aqueous sulfuric acid
DIGEST JOURNAL OF NANOMATERIALS AND BIOSTRUCTURES, (2014), 9, pp. 551-557, **1.123**, **0.209**

65. Fleaca, CT; Scarisoreanu, M; Morjan, I; Alexandrescu, R; Dumitrache, F; Luculescu, C; Morjan, IP; Birjega, R; Niculescu, AM; **Filoti, G**; **Kuncser, V**; Vasile, E; Danciu, V; Popa, M;
Recent progress in the synthesis of magnetic titania/iron-based, composite nanoparticles manufactured by laser pyrolysis
APPLIED SURFACE SCIENCE, (2014), pp. 198-204 **2.538**, **0.55**

66. Florea, M; Alifanti, M; **Kuncser, V**; **Macovei, D**; Apostol, N; Granger, P; Parvulescu, VI;
Evidence of A-B site cooperation in the EuFeO3 perovskite from Eu-151 and Fe-57 Mossbauer spectroscopy, EXAFS, and toluene catalytic oxidation
JOURNAL OF CATALYSIS, (2014), 316, pp. 130-140, **6.073**, **1.489**

67. Florian, M; **Gartner, P**; Steinhoff, A; Gies, C; Jahnke, F;
Coulomb-assisted cavity feeding in nonresonant optical emission from a quantum dot
PHYSICAL REVIEW B, (2014), 89, pp. -, **3.664**, **1.342**

68. **Florica, C**; **Matei, E**; **Costas, A**; Molares, MET; **Enculescu, I**;
Field effect transistor with electrodeposited ZnO nanowire channel
ELECTROCHIMICA ACTA, (2014), 137, pp. 290-297, **4.086**, **0.912**

69. **Florica, C**; **Preda, N**; **Enculescu, M**; **Enculescu, I**;
Micropatterned ZnO rod arrays prepared by Au-catalyzed electroless deposition
PHYSICA STATUS SOLIDI-RAPID RESEARCH LETTERS, (2014), 8, pp. 648-652, **2.343**, **0.769**

70. **Florica, C**; **Preda, N**; **Enculescu, M**; **Zgura, I**; **Socol, M**; **Enculescu, I**;
Superhydrophobic ZnO networks with high water adhesion
NANOSCALE RESEARCH LETTERS, (2014), 9, pp. -, **2.481**, **0.672**

71. **Frunza, L**; **Zgura, I**; **Enculescu, M**; **Frunza, S**; **Ganea, CP**; **Rasoga, O**; **Cotorobai, F**; Dorogan, A;
Polyester fabrics coated with SiOx nanoparticles by vacuum deposition at small angle. Structural characterization and wetting properties
JOURNAL OF OPTOELECTRONICS AND ADVANCED MATERIALS, (2014), 16, pp. 176-181, **0.563**, **0.111**

72. **Frunza, S**; **Zgura, I**; **Frunza, L**; **Rasoga, O**; Gheorghe, P; Petris, A; Vlad, VI;
Covering obliquely deposited SiOx with polyvinyl carbazole changes the orientation properties
ROMANIAN JOURNAL OF PHYSICS, (2014), 59, pp. 733-744, **0.745**, **0.125**

73. **Ganea, CP**;
Effects of the ionic association-dissociation and adsorption-desorption on the space charge polarization: A new theoretical approach
EUROPEAN PHYSICAL JOURNAL PLUS, (2014), 129, pp. -, **1.475**, **0.45**

74. **Ganea, CP**; **Frunza, L**; **Zgura, I**; **Preda, N**; **Matei, E**; **Frunza, S**;
Polyester fabrics covered with ZnO particles; particle interaction with the surface shown by dielectric properties
DIGEST JOURNAL OF NANOMATERIALS AND BIOSTRUCTURES, (2014), 9, pp. 1493-1503, **1.123**, **0.209**

75. **Ghica, C**; **Negrea, RF**; **Nistor, LC**; Chirila, CF; **Pintilie, L**;
Nanoscale monoclinic domains in epitaxial SrRuO3 thin films deposited by pulsed laser deposition
JOURNAL OF APPLIED PHYSICS, (2014), 116, pp. -, **2.185**, **0.724**

76. **Ghica, D**; **Stefan, M**; **Ghica, C**; **Stan, GE**;
Evaluation of the segregation of paramagnetic impurities at grain boundaries in nanostructured ZnO films
ACS APPLIED MATERIALS & INTERFACES, (2014), 6, pp. 14231-14238, **5.9**, **1.279**

77. Ghita, RV; Grigorescu, CEA; **Secu, M**; **Predoi, D**; **Frumosu, F**; Cotirlan, C; Feraru, ID;
Optical characteristics of sulphur-passivated n-GaAs (100) surface
DIGEST JOURNAL OF NANOMATERIALS AND BIOSTRUCTURES, (2014), 9, pp. 1471-1478, **1.123**, **0.209**

78. Ghita, RV; **Iconaru, SL**; **Popa, CL**; Costescu, A; Le Coustumer, P; Motelica-Heino, M; **Ciobanu, CS**;
Tetraethyl orthosilicate coated hydroxyapatite powders for lead ions removal from aqueous solutions
JOURNAL OF NANOMATERIALS, (2014),, pp. -, **1.611**, **0.37**

79. Granville, S., **Matei, E., Enculescu, I.**, Toimil-Molares, M. E.
Cu codoping control over magnetic precipitate formation in ZnCoO nanowires
APPLIED PHYSICS LETTERS, (2014), 105 (25), Article number 252403, **3.515**, **1.217**

80. Groza, A; Surmeian, A; Diplasu, C; Luculescu, C; **Negrila, C**; Ganciu, M;
Generation of porous alumina layers in a polydimethylsiloxane/hydrogen peroxide medium on aluminum substrate in corona discharges
JOURNAL OF NANOMATERIALS, (2014),, pp. -, **1.611**, **0.37**

81. Gyorgy, E; del Pino, AP; **Logofatu, C**; Cazan, C; Duta, A;
Simultaneous laser-induced reduction and nitrogen doping of graphene oxide in titanium oxide/graphene oxide composites
JOURNAL OF THE AMERICAN CERAMIC SOCIETY, (2014), 97, pp. 2718-2724, **2.428**, **0.691**

82. Gyorgy, E; del Pino, AP; **Logofatu, C**; Duta, A; Isac, L;
Effect of nitrogen doping on wetting and photoactive properties of laser processed zinc oxide-graphene oxide nanocomposite layers
JOURNAL OF APPLIED PHYSICS, (2014), 116, pp. -, **2.185**, **0.724**

83. **Iconaru, SL**; Chapon, P; Le Coustumer, P; **Predoi, D**;
Antimicrobial activity of thin solid films of silver doped hydroxyapatite prepared by sol-gel method
SCIENTIFIC WORLD JOURNAL, (2014),, pp. -, **1.219**, **0.343**

84. Ignat, T; **Husanu, MA**; Munoz, R; Kusko, M; Danila, M; **Teodorescu, CM**;
Gold nano-island arrays on silicon as SERS active substrate for organic molecule detection
THIN SOLID FILMS, (2014), 550, pp. 354-360, **1.867**, **0.51**

85. Ilis, M; Micutz, M; Dumitrascu, F; **Pasuk, I**; Molard, Y; Roisnel, T; Circu, V;
Enhancement of smectic C mesophase stability by using branched alkyl chains in the auxiliary ligands of luminescent Pt(II) and Pd(II) complexes
POLYHEDRON, (2014), 69, pp. 31-39, **2.047**, **0.333**

86. Iorga, S; Cojocaru, M; Chivu, A; Ciuca, S; **Burdusel, M**; **Badica, P**; Leuvrey, C; Schmerber, G; Ulhaq-Bouillet, C; Colis, S;
Influence of the carbo-chromization process on the microstructural, hardness, and corrosion properties of 316L sintered stainless steel
METALLURGICAL AND MATERIALS TRANSACTIONS A-PHYSICAL METALLURGY AND MATERIALS SCIENCE, (2014), 45A, pp. 3088-3096, **1.73**, **0.72**

87. Jepu, I; Porosnicu, C; Lungu, CP; Mustata, I; Luculescu, C; **Kuncser, V**; Iacobescu, G; Manin, A; Ciupina, V;
Combinatorial Fe-Co thin film magnetic structures obtained by thermionic vacuum arc method
SURFACE & COATINGS TECHNOLOGY, (2014), 240, pp. 344-352, **2.199**, **0.574**

88. Krishnan, G; **Negrea, RF**; **Ghica, C**; ten Brink, GH; Kooi, BJ; Palasantzas, G;
Synthesis and exceptional thermal stability of Mg-based bimetallic nanoparticles during hydrogenation
NANOSCALE, (2014), 6, pp. 11963-11970, **6.739**, **1.621**

89. Lazanu, I; **Lazanu, S**;
Thermal effects produced at cryogenic temperatures in materials used as bolometric detectors for dark matter
ROMANIAN REPORTS IN PHYSICS, (2014), 66, pp. 963-972, **1.137**, **0.133**

90. Lazarescu, V; Enache, M; Anastasescu, M; Dobrescu, G; **Negrila, C**; **Lazarescu, MF**;
Electrochemical impedance spectroscopy investigations on the L-cysteine-thiolate self-assembled monolayers formed at p-GaAs(100) electrodes
ELECTROCHIMICA ACTA, (2014), 131, pp. 42-51 **4.086, 0. 912**

91. Lazea-Stoyanova, A; **Enculescu, M**; Vizireanu, S; Marascu, V; Dinescu, G;
Effects of process parameters on growth of metal particles by atmospheric pressure plasma jet
DIGEST JOURNAL OF NANOMATERIALS AND BIOSTRUCTURES, (2014), 9, pp. 1241-1247, **1.123**, **0.209**

92. Li, SY; Chen, F; Schafranek, R; Bayer, TJM; Rachut, K; Fuchs, A; Siol, S; Weidner, M; Hohmann, M; Pfeifer, V; Morasch, J; Ghinea, C; Arveux, E; Gunzler, R; Gassmann, J; Korber, C; Gassenbauer, Y; Sauberlich, F; Rao, GV; Payan, S; Maglione, M; **Chirila, C**;
Intrinsic energy band alignment of functional oxides
PHYSICA STATUS SOLIDI-RAPID RESEARCH LETTERS, (2014), 8, pp. 571-576, **2.343**, **0.769**

93. **Lungu, GA**; Stoflea, LE; **Tanase, LC**; Bucur, IC; Radutoiu, N; **Vasiliu, F**; **Mercioniu, I**; **Kuncser, V**; **Teodorescu, CM**;
Room temperature ferromagnetic Mn:Ge(001)
MATERIALS, (2014), 7, pp. 106-129, **1.879**, **0.742**

94. Makarenko, LF; Korshunov, FP; Lastovskii, SB; Murin, LI; Moll, M; **Pintilie, I**;
Formation and annealing of metastable (interstitial oxygen)-(interstitial carbon) complexes in n- and p-type silicon
SEMICONDUCTORS, (2014), 48, pp. 1456-1462, **0.705**, **0.154**

95. Makarenko, LF; Lastovskii, SB; Yakushevich, HS; Moll, M; **Pintilie, I**;
Forward current enhanced elimination of the radiation induced boron-oxygen complex in silicon n(+)-p diodes
PHYSICA STATUS SOLIDI A-APPLICATIONS AND MATERIALS SCIENCE, (2014), 211, pp. 2558-2562, **1.525**, **0.469**

96. Micutz, M; Ilis, M; Staicu, T; Dumitrascu, F; **Pasuk, I**; Molard, Y; Roisnel, T; Circu, V;
Luminescent liquid crystalline materials based on palladium(II) imine derivatives containing the 2-phenylpyridine core
DALTON TRANSACTIONS, (2014), 43, pp. 1151-1161, **4.097**, **0.819**

97. Mihailescu, CN; **Pasuk, I**; Straticiuc, M; Nita, CR; Pantelica, D; Giapintzakis, J;
Origin of the stabilization of the metastable tetragonal high-pressure phase in SrCuO2 thin films grown on SrTiO3 substrates by pulsed laser deposition
APPLIED SURFACE SCIENCE, (2014), 320, pp. 852-857, **2.538**, **0.55**

98. **Mihalache, V**; Stefan, N; **Enculescu, I**; Mihailescu, IN; **Socol, M**; Miroi, M;
The influence of the microstructure and morphology of CeO_2 buffer layer on the properties of YBCO films PLD grown on Ni tape
JOURNAL OF SUPERCONDUCTIVITY AND NOVEL MAGNETISM, (2014), 27, pp. 2475-2485, **0.93**, **0.205**

99. Mindru, I; Gingasu, D; Marinescu, G; Patron, L; Calderon-Moreno, JM; **Bartha, C**; Andronescu, C; **Crisan, A**;
Cobalt chromite obtained by thermal decomposition of oxalate coordination compounds
CERAMICS INTERNATIONAL, (2014), 40, pp. 15249-15258, **2.086**, **0.439**

100. Mitroi, MR; Fara, L; **Ciurea, ML**;
Numerical procedure for optimizing dye-sensitized solar cells
JOURNAL OF NANOMATERIALS, (2014), pp. -, **1.611**, **0.37**

101. Miu, DN; Sima, C; Jinga, SI; Vasile, BS; **Miu, L**;
A simple approach for the magnetic relaxation in systems of weakly-interacting, dispersive nanoparticles in applied magnetic field
JOURNAL OF SUPERCONDUCTIVITY AND NOVEL MAGNETISM, (2014), 27, pp. 781-785, **0.93**, **0.205**

102. **Miu, L**; Mele, P; **Crisan, A**; Ionescu, A; Miu, D;
Evolution of vortex dynamics in YBa2Cu3O7 films with nanorods by adding nanoparticles
PHYSICA C-SUPERCONDUCTIVITY AND ITS APPLICATIONS, (2014), 500, pp. 40-43, **1.11**, **0.293**

103. **Moldoveanu, V**; **Dinu, IV**; **Dragomir, R**;
Dynamics and relaxation of sp biexcitons in disk-shaped quantum dots
PHYSICAL REVIEW B, (2014), 89, pp. -, **3.664**, **1.342**

104. Nistor, M; Seiler, W; Hebert, C; **Matei, E**; Perriere, J;
Effects of substrate and ambient gas on epitaxial growth indium oxide thin films
APPLIED SURFACE SCIENCE, (2014), 307, pp. 455-460, **2.538**, **0.55**

105. **Nistor, SV**; **Stefan, M**; **Ghica, D**;
Pulse annealing electron paramagnetic resonance with probing transition ions
JOURNAL OF THERMAL ANALYSIS AND CALORIMETRY, (2014), 118, pp. 1021-1031, **2.206**, **0.262**

106. **Nita, M**; **Tolea, M**; **Ostahie, B**;
Transmission phase lapses at zero energy in graphene quantum dots
PHYSICA STATUS SOLIDI-RAPID RESEARCH LETTERS, (2014), 8, pp. 790-793, **2.343**, **0.769**

107. O'Malley, SM; Tomko, J; del Pino, AP; **Logofatu, C**; Gyorgy, E;
Resonant infrared and ultraviolet matrix-assisted pulsed laser evaporation of titanium oxide/graphene oxide composites: a comparative study
JOURNAL OF PHYSICAL CHEMISTRY C, (2014), 118, pp. 27911-27919, **4.835**, **1.247**

108. Olar, R; Scaeteanu, G; **Vlaicu, ID**; Marutescu, L; Badea, M;
Synthesis, physico-chemical characterization and thermal behavior of new complexes with N4O2 donor set
JOURNAL OF THERMAL ANALYSIS AND CALORIMETRY, (2014), 118, pp. 1195-1202, **2.206**, **0.262**

109. Opris, CM; Pavel, OD; Moragues, A; El Haskouri, J; Beltran, D; Amoros, P; Marcos, MD; **Stoflea, LE**; Parvulescu, VI;
New multicomponent catalysts for the selective aerobic oxidative condensation of benzylamine to N-benzylidenebenzylamine
CATALYSIS SCIENCE & TECHNOLOGY, (2014), 4, pp. 4340-4355, **4.76**, **1.081**

110. **Ostahie, B**; **Nita, M**; **Aldea, A**;
Topological properties of the mesoscopic graphene plaquette: Quantum spin Hall effect due to spin imbalance
PHYSICAL REVIEW B, (2014), 89, pp. -, **3.664**, **1.342**

111. Pana, A; Ilis, M; Micutz, M; Dumitrascu, F; **Pasuk, I**; Circu, V;
Liquid crystals based on silver carbene complexes derived from dimeric bis(imidazolium) bromide salts
RSC ADVANCES, (2014), 4, pp. 59491-59497, **3.708**, **0.734**

112. Pantelica, D; Ionescu, P; Petrascu, H; Nita, CR; **Matei, E**; **Rasoga, O**; Acsente, T; Dinescu, G;
Characterization of hydrogenated and deuterated thin carbon films deposited by magnetron sputtering
NUCLEAR INSTRUMENTS & METHODS IN PHYSICS RESEARCH SECTION B-BEAM INTERACTIONS WITH MATERIALS AND ATOMS, (2014), 331, pp. 121-124, **1.186**, **0.392**

113. Papa, F; Balint, I; Negrila, C; Olaru, EA; **Zgura, I**; Bradu, C;
Supported Pd-Cu Nanoparticles for Water Phase Reduction of Nitrates. Influence of the Support and of the pH Conditions
INDUSTRIAL & ENGINEERING CHEMISTRY RESEARCH, (2014), 53, pp. 19094-19103, **2.235**, **0.6**

114. **Pintilie, I**; **Teodorescu, CM**; **Ghica, C**; **Chirila, C**; **Boni, AG**; Hrib, L; **Pasuk, I**; Negrea, R; Apostol, N; **Pintilie, L**;
Polarization-control of the potential barrier at the electrode interfaces in epitaxial ferroelectric thin films
ACS APPLIED MATERIALS & INTERFACES, (2014), 6, pp. 2929-2939, **5.9**, **1.279**

115. **Pintilie, L**; **Botea, M**; **Iuga, A**;
Enhancement of pyroelectric signal by continuous ultraviolet illumination of epitaxial Pb(Zr0. 2Ti0. 8)O-3 films
APPLIED PHYSICS LETTERS, (2014), 105, pp. -, **3.515**, **1.217**

116. **Pintilie, L**; Hrib, L; **Pasuk, I**; **Ghica, C**; **Iuga, A**; **Pintilie, I**;
General equivalent circuit derived from capacitance and impedance measurements performed on epitaxial ferroelectric thin films
JOURNAL OF APPLIED PHYSICS, (2014), 116, pp. -, **2.185**, **0.724**

117. **Plugaru, N**; **Valeanu, M**; Plugaru, R; Campo, J;
First principles calculations, neutron, and x-ray diffraction investigation of Y3Ni13B2, Y3Co13B2, and Y3Ni10Co3B2
JOURNAL OF APPLIED PHYSICS, (2014), 115, pp. -, **2.185**, **0.724**

118. **Polosan, S**; **Ciobotaru, IC**;
Electroluminescence of OLED based IrQ(ppy)(2)-5Cl organometallic compound: Theoretical considerations
JOURNAL OF OPTOELECTRONICS AND ADVANCED MATERIALS, (2014), 16, pp. 87-92, **0.563**, **0.111**

119. **Polosan, S**; **Ciobotaru, IC**; **Enculescu, I**; **Ciobotaru, CC**;
Structural characteristics of iridium dual-emitter organometallic compound
JOURNAL OF MATERIALS RESEARCH, (2014), 29, pp. 2898-2904, **1.815**, **0.569**

120. **Popa, AC**; Marques, VMF; **Stan, GE**; **Husanu, MA**; **Galca, AC**; **Ghica, C**; Tulyaganov, DU; Lemos, AF; Ferreira, JMF;
Nanomechanical characterization of bioglass films synthesized by magnetron sputtering
THIN SOLID FILMS, (2014), 553, pp. 166-172, **1.867**, **0.51**

121. **Popa, CL**; Andronescu, E; Stoicea, M; Le Coustumer, P; Galaup, S; Beuran, M; Iordache, FM; Telcian, A; Bleotu, C; Prodan, AM;
Fabrication, characterization, toxicity and biocompatibility evaluation of iron oxide nanoparticles
DIGEST JOURNAL OF NANOMATERIALS AND BIOSTRUCTURES, (2014), 9, pp. 19-25, **1.123**, **0.209**

122. **Popa, CL**; **Ciobanu, CS**; **Iconaru, SL**; Stan, M; Dinischiotu, A; **Negrila, CC**; Motelica-Heino, M; Guegan, R; **Predoi, D**;
Systematic investigation and in vitro biocompatibility studies on mesoporous europium doped hydroxyapatite
CENTRAL EUROPEAN JOURNAL OF CHEMISTRY, (2014), 12, pp. 1032-1046, **1.329**, **0.263**

123. **Popa, NC**; Balzar, D; Vogel, SC;
Elastic macro strain and stress determination by powder diffraction: spherical harmonics analysis starting from the Voigt model
JOURNAL OF APPLIED CRYSTALLOGRAPHY, (2014), 47, pp. 154-159, **3.95**, **1.784**

124. **Popescu, DG**; **Husanu, MA**;
Epitaxial growth of Au on Ge(001) surface: Photoelectron spectroscopy measurements and first-principles calculations
THIN SOLID FILMS, (2014), 552, pp. 241-249, **1.867**, **0.51**

125. **Popescu, M**; **Sava, F**; **Velea, A**; **Lorinczi, A**; **Simandan, ID**;
Simulation of the structure of GeAs4Te7 chalcogenide materials during memory switching
CANADIAN JOURNAL OF PHYSICS, (2014), 92, pp. 675-680, **0.928**, **0.262**

126. **Popescu, M**; **Velea, A**; **Sava, F**; **Lorinczi, A**;
Chalcogenide systems at the border of the glass-formation domain: A key for understanding the memory-switching phenomena
PHYSICA STATUS SOLIDI B-BASIC SOLID STATE PHYSICS, (2014), 251, pp. 1334-1339, **1.605**, **0.505**

127. **Popescu, T**; Lupu, AR; **Feder, M**; Tarabasanu-Mihaila, D; **Teodorescu, VS**; **Vlaicu, AM**; **Diamandescu, L**;
In vitro toxicity evaluation of Ti4+-stabilized gamma-Bi2O3 sillenites
TOXICOLOGY IN VITRO, (2014), 28, pp. 1523-1530, **3.207**, **0.676**

128. **Preda, N**; **Enculescu, M**; **Enculescu, I**;
Polysaccharide-assisted crystallization of ZnO micro/nanostructures
MATERIALS LETTERS, (2014), 115, pp. 256-260, **2.269**, **0.473**

129. Prodan, AM; **Ciobanu, CS**; **Popa, CL**; **Iconaru, SL**; **Predoi, D**;
Toxicity evaluation following intratracheal instillation of iron oxide in a silica matrix in rats
BIOMED RESEARCH INTERNATIONAL, (2014),, pp. -, **0**,

130. **Racec, PN**;
Cylindrical semiconductor nanowires with constrictions
PHYSICA STATUS SOLIDI B-BASIC SOLID STATE PHYSICS, (2014), 251, pp. 195-200, **1.605**, **0.505**

131. Radu, M; Gheorghiu, A; **Predoi, D**; Hermenean, A; Ardelean, A; Dinischiotu, A;
Mechanisms of pulmonary toxicity developed at low and high doses of dextran-coated magnetite nanoparticles
TOXICOLOGY LETTERS, (2014), 229, pp. S78-S78 **3.355 0. 868**

132. Radutoiu, N; **Teodorescu, CM**;
Spin waves in systems with variable size, dimensionality and different crystal structures: effects in the magnetization dependence on temperature
DIGEST JOURNAL OF NANOMATERIALS AND BIOSTRUCTURES, (2014), 9, pp. 721-737, **1.123**, **0.209**

133. Ruiz-Rivas, J; del Valle, E; Gies, C; **Gartner, P**; Hartmann, MJ;
Spontaneous collective coherence in driven dissipative cavity arrays
PHYSICAL REVIEW A, (2014), 90, pp. -, **2.991**, **1.006**

134. Rusen, E; Mocanu, A; **Nistor, LC**; Dinescu, A; Calinescu, L; Mustatea, G; Voicu, SI; Andronescu, C; Diacon, A;
Design of antimicrobial membrane based on polymer colloids/multiwall carbon nanotubes hybrid material with silver nanoparticles
ACS APPLIED MATERIALS & INTERFACES, (2014), 6, pp. 17384-17393, **5.9**, **1.279**

135. Sandu, SG; **Palade, P**; **Schinteie, G**; **Birsan, A**; **Trupina, L**; **Kuncser, V**;
Tuning structural and magnetic properties of Fe films on Si substrates by hydrogenation processing
MATERIALS SCIENCE AND ENGINEERING B-ADVANCED FUNCTIONAL SOLID-STATE MATERIALS, (2014), 181, pp. 24-32, **2.122**, **0.465**

136. **Sandu, V**; **Aldica, G**; Liu, ZY; Zhang, ZL; Suo, HL;
Effect of silver addition to superconducting $SmFeAsO_{1-x}F_x$
JOURNAL OF SUPERCONDUCTIVITY AND NOVEL MAGNETISM, (2014), 27, pp. 1635-1641, **0.93**, **0.205**

137. **Sandu, V**; **Badica, P**; **Aldica, G**; Ferbinteanu, M; Hayasaka, Y;
Doping of MgB_2 using molecular magnets as precursors
JOURNAL OF SUPERCONDUCTIVITY AND NOVEL MAGNETISM, (2014), 27, pp. 1837-1843, **0.93**, **0.205**

138. **Sandu, V**; Chee, CY;
Magnetic nanoparticles in MgB_2
PHYSICA C-SUPERCONDUCTIVITY AND ITS APPLICATIONS, (2014), 498, pp. 30-37, **1.11**, **0.293**

139. Sava, BA; Blisa, M; **Bartha, C**; Iordanescu, R; Feraru, I; **Plapcianu, C**; Patrascu, R;
Non-isothermal free-models kinetic analysis on crystallization of europium-doped phosphate glasses
CERAMICS INTERNATIONAL, (2014), 40, pp. 12387-12395, **2.086**, **0.439**

140. Scarisoreanu, ND; Craciun, F; Birjega, R; Andrei, A; Ion, V; **Negrea, RF**; **Ghica, C**; Dinescu, M;
Strain-induced long range ferroelectric order and linear electro-optic effect in epitaxial relaxor thin films
JOURNAL OF APPLIED PHYSICS, (2014), 116, pp. -, **2.185**, **0.724**

141. **Secu, CE**; **Bartha, C**; **Polosan, S**; **Secu, M**;
Thermally activated conversion of a silicate gel to an oxyfluoride glass ceramic: Optical study using Eu3+ probe ion
JOURNAL OF LUMINESCENCE, (2014), 146, pp. 539-543, **2.367**, **0.459**

142. **Secu, CE**; **Matei, E**; **Secu, M**; Damian, V;
BaFBr:Eu2+ nanophosphor-SiO2 hybrid entrapped in Anodise Alumina membrane pores array
RADIATION MEASUREMENTS, (2014), 68, pp. 38-41, **1.14**, **0.343**

143. Serban, N; Ristoscu, C; Socol, G; Stefan, N; Mihailescu, CN; **Socol, M**; Mulenko, SA; Petrov, YN; Gorbachuk, NT; Mihailescu, IN;
Laser synthesis of nanometric iron oxide films for thermo-sensing applications
MATERIALS RESEARCH BULLETIN, (2014), 50, pp. 148-154, **1.968**, **0.443**

144. **Sima, M**; Vasile, E; Buda, M; **Sima, M**;
Investigation on the electrodeposition of Pt-(Bi, Sb)(2)Te-3 nanocomposite as film and wires
ELECTROCHIMICA ACTA, (2014), 127, pp. 208-214, **4.086**, **0.912**

145. **Smaranda, I**; Benito, AM; Maser, WK; **Baltog, I**; **Baibarac, M**;
Electrochemical grafting of reduced graphene oxide with polydiphenylamine doped with heteropolyanions and its optical properties
JOURNAL OF PHYSICAL CHEMISTRY C, (2014), 118, pp. 25704-25717, **4.835**, **1.247**

146. **Smaranda, I**; **Mihut, L**; **Baibarac, M**; **Baltog, I**; Lefrant, S;
Abnormal anti-Stokes Raman scattering and coherent backscattering as manifestation of Anderson localization of light in nonlinear mesoscopic materials
OPTICAL ENGINEERING, (2014), 53, pp. -, **0.958**, **0.215**

147. Socol, G; **Galca, AC**; Craciun, D; Hanna, M; Taylor, CR; Lambers, E; Craciun, V;
Pulsed laser deposition of nanocrystalline SiC films
APPLIED SURFACE SCIENCE, (2014), 306, pp. 66-69, **2.538**, **0.55**

148. **Socol, M**; **Preda, N**; Vacareanu, L; Grigoras, M; Socol, G; Mihailescu, N; Stanculescu, F; Jelinek, M; **Stanculescu, A**; Stoicanescu, M;
Organic heterostructures based on arylenevinylene oligomers deposited by MAPLE
APPLIED SURFACE SCIENCE, (2014), 302, pp. 216-222, **2.538**, **0.55**

149. Solodkyi, I; Borodianska, H; Zhao, T; Sakka, Y; **Badica, P**; Vasylkiv, O;
B6O ceramic by in-situ reactive spark plasma sintering of a B2O3 and B powder mixture
JOURNAL OF THE CERAMIC SOCIETY OF JAPAN, (2014), 122, pp. 336-340, **0.846**, **0.21**

150. Somacescu, S; Osiceanu, P; Calderon-Moreno, JM; Sackmann, A; **Simion, CE**; **Stanoiu, A**;
Mesopororous (Sn0. 9-xIn0. 1CuxO2-delta)-O-(I) gas sensors with selectivity to H2S working under humid air conditions
MICROPOROUS AND MESOPOROUS MATERIALS, (2014), 197, pp. 63-71, **3.209**, **0.746**

151. Sorescu, M; Bushunow, V; **Diamandescu, L**; **Tolea, F**; **Valeanu, M**; Xu, TH;
Structural and magnetic properties of Li2O-Fe2O3 ceramic nanostructures
CERAMICS INTERNATIONAL, (2014), 40, pp. 5387-5395, **2.086**, **0.439**

152. Stan, MS; Memet, I; Sima, C; **Popescu, T**; **Teodorescu, VS**; Hermenean, A; Dinischiotu, A;
Si/SiO2 quantum dots cause cytotoxicity in lung cells through redox homeostasis imbalance
CHEMICO-BIOLOGICAL INTERACTIONS, (2014), 220, pp. 102-115, **2.982**, **0.704**

153. **Stanculescu, A**; Socol, G; Grigoras, M; Ivan, T; Vacareanu, L; **Socol, M**; **Rasoga, O**; Breazu, C; Mihailescu, IN; Iordache, I; **Preda, N**; Stanculescu, F;
Laser prepared organic heterostructures based on star-shaped arylenevinylene compounds
APPLIED PHYSICS A-MATERIALS SCIENCE & PROCESSING, (2014), 117, pp. 261-268, **1.694**, **0.484**

154. **Stanculescu, A**; **Socol, M**; **Rasoga, O**; Mihailescu, IN; Socol, G; **Preda, N**; Breazu, C; Stanculescu, F;
Laser prepared organic heterostuctures on glass/AZO substrates
APPLIED SURFACE SCIENCE, (2014), 302, pp. 169-176, **2.538**, **0.55**

155. Stanculescu, F; Ionita, I; **Stanculescu, A**;
Organic/inorganic-doped aromatic derivative crystals: Growth and properties
JOURNAL OF CRYSTAL GROWTH, (2014), 401, pp. 215-220, **1.693**, **0.45**

156. Stasic, J; Joksic, G; Zivkovic, L; Mihailescu, IN; **Ghica, C**; **Kuncser, A**; Trtica, M;
Focusing geometry-induced size tailoring of silver nanoparticles obtained by laser ablation in water
LASER PHYSICS, (2014), 24, pp. -, **1.025**, **0.235**

157. **Stavarache, L**; **Lepadatu, AM**; **Teodorescu, VS**; **Galca, AC**; **Ciurea, ML**;
Annealing induced changes in the structure, optical and electrical properties of GeTiO2 nanostructured films
APPLIED SURFACE SCIENCE, (2014), 309, pp. 168-174, **2.538**, **0.55**

158. **Stoflea, LE**; **Apostol, NG**; **Chirila, C**; **Trupina, L**; Negrea, R; **Pintilie, L**; **Teodorescu, CM**;
Schottky barrier versus surface ferroelectric depolarization at Cu/Pb(Zr, Ti)O-3 interfaces
JOURNAL OF MATERIALS SCIENCE, (2014), 49, pp. 3337-3351, **2.305**, **0.601**

159. **Stoflea, LE**; **Apostol, NG**; **Trupina, L**; **Teodorescu, CM**;
Selective adsorption of contaminants on Pb(Zr, Ti)O-3 surfaces shown by X-ray photoelectron spectroscopy
JOURNAL OF MATERIALS CHEMISTRY A, (2014), 2, pp. 14386-14392 **6.626** **1. 514**

160. Stokker-Cheregi, F; Matei, A; Dinescu, M; **Secu, CE**; **Secu, M**;
Photoluminescence of Eu-doped LiYF4 thin films grown by pulsed laser deposition and matrix-assisted pulsed laser evaporation
JOURNAL OF PHYSICS D-APPLIED PHYSICS, (2014), 47, pp. -, **2.521**, **0.811**

161. Tanaka, Y., **Crisan, A.**, Shivagan, D. D., Iyo, A., Tokiwa, K., Watanabe, T.
Erratum: Interpretation of abnormal AC loss peak based on vortex-molecule model for a multicomponent cuprate superconductor [Jpn. J. Appl. Phys. 46, 134 (2007)] (Erratum)
JAPANESE JOURNAL OF APPLIED PHYSICS, (2014), 53, 9, 2014, Article number 099202, **1.057**, **0.227**

162. Tiseanu, C; Parvulescu, V; Avram, D; Cojocaru, B; **Apostol, N**; Vela-Gonzalez, AV; Sanchez-Dominguez, M;
Structural, down- and phase selective up-conversion emission properties of mixed valent Pr doped into oxides with tetravalent cations
PHYSICAL CHEMISTRY CHEMICAL PHYSICS, (2014), 16, pp. 5793-5802, **4.198**, **1.184**

163. Tudorache, M; Ghemes, G; Nae, A; **Matei, E**; **Mercioniu, I**; Kemnitz, E; Ritter, B; Coman, S; Parvulescu, VI;
Biocatalytic designs for the conversion of renewable glycerol into glycerol carbonate as a value-added product
CENTRAL EUROPEAN JOURNAL OF CHEMISTRY, (2014), 12, pp. 1262-1270, **1.329**, **0.263**

164. Turcheniuk, K; Khanal, M; Motorina, A; Subramanian, P; Barras, A; Zaitsev, V; **Kuncser, V**; Leca, A; Martoriati, A; Cailliau, K; Bodart, JF; Boukherroub, R; Szunerits, S;
Insulin loaded iron magnetic nanoparticle-graphene oxide composites: synthesis, characterization and application for in vivo delivery of insulin
RSC ADVANCES, (2014), 4, pp. 865-875, **3.708**, **0.734**

165. Tyunina, M; **Pintilie, I**; **Iuga, A**; **Pintilie, L**;
Electric-field-induced transformations in epitaxial relaxor ferroelectric PbMg1/3Nb2/3O3 films
PHYSICAL REVIEW B, (2014), 89, pp. -, **3.664**, **1.342**

166. Tyunina, M; **Pintilie, I**; **Iuga, A**; Stratulat, MS; **Pintilie, L**;
Frustration of ferroelectricity in epitaxial film of relaxor ferroelectric PbSc1/2Nb1/2O3
JOURNAL OF PHYSICS-CONDENSED MATTER, (2014), 26, pp. -, **2.223**, **0.965**

167. Ulmeanu, M; Sima, LE; Ursescu, D; **Enculescu, M**; Bazan, X; Quintana, I;
Cell adhesion response on femtosecond laser initiated liquid assisted silicon surface
CURRENT TOPICS IN MEDICINAL CHEMISTRY, (2014), 14, pp. 624-629, **3.453**, **1.006**

168. **Velea, A**; Borca, CN; Socol, G; **Galca, AC**; Grolimund, D; **Popescu, M**; van Bokhoven, JA;
In-situ crystallization of GeTeGaSb phase change memory stacked films
JOURNAL OF APPLIED PHYSICS, (2014), 116, pp. -, **2.185**, **0.724**

169. Vidu, R; **Plapcianu, C**; **Bartha, C**;
Multivalence Ce and Sn Oxide Doped Materials with Controlled Porosity for Renewable Energy Applications
INDUSTRIAL & ENGINEERING CHEMISTRY RESEARCH, (2014), 53, pp. 7829-7839, **2.235**, **0.6**

170. Visan, A; Grossin, D; Stefan, N; Duta, L; Miroiu, FM; **Stan, GE**; Sopronyi, M; Luculescu, C; Freche, M; Marsan, O; Charvilat, C; Ciuca, S; Mihailescu, IN;
Biomimetic nanocrystalline apatite coatings synthesized by Matrix Assisted Pulsed Laser Evaporation for medical applications
MATERIALS SCIENCE AND ENGINEERING B-ADVANCED FUNCTIONAL SOLID-STATE MATERIALS, (2014), 181, pp. 56-63, **2.122**, **0.465**

171. Zoita, NC; Braic, V; Danila, M; **Vlaicu, AM**; **Logofatu, C**; Grigorescu, CEA; Braic, M;
Influence of film thickness on the morphological and electrical properties of epitaxial TiC films deposited by reactive magnetron sputtering on MgO substrates
JOURNAL OF CRYSTAL GROWTH, (2014), 389, pp. 92-98, **1.693**, **0.45**

Conference Proceedings

1. ***Apostol NG***
   Band bending at ferroelectric surfaces and interfaces investigated by X-ray photoelectron Spectroscopy
   In: *TIM 2013 Physics Conference* Location: *Timisoara, ROMANIA* Date: *NOV 21-24, 2013*
   TIM 2013 PHYSICS CONFERENCE Volume: 1634, Pages: 81-88 Published: 2014

2. *Avădănei OG,* ***Banciu MG, Nedelcu L***
   High-order modes in high permittivity cylindrical dielectric resonator antenna excited by a wide microstrip line
   In: *IEEE 10th International Conference on Communications, COMM 2014;*
   Bucharest; Romania; 29 - 31 May 2014
   IEEE ANTENNAS AND WIRELESS PROPAGATION LETTERS, Volume 13,
   Pages1585-1588, 2014

3. ***Badica P, Aldica GV, Burdusel M****, Borodianska H, Sakka Y, Vasylkiv O*
   Challenges of nanostructuring and functional properties for selected bulk materials obtained by reactive spark plasma sintering
   JAPANESE JOURNAL OF APPLIED PHYSICS Volume 53,
   Issue 5 SPEC. ISSUE 1, May 2014, Article number 05FB22

4. ***Banciu*** **MG,** ***Nedelcu L****, Yamamoto K, Tsuzuki S, Tani M*
   THz TDS investigations on dielectrics for microwave applications
   In: *IW-FIRT proceedings, March 2014, Fukui, Japan*

5. *Branzei M, Cristea I, Ciuca I, Bibi A,* ***Feder M***
   Correlation between microstructure and magnetic properties on MnZn ferrite with Bi_2O_3 increasing addition
   In: *5th International Conference on Advanced Materials and Structures, AMS 2013;*
   Timisoara; Romania; 24 -25 October 2013
   SOLID STATE PHENOMENA Volume 216, Pages 23-28, 2014

6. ***Ciurea ML, Lazanu S***
   Stress influenced trapping processes in Si based multi-quantum well structures and heavy ions implanted Si
   In: *International Conference of Computational Methods in Sciences and Engineering 2014 (ICCMSE)* Location: *Athens, GREECE* Date: *APR 04-07, 2014*
   INTERNATIONAL CONFERENCE OF COMPUTATIONAL METHODS IN SCIENCES AND ENGINEERING 2014 (ICCMSE 2014) Volume: 1618, Pages: 60-63 Published: 2014

7. *Endo K, Kaneko T, Moriguchi T, Takemata H, Takada T, Ikenaga N,* ***Badica P***
   Growth of (001) or (115) Bi-2201 thin films by spin coating and MOCVD targeting future electronics applications
   In: *11th European Conference on Applied Superconductivity, EUCAS 2013;*
   Genoa; Italy; 15 -19 September 2013
   JOURNAL OF PHYSICS: CONFERENCE SERIES Volume 507, Issue PART 1, 2014, Article number 012011

8. *Fleaca CT, Scarisoreanu M, Morjan I, Alexandrescu R, Dumitrache F, Luculescu C, Morjan IP, Birjega R, Niculescu AM,* ***Filoti G, Kuncser V,*** *Vasile E, Danciu V, Popa M*
   Recent progress in the synthesis of magnetic titania/iron-based, composite nanoparticles manufactured by laser pyrolysis
   In: *5th European-Materials-Research-Society Symposium on Laser Material Interactions for Micro- and Nano- Applications* Location: *Strasbourg, FRANCE* Date: *MAY 27-31, 2013*
   APPLIED SURFACE SCIENCE Volume: 302, Pages: 198-204 Published: 30-May 2014

9. *Laurent P, Mekadmini A, Le Febvrier A, Laur V, Martin N, Députier S,* ***Galca AC, Pintilie L,*** *Guilloux-Viry M, Tanné G*
   Etude en température de couches minces ferroélectriques de KTN pour des applications d'accordabilité, art 44, Actes de colloque des 13èmes Journées de Caractérisation Microondes et Matériaux (JCMM 2014), Mart 2014, Nantes, France

10. *Lazarescu V, Enache M, Anastasescu M, Dobrescu G,* ***Negrila C, Lazarescu MF***
    Electrochemical impedance spectroscopy investigations on the L-cysteine-thiolate self-assembled monolayers formed at p-GaAs(100) electrodes
    In: *9th International Symposium on Electrochemical Impedance Spectroscopy (EIS)* Location: *Okinawa, JAPAN* Date: *JUN 16-21, 2013*
    ELECTROCHIMICA ACTA Volume: 131, Pages: 42-51 Published: 10-Jun 2014

11. ***Palade C, Lazanu S, Ciurea ML***
    Trapping centers in heavy ion irradiated silicon
    In: *37th International Semiconductor Conference, CAS 2014; Sinaia; Romania; 13 -15 October 2014*
    PROCEEDINGS OF THE INTERNATIONAL SEMICONDUCTOR CONFERENCE, CAS, 24 November 2014, Article number 6966411, Pages 125-128

12. ***Palade C, Slav A, Lepadatu AM, Teodorescu VS, Ciurea ML***
    Charge storage properties of HfO_2/Ge-HfO_2/SiO_2 trilayer structures
    In: *37th International Semiconductor Conference, CAS 2014; Sinaia; Romania; 13 - 15 October 2014*
    PROCEEDINGS OF THE INTERNATIONAL SEMICONDUCTOR CONFERENCE, CAS, 24 November 2014, Article number 6966390, Pages 59-62

13. ***Palade C, Lepadatu AM, Stavarache I, Teodorescu VS, Ciurea ML***
    Transition in conduction mechanism in GeSi nanostructures
    In: *37th International Semiconductor Conference, CAS 2014; Sinaia; Romania; 13 - 15 October 2014*
    PROCEEDINGS OF THE INTERNATIONAL SEMICONDUCTOR CONFERENCE, CAS, 24 November 2014, Article number 6966389, Pages 55-58

14. ***Pintilie L, Pintilie I, Teodorescu CM, Ghica C, Hrib L, Chirila C, Trupina L, Boni AG, Iuga A, Negrea R, Pasuk I, Botea M, Filip LD, Kuncser V, Schinteie G***
    Interfaces in epitaxial structures based on oxide ferroelectrics
    SIPS2014: SHECHTMAN INTERNATIONAL SYMPOSIUM PROCEEDINGS, pp. 187-214, ISBN 978-1-987820-11-9

15. *Popa AC, Marques VMF,* ***Stan GE, Husanu MA, Galca AC, Ghica C,*** *Tulyaganov DU, Lemos AF, Ferreira JMF*
    Nanomechanical characterization of bioglass films synthesized by magnetron sputtering
    In: *European Materials Research Society (E-MRS) Spring Meeting 2013 Symposium O: Synthesis, processing and characterization of nanoscale multi functional oxide films IV*
    THIN SOLID FILMS Volume 553, Pages:166-172 Published:28 February 2014

16. ***Popa CL, Ciobanu CS**, Petre CC, Motelica-Heino M, **Iconaru SL**, Jiga G, **Predoi D***
Hydroxyapatite with environmental applications
In: *7th International Conference on Times of Polymers and Composites (TOP)* Location: *Ischia, ITALY* Date: *JUN 22-26, 2014*
AIP Conference Proceedings:TIMES OF POLYMERS (TOP) AND COMPOSITES 2014 Volume: 1599, Pages: 318-321 Published: 2014

17. ***Popescu M, Sava F, Velea A, Lorinczi A, Simandan ID***
Simulation of the structure of $GeAs_4Te_7$ chalcogenide materials during memory switching
In: *Proc of the 25th International Conference on Amorphous and Nanocrystalline Semiconductors (ICANS25), August 18–23, 2013 Toronto, Ontario Canada*
CANADIAN JOURNAL OF PHYSICS Volume 92, Issue 7-8, July 2014, Pages 675-680

18. *Radu M, Gheorghiu A, **Predoi D**, Hermenean A, Ardelean A, Dinischiotu A*
Mechanisms of pulmonary toxicity developed at low and high doses of dextran-coated magnetite nanoparticles
In: *50th Congress of the European-Societies-of-Toxicology* Location: *Edinburgh, SCOTLAND* Date: *SEP 07-10, 2014*
TOXICOLOGY LETTERS Volume: 229, Pages: S78-S78 Published: 10-Sep 2014

19. ***Sandu V, Aldica G, Badica P, Kuncser A**, Hayasaka Y*
Insertion versus growth of magnetic nanoparticles in MgB_2 superconducting composites
ADVANCED MATERIALS RESEARCH Volume 941-944, 2014, Pages 458-461

20. ***Simion CE**, Sackmann A, **Teodorescu VS**, Rusti CF, Piticescu RM, **Stanoiu A***
Tuned sensitivity towards H2S and NH3 with Cu doped barium strontium titanate materials
In: *14th Electroceramics Conference* Location: *Bucharest, ROMANIA* Date: *JUN 15-20, 2014*
ELECTROCERAMICS XIV CONFERENCE Volume: 1627, Pages: 92-97 Published: 2014

21. *Socol G, **Galca AC**, Craciun D, Hanna M, Taylor CR, Lambers E, Craciun V*
Pulsed laser deposition of nanocrystalline SiC films
In: *European Materials Research Society Fall Meeting 2013, Symposium B: Stress, structure and stoichiometry effects on the properties of nanomaterials II*
APPLIED SURFACE SCIENCE Volume: 306, Pages: 66-69 Published: 1 July 2014

22. ***Socol M, Preda N**, Vacareanu L, Grigoras M, Socol G, Mihailescu N, Stanculescu F, Jelinek M, **Stanculescu A**, Stoicanescu M*
Organic heterostructures based on arylenevinylene oligomers deposited by MAPLE
In: *5th European-Materials-Research-Society Symposium on Laser Material Interactions for Micro- and Nano- Applications* Location: *Strasbourg, FRANCE* Date: *MAY 27-31, 2013*
APPLIED SURFACE SCIENCE Volume: 302, Pages: 216-222 Published: 30-May 2014

23. ***Stanculescu A, Socol M, Rasoga O**, Mihailescu IN, Socol G, **Preda N**, Breazu C, Stanculescu F*
Laser prepared organic heterostuctures on glass/AZO substrates
In: *5th European-Materials-Research-Society Symposium on Laser Material Interactions for Micro- and Nano- Applications* Location: *Strasbourg, FRANCE* Date: *MAY 27-31, 2013*
APPLIED SURFACE SCIENCE Volume: 302, Pages: 169-176 Published: 30-May 2014

24. ***Trinca LM, Galca AC, Stancu V, Chirila C, Pintilie L***
Structural caracterization of impurified Zzinc oxide thin films
In: *14th Electroceramics Conference* Location: *Bucharest, ROMANIA* Date: *JUN 15-20, 2014*
ELECTROCERAMICS XIV CONFERENCE Volume: 1627, Pages: 123-128 Published: 2014

25. *Tudorache M, Ghemes G, Nae A,* ***Matei E, Mercioniu I****, Kemnitz E, Ritter B, Coman S, Parvulescu VI*
Biocatalytic designs for the conversion of renewable glycerol into glycerol carbonate as a value-added product
In: *Catalysis for Renewable Sources: Fuel, Energy, Chemicals, Lund, Sweden, July 22-28, 2013*
CENTRAL EUROPEAN JOURNAL OF CHEMISTRY Volume 12, Issue 12, December 2014, Pages 1262-1270

Contributed Presentations

1. ***Aldica G, Burdusel M,*** *Popa S,* ***Enculescu M, Miu L, Badica P***
   Graphene-based addition to MgB_2 superconductor obtained by *ex-situ* spark plasma sintering technique
   4th International Conference on Superconductivity and Magnetism, Antalya, Turkey
   27 April – 3 May 2014, Talk
2. ***Apostol NG***
   Band bending at ferroelectric surfaces and at metal/ferroelectric heterostructures investigated by photoelectron spectroscopy
   ECOSS 30, 30th European Conference on Surface Science, Antalya, Turkey
   31 August – 05 September 2014, Talk
3. ***Apostol NG***
   Adsorption on ferroelectric surfaces of simple polar molecules
   EMAST 1st European Symposium on Surface Science, Rome, Italy
   26-28 November 2014, Talk
4. *Axente E, Hermann J, Socol G,* ***Galca AC****, Craciun V*
   On the metrology of ternary and quaternary/complex amorphous transparent oxides by spectroscopic techniques
   Electroceramics XIV, Bucharest, Romania
   16–20 June 2014, Poster
5. *Axente E, Hermann J, Socol G,* ***Galca AC,*** *Pantelica D, Ionescu P, Craciun V*
   On the metrology of amorphous transparent oxides by spectrometry techniques
   EMRS Spring Meeting, Lille, France
   26–30 May 2014, Poster
6. *Axente E, Socol G, Dorcioman G, Craciun D,* ***Trinca LM, Galca AC****, Pantelica D, Ionescu P, Hermann J, Craciun V*
   Synthesis and characterization of doped hafnium oxide thin films for applications in thin film transistors
   EMRS Fall Meeting, Warsaw, Poland
   15–18 September 2014, Poster
7. ***Badica P***
   Structures and patterns in matter and fields
   An Inderdisciplnary Workshop devoted to Morphogenesis, Alexander von Humbold, Bucharest, Romania
   29-31 May 2014, Talk
8. ***Badica P***
   MgB_2 based composites obtained by Spark Plasma Sintering for superconductivity applications
   Adv. Workshop in solar energy conversion and Nanohysics, Magurele, Romania
   1-3 September 2014, Talk

9. ***M. Baibarac, I. Baltog, I. Smaranda,*** *A. Magrez*
   Highly separated metallic and semiconducting single-walled carbon nanotubes functionalized with polydiphenylamine: synthesis, photochemical processes evidenced by photoluminescence and applications in supercapacitors field
   Internatinal Conference on Diamond and Carbon Materials, Madrid, Spain
   7-12 September 2014, Poster

10. ***I.Baltog, I. Smaranda, M. Baibarac****, W.K. Maser, A.M. Benito*
    Electrochemical grafting of reduced graphene oxide with polydifenylamine doped with heteropolyanions – optical properties and applications in the supercapacitors field
    Internatinal Conference on Diamond and Carbon Materials, Madrid, Spain
    7-12 September 2014, Poster

11. ***Banciu MG, Nedelcu L, Chirila C, Geambasu D****, Furuya T, Tani M*
    Terahertz Time-Domain spectroscopy investigations on bulk and film microwave dielectrics
    14th International Balkan Workshop on Applied Physics, Constanta, Romania
    2-4 July 2014, Poster

12. ***Banciu MG, Nedelcu L, Geambasu D***
    Improved dielectric resonator antennas with half split resonators
    14th International Balkan Workshop on Applied Physics, Constanta, Romania
    2-4 July 2014, Poster

13. ***Banciu MG, Nedelcu L****, Nicolaescu I*
    Dielectric resonator antennas of YST and BNT materials
    COST-VISTA Workshop, Bucharest, Romania
    26-28 May, Talk

14. ***Banciu MG, Nedelcu L***
    Investigation of some microwave materials in THz range using time-domain spectroscopy
    COST-VISTA Workshop, Bucharest, Romania
    26-28 May, Talk

15. ***Banciu MG,*** *Nicolaescu I,* ***Nedelcu L, Geambasu DC***
    Investigations for bandwidth enhancement of dielectric resonator antenna
    COST-VISTA Workshop, Madrid, Spain
    22-24 October, Talk

16. ***Bartha C, Plapcianu C, Palade P, Schinteie G****, Vizman D*
    Model-free kinetic analysis of Sr2FeMoO6 re-crystallization process used for growing by Bridgman method of the double-perovskite monocrystals
    Physics Conference TIM-14, Timisoara, Romania
    20-22 November, Poster

17. *Batalu D,* ***Aldica G, Burdusel M****, Popa S,* ***Enculescu M, Pasuk I,*** *Miu D,* ***Badica P***
    Ge-added MgB_2 Superconductor obtained by *ex-situ* Spark Plasma Sintering
    4th International Conference on Superconductivity and Magnetism, Antalya, Turkey
    27 April - 3 May 2014, Poster

18. ***Besleaga C, Galca AC, Pintilie I***
Advanced characterization of amorphous oxide semiconductor thin films by x-ray reflectivity and thermal stimulated current spectroscopy
10th International Conference on Physics of Advanced Materials (ICPAM), Iasi, Romania
22-28 September 2014, Poster

19. ***Besleaga C, Galca AC, Stan GE, Ghica C, Pasuk I***
Growth evolution of sputtered zinc oxide thin films
TIM14, Timisoara, Romania
20-22 November 2014, Talk

20. ***Besleaga C, Galca AC, Stan GE, Miclea CF***
Semiconductor thin film analysis by Spectroscopic Ellipsometry; The link between optical properties and structural and electrical ones
International Conference on Spectroscopy and Applications (ICSA), Hammamet, Tunisia
2-4 May 2014, Talk

21. ***Besleaga C,*** *Antohe S,* ***Stan GE, Galca AC,*** *Barquinha P, Fortunato E, Martins R*
Fully transparent transistors based on AlN-gate dielectric and IGZO-channel semiconductor
Electroceramics XIV, Bucharest, Romania
16-20 June 2014, Talk

22. ***Bibicu I***
Spectroscopia Mössbauer: metoda de studiu a suprafetei
Simpozionul Stiintific al Inginerilor Romani de Pretutindeni, editia a XI-a SINGRO 2014: Ingineria – prezent si viitor, Chisinau, Republic of Moldova
23-24 October 2014, Talk

23. ***Birzu M, Cotorobai F, Zgura I, Ganea CP, Frunza S, Diamandescu L, Frunza L***
Contact angles of the wool fabrics functionalized with titanium dioxide
Simpozionul International PRIOCHEM, editia a X-a, Bucharest, Romania
30-31October 2014, Poster

24. ***Birzu M, Zgura I, Cotorobai F, Ganea CP, Frunza S, Frunza L***
Complex characterization of the wool fabrics deposited by TiO2 nanoparticles
A XXXIII-a Conferinta Nationala de Chimie Căciulata, județul Vâlcea, Romania
01-03 October 2014, Poster

25. *Boroica L, Sava BA, Elisa M,* ***Valeanu M, Kuncser V, Sofronie M,*** *Shikimaka O, Grabco D*
Magneto-optical and mechanical properties of rare-earth doped phosphate glasses
7th International Conference on Materials Science and Condensed Matter Physics-MSCMP 2014, Vadu lui Voda, Republic of Moldova, 2014, Abstract Book, p. 88
16-19 September 2014, Talk

26. ***Botea M, Iuga A, Stancu V, Pintilie L***
Pyroelectric effect on $Pb(Zr_{0.2}, Ti_{0.8})O_3$ structures
5th ICSP International Conference, Orastie, Romania
23–26 September 2014, Poster

27. ***Boni G, Chirila C, Stancu V, Trupina L, Negrea R, Pintilie I, Pintilie L***
The influence of the bottom electrode on the structural and electrical properties of $Pb(Zr_{0.2}, Ti_{0.8})O_3/CoFe_2O_4$ multiferroic structures
5th ICSP International Conference, Orastie, Romania
23–26 September 2014, Talk

28. ***Boni G, Dragoi C,*** *Shi Y, Vilquin B, Saint-Girons G, Robach Y, Le Rhun G,* ***Pintilie I, Pintilie L***
The effect of the different top electrodes on the electrical properties of epitaxial $Pb(Zr_{0.52}Ti_{0.48})O_3$ deposited by PLD on Si substrate with SrTiO3 buffer layer
Electroceramics XIV, Bucharest, Romania
16–20 June 2014, Talk

29. ***Botea M, Iuga A, Stancu V, Pintilie L***
Pyroelectric properties of the Pb(Zr, Ti)O_3-based structures
Electroceramics XIV, Bucharest, Romania
16–20 June 2014, Poster

30. ***Breazu C,*** *Stanculescu F,* ***Preda N, Rasoga O, Socol M,*** *Socol G,* ***Stanculescu A***
An investigation of the beta-amyloid aggregation on carbon allotropes thin films for sensing applications
E-MRS Spring Meeting, Lille, France
26-30 May 2014, Poster

31. *Bulai G,* ***Diamandescu L,*** *Dumitru I, Gurlui S,* ***Feder M,*** *Caltun O F*
Synthesis and characterization of RE (RE=Dy, Gd, La, Sm, Yb, Er, Ho) doped cobalt ferrite bulk materials
Electroceramics XIV, Bucharest, Romania
16-20 June 2014, Poster

32. *Bulai G A,* ***Diamandescu L,*** *Gurlui S,* ***Feder M,*** *Clatun O F, Dumitru I*
Magnetic and magnetostrictive behavior of rare earth doped cobalt ferrite bulk materials
10th European Conference on Magnetic Sensors and Actuators, EMSA 2014, Viena, Austria
6-9 July 2014, Poster

33. ***Busuioc C, Evanghelidis A, Florica C, Costas A, Enculescu I***
Influence of preparation conditions on the properties of electrospun ZnO fibers
E-MRS 2014 Spring Meeting, Lille, France
26-30 May 2014, Poster

34. ***Busuioc C, Evanghelidis A, Florica C, Enculescu I***
Characterization of ZnO fibers prepared via electrospinning
The 23rd European Workshop on Heterostructure Technology - HETECH, Rauischholzhausen, Germany
12-15 October 2014, Poster

35. ***Cernea M, Trupina L,*** *Vasile BS,* ***Bartha C,*** *Trusca R*
Piezoelectric and magnetic nanowires of $BiFeO_3$ doped-BNT-$BT_{0.08}$
Electroceramics XIV / COST section, Bucharest, Romania
16-20 June 2014, Poster

36. ***Ciobanu CS, Popa CL, Iconaru SL,*** *Chapon P,* ***Ghita RV, Predoi D***
Effect of annealing temperature on antibacterial activity of silver doped hydroxyapatite thin films
7th GD Day, Reims, France
11-12 June 2014, Talk

37. ***Ciobanu CS, Popa CL,*** *Groza A, Chapon P,* ***Negrila CC, Ghita RV,*** *Ganciu M,* ***Predoi D***
The role of polydimethylsiloxane layer in the deposition process of hydroxyapatite doped with silver nanoparticles as coating
The 17th International Symposium on Silicon Chemistry, Berlin, Germany
3-8 August 2014, Poster

38. ***Ciobanu CS, Iconaru SL****, Prodan AM, Motelica M, Guegan R,* ***Popa CL****, Albu MG,* ***Predoi D***
New nanocomposites based on hydroxyapatite in collagen matrix for enviromental applications
The 17th International Symposium on Silicon Chemistry, Berlin, Germany
3-8 August 2014, Poster

39. ***Ciobanu CS, Iconaru SL, Predoi D***
Antimicrobial studies on porous hydroxyapatite used in the environment and biological applications
FEBS MEBO 2014, Paris, France
30 August-4 September 2014, Poster

40. ***Ciobanu CS, Popa CL, Iconaru SL, Predoi D***
Antimicrobial activity of samarium doped hydroxyapaptite prepared by co-precipitation method
FEBS MEBO 2014, Paris, France
30 August-4 September 2014, Poster

41. ***Ciobotaru CC, Polosan S***
Embeeding of IrQ(ppy)$_2$ organometallic compounds in polypyrrole conducting polymer
E-MRS 2014 Spring Meeting, Grand Palais, Lille, France
26-30 May 2014, Poster

42. ***Ciobotaru IC, Polosan S,*** *Iovu H*
Influence of crystallization on the phosphorescence of IrQ(ppy)$_2$ organometallic compound in OLED's applications,
E-MRS 2014 Spring Meeting, Grand Palais, Lille, France
26-30 May 2014, Poster

43. ***Ciobotaru IC, Matei E***
Polypyrrole/IrQ(ppy)$_2$ composite films prepared by electrochemical deposition for OLED's applications
10th International Conference on Electroluminescence and Optoelectronic Devices (ICEL 10), Universitatea din Cologne, Germany
31 August 2014-03 September 2014, Poster

44. *Ciuchi IV,* ***Cernea M****, Vasile BS, Trusca R, Galassi C*
Synthesis and dielectric properties of one-dimensional BNT-BTCe@SiO2 core-shell heterostructures
ELECTROCERAMICS XIV, Bucharest, Romania
16-20 June 2014, Poster

45. *Ciuchi IV,* ***Cernea M,*** *Galassi C*
Piezoelectric and dielectric characterization of $BNT_{0.92}BT_{0.08}$ (5 mol% Ce doped), coated with SiO_2
Conference COST MPO904, Genova, Italy
30-31 January 2014, Poster

46. ***Ciurea ML, Lepadatu AM, Stavarache I, Teodorescu VS, Pasuk I***
GeSi nanostructured films with structure and electrical properties tailored by annealing
E-MRS 2014 Spring Meeting, Lille, France
26–30 May, Poster

47. ***Ciurea ML, Lazanu S, Slav A, Palade C***
Traps in bismuth irradiated silicon
E-MRS 2014 Spring Meeting, Lille, France
26–30 May, Poster

48. ***Ciurea ML***
Charge transport in percolative structures based on Ge nanoparticles
NanoSEA 2014 („5th Int. Conf. on NANO-Structures SElf-Assembly"), Marsilia, France
7–11 July 2014, Talk

49. ***Chirila C, Boni A,*** *Shi Y,* ***Trupina L, Pasuk I, Pintilie I,*** *Vilquin B, Saint-Girons G, Robach Y, Le Rhun G,* ***Pintilie L***
Comparison between the ferroelectric/electric properties of the $PbZr_{0.52}Ti_{0.48}O_3$ films grown on Si (100) and on STO (100) substrates
Electroceramics XIV, Bucharest, Romania
16–20 June 2014, Poster

50. ***Costas A, Florica C, Matei E,*** *Toimil Molares ME,* ***Kuncser V, Enculescu I***
Transport properties of single Ni-Cu alloy nanowires
E-MRS 2014 Spring Meeting, Lille, France
26-30 May 2014, Talk

51. ***Cotirlan-Simioniuc C, Ghita RV, Negrila CC, Logofatu C***
Evanescent-wave cavity ring-down spectroscopy system for gases monitoring
14th International Balkan Workshop on Applied Physics and Materials Science, Constanta Romania
2-4 July 2014, Poster

52. ***Cotirlan-Simioniuc C, Ghita RV, Predoi D, Popa CL***
Cavity Ring-Down Spectroscopy measurements on hydroxyapatite thin films
14th International Balkan Workshop on Applied Physics and Materials Science, Constanta Romania
2-4 July 2014, Poster

53. *Craciun F, Dimitriu E, Grigoras M, Lupu N, Vasile BS,* ***Cernea M***
Structural, ferroelectric and magnetic properties of (R, Pb)TiO_3 perovskite ceramics
Conference COST MPO904, Genova, Italy
30-31 January 2014, Talk

54. *Craciun F, Dimitriu E, Grigoras M, Lupu N,* ***Cernea M****, Stefan VB*
The emergence of magnetic properties and magnetoelectric coupling in (Re, Pb)TiO_3 perovskite ceramics
Electroceramics XIV, Bucharest, Romania
16-20 June 2014, Talk

55. *Craciun D, Socol G, Stefan N, Craciun V, Simeone D, Gosset D,* ***Galca AC, Trinca LM****, Behdad S, Bosel B, Bogdan V, Surdu A*
Investigations of radiation effects on the structure and properties of nanocrystalline SiC thin films
EMRS Fall Meeting, Warsaw, Poland
15–18 September 2014, Poster

56. *Craciun V,* ***Galca AC, Trinca LM****, Socol G, Craciun D, Lambers E*
Optical properties of nanocrystalline SiC thin films grown by pulsed laser deposition
EMRS Spring Meeting, Lille, France
26–30 May 2014, Poster

57. ***Crisan A***
Exchange coupling in nanocomposite Fe(Co)Pt(Pd)AgB magnets
SCTE 2014 - 19th International Conference on Solid Compounds of Transition Elements, Genova, Italy
21-26 June 2014, Poster

58. ***Crisan O***
Structural phase transformation and nitriding effects in FePt-based alloys
SCTE 2014 - 19th International Conference on Solid Compounds of Transition Elements, Genova, Italy
21-26 June 2014, Talk

59. *Duta L, Bakalova S,* ***Stan GE****, Mihailescu N, Szekeres A, Mihailescu IN*
Multilayered AlN thin films synthesized on silicon substrates by pulsed laser deposition at different temperatures
18th International School on Condensed Matter Physics, Varna, Bulgaria
1–6 September 2014, Poster

60. *Duta L, Popescu AC,* ***Popa AC****, Mihailescu IN*
Nanostructured glass coatings synthesized by pulsed laser deposition
6th International Workshop on "Advanced optical and X-ray characterization techniques of multifunctional materials for information and communication technologies, health and renewable energy applications", Bucharest, Romania
10–12 September 2014, Talk

61. *Duta L,* ***Stan GE****, Popescu AC,* ***Popa AC****, Miculescu F, Mihailescu IN*
Morphological, structural and biological characteristics of ultra-high molecular weight polyethylene acetabular cups functionalized with bioactive glass coatings by pulsed laser deposition
EMRS Spring Meeting, Lille, France
26–30 May 2014, Poster

62. *Duta L,* ***Stan GE****, Serban N, Oktar FN, Mihailescu IN*
Synthesis of biological hydroxyapatite thin films by pulsed laser deposition
EMRS Spring Meeting, Lille, France
26–30 May 2014, Poster

63. ***Enculescu I, Matei E, Florica C, Enculescu M, Evanghelidis A, Costas A, Busuioc C, Preda N, Oancea M***
Electrospun based electrodes for electrodeposition of tailored nanostructures
9th International Conference on Surfaces, Coatings and Nanostructured Materials (NANOSMAT) 2014, Dublin, Ireland
8-11 September 2014, Talk

64. ***Enculescu I, Matei E, Florica C, Enculescu M, Costas A, Evanghelidis A***
Zinc oxide/samaria nanowires with intense photoluminescence
225th ECS Meeting 2014, Orlando, USA
11-15 May 2014, Talk

65. ***Enculescu I, Matei E, Florica C, Enculescu M, Costas A, Evanghelidis A***
Field effect transistors with electrodeposited nanowire channels
225th ECS Meeting 2014, Orlando, USA
11-15 May 2014, Talk

66. ***Enculescu I, Matei E, Florica C, Costas A,*** *Toimil Molares ME*
Tuning of transport properties of electrodeposited CdTe nanowires
5th International Conference on Nanostructures Self-Assembly, NANOSEA 2014, Marseille, France
7-11 July 2014, Talk

67. ***Enculescu M, Evanghelidis A, Busuioc C, Preda N, Matei E. Florica C, Costas A, Oancea M, Enculescu I***
Electrospun dye-doped nanofibers with tuneable emissive properties
E-MRS 2014 Spring Meeting, Symposium Q: Hybrid materials engineering in biology, chemistry and physics, Lille, France
26-30 May 2014, Poster

68. ***Evanghelidis A, Preda N, Florica C, Zgura I, Socol M, Enculescu M, Enculescu I***
Engineering superhydrophobic hybrid ZnO/porous polymeric structures
E-MRS 2014 Spring Meeting, Lille, France
26-30 May 2014, Poster

69. ***Evanghelidis A, Busuioc C, Matei E, Enculescu I***
Zinc oxide electrodeposition using metallic/polymer nanofiber webs as electrodes
E-MRS 2014 Spring Meeting, Lille, France
26-30 May 2014, Poster

70. ***Filip LD, Pintilie L***
Theoretical current-voltage characteristics for the symmetric metal-ferroelectric-metal heterostructure
Electroceramics XIV, Bucharest, Romania
16–20 June 2014, Talk

71. ***Florica C, Preda N, Zgura I, Socol M, Enculescu M, Evanghelidis A, Enculescu I***
ZnO nanostructured films with tailored properties prepared by simple wet chemical methods
E-MRS 2014 Spring Meeting, Lille, France
26-30 May 2014, Talk

72. ***Florica C, Matei E, Costas A, Enculescu M,*** *Toimil Molares ME,* ***Enculescu I***
Field effect transistor based on electrodeposited semiconducting nanowire for sensor applications
E-MRS 2014 Spring Meeting, Lille, France
26-30 May 2014, Poster

73. ***Florica C, Oancea m, Costas A, Matei E,*** *Toimil Molares ME,* ***Enculescu I***
Influence of biocompatible hydrogel coatings on ZnO nanowire field effect transistors electrical characteristics
E-MRS 2014 Spring Meeting, Lille, France
26-30 May 2014, Poster

74. ***Frunza S, Beica T, Zgura I, Frunza L,*** *Nuta A, Sorescu AA, Zaharia CN, Bunea I*
Dispozitiv si metoda pentru detectarea interactiunilor de tip antigen viral-anticorp specific, prin determinarea unghiului de contact
6th European Exhibition of Creativity and Innovation, Iasi, Romania
22-24 May 2014, Poster and video presentation
   a) *Silver Medal at Euroinvent 2014*
   b) *Excellence Awards at Euroinvent 2014*

75. ***Frunza S, Beica T, Zgura I, Frunza L,*** *Nuta A, Sorescu AA, Zaharia CN, Bunea I*
Dispozitiv si metoda pentru detectarea interactiunilor de tip antigen viral-anticorp specific, prin determinarea unghiului de contact
Cea de a XIl-a ediție a Salonul Internațional al Cercetării, Inovării şi Inventicii PRO INVENT, Cluj-Napoca, Romania
19-21 March 2014, Poster

76. ***Galca AC,*** *Socol G,* ***Stan GE,*** *Craciun V*
Correlation between structure, composition and optical properties of nanocrystalline thin films deposited by Pulsed Laser Deposition
Electroceramics XIV, Bucharest, Romania
16–20 June 2014, Poster

77. ***Galca AC, Trinca LM,*** *Socol G, Craciun V*
Optical characterization of transparent amorphous oxide thin films by Spectroscopic Ellipsometry and UV-Vis spectroscopy
International Conference on Spectroscopy and Applications (ICSA), Hammamet, Tunisia
2–4 May 2014, Talk

78. ***Galca AC, Trinca LM,*** *Socol G, Craciun V*
Transparent amorphous oxide thin films: advanced characterization by spectroscopic ellipsometry and X-ray reflectivity
7th International Conference on Materials Science and Condensed Matter Physics, Chisinau, Republic of Moldova
14-19 September 2014, Talk

79. ***Galca AC, Trinca LM,*** *Socol G, Craciun V*
Transparent amorphous oxide thin films: advanced characterization by spectroscopic ellipsometry and X-ray reflectivity
10th International Conference on Physics of Advanced Materials (ICPAM), Iasi, Romania
22-28 September 2014, Talk

80. ***Galca AC, Trinca LM,*** *Oumezzine Ma,* ***Chirila C, Pasuk I***
Comprehensive characterization of homo- and hetero- epilayers
6th International Workshop on "Advanced optical and X-ray characterization techniques of multifunctional materials for information and communication technologies, health and renewable energy applications", Bucharest, Romania
10–12 September 2014, Talk

81. ***Ganea CP***
Influence of the processes at the interface ionic conductibility materials-electrodes on the dielectric spectroscopy measurement – a new theoretical approach
Sesiunea stiintifica anuala a Facultatii de Fizica, Bucharest, Romania
20 June 2014, Talk

82. ***Ganea CP***
Modeling the charge transfer at the ionic liquid-electrode interface in dielectric spectroscopy measurements-a more comprehensive approach
Simpozionul International PRIOCHEM, editia a X-a, Bucharest, Romania
30-31October 2014, Poster

83. ***Ganea CP,*** *Alexandru HV*
Study of phase transition ferroelectric-paraelectric Triglycine sulphate crystal by dielectric spectroscopy
International Colloquium "Physics of Materials" (PM-4), University Politehnica of Bucharest, Romania
13-14 November 2014, Poster

84. ***Geambasu CD,*** *Tuta L,* ***Banciu MG, Nedelcu L,*** *Nicolaescu I*
Compact antenna using ZST los-loss high dielectric constant material
Proceeding of the 22nd International Communications Forum, TELFOR 2014, Belgrade, Serbia
25-27 November 2014, Talk

85. ***Ghica C, Negrea RF, Nistor LC, L. Pintilie L***
Nanoscale phase transition in strained SrRuO3 thin film
12th Europhysical Conference on Defects in Insulating Materials (Eurodim 2014), Canterbury, UK
13-19 July 2014, Talk

86. ***Ghica C, Negrea R F, Teodorescu V S, Maraloiu V A, Nistor L C, Chirila C, Pintilie L***
Quantitative HRTEM analysis of epitaxial perovskite multilayer on Si(001) single crystal substrate
18th International Microscopy Congress IMC 2014, Praga, Cehia
7-12 September 2014, Poster

87. ***Ghica D, Nistor L C, Stefan M, Nistor S V***
Unusual thermal induced structure and composition changes in the nanosized ε-$Zn(OH)_2$ shell of cZnS quantum dots
Europhysical Conference on Defects in Insulating Materials (Eurodim 2014), Canterbury, UK
13-19 July 2014, Poster

88. ***Ghica D, Stefan M, Ghica C, Stan G E***
Localization and dynamics of magnetic impurities in nanostructured ZnO films
Electroceramics XIV, Bucharest, Romania
16 – 20 June 2014, Poster

89. ***Greculeasa S, Kuncser V, Schinteie G,*** *Kumar L, Kumar P, Sahoo B, Kar M*
Magnetic and Mössbauer spectroscopy study of Al and Mn substituted nanocristalline Ni ferrites
Electroceramics XIV, Bucharest, Romania
16 – 20 June 2014, Poster

90. ***Greculeasa S, Palade P, Schinteie G, Kuncser A,*** *Lungu A, Porosnicu C, Jepu I, Lungu CP,* ***Filoti G, Kuncser V***
W-Mg alloy films deposided by TVA on hydrogenated EUROFER substrates for plasma facing components
14th International Balcan Workshop on Applied Physics, Constanta, Romania
2-4 July 2014, Talk

91. ***Hrib LM, Pintilie L,*** *Alexe M*
Electrical investigations of LSMO/PZT/LSMO thin films under magnetic field
Electroceramics XIV, Bucharest, Romania
16–20 June 2014, Poster

92. ***Iconaru SL,*** *Motelica M, Guegan R,* ***Ciobanu CS, Predoi D***
Synthesis, characterization and applications of novel hydroxypatite/SiO_2 nanocomposites
ISOS XVII BERLIN 2014 - The 17th International Symposium on Silicon Chemistry, Berlin, Germany
3-8 August 2014, Poster

93. ***Iconaru SL,*** *Prodan AM,* ***Ciobanu CS,*** *Motelica-Heino M,* ***Predoi D***
In vivo toxicity studies of superparamagnetic iron oxide nanoparticles in a silica matrix
FEBS MEBO 2014, Paris, France
30 August-4 September 2014, Poster

94. ***Iconaru SL,*** *Motelica M, Guegan R, Prodan AM, P Le Coustumer,* ***Predoi D***
Characterization and toxicity evaluation of iron oxide in a silica matrix for removing arsenic ions from aqueous solutions
24th Réunion des Sciences de la Terre, Pau, France
27-31 October 2014, Poster

95. *Iordanescu R, Feraru I, Elisa M, Sava B, Boroica L,* ***Valeanu M, Kuncser V, Sofronie M***
Magnetic and magneto-optical properties of La, Y and Eu-doped phosphate glasses
The 8th International Conference on Borate Glasses, Crystals and Melts "Borate Phosphate 2014", Pardubice, Czech Republic, Published by ICARIS Ltd., p. 206
30 June-4 July 2014, Poster

96. ***Kuncser A**, Antohe S, **Ghica C, Kuncser V***
Extended Stoner-Wohlfarth model for Bi-dimensional Distributions of Easy Axes
International Conference on Superconductivity and Magnetism ICSM 2014, Antalya, Turkey
27 April-02 Mai 2014, Poster

97. ***Kuncser A, Negrea R F, Maraloiu A V, Teodorescu V S, Ghica C, Stavarache I, Lepadatu A M, Ciurea M L**, Scarisoreanu N D, Andrei A, Dinescu M*
Nano-structuring of thin amorphous films by pulsed laser irradiation in ultraviolet
EuroMat 2014, Laussanne, Switzerland
21-25 July 2014, Talk & Poster

98. ***Kuncser V, Schinteie G**, Iacob V*
Magnetic nanostructures and bio-medical applications
Advanced Workshop in Solar Energy Conversion and Nanophysics, Bucharest-Magurele, Romnia
01-03 September 2014, Talk

99. ***Kuncser V**, Bulinski M*
Building shapes and patterns by interference
An Inderdisciplnary Workshop devoted to Morphogenesis, Alexander von Humbold, Bucharest, Romania
29-31 May 2014, Talk

100. *Ionescu MA, **Aldica G**, Popa S, **Enculescu M, Sandu V, Badica P, Pasuk I, Miu L***
Superconducting MgB_2 with addition of cubic BN and C60 obtained by Spark Plasma Sintering Technique
ICPAM 10 - 10th International Conference on Physics of Advanced Materials, Iasi, Romania
20-28 September 2014, Poster

101. *Ionescu MA, **Aldica G**, Popa S, **Enculescu M, Sandu V, Badica P, Pasuk I, Miu L***
MgB_2 with addition of cubic BN and $Ge_2C_6H_{10}O_7$ obtained by Spark Plasma Sintering Technique
ICPS 2014 "International Conference of Physics Students", Heidelberg, Germany
10-17 August 2014, Poster

102. *Ivan I, Mele P, Miu D, **Miu L***
DC magnetization relaxation and the frequency dependent AC magnetic response of $YBa_2Cu_3O_7$ films with embedded nanorods and nanoparticles
ICPAM 10 - 10th International Conference on Physics of Advanced Materials, Iasi, Romania
20-28 September 2014, Poster

103. *Laurent P, Mekadmini A, Le Febvrier A, Laur V, Martin N, Députier S, **Galca AC, Pintilie P**, Guilloux-Viry M, Tanné G*
Etude en température de couches minces ferroélectriques de KTN pour des applications d'accordabilité
13èmes Journées de Caractérisation Microondes et Matériaux (JCMM 2014), Nantes, France
24-26 March 2014, Poster

104. *Lazarescu V, Anastasescu M, Dobrescu G, Enache M,* ***Lazarescu MF, Negrila CC,*** *Preda L* Field - dipole interactions in L-cysteine-thiolate self assembled at p-and n-GaAs(100) electrodes
15th Topical Meeting of the International Society of Electrochemistry, Niagara Falls, Canada
27 April – 1 May 2014, Talk

105. ***Lepadatu AM, Teodorescu VS, Pasuk I, Stavarache I, Ciurea ML***
Tuning the structure and electrical behaviour of GeSi nanostructured films by annealing temperature
ICPAM-10, Iasi, Romania
22–28 September 2014, Talk

106. ***Lepadatu AM, Stavarache I, Teodorescu VS, Ciurea ML, Stoica T****, Buca D*
Formation of Ge nanocrystals or nanoparticles in multilayer structures by tuning the annealing temperature
PM-4, Bucuresti, Romania
13–14 November 2014, Talk

107. ***Lőrinczi A, Popescu M, Sava F, Velea A, Simandan ID, Badica P, Burdusel M, Galca AC,*** *Socol G, Jipa F, Zamfirescu M, Kiss A*
Photonic arrays based on amorphous Ga_2S_3 and As_2S_3 thin films
International Conference „Smart functional materials for shaping our future" SMART 2014, Debrecen, Hungary
18 – 21 September 2014, Talk

108. *Lupu AR,* ***Popescu T***
In vitro effects of undoped and Fe^{3+}-doped TiO_2 nanoparticles on HepG2 hepatocytes
6th EFIS/EJI South East European Immunology School, SEEIS2014, Timisoara, Romania
26 – 29 September 2014, Talk

109. ***Matei E, Florica C, Enculescu M, Evanghelidis A, Costas A, Busuioc C, Preda N, Oancea M, Enculescu I***
Transport properties of electrodeposited ZnO nanowires
9th International Conference on Surfaces, Coatings and Nanostructured Materials (NANOSMAT) 2014, Dublin, Ireland
8-11 September 2014, Talk

110. ***Matei E, Evanghelidis A, Busuioc C, Enculescu I***
Electrochemical deposition of zinc oxide on metal web electrodes
5th International Conference on Nanostructures Self-Assembly, NANOSEA 2014, Marseille, France
7-11 July 2014, Poster

111. ***Miclea CF, Miclea C,*** *Hochheimer HD, Martin B, Ohtani T*
Charge density wave and superconductivity in $Tl_xV_6S_8$
4th International Conference on Superconductivity and Magnetism- ICSM2014, Antalya, Turkey 27 April - 2 May 2014, Talk

112. *Mihailescu N, Grumezescu V,* ***Stan GE****, Duta L, Chifiriuc MC, Sopronyi M, Ristoscu C, Luculescu CR, Oktar FN, Mihailescu IN*
Transfer by pulsed laser deposition of biological hydroxyapatite thin films doped with MgF_2, MgO and Ti
EMRS Spring Meeting, Lille, France
26–30 May 2014, Poster

113. *Miroiu FM, Stefan N, Visan A,* ***Rasoga OL, Zgura I****, Nita C,* ***Stanculescu A****, Dorcioman G, Cristescu R, Mihailescu IN, Socol G*
Biodegradable silk fibroin/poly(3-Hydroxy-Butyric Acid-Co-3-Hydroxy-Valeric Acid) composite coatings obtained by MAPLE and dip-coating methods
E-MRS Spring Meeting, Lille, France
26-30 May 2014, Poster

114. ***Moldoveanu V, Dinu IV,*** *Tanatar B*
Time dependent transport in single-molecule magnets
Advanced Many-Body and Statistical Methods in Mesoscopic Systems II, Brasov, Romania
1-5 September 2014, Poster

115. ***Moldoveanu*** V, Dinu IV, Dragomir R
Optical manipulation of sp biexcitons in disk-shaped quantum dots
Advanced Many-Body and Statistical Methods in Mesoscopic Systems II, Brasov, Romania
1-5 September 2014, Poster

116. ***Nedelcu L, Banciu MG, Ganea P, Geambasu D, Ciongher M, Aldica GV***
Complex permittivity of $Ba_{0.6}Sr_{0.4}TiO_3$ ferroelectric ceramics studied by temperature-dependent dielectric spectroscopy
Electroceramics XIV, Bucharest, Romania
16–20 June 2014, Poster

117. ***Nedelcu L, Geambasu D, Banciu MG***
Submillimeter-wave properties of low-loss dielectrics studied by terahertz time-domain spectroscopy
Electroceramics XIV, Bucharest, Romania
16–20 June 2014, Poster

118. ***Nedelcu L, Banciu MG, Ganea CP, Aldica GV***
Broadband Dielectric Spectroscopy of $Mg_4Nb_2O_9$ Ceramics
14th International Balkan Workshop on Applied Physics IBWAP 2014, Constanta, Romania
2-4 July 2014, Poster

119. ***Nedelcu L, Trupina L, Ganea CP, Geambasu CD, Cioangher M, Banciu MG***
Dielectric Properties of $Ba_{2/3}Sr_{1/3}TiO_3$ Ferroelectric Ceramics
14th International Balkan Workshop on Applied Physics, Constanta, Romania
2-4 July 2014, Poster

120. ***Nedelcu L, Geambasu D, Banciu MG***
Millimeter-wave ceramics for harsh environment applications
E-MRS 2014 Fall Meeting, Warsaw, Poland
15-19 September 2014, Poster

121. ***Negrea RF, Ghica C, Nistor LC, Pintilie L***
Atomic scale STEM and EELS characterization of $BaTiO_3/SrRuO_3/SrTiO_3$ ferroelectric heterostructure
Electroceramics XIV, Bucharest, Romania
16–20 June 2014, Poster

122. ***Negrea R F, Ghica C, Teodorescu V S, Maraloiu V-A, Chirila C, Pintilie L***
Microstructural studies by advanced transmission electron microscopy of interfaces in multilayered structure based on $Pb(Zr_{0.2}, Ti_{0.8})O_3$
Electroceramics XIV, Bucharest, Romania
16-20 June 2014, Talk

123. ***Negrea R F, C Ghica C, Nistor L C, Pintilie L***
Atomic scale STEM and EELS characterization of $BaTiO_3/SrRuO_3/SrTiO_3$ ferroelectric heterostructure
Europhysical Conference on Defects in Insulating Materials (Eurodim 2014), Canterbury, UK
13-19 July 2014, Poster

124. ***Negrea R F, Ghica C, Teodorescu V S, Maraloiu V A, Nistor L C***
HRTEM/STEM characterization of interfaces and strain-related distortions in epitaxial perovskite heterostructures
18th International Microscopy Congress IMC 2014, Praga, Czech Republic
7-12 September 2014, Poster

125. ***Negrila CC, Ghita RV, Logofatu C, Cotirlan-Simionuc C, Frumosu F, Lazarescu MF***
Looking for In based active layer interface on cleaved GaAs(100) surface
14th International Balkan Workshop on Applied Physics and Materials Science, Constanta Romania
2-4 July 2014, Poster

126. ***Negrila CC, Lazarescu MF, Logofatu C, Cotirlan-Simionuc C, Ghita RV, Frumosu F, Trupina L***
XPS analysis of AuGeNi/ cleaved GaAs(110) interface
The 10th International Conference on Physics of Advanced Materials (ICPAM-10), Iasi, Romania
22-28 September 2014, **Poster**

127. ***Nistor L.C, Nistor SV, Ghica D, Joita AC, Pintilie I***
Radiation defects at high radiation doses in silicon detector materials
Europhysical Conference on Defects in Insulating Materials (Eurodim 2014), Canterbury, UK
13-19 July 2014, Poster

128. ***Nistor LC, Nistor SV, Pintilie I***
High resolution transmission electron microscopy (HRTEM) investigations of silicon irradiated with high energy electrons
24th RD50-CERN Workshop, Bucharest, Romania
11-13 June 2014, Talk

129. ***Nistor S V, Ghica D, Joița A C, Radu R, Pintilie I***
Electron Spin Resonance (ESR) investigation of paramagnetic point defects in ^{17}O doped Si-FZ irradiated with 27MeV electrons
24th Workshop RD50 – Radiation Hard Semiconductor Devices for Very High Luminosity Colliders, Bucharest, Romania
11-13 June 2014, Talk

130. ***Nistor S V, Stefan M, Nistor L C, Ghica D, Vlaicu I***
Lattice defects influence on the Mn^{2+} incorporation and magnetic interactions in ZnS quantum dots
Europhysical Conference on Defects in Insulating Materials (Eurodim 2014), Canterbury, UK
13-19 July 2014, Talk

131. *Nita C, Duta L,* ***Stan GE****, Popescu C, Craciun V,* ***Husanu M****, Bita B, Ghisleni R, Himcinschi C, Popescu AC*
DLC hard protective coatings synthetisized by pulsed laser deposition
EMRS Spring Meeting, Lille, France
26-30 May 2014, Talk

132. *Nita C, Axente E, Sima F, Iordache I, Cristescu R, Visan A,* ***Zgura I, Rasoaga OL, Breazu CS, Stanculescu A****, Socol G*
Comparative study on the deposition of biodegradable PCL/PLA blend coatings
EMRS Spring Meeting, Lille, France
26-30 May 2014, Poster

133. *Olaru EA, Căpăț C, Papa F,* ***Frunza L****, Udrea I, Mihăilă E, Bradu C*
Réduction catalytique simultanée des nitrates et des polluants organochlorés en phase aqueuse
Colloque Franco-Roumaine de Chimie Appliquee, Montpellier, France
15-18 septembre 2014, Talk

134. *Oumezzine Ma,* ***Galca AC****, Oumezzine Mo,* ***Pasuk I, Chirila C, Leca A, Kuncser A, Ghica C, Tanase LC, Teodorescu CM, Kuncser V***
Room temperature Giant magnetoresistance in $La_{0.67}Ba_{0.33}Ti_{0.02}Mn_{0.98}O_3$ epilayers
10th International Conference on Physics of Advanced Materials (ICPAM), Iasi, Romania
22-28 September 2014, Talk

135. *Oumezzine Ma,* ***Galca AC****, Oumezzine Mo,* ***Pasuk I, Chirila C, Leca A, Kuncser A, Ghica C, Tanase LC, Teodorescu CM, Kuncser V***
Structural, magnetic and electrical properties of $La_{0.67}Ba_{0.33}Ti_{0.02}Mn_{0.98}O_3$ thin films
Electroceramics XIV, Bucharest, Romania
16–20 June 2014, Talk

136. ***Palade C, Slav A, Lazanu S, Ciurea ML***
Effects produced by bismuth irradiation on high resistivity silicon
PAMS-1, (1st Autumn School on Physics of Advanced Materials), Iasi, Romania
22–28 September 2014, Poster

137. ***Palade C, Lepadatu AM, Stavarache I, Teodorescu VS, Ciurea ML***
Transition in conduction mechanism in GeSi nanostructures
CAS 2014 („37th Int. Semiconductor Conf."), Sinaia, Romania
13–15 October 2014, Talk

138. ***Palade C, Slav A, Lepadatu AM, Teodorescu VS, Ciurea ML***
Charge storage properties of HfO_2/Ge-HfO_2/SiO_2 trilayer structures
CAS 2014 („37th Int. Semiconductor Conf."), Sinaia, Romania
13–15 October 2014, Talk

139. ***Palade C, Lazanu S, Ciurea ML***
Trapping centers in heavy ion irradiated silicon
CAS 2014 („37th Int. Semiconductor Conf."), Sinaia, Romania
13–15 October 2014, Talk

140. ***Pintilie I, Radu R,*** *Fretwurst E, Lindstroem G, Makarenko L,* ***Nistor LC, Nistor SV***
Point and extended defects in silicon induced by electron irradiation – dependence on the particle energy
25th RD50-CERN Workshop, Geneve, Switzerland
18-20 Novenber 2014, Talk

141. ***Pintilie L, Hrib L, Pasuk I, Ghica C, Iuga A, Pintilie I***
General equivalent circuit and polarization controlled interface properties derived from capacitance and impedance measurements performed on epitaxial ferroelectric thin films
Electroceramics XIV, Bucharest, Romania
16–20 June 2014, Talk

142. ***Plugaru N, Filip L***
First-principles electronic and magnetic structures of $BiMn_2O_5$, $GdMn_2O_5$ and $ErMn_2O_5$ under pressure
Symposium X. "Antiferromagnetic spintronics: materials, characterization, functionalities"
E-MRS 2014 Fall Meeting, Warsaw, Poland
15-19 September 2014, Talk

143. *Plugaru R, Sandu T,* ***Plugaru N***
First principles study of the semiconductor to metal transition, dc conductivity and magnetism in (Al, Ti) codoped ZnO
Symposium D: Transparent conducting oxides and related materials, E-MRS 2014 Fall Meeting, Warsaw, Poland
15-19 September 2014, Talk

144. ***Plugaru N, Filip L,*** *Plugaru R*
First-principles study of RMn_2O_5 magnetoelectric multiferroics
Electroceramics XIV Conf., Bucharest, Romania
15-20 June 2014, Poster

145. ***Polosan S***
Electrochemical deposition of organometallic/ polypyrrole composites for OLED applications
14th International Balkan Workshop on Applied Physics, Ovidius University, Constanta, Romania
2-4 July 2014, Talk

146. ***Polosan S***
Electrochemical deposition of organometallic compounds
10th International Conference on Electroluminescence and Optoelectronic Devices (ICEL 10), Koln University, Germany
31 August -03 September 2014, Poster

147. ***Popa AC, Stan GE, Husanu MA, Mercioniu I,*** *Santos LF, Kapoor S, Ferreira JMF*
Bioactivity of bioglass implant coatings in simulated body fluid environments
International Conference on Spectroscopy and Applications (ICSA), Hammamet, Tunisia
2–4 May 2014, Talk

148. *Popescu AC, Duta L, Nita C,* ***Stan GE****, Popescu C,* ***Husanu M****, Bita B, Ghisleni R, Himcinschi C, Surdu A*
Hard DLC protective coatings synthesized by pulsed laser deposition
EMRS Fall Meeting, Warsaw, Poland
15–18 September 2014, Talk

149. ***Popa CL, Ciobanu CS, Iconaru SL,*** *Chapon P, P Le Coustumer,* ***Predoi D***
Characterization and antibacterial activity of samarium doped hydroxyapatite thin films
7th GD Day, Reims, France
11-12 June 2014, Talk

150. ***Popa CL, Ciobanu CS,*** *Petre CC, Motelica-Heino M, Iconaru SL, Jiga G,* ***Predoi D***
Hydroxyapatite with environmental applications
AIP Conference, Ischia, Italy
22-26 June 2014, Poster

151. *Popescu C, Pervolaraki M, Popescu AC,* ***Stan GE, Pasuk I,*** *Iordache (Urzica) I, Athanasopoulos GI, Giapintzakis J*
Gold thin films synthesized by pulsed laser deposition with a picosecond laser source: future sensing platforms
EMRS Spring Meeting, Lille, France
26-30 May 2014, Poster

152. *Popescu-Pelin G, Axente E, Sima F, Iordache I, Nita C, Visan A, Zgura I,* ***Rasoaga OL, Breazu CS, Stanculescu A****, Socol G, Mihailescu IN*
Comparative study on the deposition of polymeric coatings based on PCL/PLGA blends
E-MRS Spring Meeting, Lille, France
26-30 May 2014, Poster

153. ***Preda N, Socol M, Zgura I, Enculescu M, Evanghelidis A, Florica C, Matei E, Enculescu I***
Designing superhydrophobic polymer surface by controlling their morphologies
14th International Balkan Workshop on Applied Physics, Constanta, Romania
2-4 July 2014, Poster

154. ***Preda N, Zgura I, Socol M, Enculescu M, Evanghelidis A, Florica C, Matei E, Enculescu I***
Tunable surface wettabillity of ZnO nanostructured films prepared by wet chemical route
14th International Balkan Workshop on Applied Physics, Constanta, Romania
2-4 July 2014, Poster

155. *Prodan AM,* ***Popa CL****, Stoicea M,* ***Ciobanu CS,*** *Motelica M, Sizaret S,* ***Predoi D***
Characterization and toxicity evaluation of iron oxide in a silica matrix by *in vitro* and *in vivo* assays
ISOS XVII BERLIN 2014 - The 17th International Symposium on Silicon Chemistry, Berlin, Germany
3-8 August 2014, Poster

156. *Prodan AM,* ***Iconaru SL, Popa CL, Predoi D***
In vivo toxicity studies of dextran coated iron oxide nanoparticles
FEBS MEBO 2014, Paris, France
30 August-4 September 2014, Poster

157. ***Radu R,*** *Fretwurst E, Lindstroem G,* ***Nistor LC, Nistor SV, Pintilie I***
Comprehensive investigations of point and cluster radiation induced defects in silicon
RAD 14 – The 2nd International Conference on Radiation and Dosimetry in Various Fields of Research, Nis, Serbia
27-30 May 2014, Talk

158. ***Radu R, Pintilie I,*** *Lindstroem G, Fretwurst E*
Investigation of point and extended defects in electron irradiated silicon – dependence on the particle energy
24th RD50-CERN Workshop, Bucharest, Romania
11-13 June 2014, Talk

159. ***Rasoga OL,*** *Stanculescu F,* ***Stanculescu A, Socol M, Preda N, Breazu CS,*** *Socol G*
Organic heterostructures with improved electrical properties for OLED Applications
E-MRS Spring Meeting, Lille, France
26-30 May 2014, Poster

160. ***Sandu V, Aldica G, Badica P, Kuncser A,*** *Hayasaka Y*
Insertion versus growth of magnetic nanoparticles in MgB_2 superconducting composites
ICMSE-5, 5th International Conference on Manufacturing Science and Engineering, Shanghai, China
19-20 April, 2014, Talk

161. ***Sarbu C***
Phase instability of stainless alloys in low-temperature (LT) gas-atmosphere – a new way for tailoring enhanced surface properties
European Conference „Condensed Matter in Paris – 2014" (joint conference CMD25-JMC14), Université Descartes, Paris, France
24-29 August 2014, Talk

162. ***Sarbu C***
The low-temperature (LT) gas-atmosphere processing of stainless alloys surfaces – a potential new technology for surface properties enhancement
European Symposium on Surface Science, Rome, Italy
26-28 November 2014, Talk

163. *Sava B, Iordanescu R, Feraru I, Elisa M, Vasiliu I, Boroica L,* ***Bartha C, Plapcianu C, Palade P, Valeanu M, Kuncser V,*** *Volceanov A, Stoleriu S*
Optical, thermal and structural properties of iron-doped phosphate glasses
12th European Society of Glass Technology-ESG 2014, Parma, Italy, Book of Abstracts, Special Glass Poster Session -13 SGP, p. 205
21-24 September 2014, Poster

164. ***Schinteie G, Palade P,*** *Iacob V, Vekas L,* ***Kuncser V***
Interparticle interactions in high volume fraction ferrofluids
International Conference on Superconductivity and Magnetism Antalya, Turkey
27 April-2 May 2014, Poster

165. ***Schinteie G, Palade P,*** *Iacob N, Vekas L,* ***Kuncser V***
Magnetic relaxation in ferrofluids with different volume fractions of magnetite
14th International Balcan Workshop on Applied Physics, Constanta, Romania
2-4 July 2014, Poster

166. **Secu CE, Secu M**, Stokker-Cheregi F, Matei A, Dinescu M
Laser processing of composite Yb^{3+}/Er^{3+} co-doped CaF_2 oxyfluoride glass ceramic thin films
International Workshop on Photoluminescence in Rare Earths (PRE'14): Photonic Materials and Devices, San Sebastian, Spain
14-16 May 2014, Poster

167. ***Secu M, Matei E, Secu CE, Sima M,*** *Damian V*
A new X-ray microimaging detector based on Anodise Alumina membrane pores array entrapping $BaFBr:Eu^{2+}$ nanophosphor-SiO_2 hybrid
Electroceramics XIV, Bucharest, Romania
16-20 June 2014, Poster

168. ***Simion CE,*** *Sackmann A,* ***Teodorescu VS,*** *Rusti CF, Piticescu RM,* ***Stănoiu A***
Tuned sensitivity towards H2S and NH3 with Cu doped barium strontium titanate materials
Electroceramics XIV, Bucharest, Romania
16-20 June 2014, Talk

169. *Socol G, Grumezescu V, Nita C, Dorcioman G, Stefan N, Miroiu M,* ***Zgura I, Socol M,*** Visan A, Popescu-Pelin G, Cristescu R, **Rasoga OL, Breazu CS,** ***Stanculescu A***
Deposition and characterization of calcium phosphates/poly(3-hydroxybutyrate-co-3-hydroxyvalerate) biocomposite coatings
E-MRS Spring Meeting, Lille, France
26-30 May 2014, Poster

170. *Socol G, Stefan N, Craciun D, Craciun V,* ***Galca AC, Trinca LM,*** *Cristea D, Stoicanescu M, Munteanu D, Lambers E, Olah N, Balazsi K*
Characteristics of nanostructured thin SiC films grown by pulsed laser deposition
EMRS Fall Meeting, Warsaw, Poland
15–18 September 2014, Poster

171. ***Socol M, Preda N, Zgura I, Enculescu M, Evanghelidis A, Florica C, Matei E, Enculescu I***
Designing superhydrophobic polymer surfaces by controlling their morphologies
14th International Balkan Workshop on Applied Physics, Constanta, Romania
2-4 July 2014, Poster

172. ***Socol M, Breazu CS, Rasoga OL, Stanculescu A, Preda N,*** *Stanculescu F, Socol G, Craciun V, Stoicanescu M*
Organic photovoltaic structures based on zinc and magnesium phthalocyanine thin films
E-MRS Spring Meeting, Lille, France
26-30 May 2014, Poster

173. ***Socol M, Preda N, Rasoga OL, Stanculescu A, Breazu CS,*** *Stanculescu F, Socol G*
MAPLE deposition of organic structures on IZO flexible substrates
E-MRS Spring Meeting, Lille, France
26-30 May 2014, Poster

174. *Soprony M, Nita C, Grumezescu V,* ***Rasoga OL,*** *Stefan N,* ***Breazu CS, Socol M, Zgura I,*** *Visan A, Popescu-Pelin G,* ***Stanculescu A,*** *Mihailescu IN, Socol G*
Deposition and characterization of polyethylene glycol/poly(3-hydroxybutyrate-co-3-hydroxyvalerate) blends,
E-MRS Spring Meeting, Lille, France
May 2014, Poster

175. ***Slav A, Palade C, Lepadatu AM, Teodorescu VS, Ciurea ML***
Nanostructured Ge-TiO_2 films with near-infrared photoconductive properties
NanoSEA 2014, Marsilia, France
7–11 July 2014, Talk

176. ***Sofronie M, Crisan AD, Tolea F, Enculescu M, Valeanu M***
Magneto-structural properties of Fe-Pd-X (X= Mn, Ga, Ti) ribbons
10th European Conference on Magnetic Sensors and Actuators, Vienna, Austria,
6 – 9 July 2014, Poster

177. *Stanculescu F,* ***Rasoga OL, Socol M, Breazu CS,*** *Albu AM, Socol G, Girtan M,* ***Stanculescu A***
Heterostructures based on maleic anhydride-aniline derivatives monomers thin films for photovoltaic applications,
E-MRS Spring Meeting, Lille, France
26-30 May 2014, Poster

178. ***Stanculescu A,*** *Socol G, Catargiu AM, Vacareanu L,* ***Socol M, Rasoga OL, Breazu CS, Preda N,*** *Stanculescu F*
MAPLE prepared heterostructures with arylene vinylene polymer:fullerene active layer for photovoltaic applications
E-MRS Spring Meeting, Lille, France
26-30 May 2014, Poster

179. ***Stanculescu A,*** *Socol G, Vacareanu L,* ***Socol M, Rosoga OL, Breazu CS,*** *Girtan M, Stanculescu F*
Organic flexible heterostructures with Al:ZnO transparent conductor electrode for photovolataic applications
5th International Symposium on Transparent Conductor Materials, TCM 2014, Creta, Greece
12-17 October 2014, Poster

180. ***Stefan M, Ghica D, Nistor S V, Ghica C, Vlaicu I***
EPR probing with Mn^{2+} ions of ZnO nanostructures
Europhysical Conference on Defects in Insulating Materials (Eurodim 2014), Canterbury, UK
13-19 July 2014, Poster

181. *Stefan N, Miroiu FM, Visan A,* ***Rasoga OL, Zgura I,*** *Nita C,* ***Stanculescu A,*** *Socol G*
MAPLE deposition of biodegradable silk fibroin/poly(sebacic acid) diacetoxy terminated composite coatings
E-MRS Spring Meeting, Lille, France
26-30 May 2014, Poster

182. *Stefan N, Miroiu FM, Visan A,* ***Rasoga OL, Zgura I, Stanculescu A****, Cristescu R, Socol G*
Biodegradable silk fibroin/poly(sebacic acid) diacetoxy terminated composite coatings obtained by matrix assisted pulsed laser evaporation
International Conference "Modern Laser Applications" 4th Edition INDLAS 2014, Bran, Romania
19-23 May 2014, Poster

183. ***Teodorescu VS, Ghica C, Maraloiu AV, Vlaicu AM, Kuncser AC, Lepadatu AM, Stavarache I, Ciurea M L,*** *Scarisoreanu N D, Andrei A, Ion V, Dinescu M*
Ge nanoparticle formation in amorphous TiGeO thin films by pulse laser annealing at low fluencies
E-MRS 2014, Symposium J „Laser interaction with advanced materials:fundamentals and applications", Lille, France
26-30 May 2014, Poster

184. ***Teodorescu VS, Ghica C, Maraloiu AV, Kuncser AC, Dinescu M****, Scarisoreanu ND, Udrea M, Zaharescu M, Blanchin MG*
Cubic phase formation by excimer laser pulse annealing of dried amorphous HfO2 sol-gel films
Electroceramics XIV, Bucharest, Romania
16-20 June 2014, Poster

185. ***Teodorescu VS, Ghica C, Maraloiu AV, Kuncser AC****, Scarisoreanu ND, Dinescu M,* ***Ciurea ML, Stavarache I, Lepadatu AM***
Nanostructuring of GeTiO amorphous film by pulsed laser irradiation
5th International Conference on Nanostructures Self-Assembly NanoSEA 2014, Marseille, France
7-11 July 2014, Talk

186. ***Trinca LM, Hrib LM, Galca AC***
Non-invasive characterization of Al – doped ZnO based transparent conductive oxides
TIM14, Timisoara, Romania
20-22 November 2014, Talk

187. ***Trinca LM, Galca AC, Chirila C, Besleaga C, Pintilie L***
ZnO-based structures: from powders to high quality thin films
14th International Balkan Workshop on Applied Physics, Constanta, Romania
2-4 July 2014, Poster

188. ***Trinca LM, Galca AC, Chirila FC, Besleaga C, Boni AG, Pintilie L***
Transparent oxides for electronic applications
1st Autumn School on Physics of Advanced Materials, Iasi, Romania
22-28 September 2014, Poster

189. ***Trinca LM, Stancu V, Galca AC, Pintilie L***
ZnO-based homo and hetero-structures – assembling and characterization
Electroceramics XIV, Bucharest, Romania
16–20 June 2014, Poster

190. ***Trupina L, Nedelcu L, Negrila CC, Cioangher M***
Highly textured iridium thin films grown on MgO and Si substrates
14th International Balkan Workshop on Applied Physics, Constanta, Romania
2-4 July 2014, Poster

191. ***Tolea F, Sofronie M, Crisan AD, Valeanu M***
Magnetic and transport properties of Ni-Fe-Ga-X (X=Al, Nd) Heusler-type alloys
7th International Conference on Materials Science and Condensed Matter Physics (MSCMP 2014), Chisinau, Republic of Moldova
11-14 September 2014, Poster

192. ***Tolea F, Sofronie M, Crisan AD, Valeanu M***
Composition and thermal treatments effects in off-stoichiometric Heusler alloys NiNdFeGa
International Conference on Martensitic Transformations ICOMAT 2014, Bilbao, Spain
6-11 July 2014, Poster

193. ***Tolea F, Sofronie M, Crisan AD, Valeanu M***
The influence of the secondary FCC phase on the transport properties in Ni-Fe-Ga - based heusler alloys
Materials Science Engineering (MSE) 2014, Darmstadt, Germany
23-25 September 2014, Poster

194. *Visan A, Erakovic S, Jankovic A, Ristoscu C, Duta L, Mihailescu (Serban) N,* ***Stan GE, Socol M****, Iordache O, Dumitrescu I, Luculescu CR, Mihailescu IN, Janackovic Dj, Miskovic-Stankovic V*
Pure and doped hydroxyapatite thin films synthesized by pulsed laser deposition for metal implant coatings
5th ICSP International Conference, Orastie, Romania
23–26 September 2014, Talk

195. *Visan A, Erakovic S, Jankovic A, Ristoscu C, Duta L, Mihailescu (Serban) N,* ***Stan GE, Socol M****, Iordache O, Dumitrescu I, Luculescu CR, Mihailescu IN, Janackovic Dj, Miskovic-Stankovic V*
Fabrication and characterizations of pure and doped hydroxyapatite coatings for medical applications
4th International Colloquium 'Physics of Materials' - PM-4, Bucharest, Romania
13–16 November 2014, Poster

196. *Visan A, Grossin D, Stefan N, Duta L, Miroiu FM,* ***Stan GE****, Sopronyi M, Luculescu C, Freche M, Marsan O, Charvilat C, Ciuca S, Mihailescu IN*
Matrix Assisted Pulsed Laser Evaporation synthesis of biomimetic nanocrystalline apatite coatings with applications in medicine
4th Edition of the Modern Laser Applications International Conference, Bran, Romania
19–23 May 2014, Talk

197. *Visan A, Grossin D, Stefan N, Duta L, Miroiu FM,* ***Stan GE****, Sopronyi M, Luculescu C, Freche M, Marsan O, Charvilat C, Ciuca S, Mihailescu IN*
Matrix Assisted Pulsed Laser Evaporation synthesis of biomimetic nanocrystalline apatite coatings for biomedical applications
EMRS Spring Meeting, Lille, France
26–30 May 2014, Poster

198. *Visan A, Miroiu M, Stefan N, Nita C, Dorcioman G,* ***Zgura I, Rasoaga OL, Breazu CS, Stanculescu A****, Cristescu R, Socol G, Mihailescu IN*
Fabrication of biodegradable polycaprolactone -polyethylene glycol composite coatings by Matrix Assisted Pulsed Laser Evaporation and Dip Coatings
E-MRS Spring Meeting, Lille, France
26-30 May 2014, Poster

199. *Visan A, Miroiu M, Stefan N, Nita C, Dorcioman G,* ***Zgura I, Rasoaga OL, Breazu CS, Stanculescu A****, Cristescu R, Socol G, Mihailescu IN*
Matrix Assisted Pulsed Laser Evaporation vs. Dip Coating techniques for fabrication of biodegradable polymer thin films with medical applications
International Conference "MODERN LASER APPLICATIONS" 4th Edition INDLAS 2014, Bran, Romania
19-23 May 2014, Poster

200. ***Vlaicu AM, Mercioniu I, Ghica C****, Manoliu V, Ionescu G, Mihailescu AD*
Oxidation dynamics in APS and HVAF deposited Amdry997alloys
ECI Conferences: Thermal Barrier Coatings IV, Irsee, Germany
22–27 June 2014, Poster

201. ***Vlaicu AM, Ghica C, Mercioniu I****, Manoliu V, Mihailescu AD, Ionescu G, Trusca I*
APS and HVAF deposited Amdry 997 bond layers for Thermal Barrier Coatings: a comparative study of oxidation processes by XRD, SEM, and EDS
International Conference of Aerospace Sciences “AEROSPATIAL 2014”, Bucharest, Romania
18-19 September 2014, Talk

202. ***Zgura I, Cotorobai F, Frunza S, Frunza L***
Wettability measurements of functionalized textile materials as a tool to evaluate the special properties
International Colloquium “Physics of Materials” (PM-4), University Politehnica of Bucharest,
13-14 November 2014, Poster

203. ***Zgura I, Frunza L****, Pasuk I, Diamandescu L,* ***Ganea CP****, Bradu C, Udrea I*
X-ray diffraction technique applied to supported (bi)metallic catalytic systems as a part of complex characterization for nanostructured materials
6th International Workshop "Advanced optical and X-ray characterization techniques of multifunctional materials for information and communication technologies, health and renewable energy applications”, Bucharest, Romania
10-12 September 2014, Poster

204. ***Zgura I, Frunza S, Frunza L, Enculescu M, Florica C, Cotorobai F***
Deposition of titanium dioxide layers upon textile materials: Checking the adherence by ultra-sonication
14th International Balkan Workshop on Applied Physics, Constanta, Romania
2-4 July 2014, Poster

205. ***Zgura I, Preda N, Socol M, Enculescu M, Evanghelidis A, Florica C, Matei E, Enculescu I***
Tunable surface wettability of ZnO nanostructured films prepared by wet chemical route
14th International Balkan Workshop on Applied Physics, Constanta, Romania
2-4 July 2014, Poster

Invited Lectures

1. ***Apostol NG, Popescu DG, Huşanu MA, Ştoflea LE, Teodorescu CM***
   Photoemission spectromicroscopy of lead zirco-titanate (001) and (111) thin films
   International Conference on Physics of Advanced Materials (ICPAM-10), Iaşi, Romania
   21-26 September 2014, Invited
2. ***Badica P***
   MgB_2 based composites
   ICCE-22, Malta
   13-19 July 2014, Invited
3. ***Badica P***
   From HTS thin films growth to single crystal objects growth
   Science and Applications of Thin Films, Conference & Exhibition (SATF 2014), Cesme, Turkey
   5-19 September 2014, Invited
4. ***Banciu MG, Nedelcu L,*** *Yamamoto K, Tsuzuki S, Tani M*
   THz TDS investigations on dielectrics for microwave applications
   The 5th International Workshop on Far-Infrared Technologies, University of Fukui, Japan
   5-7 March 2014, Invited
5. ***Ciurea ML***
   Stress influenced trapping processes in Si based multi-quantum well structures and heavy ions implanted Si
   ICCMSE 2014 ("10th International Conference of Computational Methods in Sciences and Engineering"), Atena, Greece
   4-7 April 2014, Invited
6. ***Ciurea ML***
   Photosensitive Ge-TiO_2 films with tuneable detection wavelengths from VIS to NIR
   ICPAM-10 („10th Int. Conf. on Physics of Advanced Materials"), Iasi, Romania
   22–28 September 2014, Invited
7. ***Ciurea ML***
   Photosensitive Ge-SiO_2 and Ge-TiO_2 films for environmental and biomedical applications
   PM-4 (4th Int. Colloquium 'Physics of Materials), Bucharest, Romania
   13–14 November 2014, Invited
8. ***Costas A, Florica C, Matei E,*** *Toimil Molares ME,* ***Kuncser V, Enculescu I***
   Magnetic nanowires with potential applications in biosensing
   EMRS-Fall Meeting, Warsaw, Poland
   15-18 September 2014, Invited
9. ***Crisan O***
   Multi-purpose cluster aggregation approach for surface-functionalized nanoclusters and metal-oxide core-shell bio-conjugated nanostructures
   EMRS 2014 Fall Meeting, Symposium U: U: Bioinspired and Biointegrated Materials as New Frontiers Nanomaterials, Warsaw, Poland
   15-19 September 2014, Invited

10. ***Frunza L, Frunza S**, Brás AR, Dionisio M, Schönhals A*
    Surface layers of cyanobiphenyls in composites revealed by broadband dielectric spectroscopy and FTIR
    International Colloquium "Physics of Materials" (PM-4), University Politehnica of Bucharest, Romania
    13-14 November 2014, Invited

11. ***Galca AC***
    Extensive X-ray diffraction analyses of polycrystalline textured thin films and epilayers
    Forth Tunisian Crystallographic Meeting (TCM4-2014), Djerba, Tunisia
    2-5 November 2014, Invited

12. ***Kuncser V, Schinteie G**, Iacob V*
    Specific magnetic response of functionalized Fe oxide nanoparticles in relation to bio-medical applications
    4th International Conference on Superconductivity and Magnetism, Antalya, Turkey
    27 April – 3 May 2014, Invited

13. ***Miclea CF***
    Unconventional vortex pinning in non-centrosymmetric superconductors
    Advanced workshop in solar energy conversion and nanophysics, Magurele, Romania
    1-3 September 2014, Invited

14. ***Miu L***
    DC magnetization relaxation and the AC susceptibility of YBCO films with strong pinning
    4th International Conference on Superconductivity and Magnetism, Antalya, Turkey
    27 April – 3 May 2014, Invited

15. ***Miu L***
    Vortex dynamics in striped superconductors
    ICCE-22, Malta
    13-19 July 2014, Invited

16. ***Pintilie I***
    Interface and bulk radiation induced effects in Si-based sensors
    TIM14, Timisoara, Romania
    19-22 November 2014, Plenary lecture

17. ***Pintilie I***
    Imperfections in crystal patterns: from atomic-scale defects to modern electronic devices
    Workshop "On Form and Pattern" Humboldt Kolleg, Bucharest, Romania
    29 – 31 May 2014, Invited

18. ***Pintilie L***
    Photovoltaic and Pyroelectric properties of ferroelectric thin films
    EMRS Fall Meeting, Warsaw, Poland
    15–18 September 2014, Invited

19. ***Pintilie L***
    Photovoltaic and Pyroelectric properties of ferroelectric thin films and multilayers
    TIM14, Timisoara, Romania
    19-22 November 2014, Invited

20. ***Pintilie L, Pintilie I, Teodorescu CM, Ghica C, Hrib L, Chirila C, Trupina L, Boni AG, Iuga A, Negrea R, Pasuk I, Botea M, Filip LD, Kuncser V, Schinteie G***
Interfaces in epitaxial structures based on oxide ferroelectrics
Shechtman international symposium, Cancun, Mexic
29 June -4 July 2014, Invited

21. ***Popescu M, Sava F, Lőrinczi A, Velea A, Simandan ID, Badica P, Burdusel M, Galca AC, Matei E, Preda N, Secu M,*** *Socol G, Jipa F, Zamfirescu M, Balan A*
Ceramics and amorphous thin films based on gallium sulfide doped by rare-earth sulphides
6th International Conference on Optical, Optoelectronic and Photonic Materials and Applications – ICOOPMA 2014, Leeds, UK
27 July – 1 August 2014, Invited

22. *Socol G, Axente E, Hermann J,* ***Galca AC,*** *Pantelica D, Ionescu P, Becherescu N, Martin C, Craciun V*
On the metrology of amorphous transparent and conductive oxides grown by combinatorial pulsed laser deposition
International Conference on Electronic Materials 2014 (IUMRS-ICEM 2014), Taipei, Taiwan
10-14 June 2014, Invited

23. ***Ştoflea LE, Tănase LC, Popescu DG, Huşanu MA, Apostol NG,*** *Barinov A,* ***Teodorescu CM***
Photoelectron spectroscopy and spectromicroscopy on ferroelectric single crystal layers
TIM 14 - Physics without frontiers, Timişoara, Romania
20-22 November 2014, Invited

24. ***Teodorescu CM***
Band bending analysis by X-ray photoelectron spectroscopy in ferroelectric heterostructures
EMN Spring Meeting, Las Vegas, USA
27 February – 2 March 2014, Invited

25. ***Teodorescu CM***
Chemistry and photochemistry at ferroelectric surfaces
14th International Balkan Workshop on Applied Physics, Constanța, Romania
2-4 July 2014, Invited

26. ***Teodorescu VS***
Nanostructuring of thin amorphous films by laser pulse annealing
6th International Workshop „Advanced optical and x-ray characterisation techniques of multifunctional materials for information and communication technologies, health and renewable energy applications", Bucharest, Romania
10-12 September 2014, Invited

Selected Results

Condensed Matter Physics at Mesoscale

Electric field induced processes in relaxor ferroelectrics

I. Pintilie, A. Iuga and L. Pintilie
in cooperation with
M. Tyunina and M. S. Stratulat
Microelectronics and Materials Physics Laboratories, University of Oulu, Oulunyliopisto, Finland

Relaxors are most challenging through their outstanding properties combined with our lack of understanding of their intrinsic mechanisms. Their giant dielectric, piezo-electric, piro-electric, piezo-elastic, photo-voltaic, electro-caloric constants escape an adequate explanation. These premises are sufficient to introduce such modern materials in the top of the researching list in solid-state physics, envisaging their immediate application in the various devices presently using classic ferroelectric materials. In this sense our attention was focused on some appealing materials in this class, as: cube-on-cube-type epitaxial film of relaxor ferro-electric (FE) $PbMg_{1/3}Nb_{2/3}O_3$ grown on (001) MgO substrate [1], cube-on-cube-type epitaxial $PbSc_{1/2}Nb_{1/2}O_3$ film grown on $La_{1/2}Sr_{1/2}CoO_3$ /MgO (001) [2] and epitaxial films of $PbMg_{1/3}Nb_{2/3}O_3$ and $PbSc_{1/2}Nb_{1/2}O_3$ [3]. When dealing with relaxors, the crucial test is the behavior of their dielectric constant as temperature varies. The well known Curie-Weiss law is substituted by the Vogel-Fulcher law which predicts a much broader peak at the phase-transition temperature.

The temperature dependence of the real part of the dielectric permittivity ε is inspected using zero-field cooling in order to verify relaxor behavior in the PMN film [Fig. 1(a)]. The imaginary part of the permittivity is usually analyzed in bulk RFE samples. However, the impedance of the thin-film capacitors depends on resistances of both the PMN film and the oxide film serving as a bottom electrode. The resistances are not known exactly. This makes it impossible to determine and analyze accurately the imaginary part of the permittivity in the PMN film [4, 5]. The results in Fig. 1 show that the studied PMN film is RFE. In order to quantitatively characterize the dielectric behavior, an exponential fit has been performed.

The capacitance–voltage (C-V_{dc}) charateristics obtained by sweeping the biasing dc voltage V_{dc} at a rate of 1V/s exhibit negligible hysteresis in a broad range of temperatures both below and above T_m, including high temperatures (Fig. 2) [6].

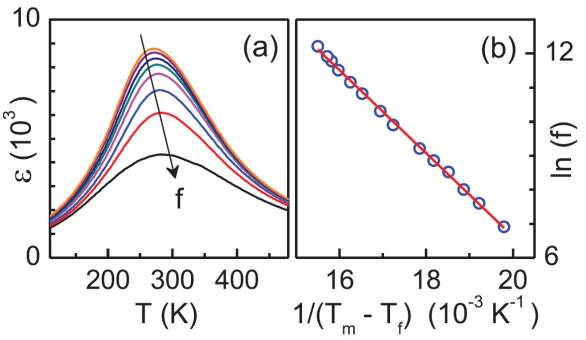

Fig. 1. RFE behavior in PMN film. (a) The real part of the dielectric permittivity ε as a function of temperature T at frequencies f = 1, 2, 5, 10, 20, 50, 100, and 200 kHz. The arrow shows the direction of frequency increase. (b) Relationship between the temperatures T_m of the dielectric peaks and the measurement frequencies. Line shows the Vogel-Fulcher fit.

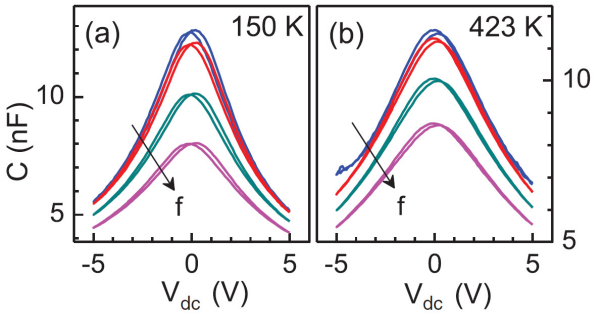

Fig. 2. Capacitance C as a function of dc biasing voltage V_{dc} at temperature T = 150 K (a) and 423 K (b). The frequency of the probing ac voltage is f = 1, 10, 100, and 1000 kHz.

The voltage V_{0C} corresponding to the maximum capacitance is close to zero and independent of the probing *ac* frequency.

The apparent decrease of the capacitance C with increasing frequency is mainly due to contribution of the resistance of the thin-film oxide electrodes to the measured impedance [5].

Arrows show direction of frequency increase. As shown before, the observed minor hysteresis can be ascribed to a relatively slow relaxation of an

internal electric field and not to FE state in thin films [5]. The similarity of the C-V_{dc} curves recorded at high temperatures, $T > T_m$, and those obtained at low temperatures, 150 K < T <T_m, implies that the biasing dc electric field does not induce any phase transitions in the PMN film at T>150 K. The butterfly-type dielectric hysteresis is observed in the PMN film at very low temperatures T<100K only (Fig. 3). The voltages V_{0C} of the capacitance maxima increase steeply on cooling below 100 K. The voltages V_{0C} in the (001) PMN film may be compared to a threshold field of the R-to-FE transformation in the (100) PMN crystal. The behavior of $V_{0C}(T)$ in the film agrees qualitatively with the field-temperature phase diagram obtained from the polarization hysteresis in the (100) PMN crystal [7]. However, compared to the crystal, the V_{0C} – T line in the film is shifted to lower temperatures by more than 100 K.

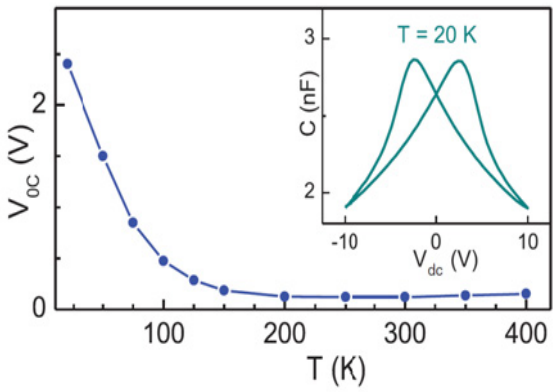

Fig. 3. The voltage V_{0C} extracted from the C-V_{dc} curves as a function of temperature. The butterfly-type C-V_{dc} curve recorded at T = 20 K is shown in the inset.

The dynamic polarization–voltage (P-V) and current voltage (I-V) loops were recorded at different temperatures using frequency f = 1 kHz and maximum voltage Vm = 15 V. The hysteresis in polarization and current is observed at all temperatures (details in Ref. [1]). The density of leakage current is small, about (5–8) x 10^2 A/m^2. The current peaks are detected at all temperatures, including the temperature as high as 475 K. The P-V loops are slim and sloped at high temperatures, but they acquire more FE-looking shape on cooling. Importantly, the P-V loops remain sloped, and the current peaks in the I-V loops remain very broad on cooling to the temperature as low as 20 K. These features make the loops in the PMN film clearly different from the dynamic loops in epitaxial films of normal FE-s and from the loops in PMN crystals [8].

Compared to crystals, the low-temperature R state is more stable in the PMN film. The robustness of the R state to electric field may be related to a spatial anisotropy of the dipolar system in the (001) epitaxial film. In contrast to spatially three-dimensional random orientations and interactions of the dipoles in bulk RFE, the dipoles are oriented along the out-of-plane direction in the film. Moreover, the strong epitaxial coupling of the film to the thick rigid substrate is likely to limit deformation of the film in directions other than the out-of-plane direction. However, such a hypothesis is rather speculative and requires theoretical analysis.

NIMP researchers acknowledge financial support from PNII 72-153/2008, 12-101/2008, PCCE ID 76, RU-TE-2011-3-0016 and Core Program PN09-45.

References

[1]. M. Tyunina, I. Pintilie, A. Iuga, and L. Pintilie, PHYS. REV B **00**, 004100 (2014), *http://dx.doi.org/10.1103/PhysRevB.00.004100*

[2]. M Tyunina, I Pintilie, A Iuga, M S Stratulat and L Pintilie. Phys.: Condens. Matter **26** (2014) 325901 (7pp), *http://dx.doi.org/10.1088/0953-8984/26/32/325901*

[3]. M. Tyunina, I. Pintilie, J. Levoska and L. Pintilie, Phase Transitions, 2014, *http://dx.doi.org/10.1080/01411594.2014.961151*

[4]. M. Tyunina,M. Plekh, and J. Levoska, Phys. Rev. B **79**, 054105 (2009).

[5]. M. Tyunina, M. Plekh, M. Antonova, and A. Kalvane, Phys. Rev. B **84**, 224105 (2011).

[6]. M. Tyunina, J. Levoska, and I. Jaakola, Phys. Rev. B **74**, 104112 (2006).

[7]. X. Zhao,W. Qu, X. Tan, A. A. Bokov, and Z.-G. Ye, Phys. Rev. B **75**, 104106 (2007).

[8]. S. M. Yang, J. Y. Jo, T. H. Kim, J.-G. Yoon, T. K. Song, H. N. Lee, Z.Marton, S. Park, Y. Jo, and T. W. Noh, Phys. Rev. B **82**, 174125 (2010).

Polarization-Control of the electrical properties in Epitaxial Ferroelectric Thin Films

I. Pintilie, C. M. Teodorescu, C. Ghica, C. Chirila, A. G. Boni, L. Hrib, I. Pasuk, R. Damian, N. Apostol, L.Pintilie

A complex study regarding the role of the electrode interfaces on the electric properties of ferroelectric capacitors based on $Pb(Zr,Ti)O_3$ (PZT) epitaxial thin films was performed, including several investigation techniques: high resolution X-ray diffraction (HR-XRD); high resolution transmission electron microscopy (HR-TEM); scanning transmission electron microscopy (STEM); X-ray photoelectron spectroscopy (XPS); macroscopic electric measurements at different temperatures (hysteresis loop; current-voltage (I-V), capacitance-voltage (C-V), capacitance-frequency (C-f) characteristics). The samples were high quality epitaxial films grown on bottom $SrRuO_3$ (SRO) electrodes and having different metals or conducting oxides as top contacts: Pt, Au, Cu, Al, SRO.

From the electrical measurements it was observed that the macroscopic quantities such as coercive voltage, leakage current, dielectric constant are affected by the change in the metal of the top electrode (see Fig. 1). Nevertheless, the value of the ferroelectric polarization remains the same, in agreement with the fact that this a property of the ferroelectric film itself. The analysis of the I-V characteristics have revealed the fact that the height of the potential barrier at the electrode-ferroelectric interface does not depends on the work function of the metals used as contacts, being in the range of 0.1-0.3 eV for all the materials mentioned above. This value is similar to the band bending obtained from XPS investigations performed during the deposition of the top contact (more details in Ref. 1).

Very interesting aspects were revealed by the TEM investigations of the electrode-ferroelectric interface. It was found that noble metals such as Au or Pt does not wet the surface of the ferroelectric layer, with the mention that epitaxial PZT grows on SRO with preferred UP orientation (polarization pointing upward). Apparently, on a surface charged with positive polarization charges the Au and Pt have the tendency to form nano-spheres, as can be seen in Fig. 2. On the other hand Cu forms a continuous layer on the epitaxial PZT, with traces of Cu oxide at the interface (details in supplementary material of Ref. 1).

Further on it was found that there is a clear control of the electronic properties of the electrode-ferroelectric interface by the polarization bound charges.

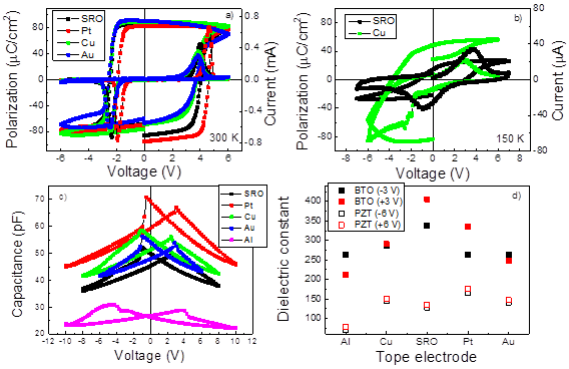

***Fig. 1** (a) Hysteresis loops, at room temperature, for PZT layer with top Cu, Au, Pt, and SRO as top contacts; (b) hysteresis loops at 150 K for BTO layer with top SRO and Cu contacts; (c) C–V characteristics for PZT with top Cu, Au, Pt, SRO, and Al contacts; (d) dielectric constants, for different top metal electrodes, calculated from the capacitance measured at voltages where the ferroelectric polarization is saturated.*

This fact was revealed not only by the fact that the height of the potential barrier is not depending on the metal electrode work function, but also by the fact that the position of the Fermi level is about the same (close to the mid-gap), the polarization values are the same, and the frequency dependence of capacitance is similar for different top contacts (see fig. 3). However, there are some differences in the value of the dielectric constant, which are attributed to the

different interface states for different metals used as top contacts.

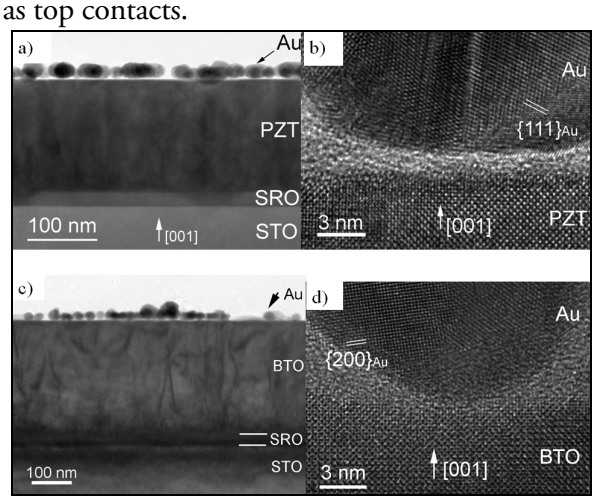

Fig. 2 *a) Low magnification TEM image of the Au/PZT/SRO/STO sampl; b). HRTEM image at the Au-PZT interface; c) Low magnification TEM image of the Au/BTO/SRO/STO sample; d) HRTEM image at the Au-BTO interface.*

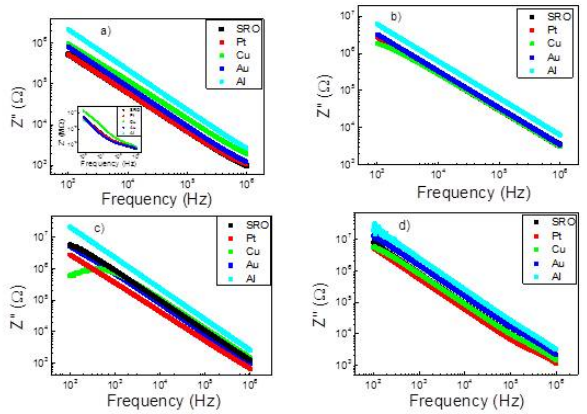

Fig. 3 *The frequency dependence of the imaginary part of the complex impedance of a ferroelectric film deposited on STO substrates with different orientation: a) BTO grown on STO(001); b) PZT grown on STO(001); c) BTO grown on STO(111); d) PZT grown on STO(111).The inset shows the frequency dependence of the real part of the complex impedance for BTO on STO(001).*

All the experimental results support the hypothesis that a Schottky-type contact is forming at the electrode-ferroelectric interface, but the properties of this contact are controlled by the magnitude and orientation of the ferroelectric polarization. A general equivalent circuit was developed for the ferroelectric capacitor, including four main elements: a voltage dependent capacitance associated to the Schottky-type contacts at the electrode interfaces; a resistance associated to the top and bottom electrodes; a capacitance and a conductance associated to the ferroelectric volume of the capacitor (see Fig. 4, with details in Ref. 2). This equivalent circuit simulates well the imaginary part of the dielectric constant, but fails to simulate the real part at low frequencies because the contribution of the trapping levels was not included.

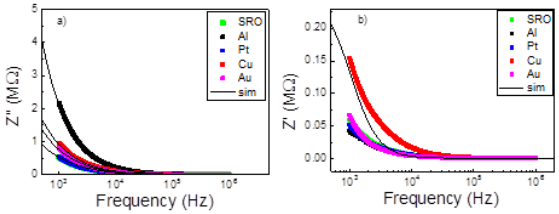

Fig. 4 *Frequency dependence of imaginary (a) and real (b) parts of the complex impedance for the case of the BTO films with bottom SRO electrode and different metals as top contacts. The marker is for experimental data and the line is simulation using the equations (2') and (2").*

In conclusion, it was shown that the macroscopic electrical properties of epitaxial ferroelectric thin films are controlled by electrode interfaces. In turn, the electronic properties of the electrode interfaces are controlled by the ferroelectric polarization.

Funding from Idea-Complex Research Grant PN-II-ID-PCCE-2011-2-0006 (contract nr. 3/2012).

References

[1] I. Pintilie, C. M. Teodorescu, C. Ghica, C. Chirila, A. G. Boni, L. Hrib, I. Pasuk, R. Negrea, N. Apostol, and L. Pintilie, "Polarization-Control of the Potential Barrier at the Electrode Interfaces in Epitaxial Ferroelectric Thin Films ACS Appl. Mater. Interfaces **6**, 2929–2939 (2014)

[2] L. Pintilie, L. Hrib, I. Pasuk, C. Ghica, A. Iuga, and I. Pintilie, "General equivalent circuit derived from capacitance and impedance measurements performed on epitaxial ferroelectric thin films", Journal of Applied Physics **116**, 044108 (2014).

Enhancement of pyroelectric signal by continuous ultraviolet illumination of epitaxial $Pb(Zr_{0.2}Ti_{0.8})O_3$ films

L. Pintilie, M. Botea, A. Iuga, V. Stancu, I. Pintilie

Pyroelectric and photovoltaic properties of epitaxial $Pb(Zr,Ti)O_3$ (PZT) thin films were investigated. It is known that ferroelectrics are also pyroelectrics, meaning that the ferroelectric polarization varies with the temperature (pyroelectric effect). The rate of variation is known as pyroelectric coefficient. The pyroelectric effect is used for the detection of the infrared (IR) radiation, which has wavelengths over 700 nm. Pyroelectric IR detectors can work in the voltage or current modes and are usually manufactured from bulk crystals like $LiNbO_3$ or ceramics like PZT. Recently it was found that epitaxial thin films can exhibit very large values of the pyroelectric coefficient, about 10 times larger than for bulk ceramics [1]. On the other hand it was shown that epitaxial PZT thin films presents interesting photovoltaic properties in the ultraviolet (UV) part of the electromagnetic spectrum, in the 200-400 nm wavelengths range [2]. Here it is shown that the pyroelectric signal can be considerably enhanced (more than two times) by continuous UV illumination. The experimental set up is presented in fig. 1 (details in Ref. 3).

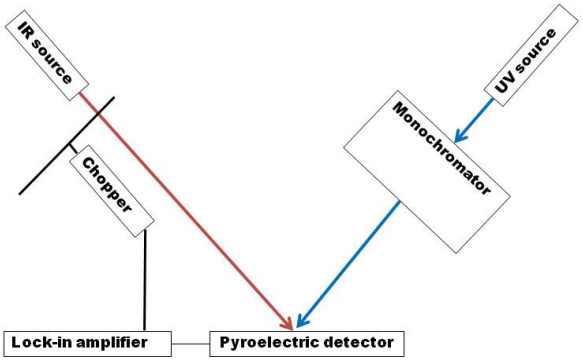

FIG. 1. *The experimental set-up used for simultaneous illumination with monochromatic continuous UV light and modulated IR radiation.*

A laser diode of 800 nm was used as an IR source, in conjunction with a mechanical chopper that modulates the IR beam incident on the surface of the active pyroelectric element working in the voltage mode. The UV light was shed on the surface of the pyroelectric element using a grating monochromator in conjunction with a Xe lamp. It was found that simultaneous illumination with modulated IR and continuous UV leads to an increase of the pyroelectric signal at low modulation frequencies (see Fig. 2). The signal in the voltage mode is given by:

$$S = \frac{\omega \eta p A P_{inc}}{2 g_H G_e (1+\omega^2 \tau_T^2)^{1/2} (1+\omega^2 \tau_e^2)^{1/2}} \qquad (1)$$

Here ω is the pulsation of the IR radiation incident on the pyroelectric element radiation ($\omega=2\pi f$, with f being the chopping frequency of the IR radiation), P_{inc} is the incident power on the active element, η is the emissivity of the front electrode (exposed to IR radiation), p is the pyroelectric coefficient, A is the area of the top electrode, g_H is the heat loss at the top surface (g_H is estimated as $4\sigma T_0^3$, where σ is the Stefan-Boltzmann constant and T_0 is the ambient temperature (298 K)), G_e is the electric conductance, τ_T is the thermal time constant (including the effect of the substrate), and τ_e is the electrical time constant ($\tau_e=C_e/G_e$, with C_e being the capacitance of the pyroelectric element).

If $(\omega\tau_e)^2>>1$ then the pyroelectric voltage S will be given by:

$$S = \frac{\eta p A P_{inc}}{2 g_H G_e \omega \tau_T \tau_e} = \frac{\eta p d P_{inc}}{2 g_H \tau_T \varepsilon_0 \varepsilon_s \omega} \qquad (2)$$

Here C_e was replaced with $\varepsilon_0\varepsilon_s A/d$, where ε_0 is the vacuum permittivity, ε_s is the static dielectric constant and d is the thickness of the ferroelectric film. Equation (2) shows that at high frequencies the pyroelectric voltage depends linearly on $1/\omega$, as presented in the inset of Fig. 2.

One can see in Fig. 2 that the maximum enhancement is obtained at a wavelength of

about 300 nm. This is close to the wavelength where the short-circuit current of the photovoltaic effect has its maximum value (see Fig. 3).

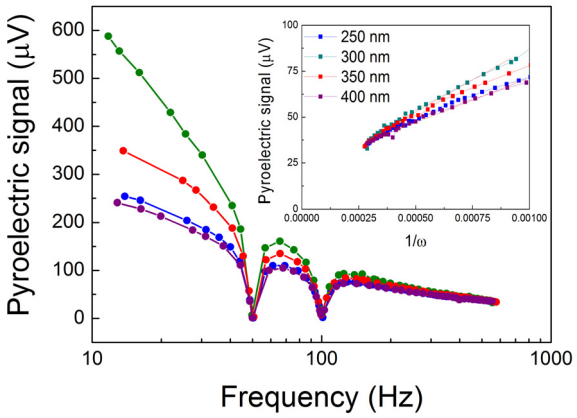

FIG. 2. *The frequency dependence of the pyroelectric signal generated for different wavelengths of the incident continuous UV light. The inset shows the dependence of the pyroelectric signal on 1/ω. The red lines show the linear fit.*

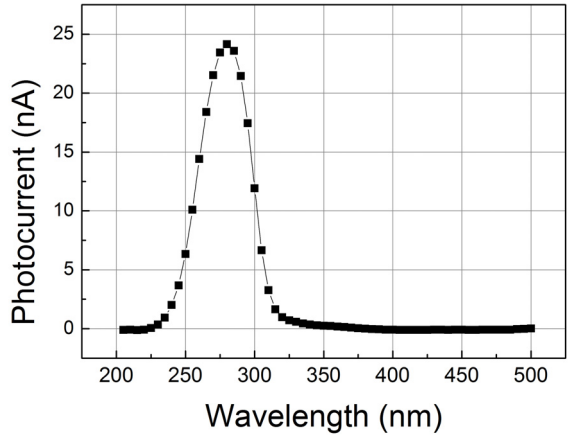

FIG. 3. *The spectral distribution of the short-circuit current measured from a PZT capacitor under illumination with continuous UV light.*

As the UV illumination is constant, then a supplement of free carriers (electrons and holes) will be generated in the active element, proportional with the absorption coefficient at the irrespective wavelength. If there is no internal electric field, then these carriers will recombine with no effect in the measuring circuit. However, the presence of the spontaneous polarization in the ferroelectric naturally generates an internal electric field, called depolarization field. This is compensated with free carriers from the ferroelectric film and from the electrodes. Nevertheless, when free carriers are generated with continuous light, the internal electric field separates these carriers and leads to the occurrence of the short-circuit current presented in Fig. 3. In the situation when the polarization is changing due to the temperature variation, the internal electric field will vary too. This means that the photo-generated carriers will produce an alternative current that is adding to the pyroelectric current. The addition is constructive because the pyroelectric current and the periodical variation of the internal electric field are generated by the same temperature variation, produced by the modulated IR light. Therefore, the current signals are in phase, and the result is an increase of the measured pyroelectric voltage.

Funding from Idea-Complex Research Grant PN-II-ID-PCCE-2011-2-0006 (contract nr. 3/2012) and through the IFA (Institute of Atomic Physics, Romania) - CEA (the Commissariat for Atomic Energy, France) cooperation program (Contract no. 04/2014).

References

[1] M. Botea, A. Iuga, and L. Pintilie, Applied Physics Letters **103**, 232902 (2013).
[2] L. Pintilie, I. Vrejoiu, G. Le Rhun, and M. Alexe, J. Appl. Phys. **101**, 064109 (2007).
[3] L. Pintilie, M. Botea, and A. Iuga, Applied Physics Letters **105**, 132901 (2014).

Influence of the average valence of Ni-Nb co-dopants on microstructure, ferroelectric and piezoelectric properties of lead titanate ceramics

L. Amarande, C. Miclea, M. Cioangher, M.N. Grecu, I. Pasuk, R. F. Negrea

Lead titanate ceramics are traditional ferroelectric materials with many applications in non-destructive testing, micro-positioning systems, underwater detection, medical imaging and therapy. In a previous work [1], we reported about the use of Ni, Nb and Mn co-dopants for titanium substitution. At various relative concen-trations of donor (Nb^{5+}) and acceptor (Ni^{2+}) co-dopants, the average valence (AV) of these ions was different from titanium valence, thus enhancing the "soft" or "hard" piezoelectric properties of PT ceramics. It was found that donor-like AV of co-dopants facilitates the reduction of Mn^{4+} to $Mn^{3+}$and Mn^{2+}, with direct influence on the domain wall mobility.

The aim of the present work is to extend our previous investigation to other new material compositions, in order to better understand the effect of these donor-acceptor co-dopants, in terms of their AV, correlated with the multiple valence of manganese, mainly on the electromechanical and ferroelectric properties of these materials.

Lead titanate ceramics co-doped with Ni, Nb and Mn, were prepared by a conventional ceramic technique. Titanium ions were substituted with different molar ratios of co-dopants, given in Table 1. The average valence of Ni-Nb co-dopants and B-site ions also given in Table 1, are higher/lower than 4+ (the valence of Ti^{4+} ions), hence the donor/acceptor behaviour of these co-dopants, expected to induce soft/hard piezoelectric properties. Dense ceramics, with relative density of 95-98%, 1-3μm average grain size (Fig.1) and single tetragonal phase, were obtained by decreasing the lattice anisotropy, from 1.057 to 1.047, while increasing the amount of co-dopants [2]. Ferroelectric behaviour of PT ceramics was investigated by measuring the *P-E* hysteresis loops. Fig. 2 shows three typical hysteresis loops of materials m 14, m 4 and m 23, with a high Mn^{2+} content, hard and soft–like properties, respectively. The hysteresis loops of m 14 and m 23 are similar, while the loop of m 4 is very slim and not saturated, typical for hard materials with increased conductivity (P_r= 2.3 μC/cm^2, E_C =1.9 kV/mm). The loop of m 14 has very asymmetrical extremes and is shifted towards the negative side of the horizontal axis, due to the positive poling field applied prior to hysteresis measurements. (P_r=6.4μC/cm^2–P_r=–3.7μC/cm^2, E_C=1.9 kV/mm and $-E_C$ =–4.4 kV/mm). The loop of m 23 shows less asymmetry due to the softer properties (P_r=6.7μC/cm^2 and $-P_r$=-6.1 μC/cm^2; E_C=3.3 kV/mm and $-E_C$=–3.9 kV/mm). All materials show the typical electromechanical anisotropy of PT based ceramics (k_p less than 0.1, while k_t is about 0.4). The thickness coupling factor k_t increases with Nb content and the AV of Ni-Nb co-dopants for the same amount of Ni (Fig. 3).

Mechanical quality factor Q_{mp} versus the average valence of Ni-Nb co-dopants is represented in Fig. 4. Materials with Ni-Nb AV > 4+ show higher coupling factors correlated with higher mechanical quality factors, due to the multivalence states of manganese and the larger size of Mn^{2+} ions, found by EPR spectroscopy.

For Ni-Nb AV < 4+, materials with hard piezoelectric properties were obtained. They show lower coupling factors and increasing mechanical quality factors with decreasing Ni-Nb AV. The two materials without manganese, with Ni-Nb

Table 1 *Average valence (AV) of Ni-Nb co-dopants and B-site ions in the investigated materials*

Material	m1	m2	m4	m6	m8	m10	m13	m14	m16	m21	m23
Amount of Ni /Nb /Mn (mol %)	1/5/2	2/5/2	4/5/2	6/5/2	2/6/2	4/6/2	1/7/2	2/7/2	4/7/2	1/5/0	1/7/0
AV of Ni-Nb co-dopants	4.5	4.14	3.67	3.36	4.25	3.8	4.62	4.33	3.91	4.5	4.62
AV of B-site ions	4.03	4.01	3.97	3.93	4.02	3.98	4.05	4.03	3.99	4.03	4.05

AV > 4+, proved to have soft-like behaviour. Their coupling/ mechanical quality factors show an increasing/ decreasing trend with increasing Ni-Nb AV. The Mn^{2+} EPR intensity (around g_{ef} = 2.004), resulted from the reduction of Mn^{4+} in the presence of donor co-dopants, is significantly higher for materials with Ni-Nb AV > 4+, (Fig. 5 (a)), than for those with AV < 4+, with acceptor co-dopants (Fig. 5 (b)).

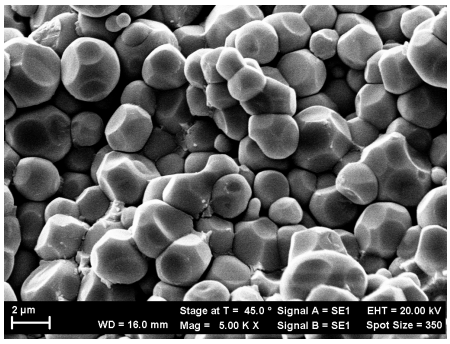

Fig. 1 SEM micrographs of fracture surfaces

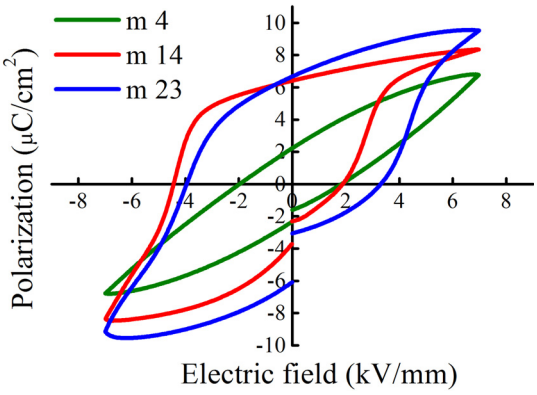

Fig. 2 P-E hysteresis loops of materials 14, 4 and 23.

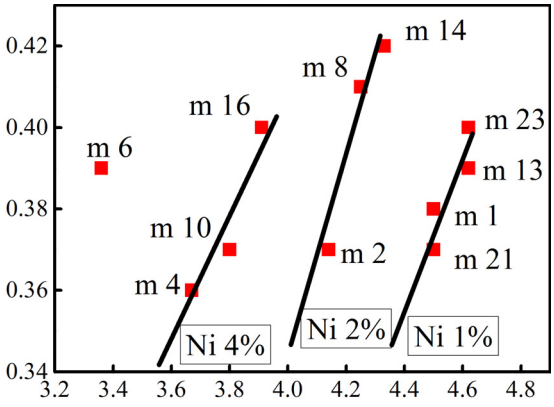

Fig. 3 Thickness coupling factor, k_t ,vs. average valence of Ni-Nb.

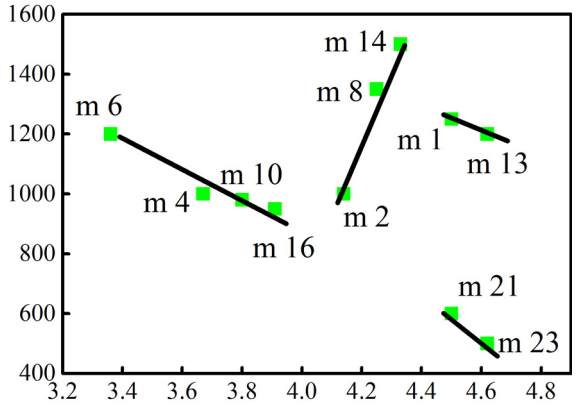

Fig. 4 Q_{mp} vs. average valence of Ni-Nb.

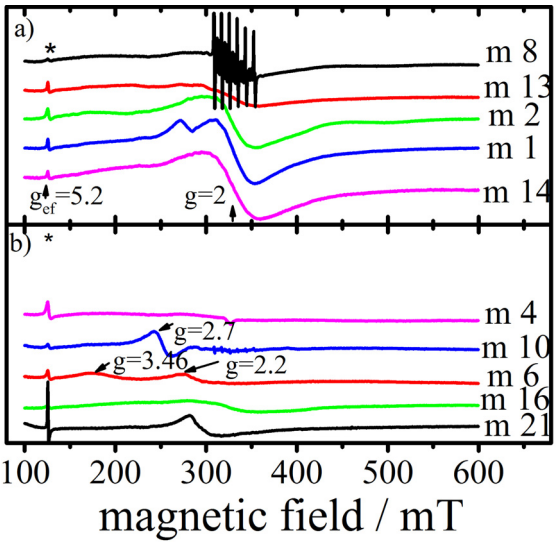

Fig. 5 EPR spectra of materials with donor (a) and acceptor (b) Ni-Nb co-dopants. The asterisk (*) marks the paramagnetic intrinsic iron impurity in PT ceramics.

This work was supported by Romanian National Authority for Scientific Research, under the project "NUCLEU" PN09-450103 and PN-II-ID-PCE-2011-3-1028. The authors are grateful to Dr. Elena Matei for SEM measurements.

References

[1] L. Amarande, C. Miclea, T. Tanasoiu, A. Iuga, M. Cioangher, L. Trupina, M.N. Grecu, I. Pasuk., IEEE Transactions on Ultrasonics Ferroelectrics and Frequency Control **56**(9) 2009; 1792-8.

[2] L. Amarande, C. Miclea, M. Cioangher, M.N. Grecu, I. Pasuk, R.F. Negrea, J. Eur. Ceram. Soc. **34**(6) 2014, 1547-1552.

Thin films deposited by sputtering at low temperature: Structural and optical properties

A.C. Galca, C. Besleaga, C.F. Miclea, I. Mercioniu, M. Enculescu, G.E. Stan
in cooperation with
A.O. Mateescu (IFIN-HH, Romania)
V. Dumitru, S. Costea (Honeywell, Romania)
S. Davidsdottir, R. Ambat (Technical University of Denmark)
R. Shabadi (University of Lille, France)
I.H. Andersen (Danish Technological Institute)
K. Dirscherl (Danish Fundamental Metrology)

Depositions of thin films at low temperatures (near room temperature) are required when flexible materials with low melting temperature (e.g. Polyethylene terephthalate) are used as substrates. The use of such deposition temperatures decrease also the cost (time and electrical power) of delivered thin films. However, mainly due to low mobility of the ad atoms on the surface, the growth of the thin films are in-depth inhomogeneous with respect to the structural properties.

One example is the growth study of TiO_2 (anatase) coatings on aluminium substrates [1], which proves a quasi-linear dependency between the crystallites in-plane size, photo-catalytic active surface area (roughness) and thickness. This dependency can be also deduced from the the optical properties of the films.

In order to get reliable and at least the best qualitatively results the simplest optical model have been used, consisting of metallic substrate, a Cauchy layer and an intermix layer between them. The fitting procedure was performed 0.7 - 3 eV spectral range, where is supposed that the TiO2 layer is fully transparent. The intermix layer (40 nm) was required due to non-perfect surface optical quality of the bare substrate. The obtained dispersions are represented in Fig. 1a.

For confirmation of the resulted optical properties, a multilayer optical model was employed. Starting from single Cauchy layer model (data) obtained for the ~100 nm thick TiO_2, were added one and two extra Cauchy (Fig. 1b) layers for ~500 nm film and ~2 micrometer thick film, respectively.

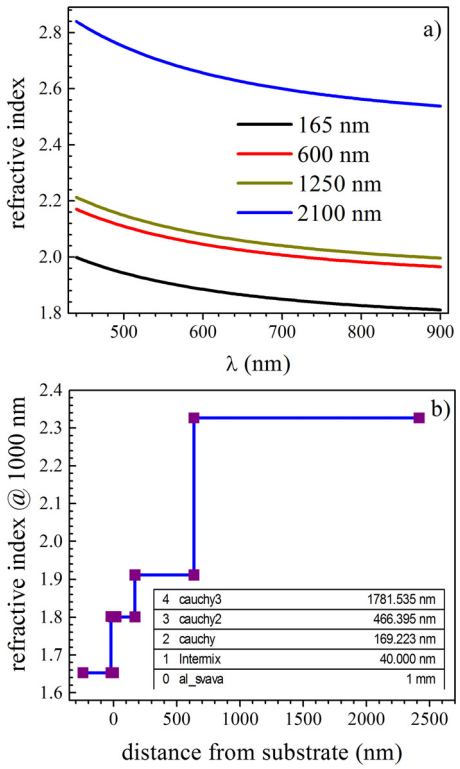

Fig.1 *a) Refractive index dispersion using single Cauchy layer b) Refractive index evolution as function of thin film thickness.*

The refractive index increases as the thickness increases (Fig. 1a). In order to understand this increase there should be considered the following mechanisms /experimental evidences: i) the 'V' shape columnar growth of the presented thin films; ii) the crystalline materials have higher refractive index than the (quasi-) amorphous counterparts, while those of polycrystalline samples lie in-between; iii) the density of the point defects, as well the density of grain boundaries (larger grains), decreases toward the top of the thin films; iv) the refractive index linear dependence on the grain (crystallite) size;

v) density of atoms at the grain boundaries is usually smaller than in the crystallites.

The methylene blue decomposition test showed an increase in photocatalytic activity by increasing coating thickness, which was greater for the thickness range of 100 nm and 500 nm compared to the increase between 500 nm and 2 microns.

$Al_xIn_{1-x}N$ layers have been obtained by reactive magnetron sputtering onto rigid (glass) and flexible (polyethylene terephthalate) substrates, using Al-In targets. $Al_xIn_{1-x}N$ alloys with a large compositional range were successfully achieved by varying only the composition of the deposition atmosphere. Insightful discussions about the bowing parameters of lattice constants, optical band gap, refractive index, and electrical properties were published [2].

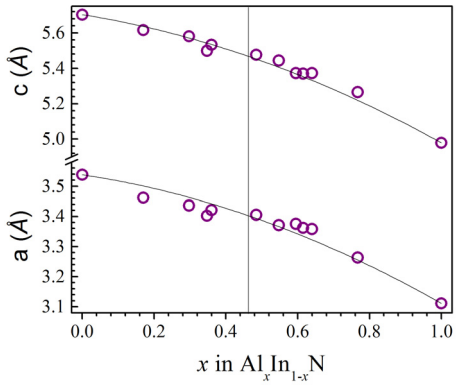

***Fig.2** Dependence of the lattice parameters versus stoichiometry of $Al_xIn_{1-x}N$ thin films.*

The *a* and *c* lattice parameters of $Al_xIn_{1-x}N$ thin films, determined from X-ray diffractograms taking into account the positions of all diffraction lines, as function of the aluminium concentration (*x*) are plotted in Fig. 2. The lattice parameters, *a* and *c*, decrease upon increasing aluminium concentration, and the relationship between the lattice parameters and the composition ratio is not a linear one. The amount of deviation from the Vegard's Law is given by Eq. 1, where a_{AlN}, c_{AlN} ,a_{InN}, c_{InN} are the lattice constants of AlN and InN, respectively.

By fitting the experimental values have been determined the deviation parameter values.

$$a_x = a_{AlN} + (a_{InN} - a_{AlN})(1-x) + \beta_a x(1-x)$$

$$c_x = c_{AlN} + (c_{InN} - c_{AlN})(1-x) + \beta_c x(1-x)$$

eq.1

Both lattice parameters of the polycrystalline AlInN thin films are slightly larger with respect to values reported in literature for single crystal-like AlInN films grown at higher temperatures and/or on lattice matched substrates. Since both deviation parameters have the same sign, in combination with a textured growth mode, the presence of the macrostrain can be ruled out. The non-uniform distribution of cations within each grain is a source of the slight isotropic expansion of the unit cell volume.

The Al content of x = 0.5 seems to be a threshold value which can be used to define two classes of AlInN films. X-ray diffraction revealed a 002-oriented preferential growth for In rich films and a shift towards a 101-oriented preferential growth for the Al rich films. Both *a* and *c* decreased with aluminium content, showing bowing parameters of -0.288 and -0.446, respectively.

In conclusion, the optical parameters, band gap energy, refractive index, the electrical properties, conductivity, and free carrier mobility, can be varied in a wide range when tuning the chemical composition of AlInN layers.

NIMP researchers acknowledge financial support from Romanian Ministry of National Education through the RU-TE-2011-3-0016 and PN-II-ID-PCE-2011-3-1028 projects.

References

1. S. Davidsdottir, R. Shabadi, A.C. Galca *et al.* Applied Surface Science 313, 677-686, 2014.
2. C. Besleaga, A.C. Galca, C.F. Miclea *et al.* Journal of Applied Physics 116 (15) 153509, 2014.

Precluded long range magnetic order in the geometrically frustrated heavy fermion $CeCu_4Ga$

C.F. Miclea, B.G. Ueland[1], K. Gofryk[2], Y. Qiu[3], F. Ronning[4], R. Movshovich[4], E. D. Bauer, J. S. Gardner[5], and J. D. Thompson[4]

[1]Ames Laboratory, U.S. DOE, Iowa State University, Ames, Iowa, USA

[2]Idaho National Laboratory, Idaho Falls, Idaho, USA

[3]NIST Center for Neutron Research, National Institute of Standards and Technology, Gaithersburg, Maryland, USA

[4]Los Alamos National Laboratory, Los Alamos, New Mexico, USA

[5]National Synchrotron Radiation Research Center, Neutron Group, Hsinchu, Taiwan

The heavy fermion $CeCu_4Ga$ belongs to the $CeCu_{5-x}M_x$ series of strongly correlated electron compounds (with x = 0,1,2 and M =Ga, Al) with a hexagonal structure described by the *P6/mmm* space group. They are prone to geometrical frustration of the magnetic moments carried by the Ce atoms which are distributed in the basal plane forming a sublattice of side sharing triangles.

$CeCu_4Ga$ display clear peaks in the specific heat and in the magnetic susceptibility at T^* = 1.2 K. $CeCu_4Ga$ has a huge Sommerfeld coefficient, γ_0 (over 1000 mJ/mol K^2) which could be the result of the mass renormalization of the conduction electrons due to the Kondo effect. However, our data suggest an alternative interpretation for this large γ_0. The crystal field environment of the Ce spins should split the putative J = 5/2 single-ion ground state multiplet into three magnetic doublets. Previous neutron scattering experiments have found that a crystal-field level transition occurs for a neutron energy transfer of E = 6 meV, and that the transition is broadened by the Kondo coupling [1]. The Hall-effect measurements reveal no unconventional behavior induced by the frustration as observed in the case of the related compound UCu_5 [2]. Also the system is highly isotropic [3].

In this work [4] we present results from experiments on both, single crystals and policrystals of $CeCu_4Ga$. Our findings indicate short-range magnetic correlations at T = 0.1 K. A peak occurs in its specific heat at T^* = 1.2 K, below which its ac magnetic susceptibility becomes temperature independent. The temperature dependence of the resistivity indicate Fermi-liquid behavior. The neutron scattering do not show any magnetic Bragg peaks down to T = 0.1 K, which would correspond to long-range magnetic order. We find a modulation in the neutron momentum transfer Q that corresponds to short-range magnetic correlations occurring across two unit cells.

Figure 1(a) shows the T dependence of χ^{-1} of a polycrystal for $\mu_0 H$ = 0.1 T. The fit yields a Weiss temperature of θ_W = -3 K, which indicates a weak antiferromagnetic (AFM) spin interaction. The effective moment is p_{eff} = 2.46 μ_B and the T independent susceptibility is $\chi_0 = 4.24\times10^{-6}$ m^3/mol. The bottom inset shows χ_{ac} for a single crystal sample measured at f = 1 kHz while applying various static fields. The upper inset shows that T^* does not change with frequency, which indicates that spin freezing does not occur on the time scale of the measurement. Figure 1(b) shows the C_{mag}/T (left axis) and the magnetic entropy S_{mag} (right axis) for a single crystal, with H along the c-axis.The inset shows C_{mag} at low temperatures. A peak in C_{mag}/T occurs at T^* which decreases, broadens, and shifts to higher temperature with increasing field. We find a large electronic term, γ_0 = 1.44 J/(mol K^2), partly due to the heavy charge carriers partly due to the low-energy magnetic excitations. C_{mag} cannot be fit to a Schottky term, which suggests that the peak at T^* does not represent a canonical crystal-field level transition. The zero field entropy does not reach expected value for a ground state doublet of $S_{mag} = R \ln 2$ J/(mol K) until $T \approx 6.6$ K.

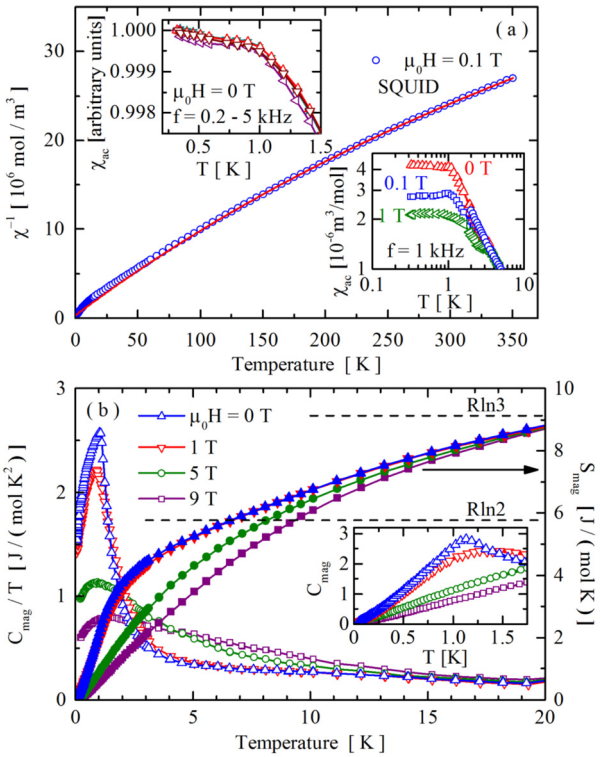

FIG. 1: (a) χ^{-1} for 0.1 T. Top inset: χ_{ac} for f = 0.1, 0.5, 1, and 5 kHz. Bottom inset: χ_{ac} for f = 1 kHz and various applied dc fields. (b)C_{mag}/T (left axis) and the magnetic entropy (right axis). Inset: C_{mag} for various fields

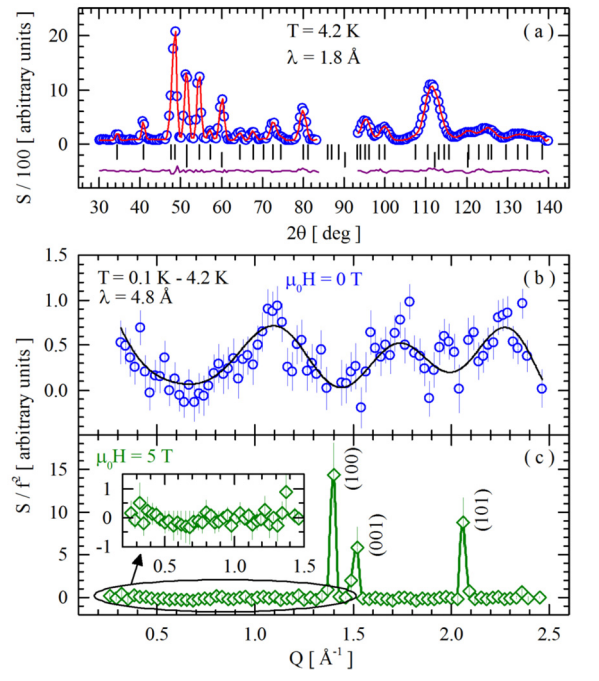

Fig. 2: (a) Diffraction pattern integrating over E = -2 to 2 meV. Vertical lines indicate Bragg peak positions for the sample (upper) and the sample holder (lower), and the bottom line is the difference between the data and fit. (b) T = 0.1 K diffuse scattering. (c) Diffuse neutron scattering data for 5 T constructed as in (b). The inset shows a blowup of the low Q data (for details see ref. [4]).

The diffraction pattern at T = 4.2 K for λ = 1.8 Å incident neutron data constructed by integrating over E = -2 to 2 meV are presented in Fig. 2(a) and reveal that the sample has the anticipated structure. To check for the existence of magnetic Bragg peaks below T*, which would indicate long-range magnetic order, the T = 0.1 K pattern was subtracted by the T = 4.2 K pattern (after integrating over E = -0.1 to 0.1 meV), and the result was divided by the square of the Ce^{3+} magnetic form factor *f*. No magnetic Bragg peaks were found (fig. 2(b)).

Magnetic diffuse scattering present as broad peaks centered at $Q \approx 1.1$, 1.75, and 2.3 $Å^{-1}$ is suppressed by the magnetic field which sharpens the peaks at Q (fig. 2(c)). By comparing these data with the magnetization and the magnetic structure, we estimate at $\mu_0H = 0$ T an ordered moment of less than $0.3\mu_B$. This is corroborated by muon spin relaxation experiments [5].

The absence of the spin freezing suggested by the frequency independence of the susceptibility (at least in the experimental frequency range) does not completely rule out a spin glass behavior. Corroborated with the broad inelastic magnetic scattering these results suggest that the correlation in $CeCu_4Ga$ may be dynamic.

References

[1] D. Gignoux, D. Schmitt, E. Bauer, and A. P. Murani, J. Magn. Magn. Mater. **88**, 63 (1990).

[2] B.G. Ueland, C.F. Miclea, Y. Kato, O. Ayala–Valenzuela, R.D. McDonald, R. Okazaki, P.H. Tobash, M.A. Torrez, F. Ronning, R. Movshovich, Z. Fisk, E.D. Bauer, I. Martin and J.D. Thompson, Nature Comm. **3**, 1067 (2012).

[3] C. F. Miclea et al. to be published.

[4] B. G. Ueland, C. F. Miclea, K. Gofryk, Y. Qiu, F. Ronning, R. Movshovich, E. D. Bauer, J. S. Gardner, and J. D. Thompson, Phys. Rev. B **90**, 121109R (2014).

[5] G. Wiesinger et al., Physica B **230-232**, 243 (1997).

Conception, development and phase structure studies of FePt-based nanocomposite magnets

A. D. Crisan, F.Vasiliu, I.Mercioniu and O. Crisan
in cooperation with
J. Bednarcik, S. Michalik,
Deutsches Elektronen Synchrotron DESY, Hamburg, Germany

The FePt system has important perspectives as high-temperature corrosion-resistant magnets. In the form of rapidly solidified melt-spun ribbons, FePt-based magnets may exhibit in certain cases a two-phase hard–soft magnetic behaviour. A microstructural and magnetic study of FePtAgB alloys with increasing Ag content was aimed at identification and confirmation of the effect of Ag addition in decreasing the temperature of the FePt disorder–order structural phase transformation [1]. A detailed high-resolution transmission electron microscopy study was employed, and the alternative disposal of hard and soft regions within the two-phase microstructure was observed and interpreted with respect to the X-ray diffraction results. The HRTEM images obtained for sample FePtAg6B is shown in Fig. 1. Small grains of tetragonal $L1_0$ phase, 2-5 nm in size are well separated by a 1 nm thick intergranular phase containing Ag, B and Fe. Many other areas contain, besides the smaller $L1_2$ grains, large regions of ordered $L1_0$ phase of 30 nm length and having a lateral extension of 10 nm. The superlattice planes (001) spaced at d_{001}=0.37 nm can also be observed in this case. Selected area electron diffraction (SAED) pattern (inset) shows besides polycrystalline rings of fcc $L1_2$ Fe_3Pt, a single crystal <1 -1 0> zone axis of L10 phase which include the (001) and (110) reflections. In the $L1_0$-rich area a composition ratio Fe: Pt of 46:49 was found by EDX. In the as-cast Ag-containing samples, we have proven that there is an optimum of the Ag content for which best magnetic properties are obtained.

Fig.2 presents the hysteresis loops of samples with optimal magnetic properties and proves the true exchange spring behavior as the recoil loops (inset) show full reversibility on the whole demagnetization curve. Ag addition creates a nonlinear (oscillatory) behavior of the coercive field and the ordering parameter (Fig.3), a behavior similar to the RKKY interaction-induced interlayer exchange coupling (IEC) observed in magnetic layers separated by non-magnetic spacer layers.

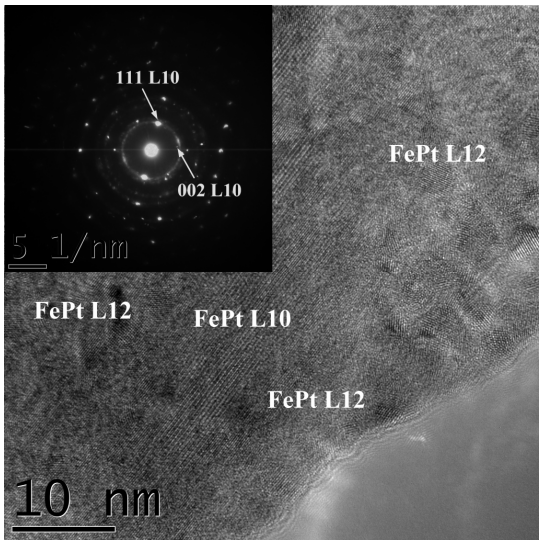

Fig.1.*HRTEM images of the sample FePtAg6B: area of $L1_0$ phase encompassed by $L1_2$ regions (inset: associated SAED pattern).*

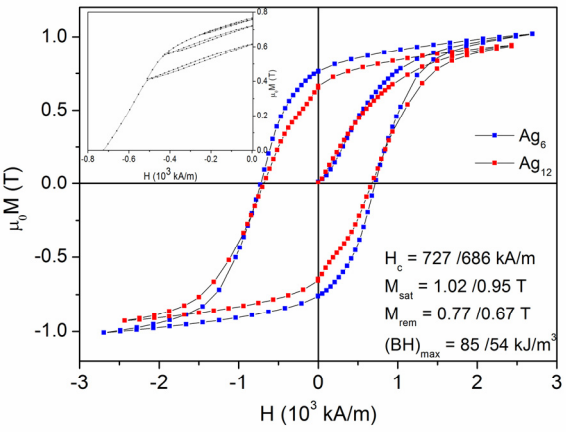

Fig.2 *270K in-plane hysteresis loops of Ag6 and Ag12 as-cast samples. Inset: recoil loops showing reversibility of the demagnetization curve of the Ag6 sample.*

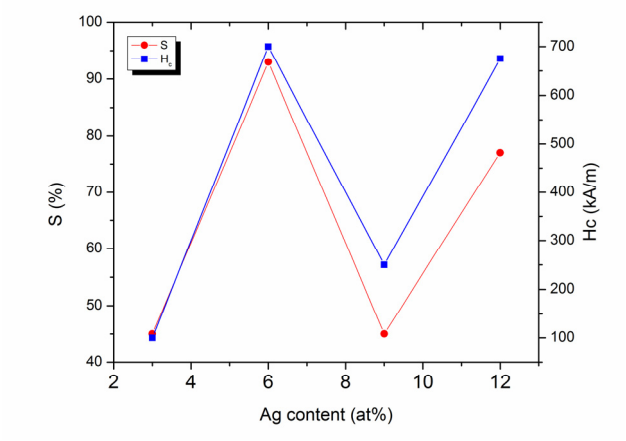

Fig.3. *The Ag content dependence of ordering parameter S and coercive field H_c for the as-cast FePtAgB samples.*

We have thus proven by XRD, HRTEM and magnetic measurements that we obtain direct formation of the $L1_0$ phase from the as-cast state in the FePtAgB alloys. Optimized magnetic parameters, comparable to other exchange spring permanent nanomagnets have been obtained.

It is to be mentioned that the tetragonal phase emerges from the A1 disordered cubic precursor via a disorder – order transformation. Such transformation in FePt-based systems with B and Nb added to the composition has been *in situ* monitored using energy dispersive X-ray diffraction of the synchrotron radiation. This experiment using high-energy photons has been performed at the BW5 wiggler beamline of the DORIS III positron storage ring at DESY/HASYLAB (Hamburg, Germany). The technique allows to observe in real time the onset of the transition and the full profile refinement of the obtained XRD patterns at each temperature value (Fig.4 top), facilitate the separation of overlapping A1 cubic and $L1_0$ tetragonal FePt and to calculate the integral relative fraction of both phases at each step of temperature from 490°C up to 750°C (Fig. 4 bottom) [2].

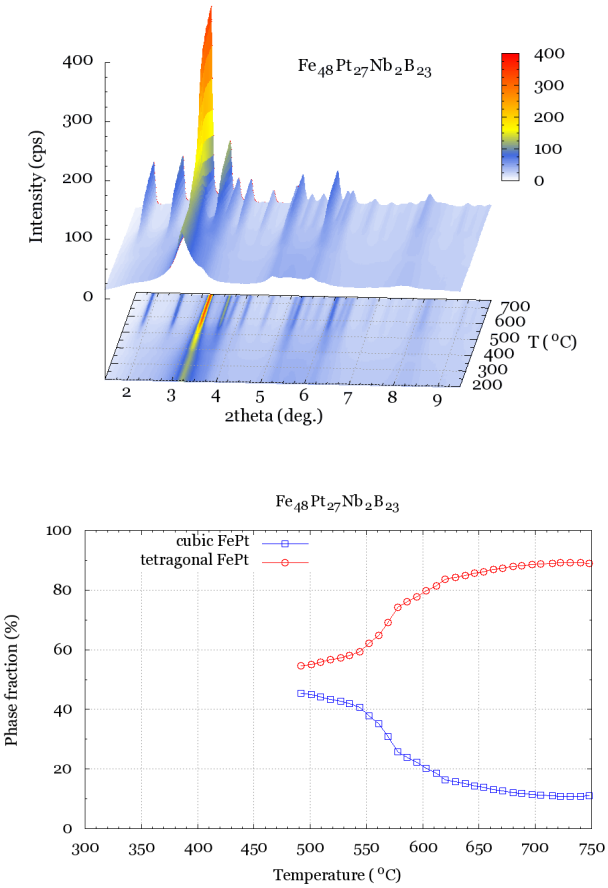

Fig.4. *3D representation of the series of XRD patterns acquired during constant rate heating (5 °C/min) (top) and T dependence of relative phase fraction of A1 and $L1_0$ phases (bottom) for $Fe_{48}Pt_{27}Nb_2B_{23}$.*

These findings open novel perspectives into utilization of such alloys as magnets operating in high-T industrial environments.

References

[1] A.D. Crisan, F. Vasiliu, I. Mercioniu, O. Crisan, Philosophical Magazine 94 (2014) 174-189

[2] A.D. Crisan, J. Bednarcik, S. Michalik, O. Crisan, Journal of Alloys and Compounds 615 (2014) S188-S191

Effect of silver addition to superconducting $SmFeAsO_{1-x}F_x$

V. Sandu and G. Aldica
in cooperation with
Z.-Y. Liu, Z. L. Zhang and Hong Li Suo,
Beijing University of Technology

Similarly to cuprates, superconducting pnictides possess a layered structure, a short coherence length, hence, a very high upper critical field H_{c2}, (over 100 T) but a much smaller anisotropy and a nodeless symmetry of the order parameter. Therefore, the detrimental effect of the grain boundaries is substantially reduced in Fe-based superconductors. This advantage might compensate the smaller critical temperature T_c. The compounds with the highest critical temperature belong to the fluorine doped LnFeAsO (Ln-1111) family where Ln is a rare earth. Critical current density J_c was found to be as high as 2×10^6 A·cm^{-2} at 5 K and 14 T [1] in single crystals but the cables made of this material show only $J_c \sim 10^3$ A·cm^{-2} [2] In addition, the always spurious, phases like FeAs are present and fluorine is very labile.

Improvements might be obtained by the addition of several compounds which attenuate the granularity and its effects. In our research, we investigated the transport and magnetic properties of a series of Ag-added $SmFeAsO_{1-x}F_x$ polycrystalline samples, focusing on the effect of the intragranular critical current density. For this aim, a series of Ag-enriched $SmFeAsO_{1-x}F_x$ (Sm-1111) samples were prepared by a two-step solid state reaction method using SmAs as precursor, Fe, Ag, Fe_2O_3 and FeF_3.

The resistive transition shows the typical temperature dependence of the resistance up to 300 K for three $SmFeAsO_{1-x}F_xAg_y$ samples: y = 0.0; 0.06 and 0.12 (Fig. 1). The critical temperature T_c decreases from 54.1 K (y = 0) to 43.0 K for y = 0.12. All samples have similar non–Fermi temperature dependence of the resistance in the normal state with a remarkable linearity of the $R(T)$ curves just beyond T_c. Above a certain crossover temperature T_{cr}, around 160 K, the dependence slows down to a logarithmic dependence $R(T) = A(x)\log(T/\Delta)$ (Fig. 2).

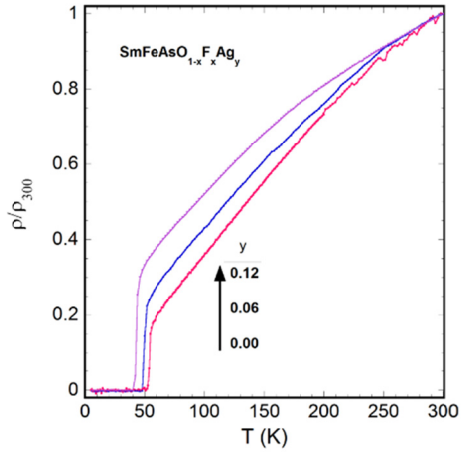

***Figure 1**. Temperature dependence of the normalized electrical resistivity of polycrystalline $SmFeAsO_{1-x}F_xAg_y$.*

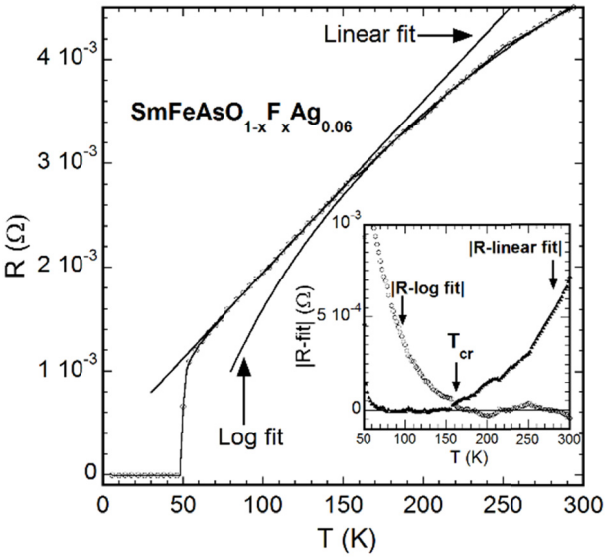

***Figure 2**. Temperature dependence of the electrical resistivity of polycrystalline $SmFeAsO_{1-x}F_xAg_{0.06}$ and the fit with linear and logarithmic function. Inset: the determination of the crossover temperature.*

T_{cr} was determined as the point of equal departure of the linear and logarithmic fit from the experimental $R(T)$. (inset to Fig. 2). The linear-in-T dependence of the resistance at low T is a signature of the *quantum criticality* [3]) which marks the suppression of the spin density waves by doping. The logarithmic dependence is

still hard to understand. The value of T_{cr} is almost identical to the structural phase transition in the undoped parent SmFeAsO which raises some questions related to the presence of the antiferromagnetic correlations and their role [4]. The dependences of the T_c and T_{cr}, on the amount of silver are shown in the Fig 3.

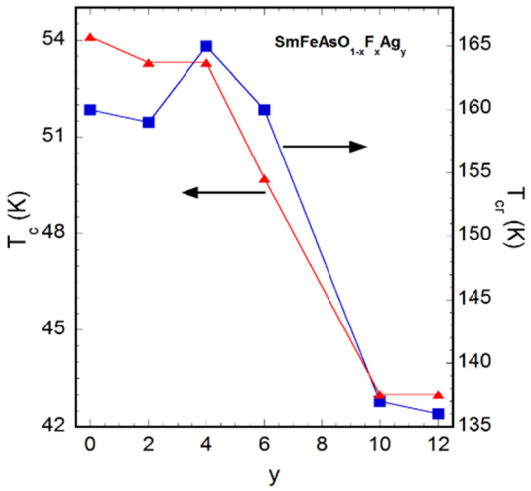

***Figure 3**. The dependence of the critical temperature T_c and crossover temperature T_{cr} as a function of Ag content y.*

Both T_c and T_{cr} show minor changes for $0 \le y \le 0.06$ with T_{cr} around 160 K and T_c slightly decreasing from 54 to 53 K. At higher Ag content they steeply fall.

Critical current. The intragranular critical current density J_{cg} at 20 K is shown in Fig. 4. The field dependence for all sample as investigated between 5 and 30 K is similar. We noticed four regimes of field dependence which are similar to the regimes depicted for single crystals. At very low fields, there is a slow decrease of J_{cg}. As the field increases, J_{cg} crosses to a power law dependence, $J_{cg} \sim B^{\alpha}$, which is followed an almost B-independent J_{cg} and, finally, by fast decrease. The B-independent plateau at higher fields is attributed to the collective pinning of single vortex due to atomic scale fluctuations of the dopant positions, hence, to mean free path fluctuations. At even higher fields, pinning crosses to small bundles regime wherer, $J_{cg} \sim \exp[-(B/B_0)^{3/2}]$. Note that small amount of Ag (y = 0.04) leads to an enhancement of J_{cg} which is more consistent at low fields but also reduces the B-range of collective pinning. The samples with Ag display a faster decrease of J_{cg}, an effect which is emphasized at high Ag content. Data show that Ag contributes to the stabilization of the high T_c phase but the price is its decrease. In addition, Ag improves the homogeneity of the dopant (fluorine) distribution but prevents the optimal fluorination for $y > 0.06$. This fact increases the density of the deep pinning potential wells sites and reduces the more shallow ones. However, the pinning gets weaker as T_c significantly decreases.

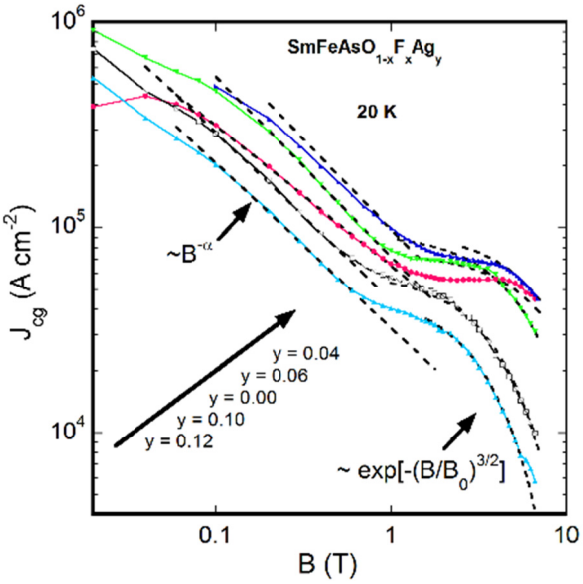

***Figure 4**. Field dependence of intragranular critical current density of polycrystalline $SmFeAsO_{1-x}F_xAg_y$ at 20 K;*

Therefore, J_{cg} is the result of a subtle balance between the diminution of the critical temperature, hence, of the density of Cooper pairs, and the enhancement of the homogeneity. Surface pinning may also be considered because Ag is detrimental for the glassy FeAs that develops at grain boundaries.

References

1. Moll, P.J.W. *et al.*, Nature Mater. 9, 628 (2010)
2. Yamamoto, A *et al.*, Supercond. Sci. Technol. 21, 095008 (2008)
3. v. Löhneysen *et al.*, Rev. Mod. Phys. 79, 1015 (2007)
4. Klingeler, R. *et al.*, Phys. Rev. B 81, 24506 (2010)

Enhancement of the critical current density of the MgB_2 superconductor using c-BN, Ge-based and Ho_2O_3 additions

P. Badica, G. Aldica, L. Miu, S. Popa, M. Burdusel, R.F. Negrea , I.Pasuk, M. Enculescu
in cooperation with
D. Batalu (University Politehnica of Bucharest) and *M Ferbinteanu* (University of Bucharest)

Additives into MgB_2 can significantly increase the superconducting functional characteristics of MgB_2, such as the critical current density J_c and the irreversibility field H_{irr}. Therefore, testing new additives is of fundamental and technical interest.

Additives should be correlated with technological approach and its specific features. This is because superconductors are very sensitive to disorder and defects controlled by additive and technology. In this work all samples were prepared by Spark Plasma Sintering (SPS). This unconventional method was applied on powder mixtures of MgB_2 and the additive with different starting compositions. The SPS processing temperature was 1150°C and the dwell time was 3 min. All samples show high relative density above 93%. Raw materials and bulk samples were characterized by FTIR, structural and microstructural observations and by complex magnetic measurements.

MgB_2 crystals are often grown in hexagonal BN (h-BN) crucibles, indicating that h-BN is inert in respect to MgB_2. Considering this observation, doping with polymorphs of a given compound such as h- and cubic BN (c-BN) may provide information on the role of the interface between MgB_2 and the additive for flux pinning. Strain was recognized to be an important ingredient for the control of the superconducting properties, and the residual strain at interfaces can play a major role in this regard through the induced local disorder. In our work [1] we added h-BN and c-BN.

Among the metalloid addition, Ge was not tested. For the first time we introduced Ge as Ge-metal, GeO_2 and $Ge_2C_6H_{10}O_7$ [2].

The Re_2O_3 (Re=rare earth) additives were often shown in literature to improve critical current density and irreversibility field in MgB_2. Two different types (A and B) of Ho_2O_3 powders (showing a much different morphology) were added to MgB_2 [3].

The most interesting results are:

(i) The variation of the critical current density J_c with the external magnetic field H for h-BN added sample is almost overlapping the $J_c(H)$ dependence for the pristine MgB_2 sample. On the other hand, J_c for the samples added with c-BN is larger at high magnetic fields (Fig. 1), while the decrease of J_c at low H is very small. At T = 20 K, a J_c of 10^2 A cm^{-2} is determined for the optimum composition $MgB_2(c\text{-}BN)_{0.005}$ at H = 58 kOe. Magnetic relaxation measurements indicate a significant flux pinning enhancement in MgB_2 samples added with c-BN. It is proposed that the disorder at the interface caused by the convenient lattice matching relationship between the lateral plane of the MgB_2 crystal prism and the face of the c-BN crystal cube is responsible for the observed vortex pinning increase.

(ii) Ge, GeO_2 and $Ge_2C_6H_{10}O_7$ additions to MgB_2 significantly enhance the critical current density J_c in high magnetic fields (Fig. 2). A J_c(T = 20 K) of 10^2 A cm^{-2} is obtained at 3.9 T in the pristine sample and at 5.8 T in the $MgB_2(Ge_2C_6H_{10}O_7)_{0.0014}$ sample. Ge does not substitute into the MgB_2 lattice.

(iii) In the 5-25 K range, the B-Ho_2O_3 does not significantly suppress the critical current density J_c at low magnetic fields and the A-Ho_2O_3 enhances it at high fields, while their mixture simultaneously controls J_c at both small and high magnetic fields so that the decrease is small at low fields and there is a notable enhancement at high fields when compared to pristine sample (Fig. 3). The control of $J_c(H)$ is discussed versus specific characteristics of the raw powders, the resulting microstructure of the added SPS-ed samples and pinning details from magnetic relaxation measurements.

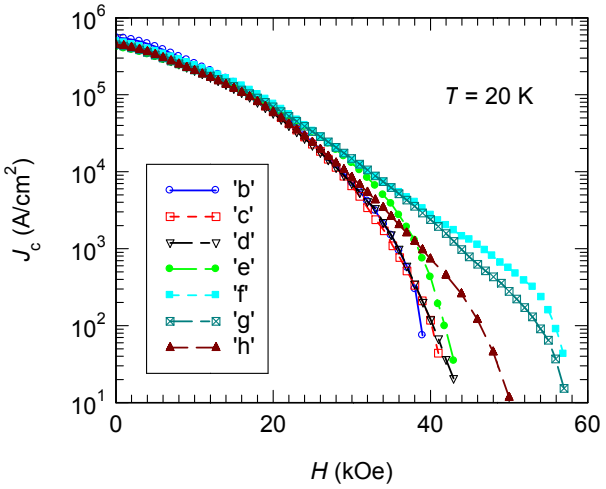

Fig. 1 *Magnetic field dependence of the critical current density J_c at 20 K. Samples are: 'b'-MgB_2, 'c'-'e'- $MgB_2(h\text{-}BN)_x$, 'f'-'h' - $MgB_2(c\text{-}BN)_x$, x=0.005, 0.01, 0.03.*

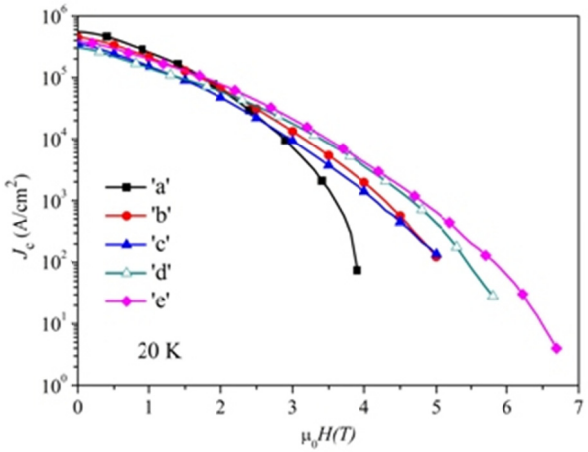

Fig. 2 *Magnetic field dependence of the critical current density J_c at 20 K. Samples are: 'a'-MgB_2, 'b'- $MgB_2(Ge)_{0.005}$, 'c'- $MgB_2(GeO_2)_{0.005}$, 'd' and 'e' - $MgB_2(Ge_2C_6H_{10}O_7)_x$, x=0.0025, 0.0014.*

(iv) Remarkable is that c-BN and $Ge_2C_6H_{10}O_7$ additives are the most effective ones for the enhancement of J_c among different additives introduced in MgB_2 processed by SPS [4].

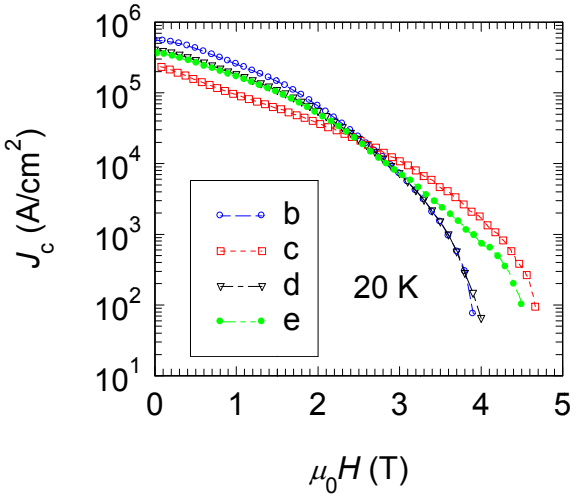

Fig. 3 *Magnetic field dependence of the critical current density J_c at 20 K. Samples are: 'b'-MgB_2, 'c'- $(MgB_2)_{0.975}(A\text{-}Ho_2O_3)_{0.0125}$, 'd'- $(MgB_2)_{0.975}(B\text{-}Ho_2O_3)_{0.0125}$, and 'e' - $(MgB_2)_{0.975}(A\text{-}Ho_2O_3)_{0.00625}(B\text{-}Ho_2O_3)_{0.00625}$.*

Authors acknowledge "Core Program"-PN09-450103/2014.

References

[1] Badica P, Aldica G., Burdusel M, Popa S, Negrea RF, Enculescu M, Pasuk I, Miu L, Superconductor Sci. & Tech, 27 9 (2014) 095013.

[2] Batalu D, Aldica G, Popa S, Miu L, Enculescu M, Negrea RF, Pasuk I, P. Badica, Scripta Mat. 82 (2014) 61-64.

[3] Aldica G, Popa S, Enculescu M, Batalu D, Miu L, Ferbinteanu M, Badica P, Mat. Chem. Phys. 146 3 (2014) 313-323

[4] Badica P, Aldica GV, Burdusel M, Borodianska H, Sakka Y, Vasylkiv O, Jpn J Appl Phys 53 (2014) 05FB22 – 1-8.

Complex thermal investigation and electronic properties in multiple-valence oxides with various structures

C. Bartha, C. Plapcianu, M. Cernea and F. Vasiliu
in cooperation with
R. Vidu
Chemical Engineering and Materials Science, University of California, California, USA

The interest in multiple-valence oxides with various structures derives both from the fundamental issues involved and the technological applications in terms of read/write heads and magnetic sensors, magnetic random access memory devices (MRAM) and spin injectors, renewable energy applications etc. The Sr_2FeMoO_6 (SFMO) double perovskite is very attractive due to the appreciable low-field magnetoresistance in granular form and a relatively high Curie temperature (410–450 K) [1, 2]. The ferrimagnetism of SFMO arises from a double exchange mechanism, which results from the ferromagnetic alignment of Fe^{3+} ($3d^5$, S=5/2) electrons and the antiferromagnetic alignment of $Mo5^+(4d^1$, S=1/2) electrons. Tetragonal Sr_2FeMoO_6 powders were prepared by the sol–gel (sample A) and solid-state reaction (sample B) methods. The thermal stability of the precursor-gel of Sr_2FeMoO_6 was analyzed using thermogravimetry (TG) and differential thermal analysis (DTA) (Fig.1). The measurements have been recorded under air atmosphere, with 10°C/min heating velocity, in the temperature range 25–1300°C. According to major changes suggested by the shape of the TG diagram we can divide the decomposition process into four steps (25–156°C, 300–447°C, 447–527°C and 527–760 °C). The mass loss of the Sr_2FeMoO_6 precursor gel powder corresponding to the first step (until 156°C) suggests the simultaneous evaporation of remaining water and trapped solvents (acetic acid and nitric acid). The exothermic peaks centered at ~418°C, 490°C and 559°C, corresponding to the weight loss intervals 300–447°C, 447–527°C and 527–760°C respectively, are attributed to loss of the organic groups (acetate, nitrate and citrate groups) by the thermal decomposition of the gel and combustion of some organic derivatives residues. No further weight loss or peaks can be seen thereafter in the TG and DTA curves, indicating that the thermal decomposition of the precursor-gel of Sr_2FeMoO_6 is completed before 760°C. In addition, there should be a small endothermic peak in the temperature range of 1000–1200°C on the DTA curve (centered at 1115°C) due to the crystallization of Sr_2FeMoO_6 and a secondary phase.

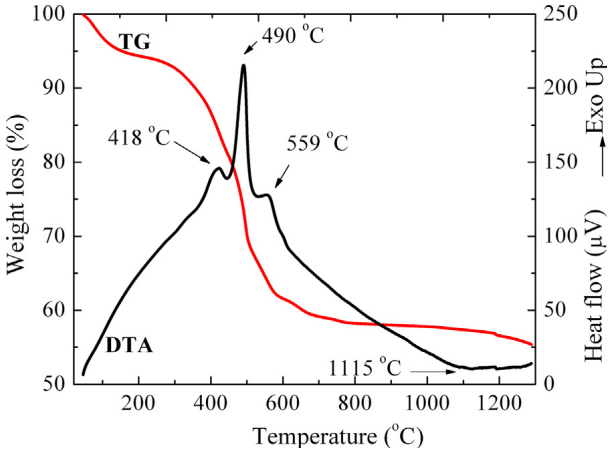

Fig.1 *TG/DTA curves of dried precursor-gel of Sr_2FeMoO_6, with a heating rate of 10 ◦C/min in air.*

Fig.2 shows the magnetic field dependence of magnetization (M) at temperatures of 5, 150 and 295 K corresponding to the two samples A (a), respectively B (b)

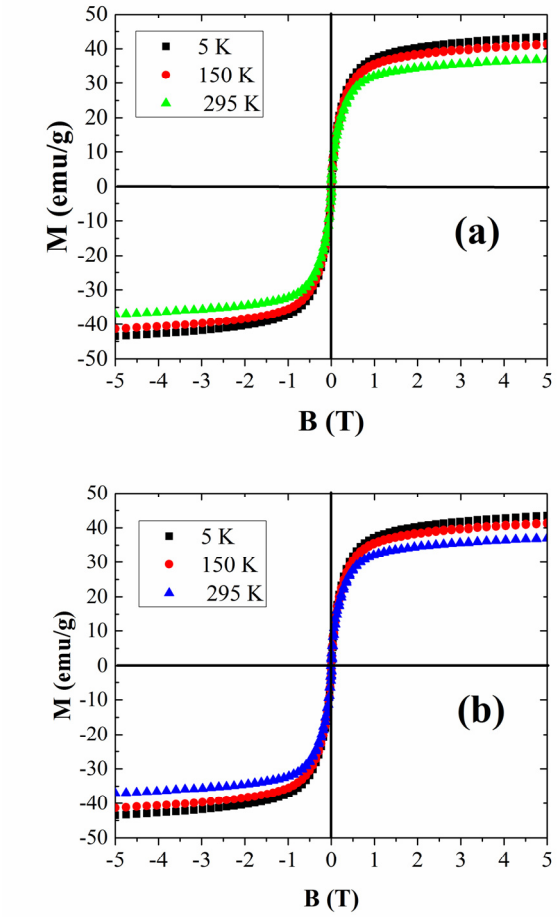

Fig.2 *Magnetic field dependence of the magnetization at temperatures of 5, 150 and 295 K for sample prepared by sol-gel method (a) and solid state reaction (b).*

The values of the total magnetic moment and saturation magnetization are listed in Table 1.

Sample	M_{sat}, (emu/g)	μ_{exp}/f.u.
A	41.18	3.26
B	40.77	3.10

As it can be seen, SFMO ceramic derived from the gel powder is characterized by an increased Fe/Mo order in comparison with the one prepared from the corresponding stoechiometric oxides mixture. Iron location on both crystallographic positions leads to the metal clusters formation due to local interactions, generating a distribution of ferromagnetic couplings. That is different from the ideal structure, which is associated with an antiferromagnetic coupling between Fe and Mo sub-lattices. Compared with literature data, our results are closed to those obtained by several groups (saturation moment: 3.1–3.2 μB). The Ce–Sn–O system is very interesting due to its application as solid electrolytes in fuel cells, catalysts, sensors, and photoanodes in solar cells (Fig.3).

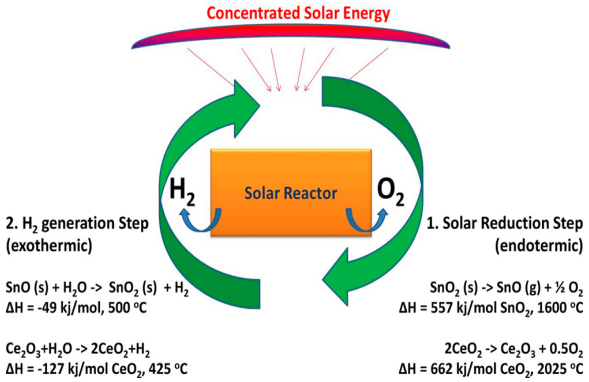

Fig.3. *Thermochemical water-splitting cycle for ceria and tin oxide.*

Ceria and ceria-based materials are studied for their electronic, magnetic (induced by dopants), optical, and catalytic properties. Ceria properties are especially appealing for applications such as gas sensors, heterogeneous catalysis, solid electrolyte fuel cells (SOFC), and especially, as catalysts for automobile exhaust systems. Because of the easy reduction of Ce^{4+} to Ce^{3+} and high oxygen ion conductivity, ceria-based materials possess high oxygen storage capacity.

References

[1] Cernea M, Vasiliu F., Bartha C., Plapcianu C. and Mercioniu M., Ceramics International, Vol. 40, Issue: 8, Pages: 11601-11609 Part: A (2014)

[2] R.Vidu, C. Plapcianu, C. Bartha, Industrial & Engineering Chemistry Research, Volume: 53 Issue:19 Pages: 7829-7839 (2014) (Review)

The spin magnetic moment of cobalt in compounds with half-metallic properties and inverse Heusler structure

A. Birsan

The interest in Heusler compounds [1] grew enormously, in the last years, due to the discovery of materials with high Curie temperature, low saturation of magnetization and high spin polarization, which may find application in new devices, related to the magnetic storage of information [2].

The feature called half-metallic ferromagnetism, proposed in 1983 by de Groot et al. [3] describes compounds behaving as hybrids between metals and semiconductors or isolators [4].

The inverse Heusler structure [5] is found in X_2YZ Heusler materials, with 2:1:1 stoichiometry, when the Y element is more electronegative than X, all symmetries adopted are T_d and no position with O_h symmetry is present. In this case, the X atoms are located in the non-equivalent 4a (0, 0, 0) and 4c (1/4, 1/4, 1/4) Wychoff positions, while the Y and Z atoms occupy the 4b (1/2, 1/2, 1/2) and 4d (3/4, 3/4, 3/4) positions, respectively.

We have used the self-consistent Full Potential Linearized Augmented Plane Wave (FPLAPW) method with the Perdew-Burke-Ernzehof (PBE) functional and Generalized Gradient Approximation (GGA) for the exchange and correlation interaction, as implemented in WIEN2k code [6] for electronic structure calculations to identify new half-metallic ferromagnetic materials, which are compatible with semiconductors, due to large enough spin-flip gaps. Therefore, the density of states, bandstructures and magnetic properties of Sc_2Co-based full-Heusler compounds with Z being an element from the fourth main group of the periodic table [7] and of Zr_2-based full-Heusler bulk system, Zr_2CoAl [8], were theoretically investigated to evaluate the possibility to obtain a high spin-polarized current through these half-metallic ferromagnetic compounds and to compare the magnetic moment carried by the cobalt atoms with those of other atoms from analyzed systems.

The investigated materials are stable against decomposition with formation enthalpies of -0.51 eV/atom (Sc_2CoSi), -0.63 eV/atom (Sc_2CoGe), -0.77 eV/atom (Sc_2CoSn) and -0.52 eV/atom (Zr_2CoAl), in ferromagnetic configurations at the calculated equilibrium lattice parameters and crystallize in the inverse Heusler structures. The negative formation enthalpies may be associated with the successful preparation of analyzed phases within experimental investigations.

For Sc_2CoSi, Sc_2CoSn and Zr_2CoAl the occurrence of an energy gap around Fermi level in the density of states from minority spin channel and the metallic behavior of majority spin electrons, lead to the half-metallic properties and the theoretically complete spin polarizations at ground state. The Fermi level, in the case of Sc_2CoGe, crosses the lower limit of the conduction band. A pseudogap is formed in the minority spin channel, which alter the spin polarization of this material by changing the density of states surrounding E_F and do not yield to half-metallic ferromagnetism.

All materials studied, fulfill the condition of having the total magnetic moments calculated at equilibrium lattice parameters, an integral number of Bohr magnetons per formula unit and follow the Slater–Pauling rule for ternary 2:1:1 compounds crystallizing in the inverse Heusler structure, $M_t = Z_t - 18$ (M_t is the total spin magnetic moments / unit cell while Z_t represents the total number of valence electrons).

To pinpoint the origin of magnetism, for all compounds, the partial magnetic moments were calculated at optimized lattice parameter. The major contributions to the total magnetic moments, for all compounds studied, come from the X atoms, located in (4a) Wyckoff positions that have tetrahedral symmetries T_d and are surrounded by Co atoms, at $a/2$ Å distances, where a are the optimized lattice parameters. This result is slightly surprising because these atoms (Sc in Sc_2Co-based full-Heusler compounds and Zr in Zr_2CoAl) in standard state do not have magnetic properties. Similar findings were reported in Ti-based half-metallic full Heusler compounds, which also follow the 18-electron-rule, where the highest spin magnetic moment contributions come from Ti atoms [9].

Despite the X atoms are ferromagnetically coupled, their dissimilar magnetic moments are determined by different neighborhoods, where the behavior of the Co magnetic moments illustrate that the X (4a)-Co interaction plays a crucial role for the prediction of half-metallic ferromagnets and for the determination of magnetic properties. Hence, in these compounds, the cobalt atoms even though, do not carry the highest spin magnetic moments, the covalent interaction with the X atoms located in (4a) Wyckoff positions determine the origin of the energy band gap.

In particular, the origin of the band gap in Sc_2CoSi case (Fig 1), results from the coupling between the d_{t2g} orbitals of Co atoms which correspond to the bonding states of valence band, 0.52 eV below E_F, and the triple degenerated d_{t2g} orbitals of Sc(4a) atoms, that have energy values in the region corresponding to the anti-bonding states of the conduction band, 0.0236 eV above E_F . An inspection of the local magnetic moments reveals that the atomic magnetic moments of X atoms from both positions (4a and 4c) decrease, in all studied materials, as the lattice expands, while the localized magnetic moments at the Co atoms are enhanced (see Fig 2 for Sc_2CoSi compound).

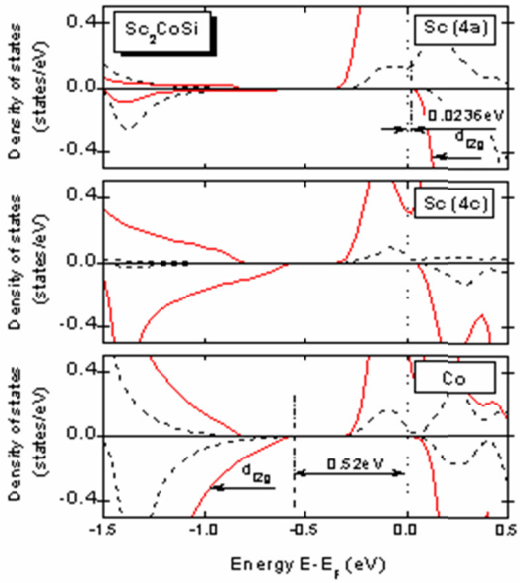

Figure 1 The main partial densities of states at optimized lattice parameters of Sc_2CoSi Fermi levels, d_{eg} and d_{t2g} being indicated by dotted, dashed and solid lines, respectively.

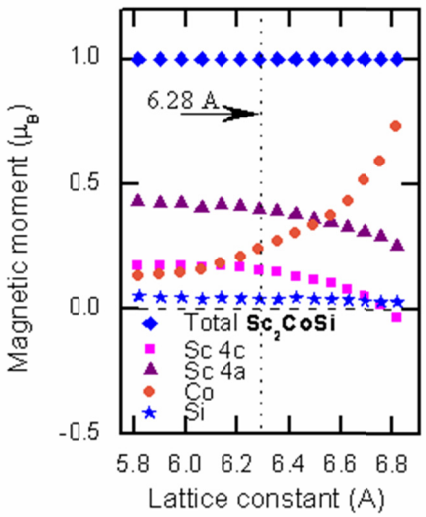

Figure 2 The total, site-projected magnetic moments as function of lattice constant for Sc_2CoSi compound.

References

[1] F. Heusler, Verh DPG 5 (1903) 219.
[2] T. Graf, C. Felser, S.S.P. Parkin, Prog. Solid State Chem. 39 (2011) 1.
[3] RA. de Groot, F.M. Mueller, P.G. van Engen, K.H.J. Buschow, Phys. Rev. Lett. 50 (1983) 2024.
[4] A.J. Bradley, J.W. Rogers, Proc. R. Soc. A 144 (852) (1934) 340.
[5] H.C. Kandpal, G.H. Fecher, C. Felser, J. Phys. D: Appl. Phys. 40 (2007) 1507.
[6] P. Blaha, K. Schwarz, G.K.H. Madsen, D. Hvasnicka, J. Luitz, WIEN2k, An Augmented Plane Wave Local Orbitals Program for Calculating Crystal Properties, Karlheinz Schwarz, Techn. Universit Wien, Austria, 2001 (ISBN: 3-9501031-1-2).
[7] A. Birsan J. Alloys and Compounds 598 (2014)230-235
[8] A. Birsan Current Applied Physics 14 (2014) 1434-1436
[9] A. Birsan, P. Palade, V. Kuncser, J. Magn. Magn. Mater. 331 (2013) 109.

Mn-based ferromagnetism in Ge(001)

G.A. Lungu, L.E. Ştoflea, L.C. Tănase, I.C. Bucur, F. Vasiliu, I. Mercioniu, V. Kuncser, C.M. Teodorescu

The Ge-Mn system is a promising diluted magnetic semiconductor (DMS), especially since it has been shown (Fig. 1) that by Mn deposition on Ge(001) (2x1) at high temperature (starting with 350 °C) the Ge surface remains unaffected [1]. Scanning tunneling measurements (STM) allowed one to identify surface Ge dimers on surfaces after Mn deposition, with a slightly elongated Ge-Ge distance with respect to the clean Ge surface (Fig. 2). Under this Ge-like surface, Mn_5Ge_3 clusters are formed, as revealed by high resolution transmission electron microscopy HRTEM (Fig. 3). However, X-ray photoelectron spectroscopy (XPS) data (Fig. 4) are interpreted in terms of a co-existence of Mn_5Ge_3 clusters with Mn diluted into the Ge matrix [1].

Thermo-magnetisation measurements revealed the influence of nanoparticles in the zero field cooled - field cooled curve (ZFC- FC) by a plateau in the ZFC curve, but also the presence of a maximum in the FC branch, which can be explained by considering the variation of the exchange integral with temperature (Fig. 5). Indeed, if the exchange interaction is intermediated by carriers in the semiconductor (Zener or RKKY models), its intensity is expected to depend strongly with temperature, as does the charge carrier density in the semiconductor. A complete model for this variation was developed in Ref. [2]. This model can be tested by fitting either the temperature dependence of the coercitive field $H_c(T)$ or that of the magnetisation $M(T)$ (Fig. 6). It was found that the RKKY model fits better the observed $H_c(T)$ and $M(T)$.

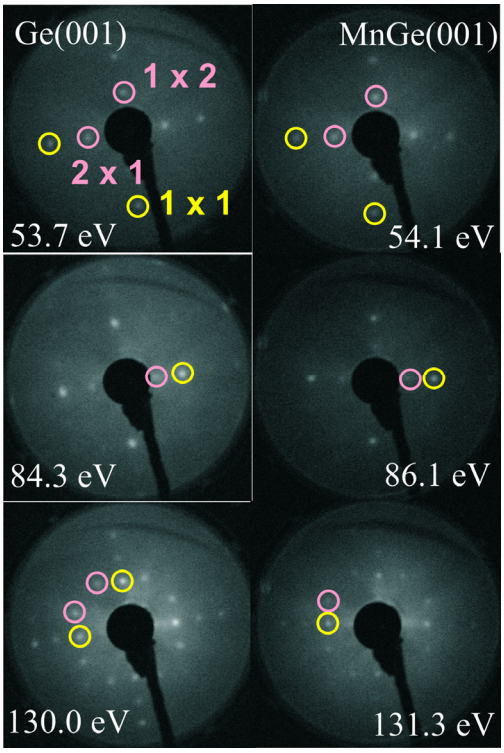

Fig. 1. *Low energy electron difraction (LEED) patterns for Ge(001) (left), and for 100 nm Mn deposited on Ge(001) at 350 °C (right). Electron energies specified on each image. The (1 × 1), (2 × 1) and (1 × 2) spots are highlighted [1,2].*

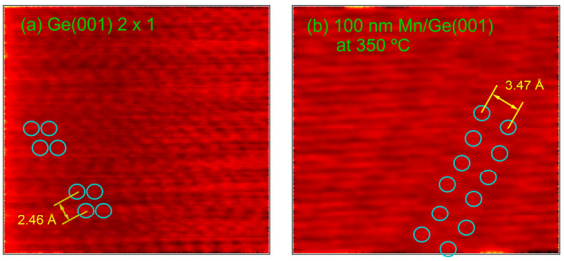

Fig. 2. *STM images obtained at a tip voltage of +150 mV (empty-states images), on (a) clean Ge(001) and (b) after the deposition of 100 nm Mn at 350 °C. The scanned area is 3 ×3 nm² [1].*

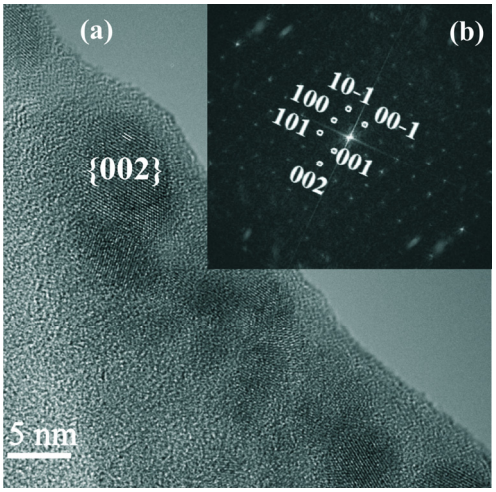

Fig. 3. *(a) Cross section HRTEM image of an area of a MnGe layer deposited at 350 °C; (b) associated FFT pattern showing the presence of Mn_5Ge_3 (electron beam direction [010]) [2].*

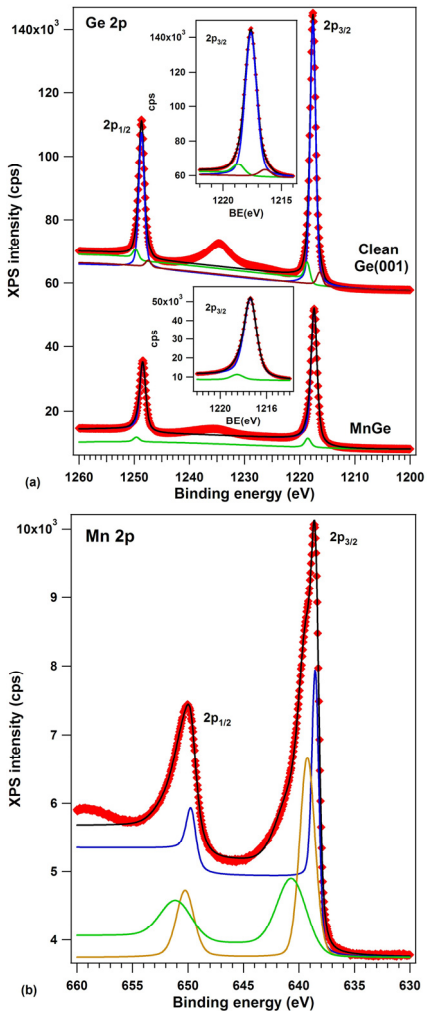

Fig. 4. X-ray photoelectron spectroscopy (XPS) results: (a) Ge 2p; (c) Mn 2p. All spectra are fitted by using Voigt doublets and backgrounds. Inserts in (a): detailed Ge $2p_{3/2}$ core level.

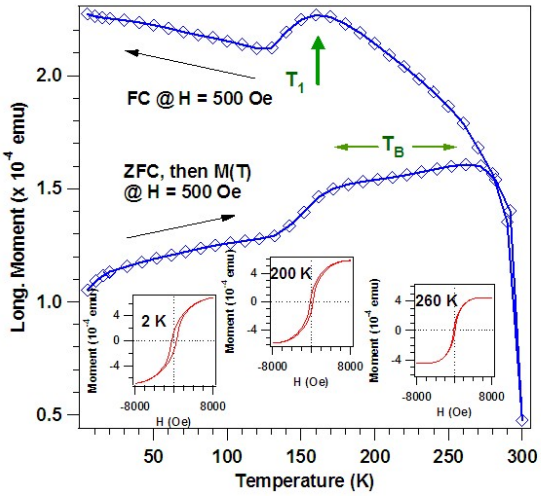

Fig. 5. Superconducting quantum inteference device (SQUID) measurement of a Mn-Ge(001) sample. The main graph represent zero field cooled - field cooled magnetization. Inserts represent magnetisation hysteresis measure-ments at the specified temperatures.

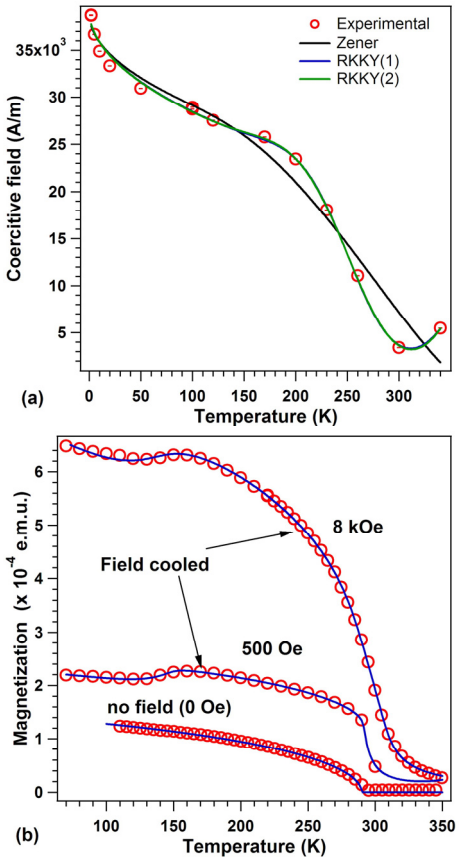

Fig. 6. Dependence of the (a) coercitive field and (b) magnetization with temperature, together with fits for Zener and for RKKY interactions.

This is an additional proof that a DMS-like material was synthesized. This material may offer opportunities of triggering its magnetic properties via the charge carrier density.

References

[1] G.A. Lungu, L.E. Stoflea, L.C. Tănase, I.C. Bucur, N. Răduțoiu, F. Vasiliu, I. Mercioniu, V. Kuncser, C.M. Teodorescu, Materials **6**, 106-129 (2014).

[2] G.A. Lungu, N.G. Apostol, C.M. Teodorescu, Chap. 4 in *Nanomagnetism*, J.M. Gonzalez Estevez (Ed.), One Central Press, Manchester, U.K. (2014), pp. 74-110, ISBN 978-1-910086-05-6.

Molecular adsorption and depolarization phenomena on ferroelectric surfaces

L.E. Şoflea, N.G. Apostol, C. Chirilă, L.Trupină, R. Negrea, L. Pintilie, C.M. Teodorescu

Ferroelectrics, such as lead zirco titanate (PZT) are intensively studied materials owing to their wide application in microelectronics, sensing and micro-electromechanical systems. Recently, increasing interest was brought to this area in view of the catalytic applications of their surfaces. The interplay between charge transfer and the polarization state is not yet well understood, therefore studies of thin ferroelectric layers with well defined polarization prepared by advanced methods (pulsed laser deposition) is of high actuality. These layers present mostly outwards polarization, as evidenced by atomic force microscopy (AFM) and piezoresponse force microscopy (PFM) [1-3].

The standard method to investigate surface composition and surface chemistry is X-ray photoelectron spectroscopy (XPS). To the surface, compositional and chemical sensitivity of the method, recently this method was validated to derive surface band bendings, assuming that core levels are shifted rigidly with the band curvature [1]. It is straightforward to apply this method to ferroelectric surfaces. Fig. 1 shows the evolution of core levels from the substrate of a PZT layer (Pb 4f) with the amount of metal deposited on surface (Cu and Au). In the case of Au, a constant band bending is observed, explained by a work function difference $\Phi_{PZT} - \Phi_{Au} \approx 0.3$ eV [1].

In the case of Cu/PZT, band bending should have occured towards higher binding energies by a serious amount exceeding 1 eV, since $\Phi_{Au} - \Phi_{Cu} \approx 0.6$ eV. In fact, this process is quenched and, starting with a given amount of Cu, the bending reverses its sign (Fig. 1(b)). Cu islands, initially insulated, form a continuous layer connected to the ground, which affects the surface polarization state of PZT (Fig. 2) [2]. This was checked by high resolution transmission electron microscopy (HRTEM, Fig. 3): after Au deposition, the PZT layer preserves its tetragonal distortion (a = 3.75 Å, c = 4.11 Å), whereas after Cu deposition, the tetragonality is lost ($a \approx c \approx 3.91$ Å).

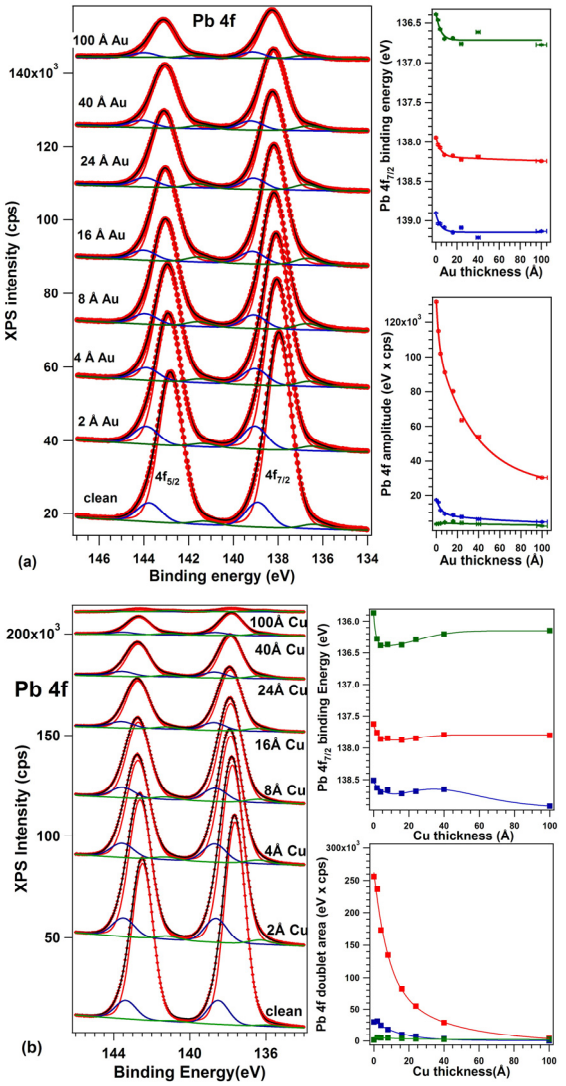

***Fig. 1**. Pb 4f XPS evolution with (a) Au deposition and (b) Cu deposition. Evolution of binding energies and of amplitudes of individual components are represented in the right panels.*

The charge state of polarized surface induce the preferential adsorption of polar molecules (such as fatty acids from standard contamination) on areas with outwards polarization [3]. The C 1s spectrum is shifted towards higher binding energies, since these molecules adsorb on positively charged surfaces, whereas in this case only the areas exhibiting inwards polarization are seen, owing to inelastic mean free path effects (Fig. 4). When the contamination exceeds a

critical thickness, it covers both kind of surfaces and the polarization of the substrate is lost by a mechanism similar to that of Cu/PZT [2,3].

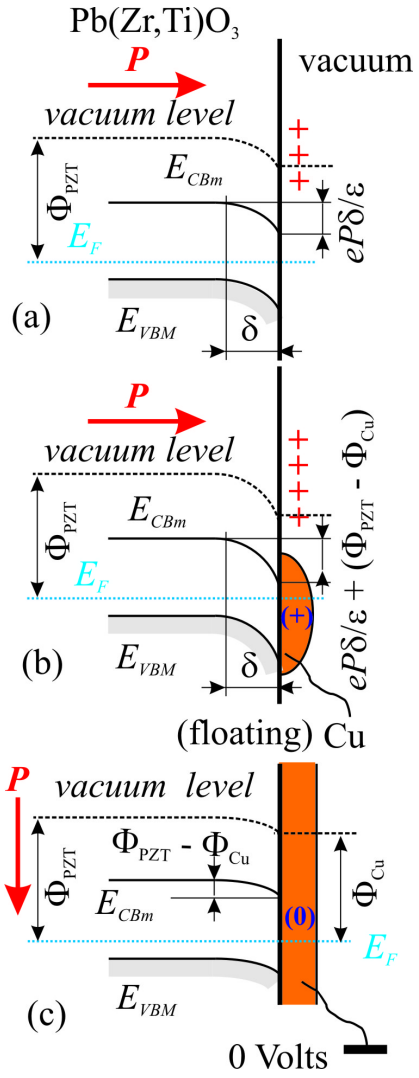

Fig. 2. Mechanism of band bending when Cu coalescing nanoparticles are deposited on PZT.

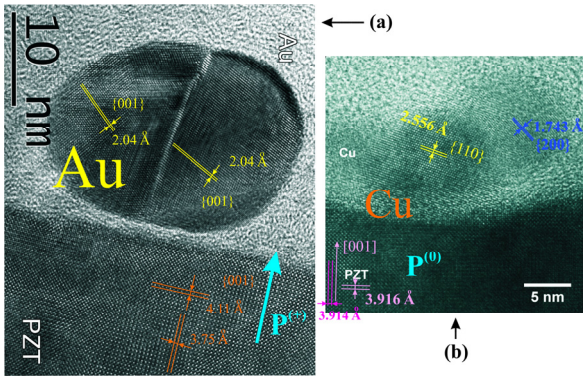

Fig. 3. HRTEM images of (a) a typical Au insulated nanoparticle and (b) Cu coalescing nanoparticles deposited on PZT.

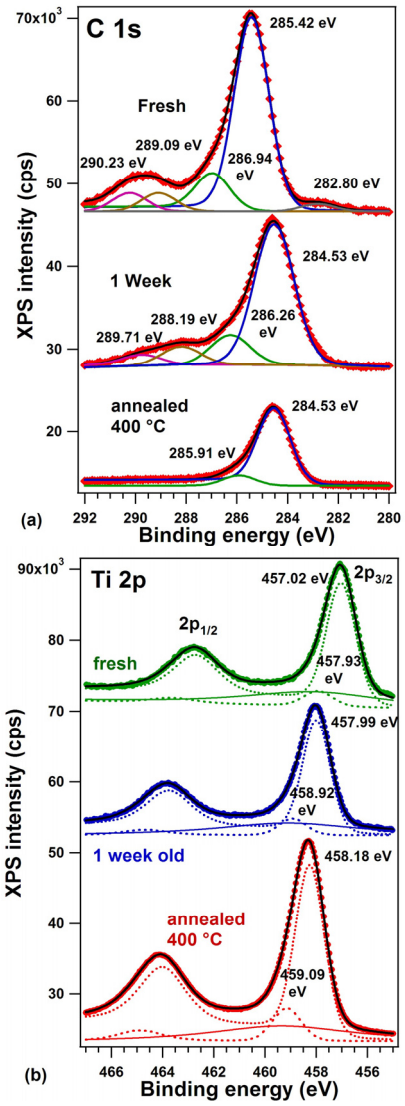

Fig. 4. XPS results for PZT samples prepared in similar conditions, but with different contamination levels (a) C 1s; (b) Ti 2p.

References:

[1] N.G. Apostol, C.M. Teodorescu, Chap. 7 in *Surface Science Characterization Techniques for Nanomaterials*, Springer Series on Characterization Tools for Nanoscience & Nanotechnology, Vol. 4, C. Kumar (Ed.), Springer, Berlin, Germany (2015), *in press*. ISBN: 978-3-662-44550-1.

[2] L.E. Ştoflea, N.G. Apostol, C. Chirilă, L. Trupină, R. Negrea, L. Pintilie, C.M. Teodorescu, J. Mater. Sci. **49**, 3337-3351 (2014).

[3] L.E. Ştoflea, N.G. Apostol, L. Trupină, C.M. Teodorescu, J. Mater. Chem. A **2**, 14386-14392 (2014).

Strain induced modification of trap parameters due to the stopped ions in Bi irradiated Si

M. L. Ciurea, S. Lazanu, A. Slav, C. Palade

Ion beam processing has long been used in manufacturing microelectronic devices for introducing dopant atoms in materials. The effects of the strain field are of great interest for microelectronic devices, as the strain in semiconductors alters the crystalline symmetry and consequently changes the materials properties from band structure to electronic transport and optoelectronic properties. By tailoring the strain, materials with suitable properties can be designed and manufactured.

There are only few studies related to effects induced by Bi irradiation on single crystal Si. As Bi atom is much heavier and has much larger size (atomic radius 1.70 A) than Si lattice atom (1.17 A), it produces a strong strain field which can be only partially relaxed by 'defect' formation. There are no reports in the literature on the influence of strain produced by the implantation of Si with heavy ions on trapping processes. To date, Bi donors in Si are shown to be excellent qubit candidates for quantum information processing, better than any other donor dopants, due to very long spin coherence times.

Float zone (100) Si wafers with 3±0.5^{O} off orientation, produced by Siltronix, P doped, with resistivity higher than 8000 Ωcm and 275±25 μm thickness were used. They have a low content of O and C impurities, of the order of 10^{16} and 10^{15} cm^{-3}, respectively, and a concentration of P less than 10^{12} cm^{-3}. The irradiation was performed with Bi^{6+} ions, at low fluence of $\mathbf{5\times10^{11}}$ ions/cm^2, with 28 MeV kinetic energy, at the Uppsala tandem accelerator.

During its slowing down, the incident Bi ion creates cascades of displacements (vacancy-interstitial pairs) following each primary interaction with the atoms placed in the sites of the lattice. As both vacancies and interstitials are mobile in Si at room temperature, they lead to the formation of 'stable' defect complexes and defect-impurity pairs, which have energy level(s) located into the band gap.

We simulated the penetration of 1000 Bi ions of 28 MeV kinetic energy into Si single crystals, for both the channelling direction and 3^{O} off orientation in respect to <100> [1], using the *Crystal-TRIM* code, based on the binary collision approximation (Fig. 1). We found that for 3^{O} off orientation, the stopped Bi ions have a nearly Gaussian distribution centred at 4.75 μm depth, with a FWHM of 0.90 μm, while for the channelling direction the distribution of stopped ions is asymmetrical, with the maximum at 7.40 μm under the surface and the FWHM of 0.82 μm. The distribution of vacancies is asymmetrical (see inset) and much broader than the distribution of Bi ions. It has the maximum at 4.25 μm and has a long tail toward the surface (for 3^{O} off orientation). Being bigger and much heavier than Si ions, Bi ions produce an important distortion in the lattice.

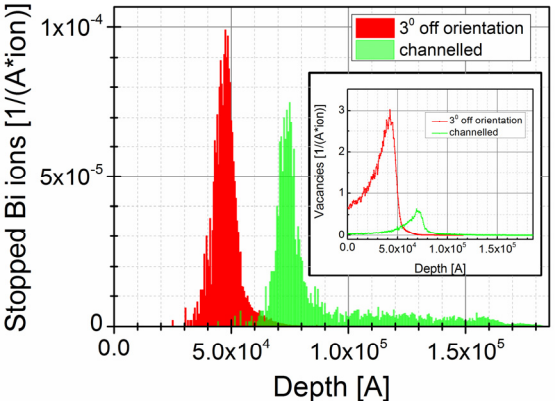

***Fig. 1** Depth distribution of Bi ions stopped into (100) Si: at perpendicular incidence and for 3^{0} off orientation. Inset: depth distribution of the vacancy – interstitial pairs.*

The method we chose for the investigation of Bi irradiation induced defects [1] is the TSC without applied bias, as it is very sensitive to trap concentrations. For this, square samples in sandwich geometry, with a semitransparent top electrode, were prepared. They are illuminated at low temperature with monochromatic light of 1000, 800 and 400 nm through the top electrode, in order to inspect the distribution of traps in the Si wafer. The traps located in the depth where light is absorbed are filled with photogenerated charge carriers, so that at low temperature a frozen-in electric field is produced in the sample. Then the sample is heated up to room temperature at a low constant rate, ensuring a quasistatic regime. During heating, the 'discharge current' due to carriers released from traps and also to equilibrium ones is recorded. The experimental set-up contains a Janis CCS-450 cryostat, a Keithley 6517A electrometer, a Lakeshore 331 temperature controller, and a Newport VIS-NIR Cornerstone 260 1/4m Monochromator System. By emission in bands of carriers from traps, the frozen-in electric field changes. The carriers move under the internal electric

field, no external bias being applied. In Bi irradiated Si samples, the internal electric field consists of two terms, namely the contribution from the carriers which are still trapped during heating, and the contribution from the strain produced by the differences in atomic size and mass between Bi stopped ions and Si. We consider the electric field which models the strain as permanent and temperature independent.

We found that the recorded maxima are very broad, suggesting that more than one trapping level contribute to the 'discharge current'. The peak intensities decrease with the wavelength from 1000 to 400 nm, and this is correlated with the decrease of the concentration of filled trapping centres which contribute to the current.

Fractionary heating measurements, performed in the aim to find out the activation energies of traps, were found usefulness in this case, due to the strong retrapping. Consequently, in modelling we have taken the start values for the activation energies from our previous results on Si irradiated with I ions [2] and from literature as well.

We calculated the 'discharge currents' in the frame of the model we developed previously. In the modelling, we considered the most probable trapping levels in high resistivity Si. The best fit was obtained with seven trapping levels. In the modelling, it appeared necessary to consider capture cross sections dependent on temperature. The best fit is for the dependence: $\sigma(T) = \sigma_0 \times (T_0 / T)^2$ for both electrons and holes, where T_0 is the start temperature of the measurement. The initial values for the cross sections σ_0 were also taken from literature and from our previous paper [2].

The trap parameters, carrier lifetimes and permanent electric field are iteratively adjusted to fit the experimental 'discharge current' curves, under the condition of strong retrapping. The 'discharge current' curves obtained for 1000, 800 and 400 nm illumination were simultaneously modelled. In Figs. 2 and 3 the experimental curves and the calculated ones for the 1000, 800 and 400 nm wavelength illumination are presented on the same graphs, showing a good fit. We resolved the 'discharge current' curves with seven traps and calculated their parameters. The three energy levels of V_2, the levels of VO/C_iC_s and C_iO_i, and also other two energy levels non-assigned have been found. From the fitting process it has resulted that all trapping levels are broadened, with a FWHM of 18–30 meV.

In conclusion, we have demonstrated that all traps are characterized by broadened energy levels with Gaussian distribution and FWHM in the interval 18–30 meV and by cross sections dependent on temperature ($\sim T^{-2}$). These characteristics of traps were not evidenced in I irradiated Si, in which the traps have discrete energy levels and temperature independent cross sections. Consequently, we attribute the broadened energy levels and the temperature dependent cross sections evidenced in Si irradiated with Bi ions to the strain field, modelled by a two times more intense electric field than in the case of Si irradiated with I. The modifications of trap parameters by the strain field are presented for the first time in literature and must be taken into account in designing and manufacturing microelectronic devices incorporating strain, including those used in quantum data storage and processing.

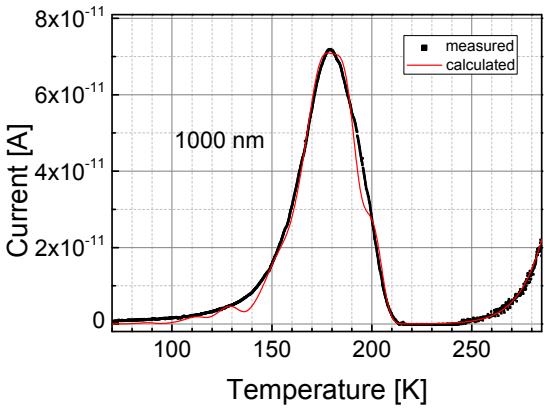

Fig. 2 Temperature dependence of the 'discharge current' after 1000 nm illumination: experimental (points) and modelled (continuous line) curves

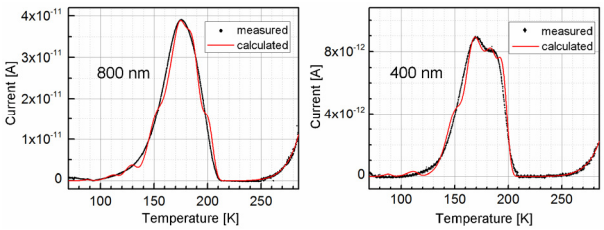

Fig. 3 Temperature dependence of the 'discharge current' after 800 nm and 400 nm illumination: experimental (points) and modelled (continuous line) curves.

References

[1] M.L. Ciurea, S. Lazanu, A. Slav, C. Palade, EPL **108** 36004 (2014).

[2] S. Lazanu, A. Slav, A.-M. Lepadatu, I. Stavarache, C. Palade, G. Iordache, and M.L. Ciurea, Appl. Phys. Lett. **101**, 242106 (2012).

Dynamics and relaxation of *sp* biexcitons in disk-shaped quantum dots

V. Moldoveanu I. V. Dinu and R. Dragomir

Self-assembled quantum dots (SAQD) are a promissing candidate for the implementation of quantum gates, the building-blocks of quantum computers [1,2]. In our work we study the effects of intraband relaxation (IBR) on the *sp* biexcitons hosted by a reallist CdTe SAQD subjected to radiation. The theorethical model investigated here goes beyond the usual two-levels systems borrowed from quantum optics and includes the Coulombian interactions. The persistence of the antiparallel *sp* electronic triplet in the ultra-fast regime is also investigated. The QD modelled here is cylindrically shaped and has radius (R) and height (W).

Using kp theory [3] we write the 4-bands Kohn-Luttinger for heavy holes(HH) and light holes(LH) that have the projection of the total spin: ±3/2, respectively ±1/2.

The single particle hole eigen-states in the valence band (VB) are found by diagonalizing the Kohn-Luttinger (KL) Hamiltonian within the anvelope approximation. The VB states are then a mixture of HH and LH in proportions that depend on the choice of the aspect ratio(R/W)[4].

Since the aspect ratio was chosen to be very small, this being the case for a nearly flat QD, the *s* and *p*-shell hole states are mostly HH[4]. The diagonalization of a 2-band Hamiltonian in the conduction band provides us with the single-particle eigenstates for electrons. The result is a mixture of products of anvelope functions and Bloch functions also known as the Luttinger spinor:

$$|\psi^{v}_{i,F_z}\rangle = \sum_{J_z,n,l} C^{i,F_z}_{n,l}\phi(F_z - J_z)_{n,l}|J_z\rangle$$

After a careful inspection we see the spectra exhibit atom-like structure: the s shell is followed by a *p* shell, than by a *d* shell, etc. It turns out [6] that the *p* shell levels need to be included in our simulations in order to have a more accurate description of the physics involved.

Having found the single-particle spectrum and the Luttinger spinors for a QD we can build the fully interacting Hamiltonian (H_0) whithin the configuration interaction method.

The relevant many-body states for our simulations are: the ground state (no electrons or holes), all excitons and all biexcitons, including the *sp* biexcitons. We focused on one particular *sp* biexciton: the one made of antiparallel hole and electron triplets. Unlike the *s* biexciton, the state of this *sp* biexciton cannot be written as a product of more simple excitonic states. We give here the expression of the *sp* biexciton with zero total electronic spin:

$$|B_{sp,0}\rangle \approx \frac{1}{\sqrt{2}}(|T^{e,0}_{sp_-}\rangle|T^{h,0}_{sp_+}\rangle + |T^{e,0}_{sp_+}\rangle|T^{h,0}_{sp_-}\rangle)$$

As we can see from the expression of the *sp* biexciton the interaction between electrons gives rise to a mixing of configurations.

The light-matter coupling is described semi-classically and modelled by a many-body operator which is added to the total Hamiltonian. We took into consideration the selection rules due to the cylindrical confinement [6].

The Neumann-Lindblad equation includes collapse Lindblad operators which describe the relaxations from higher energy levels to lower ones.

$$i\hbar\dot{\rho}(t) = [H_0 + V_R(t), \rho(t)] + i\sum_{\lambda}\mathcal{L}_{\lambda}[\rho(t)].$$

The relaxation times of electron and holes in ascending order are: the hole spin-conserving relaxation time is a few ps, the electron spin-conserving relaxation time is about 10-100 ps, the spin-flip electron relaxation time is about 100-1000 ps, while the spin-flip relaxation of holes is of the order of ns and it was neglected. The Neumann-Lindblad equation for the density matrix operator [5] was numerically solved. The diagonal elements of the density matrix operator represent the occupation probabilities of specific many-body states. The Rabi oscillations induced beetween the state of the s exciton and the state of the sp biexciton by a second laser pulse are strongly damped due to the IBR (see Fig.1).

While the spin-conserving electron relaxation time may contribute to the observed damping, the fast spin-conserving hole relaxation time is mostly responsible for damaging the *sp* biexcitonic state.

One can see that the occupations represented in the Fig. 1. don't sum up to *1* at all times. This means that other states are also involved in the dynamics. We call these states transient states (TS) since they eventually deplete in favor of the *s*-shell biexciton (recombination is neglected in the ultra-fast regime).

The mechanism of the conditional-not (CNOT) quantum gate is the following: the logical value of a target qubit is inverted if and only if the logical value of a second qubit is set to true. In our case, the occupation of the *s* exciton imposes a resonant condition on the second pulse if and only if the *s* exciton state has maximum probability.

Our two-color protocol described in Fig. 1 ressembles the CNOT operation, the control state being here the *s* exciton, while the target state being the *sp* exciton. The difference between this protocol and previous ones is that we also take into account the *p* shell states and Coulomb interaction which enables us to obtain an entangled target state.

We see from Fig. 1 that the efficiency of CNOT gate is rapidly compromised by IBR.

The simulations show that while the entangled states in the VB have rather small lifetimes, the antiparallel triplets in the conduction band can be used as a two qubit state. The temporal evolution of these electronic triplets was plotted against time for different electronic relaxation times (see Fig.2). We mention that a electron triplet state with total spin one is even more robust against decoherence due to the slower electron spin-flip relaxation rates.

The dynamics of the TS for different hole and electron relaxation times is also addressed in our paper. See [6] for further details.

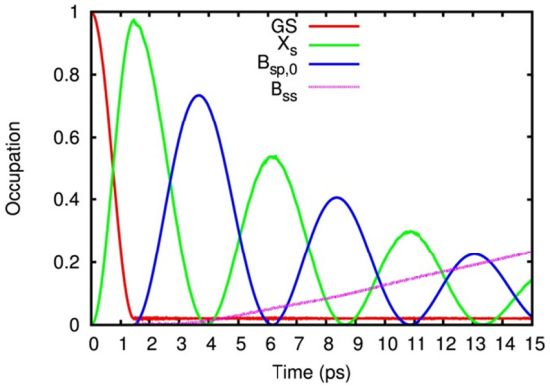

Fig.1: *The Rabi oscillations of the excitonic and biexcitonic populations P (Xs↓) and P ($B_{sp,0}$) with IBR. The first σ_+ pulse initializes the control exciton state Xs↓ and is turned off at t_s = 1.45 ps. The second σ_- pulse starts at the same time. Relaxation effects for relaxation times τ_e = 30 ps, τ_h = 4 ps. The occupations of the ground state (GS) and s-shell biexciton B_{ss} are also shown.*

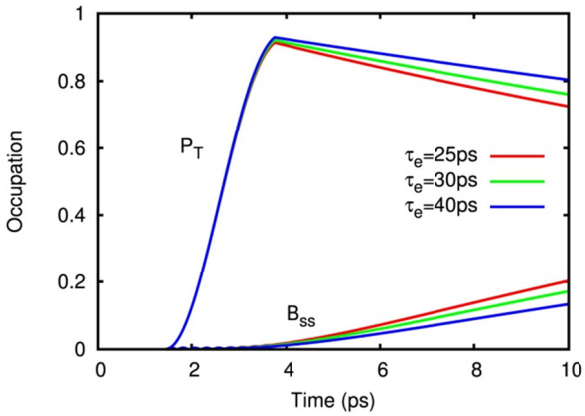

Fig.2: *The total occupation of antiparallel electronic sp triplet at different relaxation times τe . The occupation of the s-shell biexciton (B_{ss}) increases faster when the electron relaxationtime decreases. Other parameters: R = 15 nm, W = 5 nm, τ_h = 3ps, F=35kV/cm.*

References:

[1] F. Rossi, IEEE Trans. Nanotechnol. 3, 165 (2004).

[2] A. J. Ramsay, Semicond. Sci. Technol. 25, 103001 (2010).

[3] L. C. Lew, Y. Voon, and M. Willatzen, The kp Method (Springer, Berlin, 2010).

[4] J. I. Climente, M. Korkusinski, G. Goldoni, and P. Hawrylak, Phys. Rev. B 78, 115323 (2008).

[5] E. G. Kavousanaki and G. Burkard, Phys. Rev. B 86, 045122 (2012).

[6] V. Moldoveanu, I. V. Dinu and R. Dragomir, Phys. Rev. B 89, 245415 (2014).

Topological properties of the mesoscopic graphene plaquette: Quantum spin Hall effect due to spin imbalance

B. Ostahie, M.Niță, and A. Aldea

Significant conceptual interest in the properties of graphene was motivated first by the relativistic-like effects in the honeycomb structure and by the opportunity to investigate the high-temperature relativistic integer quantum Hall effect [1]. Next, interest was also stimulated by the topological insulating properties, based on the helical edge states of graphene, that support the quantum spin Hall effect (QSHE). The topological phase of graphene, predicted by Kane and Mele [2], is induced by the intrinsic spin-orbit (ISO) coupling, which opens a topological gap between the Dirac cones located at the points K and K' in the Brillouin zone. The gap is filled with helical states stretching along the edges, which appear in pairs and carry opposite spins in opposite directions. Recall that the helical states are protected against disorder by the time-reversal symmetry of the Hamiltonian, but they are not protected against the spin-flip processes.

We address the properties of the *finite (mesoscopic)* hexagonal lattice (Fig.1) with emphasis on some features of the QSHE and QHE. We adopt the tight-binding approach, introducing creation $\{a^{\dagger}_{\sigma,nm}, b^{\dagger}_{\sigma,nm}\}$ and annihilation $\{a_{\sigma,nm,}b_{\sigma,nm}\}$ operators of the localized states $|A_{\sigma,nm}\rangle, |B_{\sigma,nm}\rangle$ where $\sigma = \pm 1$ is the spin index and (n,m) stands for the cell indices. The Hamiltonian defined on the honeycomb lattices can be written as:

$$H = \sum_{\sigma} H_0^{\sigma} + \sum_{\sigma} H_{SO}^{\sigma}, \qquad (1)$$

where the first term describes the tunneling between the nearest neighbors, while the second one represents the intrinsic spin-orbit interaction. In the presence of a perpendicular magnetic field, described by the vector potential $\vec{A} = (-By, 0, 0)$ the first term reads:

$$H_0^{\sigma} = \sum_{nm} E_A a^{\dagger}_{\sigma,nm} a_{\sigma,nm} + E_B b^{\dagger}_{\sigma,nm} b_{\sigma,nm} + t(e^{i\phi(m)} a^{\dagger}_{\sigma,nm} b_{\sigma,n,m} + e^{i\phi(m)} b_{\sigma,n+1,m} a_{\sigma,nm} + b_{\sigma,n,m+1} a_{\sigma,nm} + H.c). \qquad (2).$$

$E_{A,B}$ are the atomic energies, t is the hopping integral between the sites A and B, and the Peierles phase due to magnetic field equals $\phi(m) = \pi(m + 1/6)\phi$, where the magnetic flux through the unit cell ϕ is expressed in quantum flux unit $\phi_0 = h/e$.

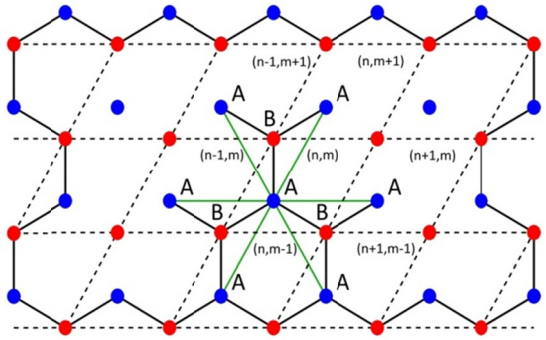

Fig.1: A sketch of the honeycomb lattice plaquette with horizontal zigzag and vertical armchair edges. The two type of atoms in the unit cell are A (blue) and B (red); (n, m) are the cell indices. The green lines connect an atom A to the six next-nearest neighbors, while the nearest neighbors are connected by the black lines; the unit cells are drawn with dashed lines. The number of lattices sites is 11×4.

The intrinsic spin-orbit Hamiltonian [2] conserves the electron spin S_z, and invokes the hopping to the six next-nearest neighbors (NNN), keeping also in mind the chirality of the trajectory between the two sites. In the presence of magnetic field the intrinsic spin –orbit Hamiltonian can be written in a compact form as [3]:

$$H_{SO}^{\sigma} H_{SO}^{\sigma} = i\lambda_{SO} \frac{1}{2} \sigma \sum_{\langle\langle nm,n'm' \rangle\rangle} \nu_{nm} e^{i\phi^{a}_{nm}} a^{\dagger}_{\sigma,n'm'} a_{\sigma,nm} + (a \to b) + H.c., \qquad (3)$$

where λ_{SO} is the spin-orbit coupling constant, $\nu_{nm} = \pm 1$ express the clockwise or anticlockwise chirality of the trajectory between the NNN and the phases ϕ^{a}_{nm}, ϕ^{b}_{nm} should be calculated by the integration of the vector potential along each trajectory.

In the presence of a small spin-orbit coupling (meaning $\lambda_{SO} \ll t$), a topological gap appear in the middle of Hofstadter spectrum. This gap is filled with helical edge states that give rise to very interesting results in the quantum Hall and quantum spin Hall transport. Also the Hofstadter spectrum exhibits the splitting of each relativistic band in two spin-dependent subbands. The small spin-orbit gap created in between is filled with edge states of both spins; however, essentially, the number of spin-up sates differs from the number of states with spin-down. This denotes the existence in the energy spectrum of "*spin-imbalance*" gaps induced by the spin-orbit coupling. This finding should not be overlooked as it is associated obviously with an imbalance of the spin currents, which may account for a nonzero QSHE in the corresponding energy range.

Simulating a quantum Hall device by attaching four leads to the finite hexagonal lattice we measure the quantum Hall spin and charge conductance. Concerning the charge conductance, we observe not only the vanishing value in the topological range and the known plateaus at 2, 6, and 10 in the relativistic one, but also some unexpected plateaus at 4 and 8 (in units of e^2/h). A similar behavior is proved by the spin Hall conductance, which shows the expected value 2e/4π in the topological range, and then vanishes everywhere except the same energy stripes where the unusual values of the charge Hall conductance occur (Fig.2). In the respective stripes the spin Hall conductance equals −2e/4π. According to the previous discussions, it is obvious that they appear in the *spin-imbalanced* gaps generated by the intrinsic spin-orbit interaction in the presence of the magnetic field.

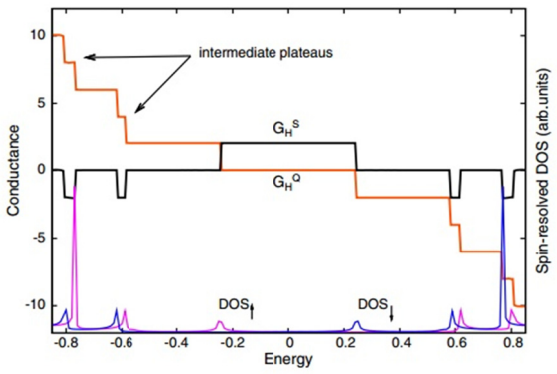

Fig.2: The spin and charge Hall conductance in the quantum regime (in $e/4\pi$ and e^2/h units, respectively); novel plateaus are visible in the imbalance gaps opened by the intrinsic spin-orbit coupling. The spin-resolved density of the states are also shown ($\phi = 0.03\phi_0$, $\lambda_{SO} = 0.05$ and the number of sites 105×40).

The density of states (shown in Fig.2) is calculated as $DOS = -\frac{1}{\pi} Tr[ImG^+(E)]$, where $G^+(E)$ is the retarded Green function for the mesoscopic graphene connected to the leads.

The main result of this work counts in finding anomalous plateaus of the QSHE outside the topological gap and namely in the spin-imbalanced gaps [4], as one can clearly see in Fig.2.

References:

[1] K. S. Novoselov, A. K. Geim, S. V. Morozov, D. Jiang, M. I. Katsnelson, I. V. Grigorieva, S. V. Dubonos, and A. A. Firsov, Nature **438** 197 (2005).

[2] C. L. Kane and E. J. Mele, Phys. Rev. Lett. **95**, 226801 (2005).

[3] O. Shevtsov, P. Camier, C. Petitjean, C. Groth, D. Carpentier, and X. Waintal Phys. Rev. X **2**, 031004 (2012).

[4] B. Ostahie, M. Nita and A. Aldea, Phys. Rev. B **89**, 165412 (2014).

Electrochemical Grafting of Reduced Graphene Oxide with Polydiphenylamine Doped with Heteropolyanions and Its Optical Properties

I. Smaranda, I. Baltog, M. Baibarac
in cooperation with
A.M. Benito, W. K. Maser
Instituto de Carboquímica ICB-CSIC, Zaragoza, Spain

In the last two decades, composite materials based on conjugated polymers (CPs), hetero-polyacids, and carbon nano-tubes have been considered as promising active materials in the field of energy sto-rage. Alternatively, less expensive graphene based materials, namely graphene oxide (RGO), have gained increased interest for the development of functional composites. This work reports new results obtained by photo-luminescence (PL) and vibrational spectroscopic studies on RGO/polydiphenyl-amine (PDPA) composites doped with phos-photungstic acid ($H_3PW_{12}O_{40}$) heteropoly-anions (RGO/PDPA:PT) synthesized by cyclic voltammetry [1]. The adding of RGO at the DPA-DMF solution leads to the appearance of an additional absorption band at 600 nm (Fig.1b), that belongs to PDPA in the un-doped (Fig.1c) and doped state (Fig.1d).

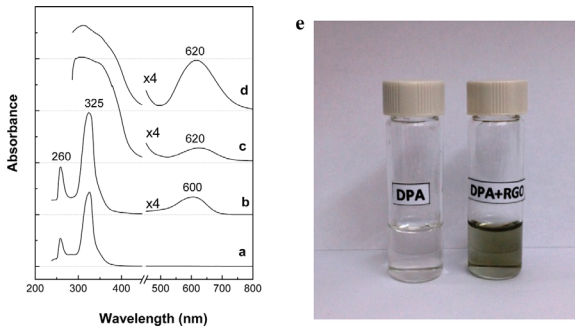

Fig 1 *UV–VIS spectra of the DPA in DMF (a), RGO/DPA blend 1 in DMF (b), the PDPA and PDPA:PT films electro-chemically synthesized onto ITO supports at stopping potentials of +100 mV (c) and +960 mV (d), respectively. Photo of solutions of DPA and RGO/DPA blend 1 after an aging time of 24 h (e).*

Fig. 2 shows the PL spectra of DPA and the DPA/RGO blend. Comparing Figs c_1 and d_1, one observes that the presence of RGO in DPA leads to a decrease of the global intensity of the complex PL band of DPA while its maximum shifts from 3.58 to 3.66 eV. Such an upshift in the PL spectrum is correlated with changes in the vibration spectrum of DPA.

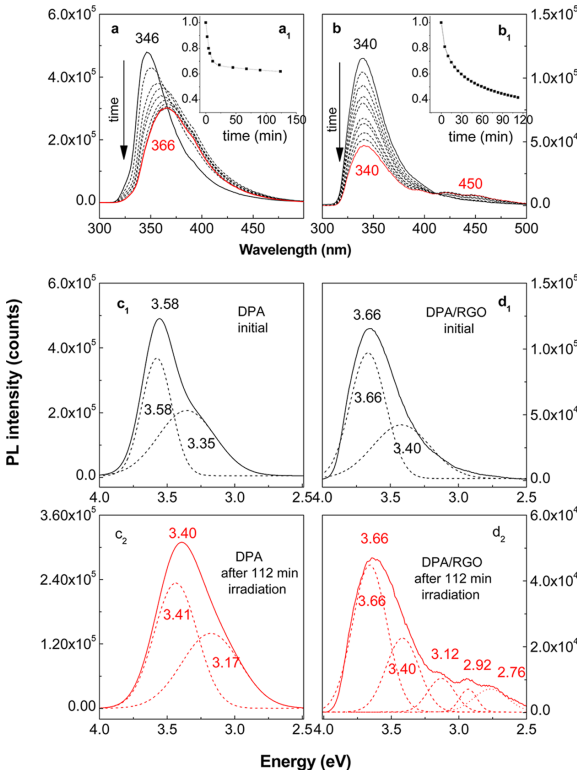

Fig. 2 *PL spectra recorded at room temperature under λ_{exc} = 275 nm of DPA (a) and DPA/RGO blend 2 (b) under UV irradiation time of 112 min (black curves with solid and dashed lines correspond to the initial state and the interme-diary state; red curves correspond to the final state after irradiation). Insets a_1 and b_1 show the PL decay as a function of the UV irradiation time. Figs. c_1 and d_1 depict the deconvoluted PL spectra at the initial state of DPA and RGO/DPA blend 2, respectively. Figs. c_2 and d_2 show the deconvoluted PL spectra after 112 min of UV irradiation of DPA and RGO/DPA blend 2, respectively.*

Fig. 3 depicts the FTIR spectra of DPA and the DPA/RGO blend. In the case of the DPA/RGO blend, clearly the appearance of a

new absorption band at 1632 cm^{-1} can be seen. This band originates from the formation of new C–C covalent bonds between different carbon nanoparticles and polymers via the transformation of aromatic rings of carbon nanotubes into orthodisubstituted cyclic hydrocarbon rings. [1]

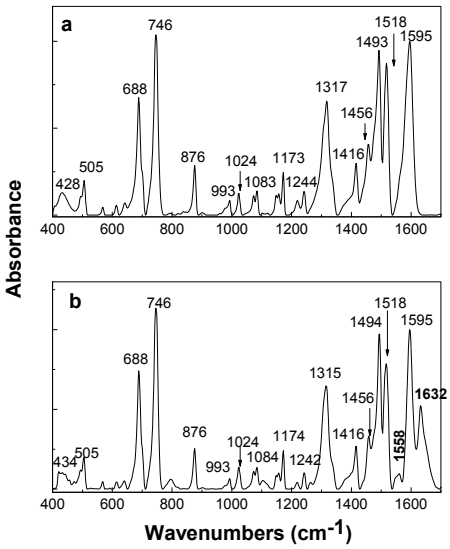

*Fig. 3 FTIR spectra of DPA (**a**) and the DPA/RGO blend after UV-Vis irradiation (**b**).*

The formation of new C–C covalent bonds indicates a covalent grafting of RGO with DPA. The PL quenching effect induced by the irradiation with light of 275 nm for 112 min is accompanied by: (i) a down shift of the complex PL bands of DPA from 3.58 and 3.35 eV to 3.41 and 3.17 eV, respectively (Figure $2c_2$,c_1), and (ii) the appearance of new PL bands with maxima at 3.12, 2.92, and2.76 eV (Figure $2d_1$,d_2) in the case of the RGO/DPA blend, which indicates the development of chemical reactions under UV irradiation. According to Ref. [1], these PL bands at 3.12, 2.91, and 2.76 eV are also found in the PL spectrum of PDPA. These photochemical reactions concern the homolytic breaking of the C–H bond in DPA, which results in two very instable free radicals that react rapidly with themselves, leading to the formation of dimers and oligomers in the case of DPA. The homolytic breaking of the C–H bond leads to a covalent grafting of RGO with monomers that are transformed into oligomers. UV–VIS spectroscopy and PL on blends of RGO/DPA evidence the partial transformation of the DPA monomers into oligomers of PDPA upon UV irradiation. The absence of light is a critical condition for the electrochemical synthesis of RGO/PDPA composites.

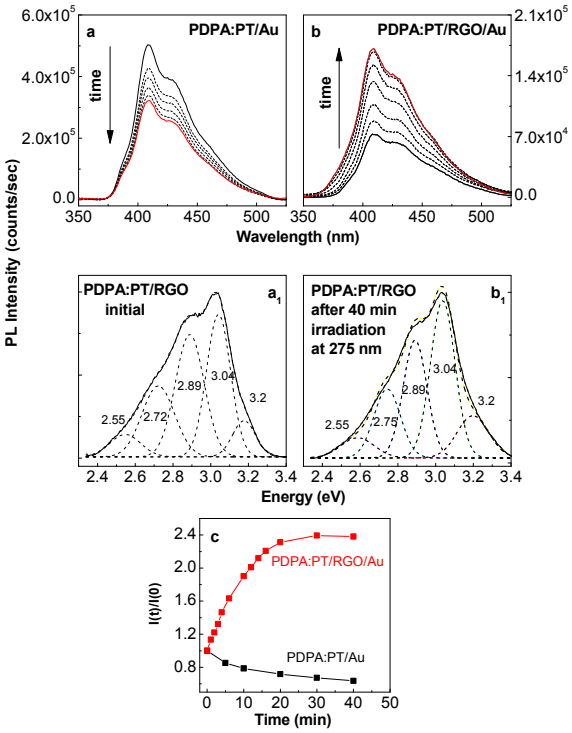

Fig. 4 The variation of the PL intensity of PDPA:PT, electrochemically synthesized (on the Au electrode and on the Au plate covered with RGO film, depending on the irradiation time at a 275 nm excitation wavelength.

According to Fig.4, the increase in the relative intensity of the PL spectrum of RGO covalently graphted with PDPA:PT reveals photochemical reactions under UV irradiation that involve the transformation of the RGO/PDPA:PT composite containing $HPW_{12}O_{40}^{2-}$ anions into an RGO/PDPA:PT composite stabilized by $PW_{12}O_{40}^{3-}$ anions. This work provides new insights on the interactions between RGO, conjugated polymers and stabilizing dopant ions.

References

[1] I. Smaranda, A. M. Benito, W. K. Maser, I. Baltog, and M. Baibarac, J. Phys. Chem. C 118, 25704, (2014).

Effects of the ionic association-dissociation and adsorption-desorption on the space charge polarization

C.P. Ganea,
in cooperation with
D. Manaila - Maximean, Politehnica University, Bucharest

The need to develop a theoretical model for studying the effect of electrode polarization appeared after performing and processing the experimental results presented in ref. [1]. The phenomena that occur both in volume and at surface due to the free carriers (ions) are rather complicated. Theoretical study was conducted progressively being developed a hierarchical ensemble of models, from the simplest to the most comprehensive ones [2, 3, 4].

In materials with mobile ions the electrode polarization effects and the ionic conductivity overlap at low frequencies in the spectrum of complex functions $\varepsilon^*(\omega)$, $\sigma^*(\omega)$. High-frequency parts of ac conductivity and permittivity spectra are governed by ion movements in the bulk of the ionic liquid, while the low-frequency part is governed by electrode polarization effects, as shown in Fig. 1 (5CB/TiO2 (5:1)) also a representative one [1]. For TiO_2 with liquid crystal 5CB (5: 1) composite system the common values are $\varepsilon = 6$, $\sigma = 10^{-11} S/m$, at room temperature. The ac electrode polarization effect is manifested by increase of the dielectric permittivity, well above the normal values, compared with the bulk at lower frequencies.

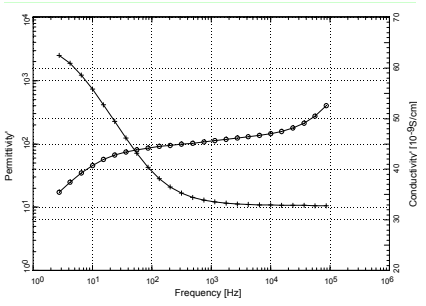

Fig. 1 Dependence on the frequency of electrical conductivity (o) and the permittivity (+), at the temperature of 321.1 K of the system 5CB/TiO_2 [1].

Accumulation of charge carriers at the electrode-sample interface leads to lower conductivity and the redistribution of local electric field. At contact surface between the electrode and the sample the adsorbed molecules of the liquid form a compact monolayer (Helmholtz layer) which prevents or limits the electric charge transfer between the electrode and the sample. Since the ions are blocked at the electrode-sample interface, there is an accumulation of ions near the electrodes, leading to the formation of space-charge layers, so called electrode polarization (EP). The voltage drops rapidly in these layers, which implies a huge electrical polarization of the material and a near absence of electric field in the bulk sample at low frequencies. The build-up of electrical polarization and the drop of the electric field in the bulk are reflected in an increase in the ac permittivity and a decrease in the ac conductivity with decreasing frequency. This process occurs dynamically and is specific to the ion electrical charge transport in the ac regime.

The work presented here [4] contains the more general theoretical model developed so far by us to study the electrode polarization. This model re-writes the well known system of the continuity equations for the mobile charge carriers and the Poisson equation of the electric potential as well by choosing new variables. Since the applied ac voltage is small enough, the equations were linearization. The mobile ions may come from impurities or from dissociation of molecules. We suppose that the ions have different mobilities and diffusion coefficients; the equilibrium concentrations of the carriers are uniform and equal each other. The mechanism of generation-recombination considered here is the dissociation and association of the neutral center, such as ion pairs in weak electrolytes. This recombination process is the best approximation for small deviation from equilibrium. It can provide an adequate

description of the wide variety of other recombination processes. Thus the generation-recombination rates are:

$$-r_p = -r_n = i\omega R p_0 (p+n)/(i\omega + G)$$

where R is the recombination (association) rate, G is the generation (dissociation) rate. The electrodes are either completely blocking or blocking by adsorption-desorption processes. A voltage U_A is applied to a dilute, binary ionic liquid placed between parallel plate blocking electrodes separated by L (Fig. 2) [2].

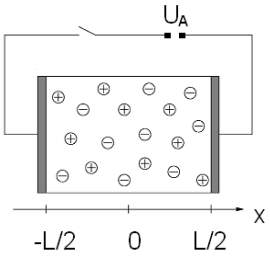

Fig. 2 Sketch of the sample cell measurement [2].

For low rates of the adsorption/desorption, the kinetic equation describing the time variation of surface concentration of ions adsorbed on the electrodes Σ_p, Σ_n, contain two phenomenological parameters: one associated with the adsorption (the adsorption coefficients K_p, K_n) and the other to the desorption phenomena (the desorption times γ_p, γ_n):

$$\dot{\Sigma}_m = K_m m(\pm L/2) - \gamma_m^{-1}\Sigma_m,$$

where $m = p$ or $m = n$.

The electric current densities must be equal to the temporal variation of the surface concentration of the adsorbed ions, and the boundary conditions are:

$$j_m = q_m \dot{\Sigma}_m = q_m K_m^*(\omega) m(\pm L/2),$$

where $K_m^*(\omega) = i\omega\gamma_m K_m / (1 + i\omega\gamma_m)$.

With original independent variables $n(x)$ and $p(x)$, we define new variables that are equal to the average concentration of charge carriers and the difference of the concentrations $n_c = (p+n)/2$ and $n_d = p - n$.

The quantity calculated as the difference of the concentrations is proportional to the net local electric charge density $\rho = q(p-n) = qn_d$. All the other physical parameters associated with charge carriers can be reformulated by the same operations and obtain the corresponding mean and differential values. Using the new variables, we reformulated the basic system of equation of continuity for ions and the Poisson equation for the electric field. It allows us solving the problem and to obtain exact analytical expression for the admittance $Y(\omega) = I/U_A$ of the considered physical system. The admittance (or impedance) final expression highlights the contribution of the bulk ionic conductivity and the electrode-sample interface polarization

$$Y = Y_{bulk} + Y_{EP}$$

$$Y_{bulk} = \frac{S}{L}(\sigma_0 + i\omega\varepsilon_0\varepsilon_r)$$

$$Y_{EP} = \frac{2q}{U_A}\frac{S}{L}(D_d n_d + D_c n_c).$$

The analytical form of the admittance highlights a distinctive term that is proportional to one a-dimensional parameter which estimates the relative effects of the bulk process in comparison with the interfaces process: $\psi = K_c\gamma_c / L_D$. The structure of admittance expression suggests an electric equivalent circuit in correspondence with the physical processes that occur in volume and at surface (Fig.3) [4].

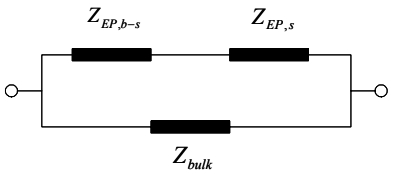

Fig. 3 Equivalent electric circuits in accordance with the admittance (impedance) structure [4].

References

[1] C. P. Ganea, D. Manaila-Maximean, Politehn. Univ. Bucharest Sci. Bull. Ser. A Appl. Math. Phys. 73, 209-216 (2011).
[2] C. P.Ganea, Rom. J. Phys. 57, 664–675 (2012).
[3] C. P. Ganea, Cent. Eur. J. Phys. 11, 497-511 (2013).
[4] C. P. Ganea, Eur. Phys. J. Plus 129, 238 -250 (2014).

In vitro biological interactions of titanium sillenite ($Bi_{12}TiO_{20}$) and Si/SiO_2 micro and nanomaterials

T. Popescu, M. Feder, D. Tarabasanu-Mihaila, V.S. Teodorescu, A.M. Vlaicu, L. Diamandescu
in cooperation with
A.R. Lupu
Cantacuzino National Institute for Microbiology and Immunology, Bucharest, Romania
M. S. Stan, I. Memet, A. Dinischiotu
Faculty of Biology, University of Bucharest, Romania
C. Sima
National Institute for Laser, Plasma and Radiation Physics, Magurele, Romania
A. Hermenean
Faculty of Medicine, Vasile Goldis Western University of Arad, Romania

$Bi_{12}TiO_{20}$ study

The monoclinic α-Bi_2O_3 has been traditionally used as a main component of endodontic materials and has been recently shown to possess antifungal properties and considered a potential candidate for related biomedical applications.

In this study we investigate the basic toxicological effects of the cubic γ-Bi_2O_3 structure, synthesized as titanium sillenite $Bi_{12}TiO_{20}$ (γ-BTO) by coprecipitation and solid state reaction [1]. The composition, crystal structure and morphology of the produced materials were assessed by XRD, SAED, TEM, SEM and EDS). The cytotoxicity, nitric oxide (NO) release and intracellular reactive oxygen species (ROS) production were determined on three cell lines-HepG2 (human hepatocellular carcinoma), SH-SY5Y (human neuroblastoma) and 3T3-L1 (murine normal fibroblasts)-with respect to material type, concentration and cell treatment time [1].

Pure phase nanometric γ-BTO monocrystals were obtained by both synthesis methods. The polycrystalline nucleation observed on the surface of the obtained particles was identified (by structure and composition) as γ-BTO (Fig.1). The *in vitro* biological tests indicated low or no cytotoxicity (Fig.2) and nitrosative/oxidative stress tendencies in agreement to the functional characteristics of the used cell lines [1]. The observed effects of γ-BTO may involve the role of NO as immune and neural mediator and its use in specific defense mechanisms as well as the function of ROS in redox-sensitive cell proliferation mechanisms.

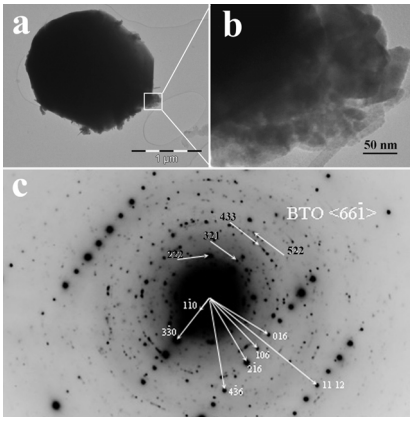

Fig. 1 *TEM/SAED details of the polycrystalline nucleation on the surface of the γ-BTO monocrystal.*

The obtained results recommend γ-BTO for further studies regarding its biocompatibility and potential for biomedical applications.

Si/SiO_2 study

Quantum dots (QDs) are used in many biological applications including cancer therapy, cellular imaging and delivery of various molecules (drugs, peptides, nucleic acids) into cells. Although silicon QDs are known to exhibit lower toxicity compared to those that contain heavy metals, it has been proposed that high concentrations of Si QDs may generate oxygen radicals that could affect the structural integrity of cell membranes and induce cytotoxicity.

In this study we investigate the impact of Si/SiO_2 QDs, produced by pulsed laser ablation,

on the cell redox status and intracellular distribution of glutathione [2].

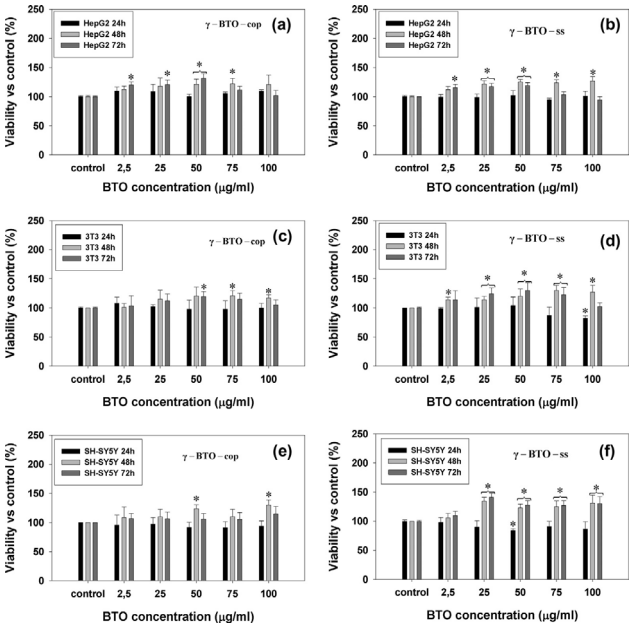

Fig. 2 *Viability results for: HepG2 (a and b), 3T3-L1 (c and d), SH-SY5Y (e and f); (*) – significant differences with respect to control ($p < 0.05$ – calculated based on four biological replicates).*

Material characterization (by EDX, XRD, SAED, HRTEM,) revealed nanoparticles aggregates composed of crystalline Si cores surrounded by amorphous SiO_2 shells (Fig.3). Micron sized silicon drops were also found in the studied samples (Fig.4) [2].

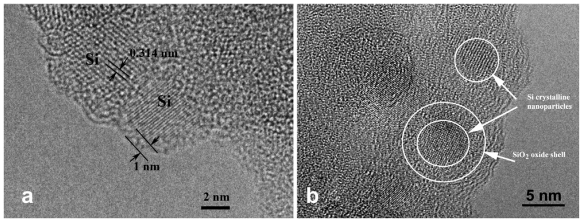

Fig. 3 *HRTEM image showing: (a) the crystalline silicon core surrounded by a thin amorphous SiO_2 layer; (b) detailed view of a nanoparticle aggregate.*

Biological tests indicated increased levels of ROS, the decrease of glutathione (GSH) content (Fig. 5) and accumulation of oxidized proteins, contributing to the formation of a highly oxidative environment that affected cell viability and morphology [2].

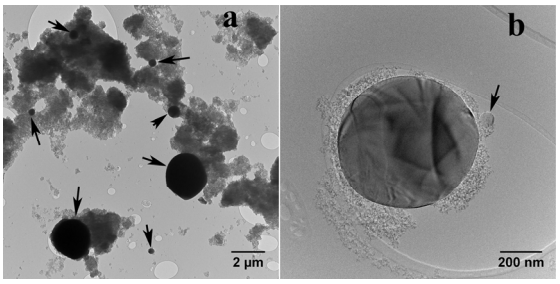

Fig. 4 *Particle morphology. (a) Micron-sized spherical silicon monocrystals (arrowed). (b) A larger (600 nm) and a smaller (60 nm) silicon spheres surrounded by aggregates of Si/SiO_2 nanoparticles.*

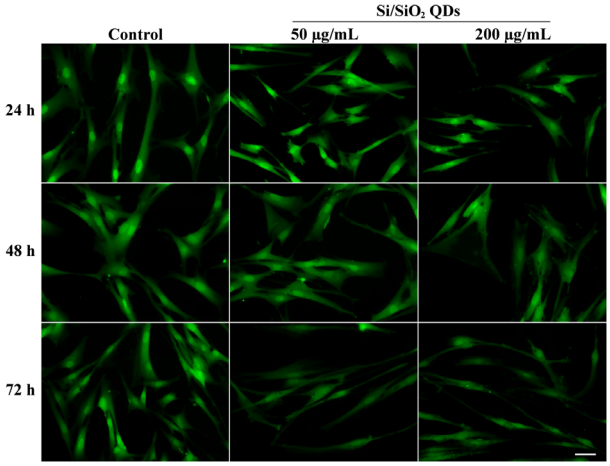

Fig. 5 *Cellular distribution of GSH is altered by Si/SiO_2 QDs exposure. Cells were incubated in the presence of 50 and 200 μg/mL QDs for 24, 48 and 72 h and were labeled with CMFDA to mark GSH. Representative fluorescence images of GSH staining are shown. Scale bar = 50 μm.*

Acknowledgements

T. Popescu acknowledges support under projects SOPHRD/107/1.5/S/82514 and PN09-450103.

References

[1] T. Popescu, A.R. Lupu, M. Feder, D. Tarabasanu-Mihaila, V.S. Teodorescu, A.M. Vlaicu, L. Diamandescu, Toxicology in Vitro, 28(8), 2014, 1523-1530

[2] M. S. Stan, I. Memet, C. Sima, T. Popescu, V. S. Teodorescu, A. Hermenean, A. Dinischiotu, Chemico-Biological Interactions, Volume 220, p.102-115 (2014)

Toxicity Evaluation following Intratracheal Instillation of Iron Oxide in a Silica Matrix in Rats

C. S. Ciobanu, C. L. Popa, S. L. Iconaru, D. Predoi
in cooperation with
A. M. Prodan
Emergency Hospital Floreasca, Bucharest, Romania

In recent years, an increasing interest has been registered for developing the field of nanotechnology. The unique chemical, physical, optical, electronic, and magnetic properties show that nanoparticles could be used in biotechnology and biomedicine. The size of these nanoparticles facilitates their use in engineering of surfaces and in creating functional nanostructures [1]. Among the many types of nanoparticles, superparamagnetic iron oxide nanoparticles (SPIONs) have been already used for several in vivo applications, showing promising results. They were used as contrast enhancement in magnetic resonance imaging [2], for tissue repair [2], for drug delivery in tumour therapy [2], etc. In order to be used for these types of applications, the nanoparticles biocompatibility could be increased by adding a silica shell. Due to the biocompatible properties, silica is less likely to degrade in a biological environment [3].

The goal of this study was to prepare iron oxide-silica nanoparticles froma mixture of ferrous chloride tetrahydrate and ferric chloride hexahydrate dropped into a silica xerogel composite. The structure and morphology of the synthesized maghemite nanoparticles into the silica xerogel were analysed by X-ray diffraction (XRD) measurements and scanning electron microscopy (SEM). On the other hand, histological evaluation of the effect caused by the obtained nanoparticles on the lungs of male Brown Norway rats after a single intratracheal instillation of a solution containing various concentrations of IOSi-NPs was performed in order to clarify the controversial toxicity of these nanoparticles.

In Figure 1 the XRD pattern is presented. The experimental data in blue and the calculated data are represented by a grey line. Vertical lines represent the positions of diffraction lines of maghemite and amorphous silica. The line below the grey plot is the difference profile. It resulted in that each sample is constituted of spherical nanocrystallites. The diffraction peak at about 2θ=23 is related to amorphous silica. Another diffraction peaks corresponding to the Miller indices value (hkl) of (220), (311), (400), (422), (511), and (440) agree with the cubic structure of maghemite in Fd3m space group (ICSD-PDF no. 79196) with a lattice parameter of 8.35 A. The XRD showed a slight broadening of the diffraction lines which can be interpreted in terms of small sized crystallites [4]. The calculated particle size of maghemite silica nanocomposites was estimated at around 12.5 nm. Based on the XRD data refinement, the formation of single-phase spinel cubic structure belonging to the Fd3m space group has been confirmed.

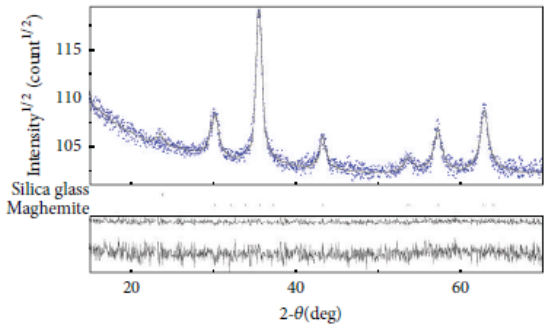

Figure 1: Experimental (blue), calculated (solid line gray), and difference plot (lower line) of γ-Fe2O3 and silica.

Information about the size and typical shape of the IOSi-NPs obtained after heat treatment at 400^0 C of the obtained initial nanocomposites powder based iron oxide and silica was provided from SEM analysis. SEM image of maghemite silica nanocomposites showed very small particle sizes and uniform spherical shapes (Figure 2(a)). EDAX spectrum and elemental maps (Figure 2(b)) of Fe, O, and Si for the maghemite-silica

nanocomposites are also presented. The uniform distributions of Fe, O, and Si could be observed.

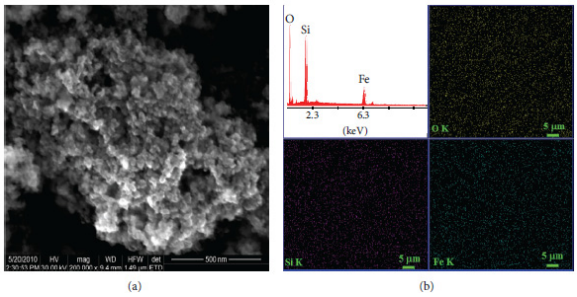

Figure 2: SEM micrograph (a) and elemental maps of maghemite-silica nanocomposite (b).

The toxicity evaluation of the lung after 24 h from intratracheal instillation of various concentrations of IOSi-NPs in rats was observed by histopathological investigations (Figure 3). After 24 h from intratracheal instillation, the rats showed particle-induced modifications that were dependent on the concentrations used. After 24 h from the intratracheal instillationwith 0.5mg/kg of IOSi-NPs, the lung parenchyma of the rats showed preserved alveolar architecturewith raremacrophages in the alveolar septa.We could see that the pathological micrographs of lung in rats after the intratracheal instillation with 0.5mg/kg dose of IOSi-NPs (Figure 3(b)) show.that the lung has preserved the architecture of the control specimen (Figure 3(a)), with no significant differences. After the intratracheal instillation of the rats with a 2.5mg/kg (Figure 3(c)) dose of IOSi-NPs, the lung parenchyma of the rats showed preserved alveolar architecture with rare macrophages in the alveolar septa, discreet anisokaryosis, and anisochromia of type II pneumocytes with rare nucleoli. Lung parenchyma of the specimen after intratracheal instillation of IOSi-NPs in rats at concentration of 5mg/kg (Figure 3(d)) showed preserved alveolar architecture with macrophages in the alveolar septa, discreet anisokaryosis, and anisochromia of type II pneumocytes, with chromocenters and nucleoli. In the lung parenchyma, focal ectatic capillaries were also observed in the alveolar septa

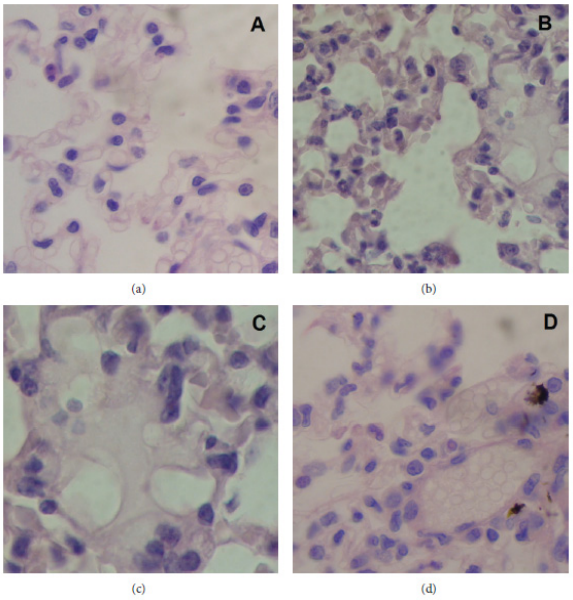

Figure 3: Light optical image of the lung at 24 h after intratracheal instillation of IOSi-NPs in rats at various concentrations. The reference sample is also presented (a). Lung after 24 hours: control (a), 0.5mg/kg (b), 2.5mg/kg (c), and 5mg/kg (d).

In conclusion, we demonstrated that intratracheal exposure with doses containing 0.5mg/kg, 2.5mg/kg, and 5mg/kg IOSi-NPs did not initiate acute lung injury and that the synthesized nanoparticles with sizes around 12.5 nm are not able to enter into the circulatory system. In this study we tried to answer some questions of the currently pressing problems regarding the toxicity of nanoparticles and their behaviour *in vitro* and *in vivo*.

References

[1] M. Mahmoudi et al., Advanced Drug Delivery Reviews, (63), 24–46, 2011.
[2] H. Maleki et al., Journal of Magnetism and Magnetic Materials, (324), 3997–4005, 2012.
[3] Z. Xu et al., The Journal of Physical Chemistry C, (114) 16343–16350, 2010.
[4] S. Music et al., Journal of Materials Science, (29), 1991–1998, 1994.

Chalcogenide systems at the border of the glass-formation domain

M. Popescu, F. Sava, A. Velea, A. Lőrinczi, I. D. Simandan

The compositions in the ternary chalcogenide systems from the demarcation region between the glass-formation domain (GFD) and the partially or fully crystalline formation domain seem to exhibit outstanding properties. We have shown [1] that the compositions with the best memory-switching properties are situated at the border of the GFD in many systems. One can use this correlation to find new phase-change materials with better switching properties or to discover GFDs that were not observed yet. Phase-change materials are intensely investigated due to their nonvolatile memory applications. These applications are based on the memory-switching effect between the amorphous and the crystalline state in a chalcogenide material. The compositions situated close to the GFD borderline contain very probably, a mixture of nanocrystalline and nanoamorphous particles. These amorphous clusters with such very small dimensions can change relatively easily the amorphous structure towards a crystalline one, and back, thus ensuring a rapid switching from insulating (amorphous) structure to the conducting (crystallized) phase.

In Fig. 1 is represented by green dotted line the GFD for the Ge–As–Te system [2] and by filled circles some memory switching compositions. Most of the memory switching compositions are very close to the margin of the GFD, while others are outside or inside of GFDs but not very far from this border (Fig. 1).

The simulation of the structural changes occurring during the memory switching process of the ternary chalcogenide composition, $GeAs_4Te_7$, has been carried out.

The transition of a high resistivity $GeAs_4Te_7$ amorphous cluster with 120 atoms to a low resistivity crystalline cluster was analyzed (Fig. 2).

The coordination of atoms changes from that corresponding to 8-N coordination rule (two for Tellurium, three for Arsenic and four for Germanium) in the amorphous phase to six (the same for all atoms) in metastable crystalline phase. Because of spatial constraints exercised by the amorphous matrix, the amorphous cluster cannot expand (Fig. 3).

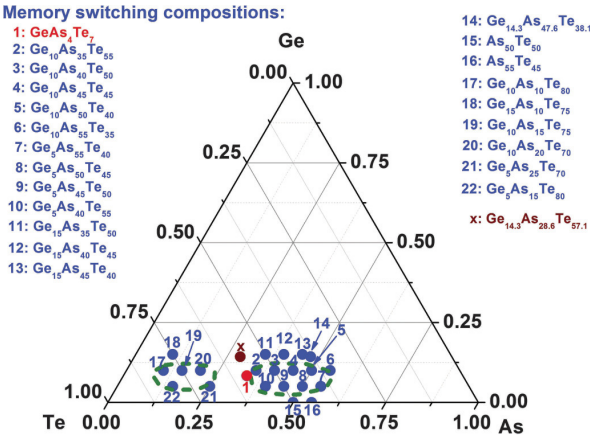

Fig. 1. Glass formation domain (defined by the green dotted line) for Ge–As–Te system. Blue filled circles represent phase change compositions with excellent switching properties. One can see in red colour the simulated composition (no. 1) and with azure colour the nearest experimentally investigated composition (after our knowledge) to the simulated composition (noted by x).

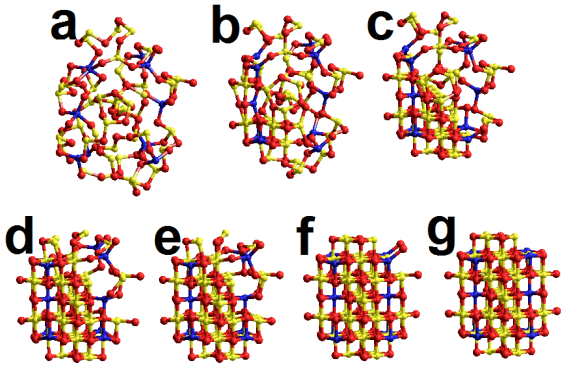

Fig. 2. The modelling of transition from amorphous (a) to metastable crystalline (g) structure in the system $GeAs_4Te_7$ (each network with 120 atoms is at the minimum mean free energy at T = 0 K and in vacuum). Intermediary steps can be seen from (b) to (f).

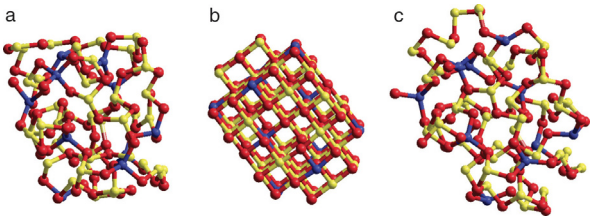

Fig. 3. The amorphous (a, c) and metastable crystalline (b) networks (models) in the system $GeAs_4Te_7$ ($GeTe-(As_2Te_3)_2$ or $Ge_{8.34}As_{33.33}Te5_{8.33}$).

Figure 4 shows the X-ray radial distribution functions, g(r), of experimentally determined a-$Ge_{14.3}As_{28.6}Te_{57.1}$ (Fig. 4a) and the pair distribution functions for a-$Ge_{8.34}As_{33.33}Te_{58.33}$ networks (initial state) at 300 K in vacuum (Fig. 4b) and in the amorphous matrix (Fig. 4c). It is found that by compression there is a shoulder in the second coordination sphere at 3.53 Å, making the distribution from Fig. 4c to be much closer to the experimental one. In these circumstances Te atoms seem to be over-coordinated (up to sixfold-coordinated) (Fig. 5).

Fig. 6 shows the structure factors for a-$Ge_{14.3}As_{28.6}Te_{57.1}$ (experimentally determined) and for the compressed and uncompressed clusters of a-$Ge_{8.34}As_{33.33}Te_{58.33}$ at T = 300K. By compression, FSDP intensity increases relative to the next maximum and so this factor structure is nearest to that experimental than the factor structure of the cluster in vacuum.

During the switching process, the atoms are moving on distances up to 4.0 Å. The average displacement is of 2.36 Å.

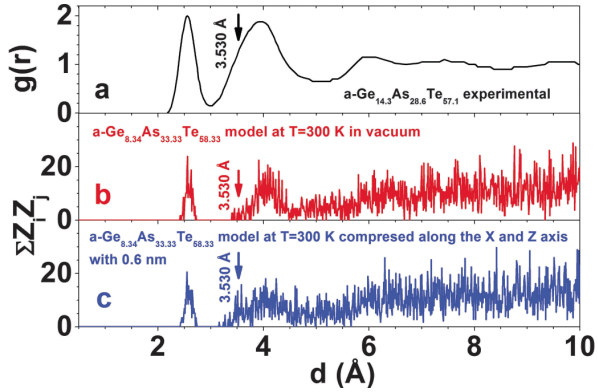

Fig. 4. The comparison between X-ray radial distribution functions g(r) of (a) experimentally determined a-$Ge_{14.3}As_{28.6}Te_{57.1}$ and pair distribution functions for a-$Ge_{8.34}As_{33.33}Te_{58.33}$ networks (initial state) at 300 K: (b) in vacuum and (c) in the amorphous matrix.

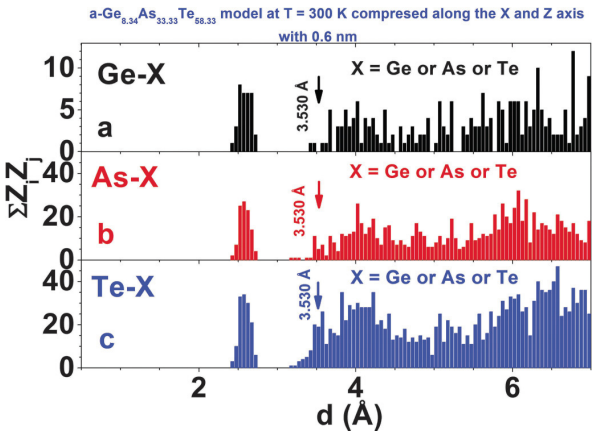

Fig. 5. The partial pair distribution functions for a-$Ge_{8.34}As_{33.33}Te_{58.33}$ networks (initial state) at 300 K inside the amorphous matrix: (a) between Ge and all other atoms, (b) between As and all other atoms, and (c) between Te and all other atoms.

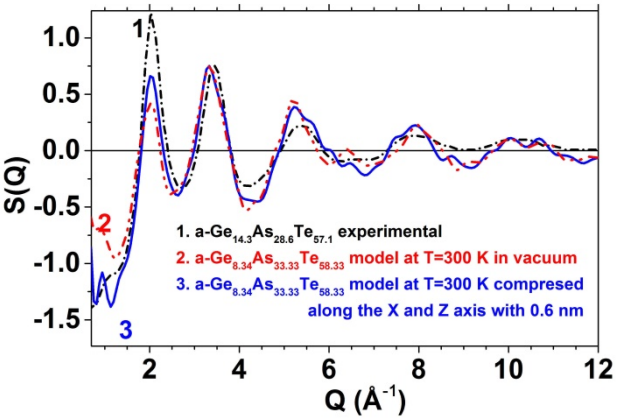

Fig. 6. The comparison between structure factors of experimentally determined a-$Ge_{14.3}As_{28.6}Te_{57.1}$ (1) and modelled a-$Ge_{8.34}As_{33.33}Te_{58.33}$ networks (initial state) at 300 K: in vacuum (2) and in amorphous matrix (3).

References

[1] M. Popescu, A. Velea, F. Sava, A. Lorinczi, Phys. Status Solidi B, 251(7), 1334-1339 (2014).

[2] M. Popescu, F. Sava, A. Velea, A. Lorinczi, I.D. Simandan, Canadian Journal of Physics, 92(7/8), 675-680 (2014).

The authors kindly acknowledge the financial support of the Ministry of National Education (Romania) in the frame of the contract NANOVISMAT PN2-162/2012.

Nanoscale Physics

Optical and morphological properties of dye-doped polymer nanofibers obtained by electrospinning

M. Enculescu, A. Evanghelidis, C. Busuioc, C. Florica, A. Costas, M. Oancea, N. Preda, E. Matei, I. Enculescu

The elecrospinning process is a facile way of producing polymer nanofibers with special morphological properties. Electrospun fibers have been studied as materials for applications varying from advanced photonic to biological applications. The modification of the process' parameters (the molecular weight and the concentration of the polymer, the electric potential, the flow rate and the distance between electrodes) allows tuning of the nanofibers' characteristics [1, 2]. Polymer nanofibers with special optical properties [3, 4] attracted an increased attention with regards towards their synthesis and characterization. Doping of the fibers with different nanoparticles or compounds is used in order to improve and tailor their optical behaviors. When used as dopants in polymer nanofibers, dyes can generate very efficient and intense emissions over the whole visible spectral region [5-8].

The dye-doped fibers with tunable wavelength of the emission band have great potential for optical applications. A major application of this phenomenon can be found in obtaining luminescent materials with extremely wide emission for lighting devices. We studied the morphological and optical properties of the beads and nanofibers of dye doped polyvinylpyrrolidone (PVP) [1, 2].

Dye-doped nanofibers were produced by the electrospinning process using 8% solution of polyvinylpyrrolidone (PVP) in ethanol doped with Rhodamine 6G (Rh 6G) in a concentration of 10^{-4} M [1]. By varying the parameters of the electrospinning method (the electric potential and the distance between electrodes) we succeeded in changing the wavelength of the emission peak for different samples deposited on glass substrates from the same Rh 6G doped PVP solution. Thus, the wavelength gradually increases from the value obtained for spin coated thin films, first to the value for the beaded nanofibers and then to the value that was obtained for the uniform nanofibers deposited by electrospinning, leading to a shift of the emission peak to the red (Fig. 1). The scanning electron microscopy confirmed that the largest wavelengths were obtained for the nanofibers with uniform surfaces and diameters of less than 500 nm (Fig. 2). The dye was uniformly distributed in the electrospun nanofibers.

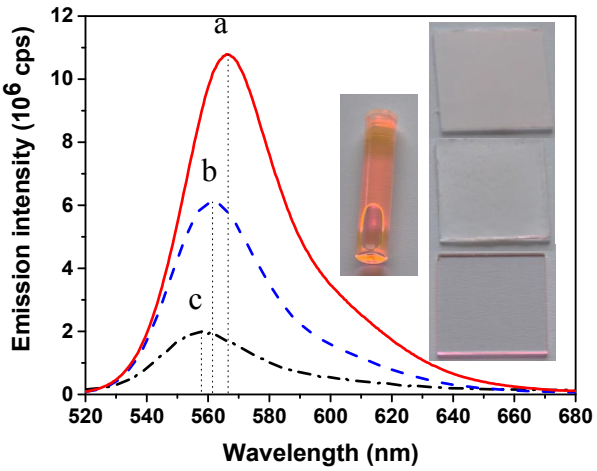

Fig.1. Emission spectra of Rh 6G doped PVP nanofibers (a) and beaded fibers (b), compared with emission of spin-coated thin film (c).

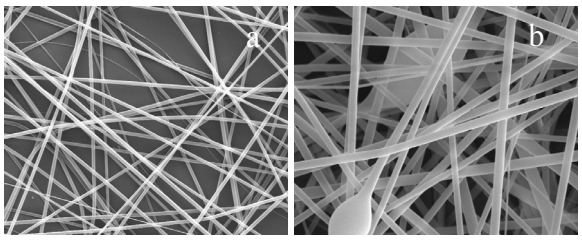

Fig. 2. SEM images of Rh 6G doped PVP nanofibers (a) and beaded nanofibers (b) produced using different parameters for the electrospinning process.

We evaluated the influence of the dye's type on the morphology of electrospun PVP (polyvynilpyrolidone) nanofibers doped with different dyes (coumarin 6 which presents a very strong emission in the green-blue region of the visible spectrum and sulforhodamine 101 and rhodamine 6G which have strong emissions in the orange-red spectral domain). Using the same

parameters for the electrospinning technique we obtained nanofibers with the "beads on string" morphology and diameters between 200 nm and 800 nm (Fig. 3). For the same concentration of the dye we observed a direct dependence between the dye's molecular weight and the fibers' diameters (smaller for coumarin 6 and larger for sulforhodamine 101 and rhodamine 6G) [2]. Instead, the diameters and number of the beads are indirect proportional with the molecular weight of the dyes (larger for coumarin 6 and smaller for sulforhodamine 101 and rhodamine 6G).

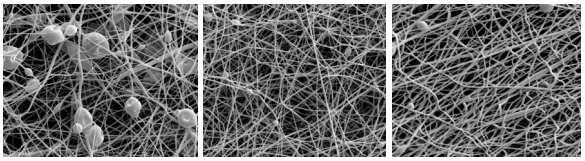

Fig.3. SEM images of PVP nanofibers doped with: C 6, Rh 6G and SRh 101.

We further evaluated the emissive properties for the PVP nanofibers doped with different dyes. In Figure 4 are presented the emission spectra of PVP nanofibers doped with 10^{-3} M concentration of SRh 101, Rh 6G and C 6. For the SRh 101 doped PVP fibers we used an excitation wavelength of 560 nm and we obtained an emission band with a maximum around 615 nm. The Rh 6G doped PVP nanofibers show an intense emission peaking at approximately 572 nm when excited with 500 nm. The most intense luminescence is observed for the C6 doped PVP nanofibers which present a very intense emission with the maximum at 523 nm when using an excitation of 470 nm.

Thus, for the same concentration of the dye in the polymeric solutions (10^{-3} M) we obtain a higher intensity for the emission peaking at smaller wavelength (523 nm for coumarin 6), and the value decreased with the increasing of the peak's wavelength (572 nm for rhodamine 6G and 614 nm for sulforhodamine 101).

Our studies demonstrate the possibility of obtaining completely organic and highly fluorescent materials for lasers, photonic and organic light emitting devices with tunable luminescence.

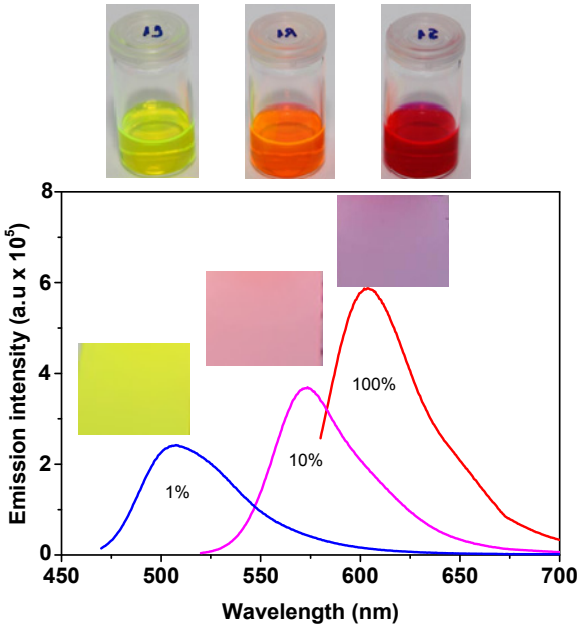

Fig.4. Emission spectra of PVP nanofibers doped with 10^{-3} M concentration of C 6, Rh 6G and SRh 101.

The authors acknowledge financial support from PNII RU-TE-2011-3-0107 and Core Program PN09-45.

References

[1] M. Enculescu, A. Evanghelidis, I. Enculescu, Journal of Physics and Chemistry of Solids, 75 (2014) 1365

[2] M. Enculescu, A. Evanghelidis, C. Busuioc, C. Florica, A. Costas, M. Oancea, N. Preda, E. Matei, I. Enculescu, Digest Journal of Nanomaterials Biostructures, 9 (2) (2014) 809

[3] A. Composeo, F. Di. Benedetto, R. Stabile, A.A.R. Neves R. Cingolani, D. Pisignato, Small, 5 (2009) 562

[4] A. Composeo, F. Di. Benedetto, R. Stabile, R. Cingolani, D. Pisignato, Applied Physics Letters, 90 (2007) 143115.

[5] J. Bohm, J. Hausselt, P. Henzi, K. Litfin, T. Hanemann, Adv. Eng. Materials, 6 (2004) 52-57.

[7] Y. Ner, J. G. Grote, J. A. Stuart, G. A. Sotzing, Angew. Chemie. Int. Ed., 48 (2009) 5734.

[8] K. J. Lee, J. H. On, Y. Kim, Jyongsik Jang, Advanced Materials, 18 (2006) 2216

Abnormal anti-Stokes Raman scattering as spectroscopic tool in the study of carbon nanotubes and carbon nanotubes/polymer composites

M. Baibarac, I. Baltog, I. L. Mihut, Smaranda, M. Scocioreanu,
in cooperation with
J.Y. Mevellec, S. Lefrant
Institut des Materiaux "Jean Rouxel", Nantes, France

The asymmetry between the Stokes and anti-Stokes spectra has generally been interpreted as a resonant Raman scattering effect produced by the excitation of different metallic (n, m) nanotubes, but considering a mixture of carbon nanotubes what are the specific anti-Stokes Raman signa-tures of separated metallic and semiconducting nanotubes? Using separated samples of C-SWNTs that are metallic and semiconducting with purities of 98% and 99%, respectively, and using the SERS measurement technique, we demonstrate that the dominant signature in the anti-Stokes branch of the G Raman band is attributed to the semiconducting nanotubes, even when resonantly exciting the metallic tubes.

To evaluate the enhancement efficiency quantitatively, the intensities of the Stokes and anti-Stokes Raman branches obtained on glass substrates were compared with those measured on Au and Ag substrates. This more conclusive approach generated the diagrams shown in Figs. 1 and 2.

Semiconducting nanotubes behave diffe-rently; they show a similar plasmonic SERS enhancement in both branches, which is stronger under excitation at 514.5 nm on the Stokes side.

Using comparative measurements performed on C-SWNTs films deposited on glass, as well as Au and Ag substrates, we showed that the SERS effect has specific characteristics under nonresonant and resonant optical excitations for the semiconducting and metallic nanotubes. Under the nonresonant optical excitation, the SERS mechanism mainly arises from the coupling of the plasmons [SPs(ωl), SPs(ωl Ω) and SPs(ωl+ Ω)] associated with the incident excitation light and the Stokes and anti-Stokes spontaneous Raman emissions, respectively.

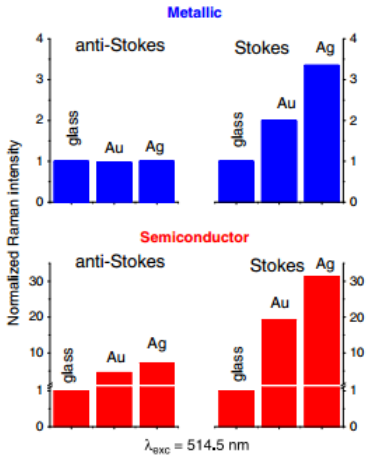

Fig. 1. *Intensities of the anti-Stokes and Stokes Raman lines at 1595 cm1 (G band) under 514.5-nm excitation for metallic and semiconducting single-walled nanotube thin films deposited on glass, Au and Ag supports. The intensity of the laser light focused on all samples was 2mW.*

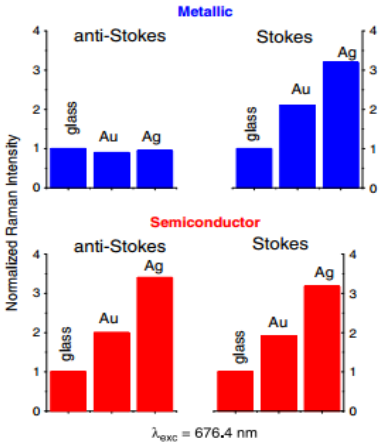

Fig. 2. *Intensities of the anti-Stokes and Stokes G band (1595 cm1) Raman lines excited at 676.4 nm for the metallic and semiconducting single-walled carbon nanotube thin films deposited on glass, Au and Ag supports. The intensity of the laser light focused on the samples was 2mW.*

Composites based on carbon nanotubes (CNTs) and conducting copolymers have received special attention since 2008 due to the interest for basic research and applications. In the preceding context we report the electrochemical synthesis of a new composite material based on poly(2,2'-

bithiophene-co-pyrene) (PBTh–Py) and SWNTs and its vibrational properties studied by anti-Stokes and Stokes Raman light scattering and polarized FTIR spectroscopy performed in grazing-incidence angle reflection geometry. New observations of AASRE from PBTh-Py copolymers synthesized in the absence and the presence of SWNTs permit the elucidation of the types of interactions between the copolymer molecules and the CNTs.

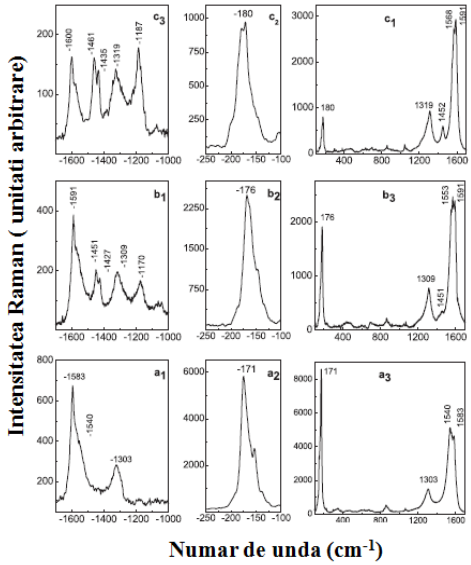

Fig. 3. Anti-Stokes and Stokes Raman spectra at α_{exc}= 676 nm of the films of SWNTs in the initial state (a1, a2, a3) and after the electropolymerization of 2,2'-bithiopheneand pyrene by 10 (b1, b2, b3) and 25 cycles (c1, c2, c3) stopped at a potential of -1 V.

The appearance of new Raman lines in the anti-Stokes rangewith maxima at -1435 and -1187 cm^{-1} (Fig.3) is reported when thecopolymer PBTh-Py is electrochemically synthetized onto aAu support coated with a SWNT film by cyclic voltammetry stopped at a potential of -1 V. This experimental result reveals acharge transfer at the interface of the SWNTs and the copolymer PBTh-Py.The functionalization of SWNTs with the copolymer PBTh-Py induce significant steric hindrance effects and this fact is demonstrated in Fig. 4 by the enhancement of the absorption of the bands at 793 and 846 cm^{-1}, which are assigned to the C-S-C deformation vibrational mode and the substituted benzene ring, respectively.

The dependence of the FTIR spectra of the SWNTs functionalizedwith PBTh-Py on the polarization angle (Fig.4) indicates a preferential orientation of the copolymer molecules on the carbon nanotube surface. Using the ratio of the absorbance recorded under the p polarization of the FTIR spectra of the copolymer PBTh-Py electrosynthesized onto the SWNT surface, we estimated that the transition dipole moment vectors of the vibrational modes associated with the absorption bands peaked at 794, 845, 1106-1118 and 1630 cm^{-1} were oriented at θ angles of 74°, 74°, 72°and 57°, respectively. The differences between the angles, observed for the FTIR bands peaked at 794, 845 and 1630 cm^{-1} when the PBTh–Py copolymer was synthetized onto the Au support (85◦, 83◦ and 71◦) and onto the SWNT surface (74◦, 74◦ and 57◦), originate in the functionalization process of the carbon nanotubes with the macromolecular compound, as a result of the steric-hindrance effects induced by the SWNTs onto the macromolecular chains.

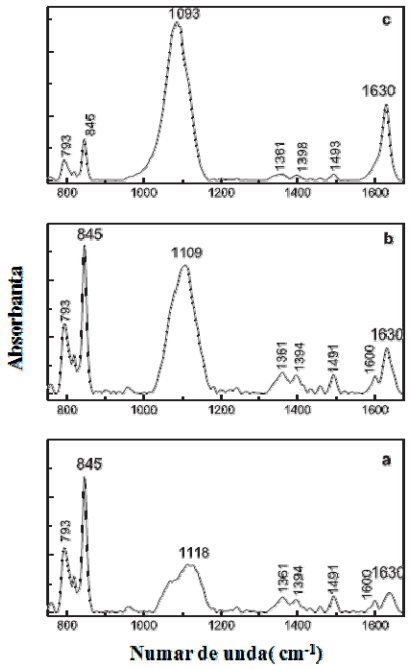

Fig. 4 FTIR spectra of the PBTh–Py copolymer film prepared by 2 (a), 10 (b) and25 cycles (c) stopped at a potential of -1 V and using as a working electrode an Ausupport coated with a SWNT film. All FTIR spectra were recorded in the grazing-incidence angle reflection geometry with p-polarization.

References

M. Baibarac, I. Baltog, I. Smaranda, M. Scocioreanu, J.Y. Mevellec, S. Lefrant,v Applied Surface Science 309 (2014) 11–21

Magnetic properties of α-Fe_2O_3 based nanostructured oxide semiconductors

F. Tolea, M Valeanu, L. Diamandescu
in cooperation with
M. Sorescu
Duquesne University, Department of Physics, Pittsburgh, PA 15282, USA

Hematite has various applications in scientific and industrial fields and can be used as semiconductor compound, magnetic material, catalyst and gas sensor. Moreover, the incorporation of other active ions into α-Fe_2O_3 structure lead to changes in unit-cell dimensions, particle size as well as magnetic and optical properties and new applications may be developed.

The magnetic state of hematite is antiferromagnetic with the Neel temperature T_N=960 K; its two magnetic sublattices have equal moment and anti-parallel orientation. However at temperatures above the Morin transition temperature (TM), the two sublattices are slightly canted leading to weak ferromagnetism. For pure, stoichiometric hematite, TM ≈ 262 K, but is strongly dependent on grain size, lattice defects, deviations from stoichiometry and surface effects.

Here we report on the evolution of the magnetic properties of IrO_2 or Li_2O and α-Fe_2O_3 equimolar mixtures after different ball-milling times. High-energy ball milling technique is a well-established method for mechanochemical synthesis of nanostruc-tured or nanocomposite materials in which non-equilibrium phases, extended solid solutions or complex structures can be formed at fairly low temperatures.

Magnetic measurements performed at high temperatures on the unmilled powder evidenced a weak ferromagnetism super-imposed on a Pauli paramagnetic behaviour. The hysteresis at 5 K, after extracting the paramagnetic contribution, reveal an antiferromagnetic behaviour as expected for hematite at low temperatures. In addition, a magnetic field induced spin flop is evidenced for H=3T and the transition is reversible and hysteretic by lowering the field. Such a field induced transition is for the first time reported and seems to have the same nature as the Morin one.

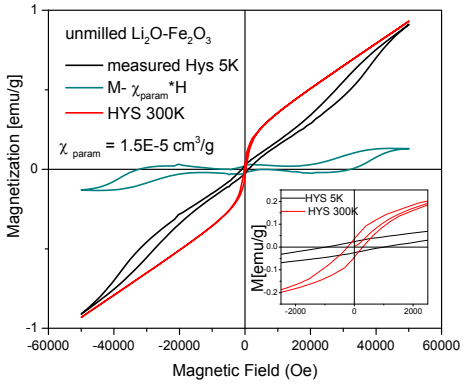

***Fig 1**. Hysteresis loop at 5 K and 300 K on unmilled Li_2O -α-Fe_2O_3.*

MT being a first-order thermodynamic transition is characterized by a thermal hysteresis. In Fig 2 the Morin transformation is evidenced by ZFC-FC measurements in 200 Oe and 1T. For the unmilled powder, T_M (measured under 200 Oe) is only 206 K, lower than for bulk (265 K). The thermal hysteresis width is influenced by the magnetic field, so it increases from 40 K for 200 Oe to 60 K for 1T and the transformation characteristic temperatures are shifted to lower values.

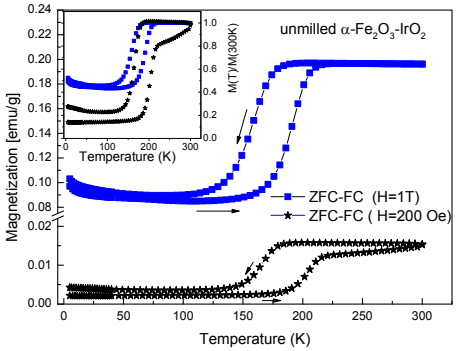

***Fig 2**. Morin transition evidenced by ZFC-FC measurements in 200 Oe and 1T for the unmilled powder.*

In the both mixtures, as effect of ball milling the grains microstructure is affected. The ZFC-FC curves measured on milled powder show only weak curvature and no apparent Morin transition. In addition, by increasing the milling

time the saturation magnetization (Fig 3.) as well as the paramagnetic contribution increases. In good agreement with the XRD and Mössbauer data [1, 2] these behaviour can be assigned to Ir substituting Fe in hematite or Fe substituting Ir in the iridium oxide lattice, generating new ferromagnetic, respectively para-magnetic phases.

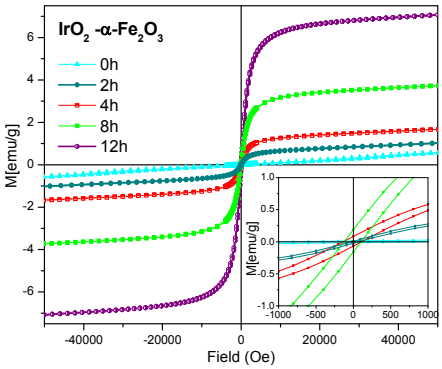

Fig 3. Hysteresis loops of the 0-12-hour milled powders recorded at 5 K.

Fig 4 shows the ZFC– FC curves for lithium-oxide-hematite system after different ball milling times. For ball milling time higher than 4h, the mixtures show a superparamagnetic behaviour and the blocking temperatures may be derived. For instance, the sample with a ball milling time of 4 h exhibits a blocking temperature of 98K, the sample with 8 h has a blocking temperature of 55 K and the specimen with 12 h of milling time has a blocking temperature of 52 K. These results show that large milling times correlate with small particle sizes and consequently, low blocking temperatures.

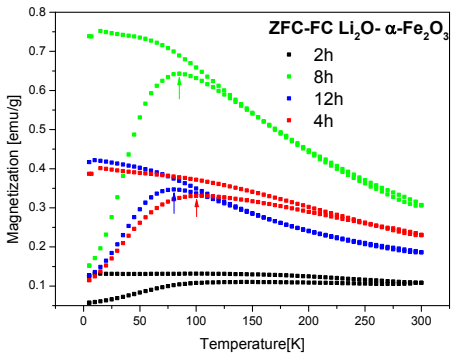

Fig 4. ZFC-FC measurements of the lithium oxide-hematite system after various ball milling times.

Fig 5 displays the hysteresis curves of the equimolar lithium oxide-hematite system at 5, 10, 20, 80, 150 and 300 K, after 12h of milling time in an applied magnetic field of 50,000 Oe. For temperatures higher than 80K the magnetic behaviour reflects a superparamagnetic state with zero coercitive field (see lower insert); for lower temperatures, the hysteresis loops show the specific features of nanopowder in the blocking state. In the blocking regime the coercive field decreases with the temperature as $T^{1/2}$; the upper inset in Fig 5 shows the dependence of the coercive field on temperature, which is in excellent agreement with the theoretical one.

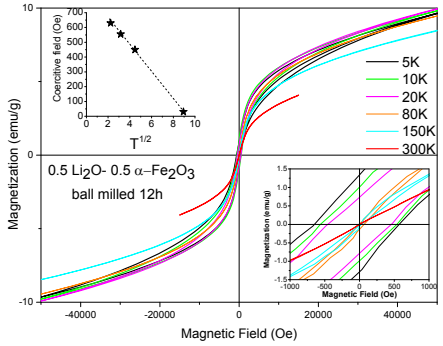

Fig 5. Hysteresis loops of the 12-h milled lithium oxide-hematite equimolar system recorded at various temperatures between 5 and 300 K.

Lithium oxide or iridium oxides-hematite nanocomposite system were successfully synthesized using mechanochemical activation for times ranging from 2 to12 h. Magnetic properties reflect the effect of grain size reduction from weak ferromagnetism to superparamagnetism.

References

[1] Sorescu, M; Bushunow, V; Diamandescu, L; Tolea, F; Valeanu, M; Xu, TH; Ceram. Int. 40 (2014) 5387-5395.

[2] Limongelli, J; Tolea, F; Valeanu, M; Diamandescu, L; Xu, TH; Sorescu, M; Ceram. Int. DOI: 10.1016/j.ceramint.2014.08.076

Electrical properties related to the structure of GeSi nanostructured films

M. L. Ciurea, I. Stavarache, A.M. Lepadatu, I. Pasuk, V. S. Teodorescu

GeSi based materials, in particular the ones based on GeSi nanocrystals (NCs) are very interesting for a wide range of applications such as memory devices and photodetectors [1]. By tuning the composition of GeSi, the energy band gap can be continuously varied from the one of Si to the one of Ge. More than that, in GeSi NCs the quantum confinement effect is stronger than in Si NCs.

One route to obtain GeSi NCs with tunable properties is to deposit GeSi films with different compositions and to subsequently anneal them under different conditions. More than that, by choosing the proper preparation conditions (deposition and annealing), the structure and morphology can be tailored, and consequently, the electrical properties can be tuned.

In this study, GeSi films with composition of 55:45 and thickness of 185 nm were co-deposited by magnetron sputtering from two targets of Ge and Si, on Si substrates [2]. The as-deposited films are amorphous, and therefore they were nanostructured by annealing in a conventional furnace in N_2 at different temperatures of 700, 800 and 900 °C.

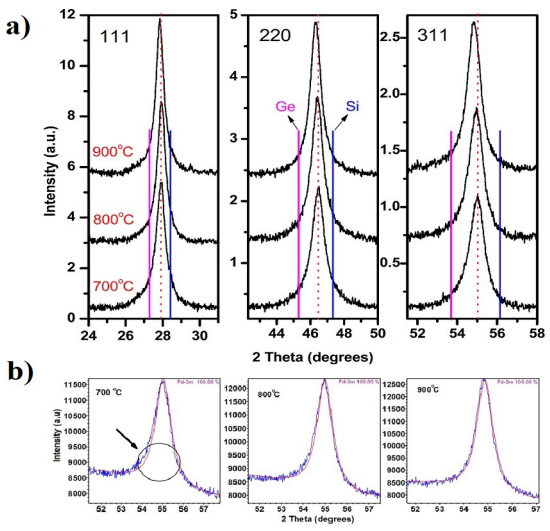

***Fig. 1** (a) XRD diagrams of the annealed GeSi films. The most intense lines are presented. The lines of pure Si and Ge are given for comparison; (b) The (311) XRD line profiles (experimental – blue, simulated – red).*

XRD, TEM and electrical measurements were employed for demonstrating the tunability of the electrical properties through tailoring of structure and morphology parameters by means of annealing temperature variation [2, 3]. XRD (Fig. 1a) shows the presence of GeSi NCs with cubic structure in all annealed films. By increasing the annealing temperature from 700 to 800 and 900°C, the Ge content of GeSi NCs increases from 45.2% to 50.2% and 52.5%, respectively, as well as the average size (coherence length) from 11.7 to 13.8 and 14.4 nm. The (311) XRD line profiles (Fig. 1b) present a small asymmetry, the most pronounced being for the 700°C annealed films, indicating the presence of some small NCs with high Ge concentration. The selected area electron diffraction pattern measurements confirm the presence of NCs enriched in Ge up to 85%.

The XTEM images in Fig. 2 taken on 700°C GeSi annealed (GeSi-700°C) film show that the film is almost completely crystallized with crystalline domains of 7–15 nm size revealed by Bragg contrast (Fig. 2a), separated by amorphous areas extended over 1–2 nm (Fig. 2b).

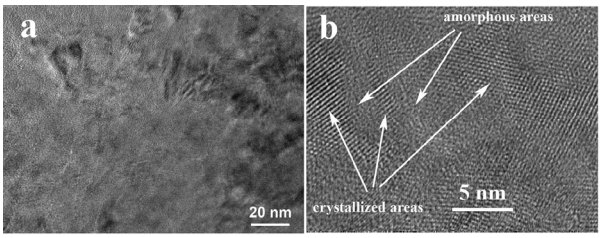

***Fig. 2** XTEM images on GeSi-700°C film: (a) high magnification and (b) high resolution detail.*

In contrast, the GeSi-800°C films are completely crystallized (HRTEM images), the NCs are larger (10–30 nm) and the boundaries between them are crystallized. Inside the NCs, stacking faults (SFs) and nanotwins (NTs) are present. In the GeSi-900°C films, the NCs are larger (20–60 nm) than in GeSi-800°C films. Inside NCs, there is a higher density of SFs and NTs (Fig. 3) compared to GeSi-800 °C films.

The crystallization process in GeSi-700°C films can be explained as follows: in the beginning of annealing, small domains with a high Ge concentration are formed by Ge segregation, while the rest of film volume crystallizes with less Ge content than the average composition. If the annealing temperature is higher, the crystallization process is faster, Ge segregation is less, and the GeSi NCs have composition closer to the average composition of film.

The electrical behaviour of GeSi films annealed at 700, 800 and 900 °C reflect the changes in structure and morphology. So, the GeSi-700°C films present thermally activated tunnelling of carriers between neighbouring GeSi NCs (through barriers given by the amorphous boundary regions) at low temperatures and low electric field, following $I \propto \exp\left(-\sqrt{T_0/T}\right)$ law with T_0 = 92380 K. At high temperatures, the current has Arrhenius dependence with activation energy $E_a^{(700)} = 0.23$ eV (Fig. 4).

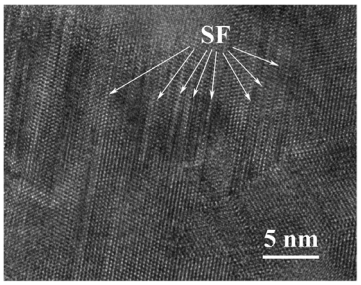

Fig. 3 HRTEM image of GeSi-900°C film.

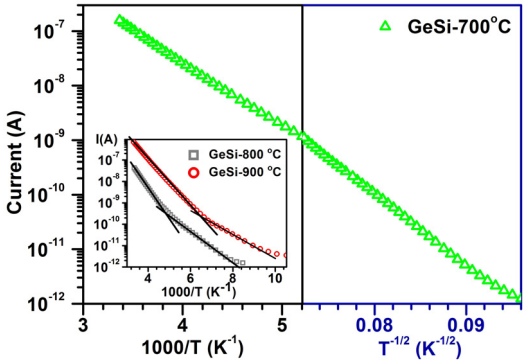

Fig. 4 I – T curves measured on GeSi-700°C, GeSi-800°C and GeSi-900°C films.

For the polycrystalline GeSi-800°C and GeSi-900°C films, the *I–T* curves have Arrhenius temperature dependence with different activation energies at low and high temperatures (Fig. 4). The activation energies for GeSi-800°C films are $E_{a,1}^{(800)} = 0.15$ eV and $E_{a,2}^{(800)} = 0.26$ eV at low and high temperatures, respectively, while for GeSi-900°C films are $E_{a,1}^{(900)} = 0.11$ eV and $E_{a,2}^{(900)} = 0.22$ eV.

The *I – V* characteristics support the *I – T* behaviour. So, the *I – V* characteristics taken on GeSi-700°C films (Fig. 5a) show a transport mechanism of high electric field ($eU >> k_BT$) assisted tunnelling:

$$I = I_0 \text{sign}(U) \times \left[\left(1 - \frac{|U|}{U_0}\right) \exp\left(-\alpha\sqrt{1 - \frac{|U|}{U_0}}\right) - \exp(-\alpha) \right]$$

of carriers between NCs, $I_0 = |a|\varphi$, $U_0 = N\varphi/e$ and $\alpha = \delta(8m_e/\hbar^2)^{1/2}\varphi^{1/2}$, the constant a is proportional to the number of equivalent paths, φ and δ are the mean height and width of the potential barrier between NCs, N is the average number of barriers. We found a small number of potential barriers (of the order of magnitude of 10^2), and we used the experimentally determined values of δ = 2.5 nm and φ = 0.23 eV.

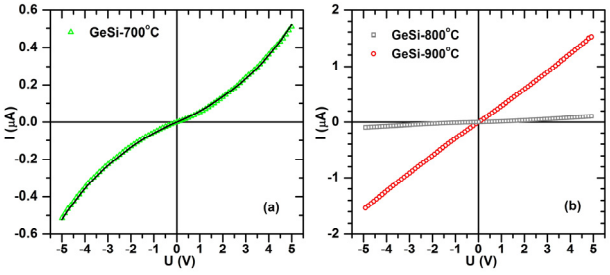

Fig. 5 I – V curves:
(a) experimental and fit for GeSi-700°C film;
(b) measured on GeSi-800°C and GeSi-900°C films.

The *I – V* characteristics measured on the polycrystalline GeSi-800°C and GeSi-900°C films (Fig. 5b) are linear in good agreement with the (micro)structure of the films.

In conclusion, we demonstrate the tuning of the electrical properties correlated with structure of GeSi nanostructured films by changing the annealing temperature. Thus, GeSi-700°C films are formed of GeSi NCs separated by very thin amorphous regions and present transport mechanisms of thermally activated tunneling between neighboring NCs (*I – T* curves at low electric field) and high field-assisted tunneling (*I – V* curves). The polycrystalline GeSi-800°C and GeSi-900°C films present a typical Arrhenius behaviour in *I – T* dependence, and a linear behavior in the *I – V* curves.

References

[1] W.T. Lai, P.H. Liao, A.P. Homyk, A. Scherer, P.W. Li, IEEE Photonic. Tech. Lett. **25**, 1520 (2013).

[2] M.L. Ciurea, I. Stavarache, A.M. Lepadatu, I. Pasuk, V.S. Teodorescu, Phys. Status Solidi B **251**, 1340 (2014).

[3] C. Palade, A.M. Lepadatu, I. Stavarache, V.S. Teodorescu, M.L. Ciurea, "Transition in conduction mechanism in GeSi nanostructures", CAS 2014 IEEE Proceedings (2014 International Semiconductor Conference, October 13-15, Sinaia, Romania), pages 55–58, New York (2014).

Covering fabrics with oxide nanoparticles: Complex characterization and wetting properties

L. Frunza, I. Zgura, S. Frunza, C.P. Ganea, V.F. Cotorobai
in cooperation with
M. Enculescu, N. Preda, E. Matei, C. Florica, C. C. Negrila and L. Diamandescu

There are many studies in the literature concerning deposition of nanoparticles/nanostructures upon textile materials. The group performed ZnO electroless deposition upon fabrics made from cotton [1], polyester (PES), polyamide (PA), poly(lactic acid) (PLA) and hemp (H) [2]. The systems were wholly characterized from structural, morphological and wetting point of view. Oxide (ZnO, TiO_2, SiOx) nanostructures were deposited by sol-gel, thermal evaporation, sputtering, chemical bath deposition as well. ZnO was chosen to be deposited on textile materials in order to develop super hydrophobic, UV-blocking, self-cleaning and antibacterial properties. TiO_2 has UV absorbing properties which can lead to many technological applications: High photocatalytic efficiency, great stability and low production cost are features which stand for TiO_2 photocatalytic properties. In addition to bulk applications, TiO_2 thin layers were obtained upon different materials for UV blocking, antibacterial or/and photocatalytic properties. SiOx was deposited onto polymeric substrates to produce (under special conditions) hydrophobic and possibly flame retardant properties.

Here we focus on the low temperature deposition of TiO_2 upon PES fabrics [2,3,4].

Due to their low thermal stability, PES fibres should be covered at rather low temperature, lower than that used for natural fibres. This fact limits the choice of deposition methods to be used. We have applied by two methods, sputtering or sol-gel, both of them at temperature close to ambient conditions. Thus, sputtering (SP) deposition used a Sputter-Coater (Tectra GmbH) installation and a TiO_2 target (99.9% oxide, K.J. Lesker), at pressure of $4x10^{-3}$, $8.6x10^{-3}$ or $4x10^{-2}$ bar. Sol-gel (SG) deposition was performed by dip coating the textile samples from a TiO_2 sol in a homemade installation. As precursor for TiO_2 sol was used titanium(IV) tetraisopropoxide.

TiO_2 coated particles are amorphous as indicated by X-ray diffraction and scanning electron microscopy. Sputtered layers consist in aggregates randomly distributed on the substrate while the sol gel layers show a uniform coverage of nanoparticles having a mosaic-like structure (Fig. 1).

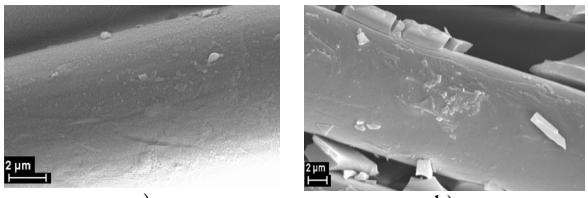

a) b)

Fig. 1*. SEM images of a) TiO_2 sputtering on PES2; b) TiO_2 sol-gel on PES2 sample [3].*

The loading degree was estimated on the basis of the thermogravimetric data and it is rather low (ca. 2%).

The surface composition of coated TiO_2 layer was studied by XPS. Taking into consideration the intensity of the main peaks and the sensitivity coefficients of each element it was possible to determine the surface elemental compositions for the series of samples. Deposition treatment adds titanium, in a higher proportion by sputtering than in the sol-gel case. Position of the O1s is shifted with ca. 0.2 eV as compared with those in pure oxides. In addition, the Ti peaks are shifted ~1 eV toward lower binding energies, possibly due to the roughness introduced by the particles. As a consequence some C is bonded to the exposed centres.

Once obtained the deposited surfaces, the adherence of the layer and their functionalization were checked by submitting the deposited samples to a sonication treatment [4] for 3 min in an equipment UIS250V (Hilscher Ultrasound Technology). The sample immersed in water was very close to the resonant horn. See Figure 2 for SEM images showing the sonication effect.

It is well known that wetting of a surface by a liquid is affected by the roughness of the surface. In the case of textile materials, this roughness is related to the topography of the fibre, the construction of the yarn, and the construction of the fabric, which is very complex. Since (nano)particles add new roughness to the materials, static contact angles (CAs) measured at room temperature with Drop Shape Analyzer DSA 100 (Krüss) on textile substrates are useful quantities for comparative measurements to characterize the effects of surface modifications (Fig. 3).

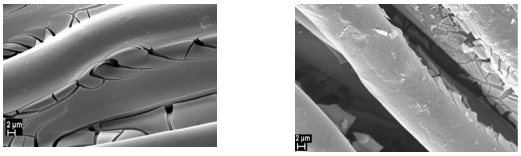

a) b)

Fig. 2*. SEM micrograph a) before and b) after sonication of TiO_2/PES2 sample SG deposited.*

a) b)

Fig. 3*. Water droplets in contact with the surface of; a) TiO_2 sol-gel on PES2 (169.3º); b) TiO_2 sputtering on PES2 (133.8º) [**Error! Bookmark not defined.**].*

The raw materials are all, hydrophobic, with CA>90°. Due to their morphology, the TiO_2 structures present different degrees of compactness, trapping more or less air in-between, and the surface has a superhydrophobic behavior.

The wetting properties changes under alternating illumination and darkening conditions. Irradiation with white light was performed for 210 min using an AM 1.5G solar simulator (Lot Oriel) with collimated output beam. Darkening conditions were ensured in a specially designed black box.

We found that amorphous coated layers respond to illumination becoming hydrophilic, meaning that the investigated systems might be involved in photocatalytic applications (Fig. 4).

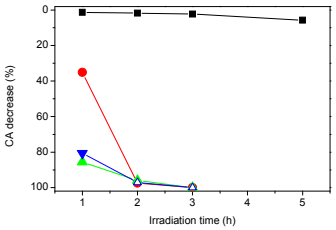

Fig. 4*. Decrease of the contact angle vs. time of UV irradiation for the samples TiO_2SG/PES2 (squares); TiO_2SP8.6/PES2 (circles); TiO_2SG/PLA (up triangles); TiO_2SP8.6/PLA (down triangles). Errors are +/- 4.2%.*

Photocatalytic activity of deposited TiO_2 particles was studied using PCC2 Evaluation Checker (ULVAC), with methylene blue as the test dye to be degraded. The level of photocatalytic activity was measured by the intensity of visible pulsed light (610 nm) reflected from the sample surfaces coated with the dye, over a period of 60 min (see Fig. 5).

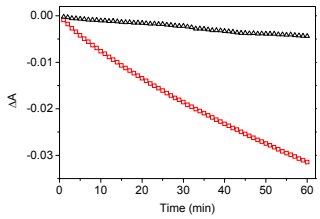

Fig. 5*. Changes in absorbance of MB removal vs. irradiation time in the case of coated TiO_2/PES30 fabric (open squares) and original PES30 (open up triangles) [**Error! Bookmark not defined.**].*

References

1. L. Frunza, N. Preda, E. Matei, S. Frunza, *et al.* J. Polymer Sci., B Polymer Phys. 51, 1427–1437 (2013)
2. I. Zgura, S. Frunza, L. Frunza, M. Enculescu, *et al.* J. Optoelectron. Adv. Mater., accepted 2014
3. I. Zgura, S. Frunza, M. Enculescu, C. Florica, F. Cotorobai, Rom. J. Phys., in press 2014
4. I. Zgura, S. Frunza, L. Frunza, M. Enculescu, *et al.* Rom. Rep. Phys., submitted 2014

Thermal analysis by electron paramagnetic resonance of probing transition ions. The thermal formation and growth of nanoZnO

S. V. Nistor, M. Stefan and D. Ghica

Thermal analysis (TA), where the temperature induced changes in the material properties are studied, is a well-established branch of materials science [1]. Specific methods have been developed, in which a certain temperature sensitive property, such as mass or heat difference, is investigated.

The electron paramagnetic resonance (EPR) spectra of weakly perturbing paramagnetic transition metal ions, inserted substitutionally in low concentrations (< 10^3 ppm) in (nano)crystalline semiconductors and insulators, are extremely sensitive to small changes in the nature and configuration of the neighboring ligands [2].

Thus, the analysis of the sequence of EPR spectra recorded during isothermal and isochronal pulse annealing treatments offers a wealth of information on both thermally induced compositional and structural changes of the host (nano)material [3]. The paramagnetic probing ions should be chosen in such a manner as to perturb as little as possible the host lattice, i.e., with the same charge state as the host lattice cations they substitute and close ionic radii. In the case of Zn^{2+}-based compounds the Mn^{2+} ion is the best choice, as it has a close ionic radius and identical charge state.

The potential of this newly proposed TA method is illustrated here with investigations on the thermal decomposition of crystalline zinc hydroxide $Zn(OH)_2$ and anhydrous zinc carbonate basic $Zn_5(CO_3)_2(OH)_6$ (ZCB), containing trace amounts of substitutional Mn^{2+} probing ions, into nanoZnO [4-6]. The TA by EPR is based on pulse annealing experiments, in which the investigated samples, lightly doped with Mn^{2+} ions, are subjected to thermal annealing into a programmable furnace. After each pulse annealing step the sample tube is extracted from the furnace, cooled down to room temperature (RT), or even to lower temperatures if needed, and its EPR spectrum is recorded. Two types of pulse annealing sequences have been employed in our investigations, namely the isochronal and the isothermal sequences [3]. A schematic of the isochronal pulse annealing procedure is presented in Fig. 1. The right hand side displays the sequence of annealing pulses of Δt = 10 min, at annealing temperatures T_{ann} which increase in equal ΔT = 10 °C steps, employed for the experiment presented on the left side. The left hand side displays the resulting sequence of Q-band EPR spectra (only the first three lowest field lines are shown) of substitutional Mn^{2+} ions in crystalline $Zn(OH)_2$, pulse annealed in vacuum. One can see a clear change in the EPR spectra at T_{ann} ~ 80 °C.

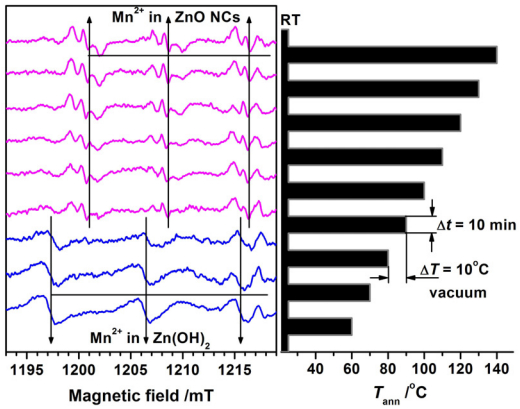

***Figure 1**. Isochronal pulse annealing EPR experiment reflecting the thermal decomposition in vacuum of crystalline $Zn(OH)_2$ around 80 °C, resulting in nanoZnO [3,4].*

The quantitative analysis of the EPR spectra at low and high microwave frequencies resulted in the spin Hamiltonian (SH) parameters presented in Table 1. The first two columns correspond to Mn^{2+} ions in crystalline ε-$Zn(OH)_2$ for T_{ann} < 80 °C and in nanocrystalline ZnO for T_{ann} > 80 °C. The intensity ratio of the EPR spectra from the different Mn^{2+} centers in a multiphase system, such as the decomposing $Zn(OH)_2$, is equal to the concentration ratio of the host phases in the investigated sample. One can thus determine from the sequence of pulse annealing EPR spectra the variation in the concentration of the starting ε-$Zn(OH)_2$ and resulting ZnO phases *vs.* T_{ann}.

Table I. *The SH parameters of the Mn^{2+} ions in $Zn(OH)_2$ and ZCB and ZnO produced by thermal decomposition of the first two. The A and D parameters are given in 10^{-4} cm^{-1}.*

SH param.	Mn^{2+} / $Zn(OH)_2$	Mn^{2+} / ZnO NCs	Mn^{2+} / ZnO disord.	Mn^{2+}-A / ZCB	Mn^{2+}-B / ZCB
g	2.0010	2.0012	2.0012	2.0012	2.0055
A	-87.0	-74.0	-73.5	-84.7	-86
$\|D\|$	70-600	242	242	150-220	150-240
$\sigma(D)$ [%*D*]	40	7	42	33	30
Ref.	4	4,5	5	5	5

As shown in Fig. 2, a transformation takes place in the 60 °C < T_{ann} < 140 °C range.

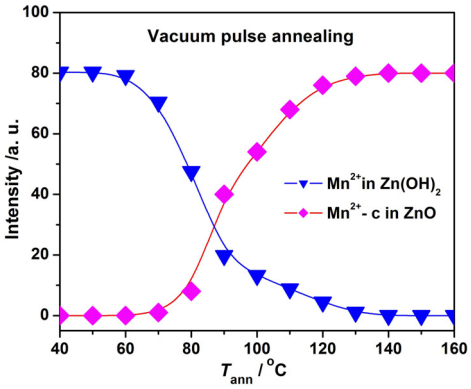

Figure 2. *The variation in the relative amount of $Zn(OH)_2$ and resulting ZnO in the EPR pulse annealing experiments in vacuum from Fig.1.*

The temperature induced decomposition in air of the ZCB in ZnO resulted in the sequence of isochronal annealing EPR spectra presented in Fig. 3. The analysis of the recorded EPR spectra points to a process different from the decomposition of $Zn(OH)_2$ [5], namely the initial formation of disordered ZnO above 225°C, which further crystallizes in nanocrystalline ZnO. This is observed as the transformation of the Mn^{2+}(A) and Mn^{2+}(B) centers, corresponding to two substitutional sites in ZCB, into Mn^{2+} ions in disordered ZnO (Mn^{2+}-d centers) and further on in ZnO nanocrystals (Mn^{2+}-c centers) (Table 1).

The corresponding variation in the amount of starting ZCB and resulting ZnO decompo-sition products are shown in Fig. 4.

Isothermal pulse annealing EPR data have been further used to study the crystallization of disordered ZnO at T_{ann} > 225 °C [6].

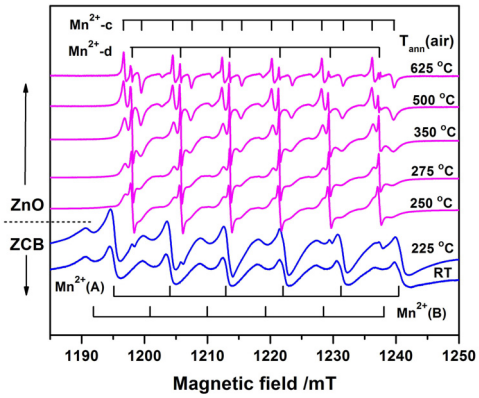

Figure 3. *Selected EPR spectra from an isochronal pulse annealing sequence with ΔT = 25 °C and Δt = 15 min [5].*

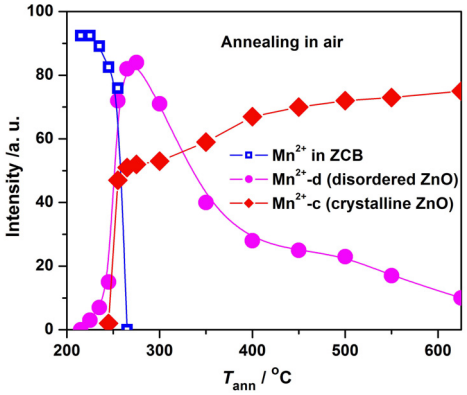

Figure 4. *The relative amount of ZCB and resulting ZnO observed in the EPR pulse annealing experiments in air shown in Fig. 3.*

References

[1] P. Gabbott, Principles and applications of thermal analysis. Blackwell Publ., Oxford, 2008

[2] J. R. Pilbrow, Transition ion EPR. Clarendon Press, Oxford, 1990

[3] S. V. Nistor, M. Stefan, D. Ghica, J. Therm. Anal. Calorim. (Springer) 118, 1021 (2014)

[4] S.V. Nistor, D. Ghica, M. Stefan, I. Vlaicu, J. N. Barascu, C. Bartha, J. Alloys Comp. 548, 222 (2013)

[5] S. V. Nistor, L. C. Nistor, M. Stefan, D. Ghica, Gh. Aldica, J. N. Barascu, Cryst. Growth Des. 11, 5030 (2011)

[6] M. Stefan, S. V. Nistor, D. Ghica. Cryst. Growth Des. 13, 1350 (2013)

Indium-tin nanoscaled oxides synthesized under hydrothermal supercritical and postannealing pathway: phase dynamics and characterization

L. Diamandescu, D. Tarabasanu-Mihaila, M. Feder, M. Enculescu, V.S. Teodorescu, S. Constantinescu, T. Popescu, C. Bartha
in cooperation with
Zs. Pap
Institute of Material Science and Engineering, University of Szeged, Szeged, Hungary

In the last decade much attention has been paid to the synthesis and study of mixed nanoscaled semiconducting oxides due to their applications in sensing, optoelectronic devices or catalysis [1, 2]. In particular, the mixed system tin oxide - indium oxide is of great importance mainly due to the representative transparent conducting oxide called ITO (usually 10% SnO_2-90% In_2O_3 -cubic phase, by weight). With the aim to obtain nanoscaled indium-tin oxides in an extended solubility range, this paper proposes the study of indium-tin hydrogel (obtained starting with $InCl_3$-$SnCl_4$ water solution) under hydrothermal supercritical conditions and post annealing pathway. Indium–tin nanoscaled mixed oxides, xIn_2O_3—$(1-x)SnO_2$ ($0 \le x \le 1$), were synthesized under hydrothermal supercritical conditions and postannealing route, starting with $InCl_3$-$SnCl_4$ water solution.

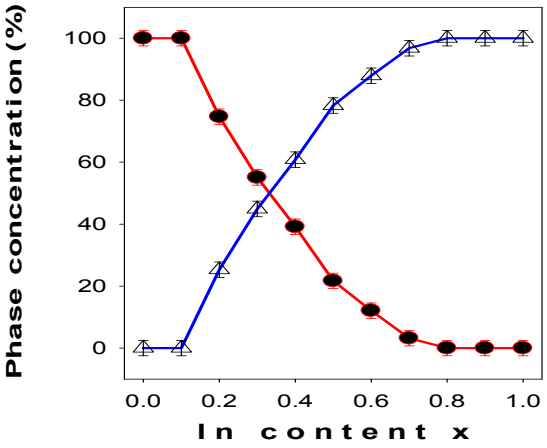

Fig 1. *Phase balance in the supercritical hydrothermal samples as resulted from Rietveld refinements of X-ray diffractograms. Phase index Sx: (●) isostructural with SnO_2; Ix (Δ) isostructural with InOOH phase.*

In the conentration range $0.1 \le x \le 0.7$, by hydrothermal reaction at 400 °C, mixtures of phases isostructural with InOOH and SnO_2, were obtained (Fig 1).

In the absence of tin (x = 1) the InOOH hydrothermal precursor transforms, by thermal treatment at 500 °C for 1 hour, into cubic indium oxide (Fig 2).

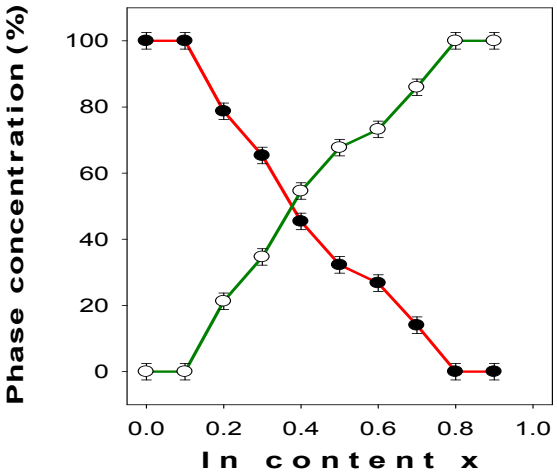

Fig 2. *Phase balance in the supercritical hydrothermal samples after the thermal treatment at 500 °C for 1h, as resulted from Rietveld refinements. Phase index Sx: (●) isostructural with SnO_2; phase index Inr: (○) isostructural with rhombohedral phase In_2O_3.*

In the presence of tin, the calcined samples with the nominal indium concentrations $0.2 \le x \le 0.7$ contain two nanoscaled phases: first one isostructural with rhombohedral In_2O_3 and the second one isostructural with tetrahedral SnO_2; the abundance of the tin oxide like phase decreases continuously with increasing indium concentration. At high indium concentrations (x = 0.8 and x = 0.9) only one phase isostructural with rhombohedral In_2O_3 appears; this is an ITO like phase based on rhombohedral indium oxide. No other In-Sn structures are detected in the calcined samples.

XRD refinements and TEM analyses (Fig 3) indicate the formation of nanoscaled phases (15-

50 nm) in both hydrothermal system and calcined samples [3].

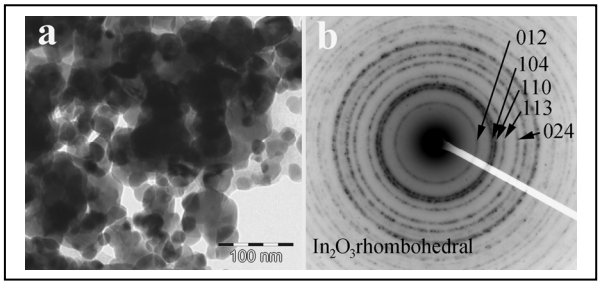

Fig 3. *TEM image (a), and electron diffraction pattern (b) of the calcined xIn_2O_3-(1-x)SnO_2 sample with nominal concentration x = 0.8.*

The solubility limit of tin in rhombohedral indium oxide under the synthesis conditions used in this study was evaluated to be close to ~ 20 mol % (~ 12 wt %), both by XRD and EDX. The solubility limits of In^{3+} in SnO_2 is close to 10 mol % (~ 17 wt %). A reaction sequence describing the main steps in the synthesis of indium-tin nanoscaled oxides, under hydrothermal supercritical and postannealing pathway, was proposed [3]. UV-vis diffuse reflectance measurements were performed to reveal the optical properties in the interesting concentration range of x = 0.7 – 1.0, for the calcined samples. The lower band gap energy (~ 2.5 eV) was found at x=0.9. (Fig 4).

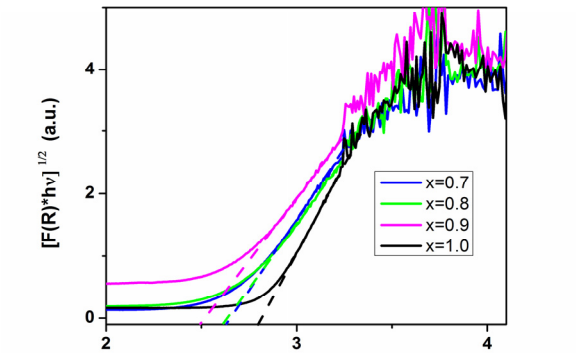

Fig 4. *Tauc plot for the hydrothermally samples at x=0.7-1.0, after calcination at 500 °C for 1h.*

The band gap energy values in the range of 2.5-2.6 eV could recommend the calcined samples with x=0.8 and x=0.9 (the rhombohedral ITO, synthesized under hydrothermal supercritical and postannealing pathway) for applications in visible light photocatalysis.

In the recent literature [4], ITO based materials are mentioned to have the "ability" to produce hydrogen under visible light. The experiments on our samples in Szeged-Hungary were irrelevant in spite of these E_g values, and the materials cannot be used -as resulted- in such kind of applications [3]. Some other strategies have to be applied to activate these materials for photocatalytic hydrogen production, such as noble metal deposition [5] or coupling with other oxides.

By our knowledge this report is the first study on nanophase dynamics in the synthesis of the nanoparticle system xIn_2O_3-(1-x)SnO_2 under hydrothermal supercritical conditions and postannealing pathway, over all molar concentration range x, starting with $InCl_3$-$SnCl_4$ water solution. Moreover, we obtained the ITO powder based on rhombohedral In_2O_3 – a phase which until the years 2005 was hardly obtained at high temperatures and pressures [6].

References

[1] A. Fujishima, X. Zhang, D.A. Tryk, Surface Science Reports, 63 (2008) 515-582.

[2] H. Gu, Z. Wang, Y. Hu, Sensors, 12 (2012) 5517-5550.

[3] L. Diamandescu, D. Tarabasanu-Mihaila, M. Feder, M. Enculescu, V.S. Teodorescu, S. Constantinescu, T. Popescu, C. Bartha, Zs. Pap, Mat. Chem. Phys., 143(2014) 1540-1549.

[4] R. Dholam, N. Patel, A. Miotello, Int. J. Hydrogen Energy, 36 (2011) 6519-6528.

[5] É. Karácsonyi, L. Baia, A. Dombi, V. Danciu, K. Mogyorósi, L.C. Pop, G. Kovács, V. Coşoveanu, A. Vulpoi, S. Simon, Zs. Pap, Catal. Today, 208 (2013) 19-27.

[6] M. Sorescu, L. Diamandescu, D. Tarabasanu-Mihaila, V.S. Teodorescu, J. Mat. Sci., 39 (2004) 675-677.

Evaluation of the paramagnetic impurities segregation at grain boundaries in nanostructured ZnO films

D. Ghica, M. Stefan, C. Ghica, G. E. Stan

Magnetic and electrical properties of the nanostructured ZnO films are affected by the non-random impurities distribution in the film due to segregation at grain boundaries (GBs) or extended defects. However, mapping the nature and distribution of the impurities in the film is not trivial and quite elaborate and time-consuming methods have been used for this purpose [1, 2]. We have recently demonstrated a comparingly simple, statistically relevant and non-destructive procedure of quantitative determination of the paramagnetic impurities segregated at the GBs in nanostructured semiconducting and insulating films [3].

We have investigated the segregation process of the Mn^{2+} ions present in low concentrations (~1 ppm) in a nanostructured ZnO film deposited onto r-cut sapphire substrates by RF magnetron sputtering at room temperature (RT). From correlated electron paramagnetic resonance (EPR) and transmission electron microscopy/high resolution transmission electron microscopy (TEM /HRTEM) investigations we have determined the localization of the Mn^{2+} ions in both as-deposited and thermally treated nanostructured ZnO thin film.

The EPR investigations were carried out in the Center for advanced ESR techniques (CetRESav) from our institute (*http://cetresav.infim.ro*). The analysis of the EPR spectra of the Mn^{2+} ions was performed with the spin Hamiltonian (SH) and lineshape simulation procedure developed for nanopowder samples [4, 5]. The SH parameter values determined for the Mn^{2+} ions in the as-deposited ZnO film match the values reported for the Mn^{2+}-d centers in ZnO nanopowders [5] and correspond to a substitutional localization of the impurity ions at Zn^{2+} sites in disordered regions of the ZnO film. Thus, we have experimentally demonstrated by EPR that in a nanostructured ZnO thin film, even at very low Mn concentration, all the Mn^{2+} ions accumulate in the disordered regions of the film (Fig. 1 – left) [3]. As seen by HRTEM, such regions correspond to nanometric pockets filled with amorphous phase along the GBs of nanocrystalline ZnO columns (Fig. 1 – right). To our knowledge, this is the first direct observation of the complete segregation at GBs of very low impurity concentrations, and also the first time that EPR was used to probe the segregation process.

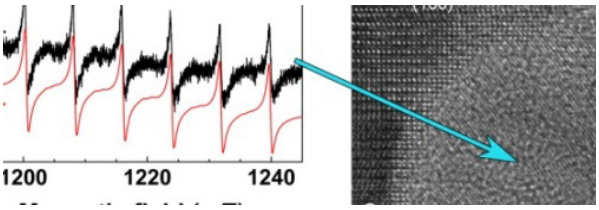

***Figure 1. Left** - Experimental (exp. - black) Q-band EPR spectrum (20 scans) of the ZnO film at RT and the simulated one (sim. - red) for substitutional Mn^{2+} ions in disordered ZnO. **Right** - HRTEM image of the as-deposited ZnO film showing the amorphous / poorly-crystallized phase of nanometric size (blue arrow) at the interface between the ZnO columns.*

By annealing the ZnO film in air, the lineshape of the EPR spectrum of Mn^{2+} changes progressively, signaling a change in the Mn^{2+} ions environment. For pulse annealing temperatures above 400 °C, another Mn^{2+} spectrum starts to grow, while the intensity of the Mn^{2+}-d spectrum from the disordered ZnO decreases. We have determined the SH parameters of the new Mn^{2+} centers from the EPR spectrum measured after annealing the ZnO film at 600 °C for 45 min (Fig. 2). They are further called Mn^{2+}-c centers, as they resemble the Mn^{2+}-c centers in ZnO nanocrystals [5] in both SH parameter values and behavior.

The intensity of the EPR spectrum of a center, calculated by the double integration of the spectrum, is proportional to the concentration of the respective center in the host lattice. Therefore, the changes in the

relative intensities of the two centers with the annealing temperature show the increase of the Mn^{2+}-c centers concentration at the expense of the Mn^{2+}-d centers. If we define f_c and f_d as the concentration fractions in % of the Mn^{2+} ions in the crystalline and disordered ZnO phases, respectively, with $f_c + f_d = 100$ %, the double integration of the simulated spectra of the Mn^{2+}-c and Mn^{2+}-d centers represented in Fig. 2 results in $f_c = 63$ % and $f_d = 37$ %.

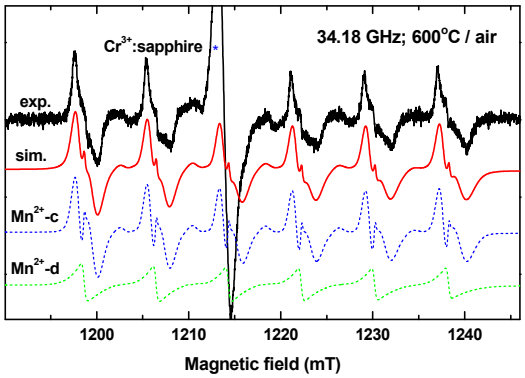

Figure 2. *Experimental (exp., 20 scans) and simulated (sim.) Q-band EPR spectra at RT of the ZnO film annealed in air at 600 °C for 45 min. Dot lines: the calculated spectra of the Mn^{2+} ions in the nanocrystalline (Mn^{2+}-c) and disordered (Mn^{2+}-d) ZnO. The intense EPR line of the Cr^{3+} ions from the sapphire substrate is marked with a blue star.*

As further observed by HRTEM (not shown here), the disordered pockets disappeared in the annealed film. We can conclude that, even after thermal annealing at 600 °C for 45 min, when equilibrium was achieved, the distribution of the Mn^{2+} ions was still non-uniform in the nanostructured ZnO film, 37 % of the Mn^{2+} ions remaining at the GBs, while the rest were localized in the peripheral strained regions of the ZnO columns neighboring the GBs.

Our results demonstrate a new procedure to evaluate the amount of paramagnetic impurities segregated at the GBs in a nanostructured film, which can be further used to establish the preparation conditions for films designed for specific applications. Moreover, the proposed EPR-based method can be adapted as a regular test for the quality assurance of the defect-engineered thin films. Such applications could be of real interest for nanotechnology.

This method can be applied only for paramagnetic impurities in concentrations lower than 1 %, for which the dipolar interactions do not wipe out the relevant information in the EPR spectra.

Our findings bear a high importance for any application involving doped nanostruc-tured ZnO films, as they show that even in nominally pure films the native impurities could accumulate in quite high local concentrations at the GBs, being able to affect the magnetic and electrical properties of the films. This effect could be further controlled by defect engineering for specific applications. We expect that these results are of interest for a broad research and technology community, as they can help improve the knowledge for top-applications in spintronics, opto- and nanoelectronics.

This work was supported by UEFISCDI through the projects PN-II-ID-PCCE-2011-2-0006 (contract #3/2012) and PN-II-ID-PCE-2012-4-0362 (contract #36/2013).

References

[1] Z. Wang, M. Saito, K. P. McKenna, L. Gu, S. Tsukimoto, A. L. Shluger, Y. Ikuhara, *Nature* **479**, 380 (2011).

[2] M. Herbig, D. Raabe, Y. J. Li, P. Choi, S. Zaefferer, S. Goto, *Phys. Rev. Lett.* **112**, 126103 (2014).

[3] D. Ghica, M. Stefan, C. Ghica, G. E Stan, *ACS Appl. Mater. Interfaces* **6**, 14231 (2014).

[4] M. Stefan, S. V. Nistor, D. Ghica, *Cryst. Growth Des.* **13**, 1350 (2013).

[5] S. V. Nistor, L. C. Nistor, M. Stefan, D. Ghica, Gh. Aldica, J. N. Barascu, *Cryst. Growth Des.* **11**, 5030 (2011).

Nanoscale monoclinic domains in epitaxial $SrRuO_3$ thin films deposited by pulsed laser deposition

C. Ghica, R. F. Negrea, L. C. Nistor, C. F. Chirila and L. Pintilie

During the last decade or more, a great deal of effort has been invested in developing applications based on ferroelectric materials such as static random access memories, pyroelectric detectors, high-k capacitors and, more recently, artificial multiferroics. Most of the currently studied artificial multiferroic systems are based on epitaxial multilayers grown onto $SrTiO_3$ (001) single crystals (STO). $SrRuO_3$ (denoted SRO hereafter) epitaxial layers are frequently used as bottom electrode for two reasons: i. SRO has a good electrical conductivity and ii. SRO allows for further epitaxial growth of ferroelectric layers with perovskite structure. The quality of the epitaxial layers grown on top of the SRO electrode is strongly influenced by the crystalline status of the SRO layer itself, the presence of structural defects inside the SRO film or at the interfaces, the strain field effects, the presence of secondary phases, etc. SRO is a pseudocubic perovskite exhibiting three different crystalline phases: orthorhombic at room temperature, tetragonal between 547-677 °C and cubic above 677 °C. Our work [1] proves the formation of nanosized domains of a yet another phase, monoclinic SRO, inside epitaxial SRO layers under compressive stress. This was done via strain mapping at atomic resolution by quantitative HRTEM on epitaxial SRO thin films embedded in multilayered perovskite coatings onto STO(001). Transmission electron microscopy on cross-section specimens has been carried out on a high-resolution JEM ARM 200F electron microscope operated at 200 kV.

The selected-area electron diffraction (SAED) patterns revealed the presence of supplementary diffraction spots attributed to SRO appearing in positions which are forbidden in all the three space groups describing the known SRO structural phases.

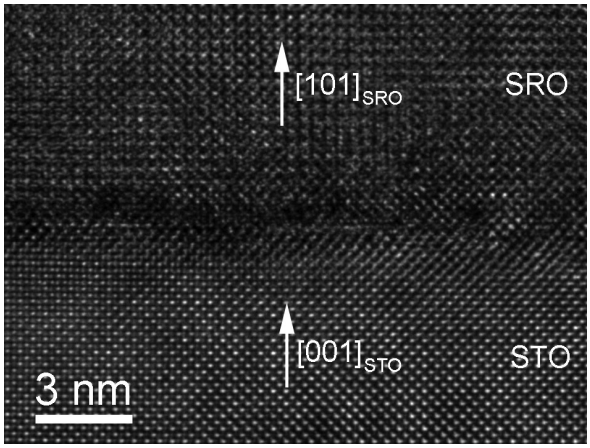

Figure 1. *HRTEM image at the SRO-STO interface showing the epitaxial growth of the SRO layer.*

To elucidate the origin of these supplementary spots, we have performed an in-depth study by quantitative HRTEM and image simulation regarding the SRO layer. The HRTEM micrograph at the SRO-STO interface (Figure 1) proves the epitaxial growth of the SRO layer. Strain field effects may be noticed as dark contrast at the SRO-STO interface or inside the SRO layer.

The high-resolution image in figure 2a, representing the SRO layer and neighboring areas from the STO substrate and the overgrown PZT layer, has been recorded in a thin area where the $0k0_{SRO}$, k=2n+1, diffraction spots have been noticed in the SAED pattern. Selected-area power spectra, obtained from two neighboring areas denoted 1 and 2 are presented in figures 2 c and d. One can clearly see that the power spectrum corresponding to area 1 does not show spots in the forbidden positions, while the selected area 2 generates spots in forbidden positions (white arrowheads). The dynamical effects due to local variations of the specimen thickness have been ruled out. We have searched for a different explanation using the Geometrical Phase Analysis [2].

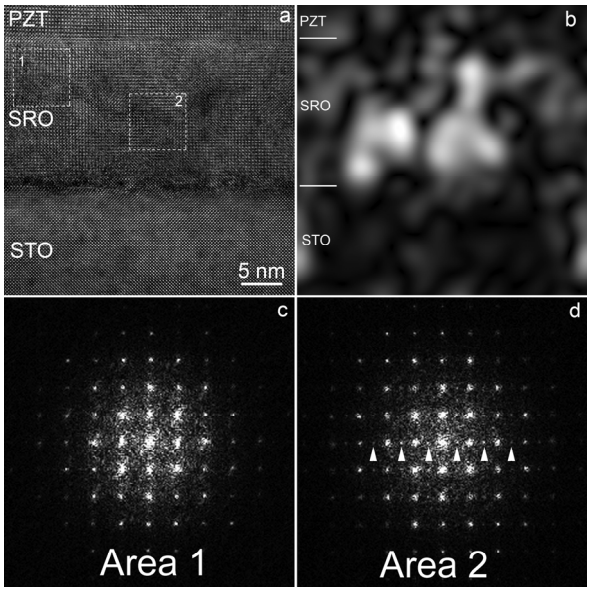

Figure 2. *(a) HRTEM image including the SRO layer and neighboring areas from the STO substrate and PZT layer; (b) Amplitude Image obtained by selecting one forbidden spot; (c), (d) Power spectra from areas 1 and 2.*

By selecting one of the forbidden spots on the FFT diagram, we have extracted the Amplitude Image where the bright areas correspond to regions with significant contribution to the intensity of the selected spot. The revealed bright areas generating the 0-30$_{SRO}$ spot represent nanometric domains inside the SRO layer, in the neighborhood of the dislocations revealed by Fourier filtering (not shown here).

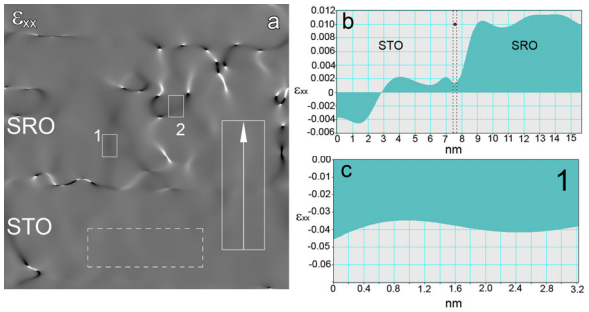

Figure 3. *(a) Map of the ε_{xx} strain field; (b) Line profile of ε_{xx} across the STO-SRO interface; (c) Line profile of ε_{xx} strain field inside area 1.*

The calculated strain field maps reveal the strain accumulation along the interfaces and around the dislocations inside SRO. The line-profile of the ε_{xx} strain across the STO-SRO interface oscillates around zero on the STO side, showing a jump to a plateau around +1% when crossing the interface into the SRO layer, in perfect agreement with the SRO-STO lattice mismatch (Fig. 3). The lattice distortion in areas close to the dislocations inside the SRO layer (1 and 2 on the ε_{xx} map) has negative values (-4 ÷ -5 %), representing nanodomains of compressive strain overlapped with the bright nanometric areas on the amplitude image. We claim, therefore, that the source of the faint forbidden SRO diffraction spots is the presence inside the SRO layer of heavily distorted nanometric domains under compressive strain. We have further confirmed this hypothesis by image simulation on monoclinically distorted SRO (Fig. 4).

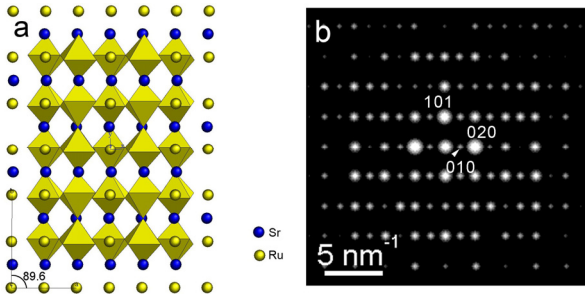

Figure 4. *(a) Monoclinic distortion (γ = 89.6°) applied to orthorhombic SRO; (b) Simulated electron diffraction patterns for SRO along **B**=[10-1] for the monoclinic distorted SRO.*

In conclusion, we have shown that the forbidden diffraction spots observed in the SAED patterns originate from nanometric areas inside the SRO layer, where high values of a local compressive strain have been measured. The high local strain leads to a local monoclinic distortion of the orthorhombic lattice of SRO, suppressing the screw axis along [010]$_{SRO}$ and enabling the appearance of diffraction spots in forbidden positions.

References

[1] C. Ghica, R. F. Negrea, L. C. Nistor, C. F. Chirila and L. Pintilie, J. Appl. Phys. **116**, 023516 (2014).

[2] M. J. Hÿtch, J.-L. Putaux, and J.-M. Pénisson, Nature **423**, 270 (2003).

Potential Applications

Dual emitter organometallic compounds and their applications

I.C. Ciobotaru, C.C. Ciobotaru, E. Matei, I. Enculescu, S. Polosan

Chemical synthesis of organometallic compound with two types of ligands, quinoline and phenylpyridine, was successfully done. The two step synthesis produces an iridium organometallic compound $IrQ(ppy)_2$ with dual emission (figure 1). In the first step, reaction of $IrCl_3$ with phenylpyridine results in a yellow powder with bimolecular structure, which was used in the second step of reaction with hydroxiquinoline. The chemical yield was between 75%-80% for the first step and 55–60% in the second step of reaction [1].

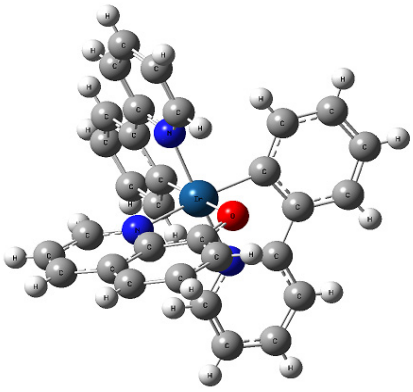

***Fig. 1** Structure of synthetized $IrQ(ppy)_2$*

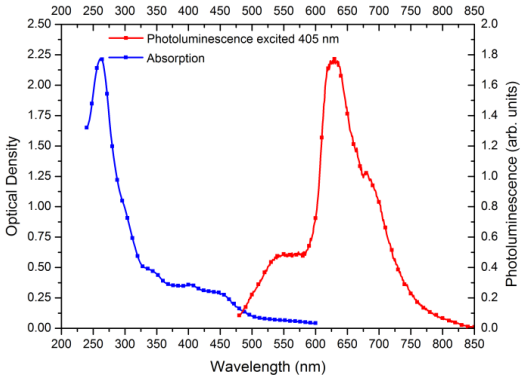

***Fig. 2** Absorption and photoluminescence of $IrQ(ppy)_2$ in dichlorometane*

The absorption spectrum of $IrQ(ppy)_2$ in dichloromethane is an ovelap of broad peaks in a visible region assigned to metal-to-ligands charge transfer and UV region assigned to intraligand absorptions (figure 2).

The photoluminescence spectrum exhibits the expected dual emission. Red emission is more intense than the green one, probably due to the π–π stacking of the quinoline ligands in the nanocrystaline powder.

Under electrons beam, $IrQ(ppy)_2$ powder reveals similar behaviors with photo-luminescence spectra (figure 3). The cathodo-luminescence (CL) images show a triclinic structure.

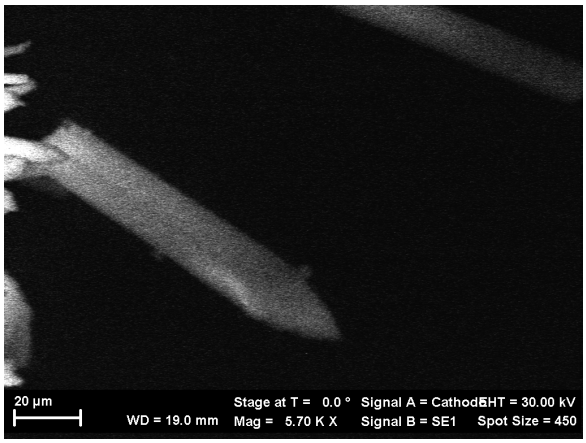

***Fig.3** Cathodoluminescence image of $IrQ(pyy)_2$ powder.*

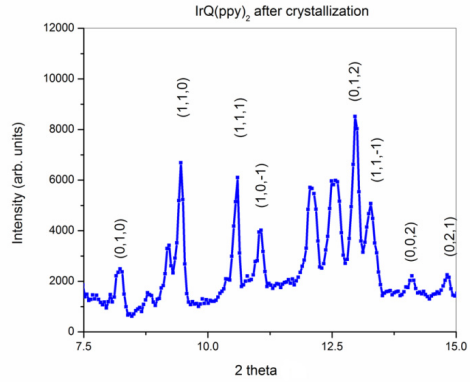

***Fig.4** XRD patterns of IrQ(ppy)2 after recrystallization.*

X-ray diffraction patterns of partially crystal-line powder, obtained from dichloro-methane, show a *P-1* triclinic structure (figure 4) confirmed by CL images [2].

In the case of the final compound, DSC patterns show higher stability, the melting point being centered at around 355 and 390 °C with an enthalpy of about 28.64 J/g. These peaks are assigned to the melting process of each ligand (figure 5).

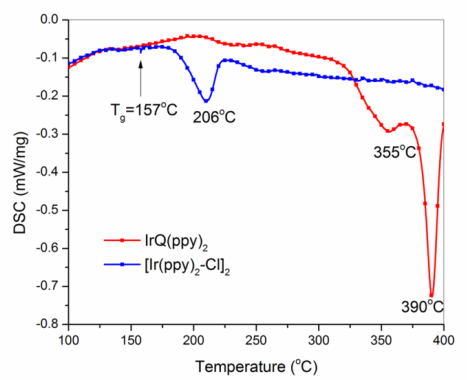

Fig.5. *DSC patterns of the intermediate and final compound.*

To investigate the thermal stability of the organometallic compounds, thermogravimetric analysis (TGA) was performed (figure 6).

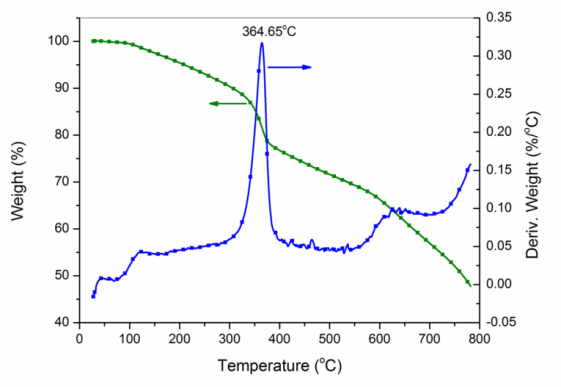

Fig. 6. *TGA of the final compound*

In the case of mixed ligands, the weight loss depends on the type of ligands in question. For IrQ(ppy)$_2$, the weight loss is centered at approximately 365°C and the temperature decrease is due to the weak coupling of the quinoline ligand.

Embedding of organometallic compound in conducting polymers is the key role of OLED's functionality [3]. Thin layers of polypyrrole:IrQ(ppy)$_2$ and polypyrrole were electrochemically deposited at 0.7–0.8 V on the ITO/glass substrate for 3 minutes (figure 7).

These thin films were characterized by spectroscopic methods to underline the properties of dispersed organometallic compound in the conducting polymer matrix.

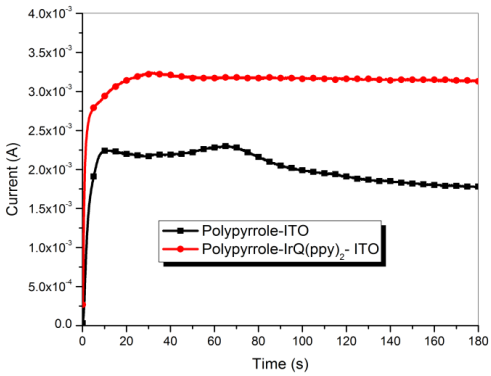

Fig. 7. *Electrochemical deposition of polypyrrole:IrQ(ppy)$_2$ and polypyrrole.*

Good dispersion of the IrQ(ppy)$_2$ in the polypyrrole matrix is supported by the CIE chromaticity in which the sum of the emissions is centered at 570 nm (figure 8).

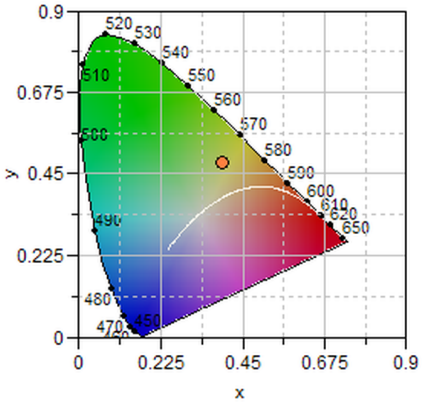

Fig. 8. *CIE chromaticity of the polypyrrole:IrQ(ppy)$_2$ thin layer under UV excitation*

Apart of the CIE coordinates (x = 0.3933; y = 0.4795), three other parameters can be detected: luminance (L_v = 0.33); correlated color temperature (T= 4282) and color difference from blackbody (d_{uv} = 0.0379).

Reference:

[1] I.C. Ciobotaru, S. Polosan, C.C. Ciobotaru, *Journal of Luminescence*, **145** (2014) 259-262.

[2] S. Polosan, I.C. Ciobotaru, I. Enculescu, C.C. Ciobotaru, *Journal of Materials Research*, **29(23)** (2014) 2898-2904.

[3] I.C. Ciobotaru, E. Matei, C.C. Ciobotaru, S. Polosan, *Synthetic Metals*, **198** (2014) 323-328.

Single nanowire based devices

C. Florica, A. Costas, E. Matei, I. Enculescu,

Quasi one-dimensional nanostructures are considered effective building blocks for future electronic devices. Their extremely interesting properties are given by their dimensions and their high aspect ratio.

Various ways to fabricate nanostructures, from straightforward wet chemistry approaches, like electroless deposition [1] or chemical bath deposition [2], to complex multistep approaches, were developed in the last years.

Nanowires represent an important class of nanostructures. The possibility of controlling their functionality raises with the ability to tune the morphological, structural and compositional properties via the preparation methods.

Electrodeposition of semiconductor materials in a polymeric template is a method which allows the growth of nanowires with high reproducibility and a narrow distribution of the geometrical characteristics. The properties of the nanowires grown using the template method can be controlled by changing the electrodeposition overpotential. However, the investigations of the electrical properties of individual ZnO or CdTe nanowires obtained in this way are scarce.

As semiconducting materials, ZnO and CdTe are studied due to the large applications range from energy production to light emitting devices, detectors, sensors or logic circuits. The morphology of ZnO and CdTe nanowire arrays was studied by scanning electron microscopy (SEM) and it is shown in Fig. 1 (a), (b). The band gaps of 3.3 eV for ZnO nanowires and 1.49 eV for CdTe nanowires were evaluated using the reflectance spectra depicted in Fig. 1 (c) and (d), respectively. For assessing the electrical properties of single nanowires, primarily, interdigitated electrodes of Ti/Au (10/100 nm) were fabricated on n++ doped Si wafers covered with 50 nm of SiO_2 using photolithography (Fig. 2 (a) and (b)). The nanowires were harvested by ultrasonication in isopropyl for being placed onto the interdigitated electrodes.

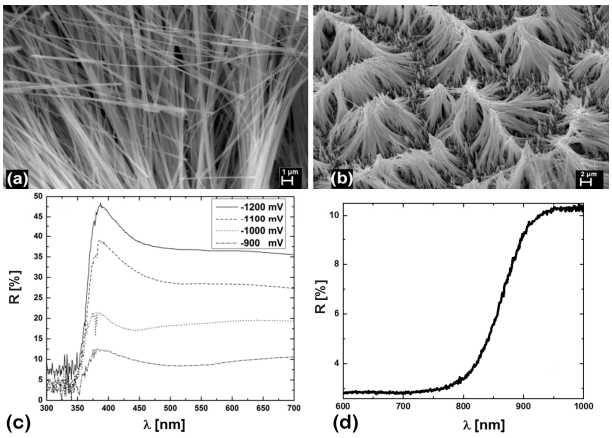

Fig.1 SEM images of (a) ZnO and (b) CdTe nanowire arrays with the corresponding reflectance spectra (c) and (d), respectively.

The ZnO nanowires were contacted by means of e-beam lithography (EBL), as it can be seen in Fig. 2 (c). By depositing Ti/Au (10/100 nm) thin layers at different angles between the sample and the deposition direction (0 and 60 degrees) and performing a thermal annealing at 350˚C, linear current-voltage characteristics were obtained for the investigated nanowires [3].

In the case of CdTe nanowires (Fig. 2 (d)), the linear current – voltage characteristics were obtained by contacting the nanowires with the help of Focused Ion Beam Induced Metallization (FIBIM), employing Pt as metallic electrodes [4].

Having linear current–voltage characteristics, devices such as field effect transistors can be fabricated in order to use them in different application, i.e. sensors.

The contacted nanowires were measured in the back-gate field effect transistor configuration having the n++ doped Si acting as the gate electrode.

Initially, the current – voltage characteristics of ZnO and CdTe nanowire based transistors are strongly dependent on surface states and as it can be noticed in Fig. 3 (a) and (b) respectively.

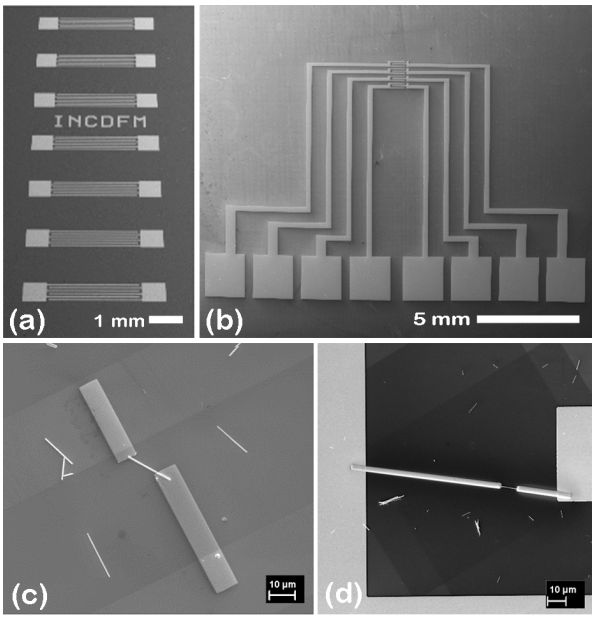

Fig.2 (a), (b) SEM images of two types of interdigitated metallic electrodes (Ti/Au); (c) ZnO single nanowire contacted using EBL and (d) CdTe single nanowire contacted using FIBIM.

An effect of the applied gate voltage is noticed but is weak and the current – voltage characteristics are not saturated.

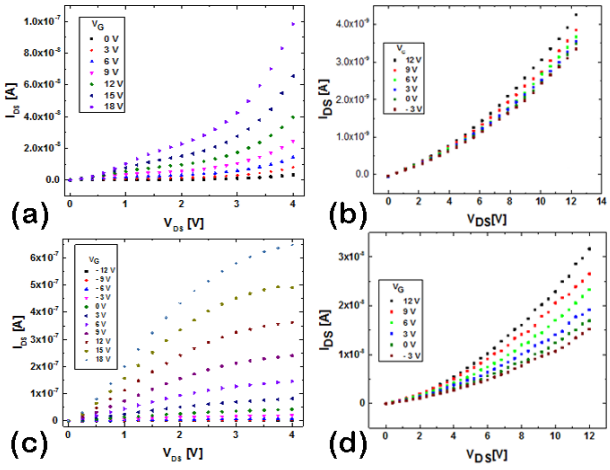

Fig.3 Source drain current - voltage characteristics for ZnO (a, c) and CdTe (b, d) nanowires before (a, b) and after (c, d) PMMA passivation.

The interaction between the surrounding environment and the surface of the nanowire can lead to the extraction of electrons from the conduction band leading to an increased resistivity. A passivation of the nanowire's surface with a thin layer of polymer (PMMA) leads to a lower resistivity and an improvement of the transport characteristics for both semiconductors.

For the ZnO single nanowires we have obtained field effect transistors with excellent properties, having saturated source – drain current – voltage characteristics, I_{ON}/I_{OFF} values of 10^4, electron mobility of 100 cm^2/Vs and the charge carriers concentration of about $10^{16}\,cm^{-3}$.

The saturation of the source – drain current – voltage characteristics for CdTe nanowires is not occurring, even after the passivation with PMMA, most probably because of the high resistivity of the FIBIM deposited contacts, which are not purely metallic, but a mixture of Pt, C and Ga^+. An improvement of the elecrodes can lead to the saturated – like desired characteristics.

The results show that these electrodeposited nanowires are suitable for being used as channels in field effect transistors. By functionalizing the nanowire's surface, highly selective and sensitive sensors can be prepared.

NIMP researchers acknowledge the financial support from Romanian Government through UEFISCDI contracts EUROC 5 and 24/2013.

References

[1] C. Florica, N. Preda, M. Enculescu, I. Enculescu, Physica Status Solidi Rapid Research Letters, 8, 648–652, 2014

[2] C. Florica, N. Preda, M. Enculescu, I. Zgura, M. Socol, I. Enculescu, Nanoscale Research Letters, 9:385, 2014

[3] C. Florica, E. Matei, A. Costas, M. E. Toimil Molares, I. Enculescu, Electrochimica Acta, 137, 290-297, 2014

[4] E. Matei, C. Florica, A. Costas, I. Enculescu, Beilstein Journal of Nanotechnology, 6, 444–450, 2015

Electronic mechanisms in Fe based oxides with catalytic applications

V. Kuncser, D. Macovei, N. Apostol, G. Filoti
in cooperation with
V. Parvulescu (University of Bucharest, Faculty of Chemistry, Department of Organic Chemistry, Biochemistry and Catalysis) and *I. Morjan, M. Scarisoreanu, C.T. Fleaca* (National Institute for Plasma, Laser and Radiation Physics, Bucharest-Magurele)

There is currently a growing interest related to oxide/semiconductor catalysts, with respect to both controlable synthesys, reaction mechanisms and applications. Among them, nanosized rare-earth ferrites belonging to the class of distorted perovskites with orthorhombic symmetry and TiO_2 nanoparticulate systems, present many advantages related peculiar electronic structures and accomodation of defects, with direct implications on the catalytic activity (in the first case) and the photocatalitic one (in the second case). While the catalytic /photocatalitic activity of such systems depends on both the crystalline structure and the specific morphology (including shape, size distribution, dispersion, surface penetrability and hydrolysis) and in case of supported catalyst on the specific interaction with the support, special synthesis procedures assuring a large variety of the above parameters in an as much as controlled way are desired. On the other hand, the understanding of the relationship between structure and catalytic behaviour is of capital importance for such applications. This can be obtained only by corroborating specific morpho-structural characterization techniques (XRD, TEM) with powerful local microscopic techniques (Mössbauer, EXAFS, XPS) and with catalytic measure-ments (pulse chemisorption, temperature programmed oxidation/ reduction, etc.)

The $EuFeO_3$ perovskite (as prepared by the citrate route) was considered in this respect as a case study for cooperative efects of the rare earth and transition metal elements in the total catalytic oxidation of aromatic hydrocarbonns [1]. XRD characte-rization pointed for a well-crystallized perovskite stucture without unreacted phases. XPS has emphasized the presence of only Fe^{3+} and Eu^{3+} species as well as a faint satellite structure in the Fe2p spectrum, pointing for enhanced ionic character of Fe-O bonds at heavier rare-earth species. The EXAFS analysis indicated distributed oxygen vacancies in the nearest neighbouhood of Fe and next nearest neighborhood of Eu, remaining almsot unchanged after toluene exposure, proving so the insignifican role of the oxygen in the perovskite structure during the reaction.

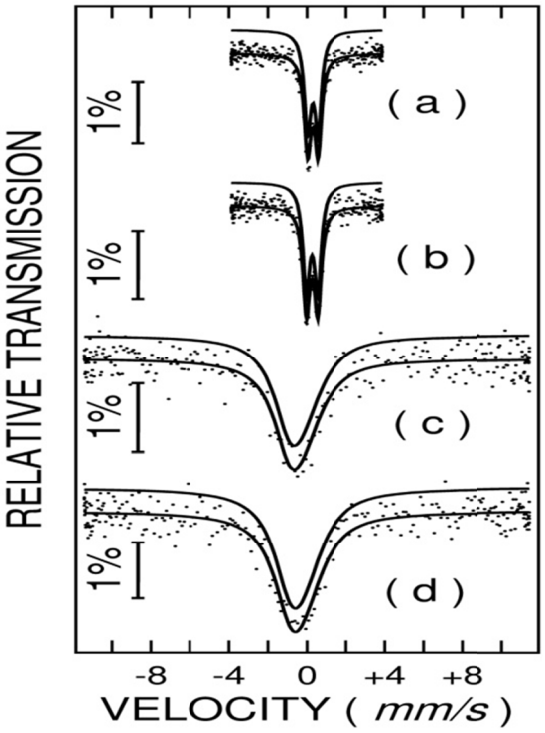

Fig.1. ^{57}Fe (a and b) and ^{151}Eu (c and d) Mossbauer spectra of the EuFeO3 perovskite structure analyzed in air: at 295 K (a and c) and at 623 K (b and d).

Combined ^{57}Fe and ^{151}Eu Mössbauer charac-terization (e.g. Fig.1) provided complementary information on the involved electronic mechanisms at the transition and rare earth metal ions. Supporting the presence of just Fe^{3+} and Eu^{3+} species, it inferred that the activation of the catalyst by calcination at 623 K in air corresponds to a tiny reduction of iron, as compensated by a slight oxidation of Eu during the reaction.

Concerning the system of TiO_2 nanoparticles, two samples obtained by laser pirolysis will be considered: a simple one and a composite sample doped with Fe in order to form additional magnetic nanoparticles, for the catalyst recovery [2].

Different HRTEM images obtained on the two samples prove clearly the formation of TiO_2 nanoparticles of average size of about 30 nm of anatase, with thin coating layers (2-3 nm) of turbostratic carbon. In the Fe/TiO_2 sample, nanosized nodules assigned to metallic/carbidic Fe were also observed.

According to the Mössbauer spectra acquired at different temperatures, the following Fe phases were evidenced (in percentage from total Fe): 22 % of Fe oxide (magnetite/maghemite), (ii) 16 % of metallic Fe, (iii) 18% of iron carbide and 35% of very small and poorly crystallized clusters (less than 1-2 nm in size) of Fe oxide or Fe carbide or even to dissolved Fe in the carbon shell. Magnetic hysteresis loops obtained on on the Fe/TiO_2 nanocomposite are shown in Fig 2. Surprisingly, even simple TiO_2 nanoparticles presented hysteresis loop at 300 K.

If the magnetization and the coercive field are expectable in this sample as due to a low amount (a few at. % and about 10 wt. %) of metallic Fe and Fe carbide phases, the presence of the magnetic signal of finite coercive field in sample containg just TiO_2 nanoparticles is quite unexpected and can be interpreted only in terms of the specific magnetism appearing in diluted magnetic oxides/semiconductors without transition metal doping.

It is worth mentioning that the elemental difference between the two samples (due to the absence/presence of Fe) is the lower amount of anatase phase and the higher amount of Carbon in Fe containing sample, both ingredients having a negative impact on the photo-catalytic activity of the product.

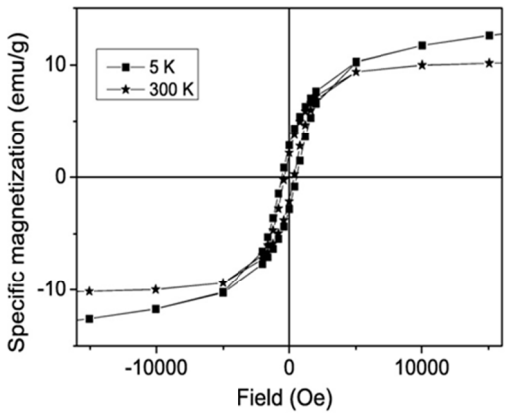

Fig.2. Hysteresys loops at two temperatures obtained on the Fe/TiO_2 nanocomposite.

Indeed, experiments concerning the photo-catalytic activity of such samples [2] confirmed the higher activity of the undoped sample. Hence, at a first view it seems that the Fe addition aimed for a possible recovery of the catalyst under the magnetic field would be not recommended in respect to the activity of the catalyst. In this case, a new direction remains to be exploited in auch nanocomposites, as based on the week intrinsic magnetisms of diluted magnetic semiconductor systems.

Authors acknowledge "Core Program"-PN09-450103/2014.

References

[1] M. Florea, M. Alifanti, V. Kuncser, D. Macovei, N. Apostol, N. Granger and V.I. Parvulescvu, Evidence of A-B site cooperation in the $EuFeO_3$ persovskite from Eu-151 and Fe-57 Mössbauer spectroscopy, EXAFS and toluene catalytic oxidation, Journal of Catalysis 316 (2014) 130-140

[2] C.T. Fleaca, M. Scarisoreanu, I. Morjan, R. Alexandrescu, F. Dumitrache, C. Luculescu, I.P. Morjan, R. Birjega, A.M. Niculescu, G. Filoti, V. Kuncser, E. Vasile, V. Danciu and M. Popa, Recent progress in the synthesis of magnetic titania/iron based composite nanoparticles manufactured by laser pyrolysis, Appl. Surf. Sci. 302 (2014) 198-204.

MgB_2 as a potential material for biomedical applications

G. Aldica and P. Badica
in cooperation with
D. Batalu (University 'Politehnica' of Bucharest),
and *A.M. Stanciuc, L. Moldovan* (National Institute for Biological Sciences)

The first use of a magnesium implant was mentioned in 1907 [1]. A high rate of degradation (within 8 days) and a large hydrogen release were observed. Due to this behavior, the use of magnesium was abandoned. In 1938, it was reported a decrease of the corrosion rate for Mg-Al-Mn alloy [2], hence a slower rate of hydrogen release, and no side effects were noticed. Recent studies show the importance of magnesium based materials [3], due to their low density, good initial mechanical properties (close to those of the bones) and biodegradability. At the same time, there are some negative issues such as corrosion rate being still high. The consequence is a fast decrease of the mechanical properties of the implant before the newly formed bone can sustain the necessary mechanical load. Another issue is the hydrogen release (as a reaction product, 1 liter per 1 g of Mg), and pH values of solution, up to 11 for pure Mg For overcoming these disadvantages, some methods were proposed:

(i) surface improvement (roughness control) [4], (ii) plasma surface modification [5], (iii) alloying [6] or use of new compounds [7], (iv) application of coatings [6, 8], (v) use of certain technologies to control microstructure [9].

In our work [10] micro (type A) or nano (Type B) powders of Eu_2O_3 were added to MgB_2. Composition was $(MgB_2)_{0.975}(EuO_{1.5})_{0.025}$. Pristine and doped samples were prepared by Spark Plasma Sintering and tested for (i) Vickers hardness, (ii) pH evolution in Phosphate Buffer Saline solution, (iii) corrosion resistance (Tafel polarization curves), (iv) cytotoxicity (*in vitro* tests), and (v) antibacterial activity. Eu_2O_3 additions influence investigated properties. Solution incubated with MgB_2-based samples show a relatively high saturation pH of 8.5 (Fig. 1). This value is lower than for solutions incubated with Mg or other Mg based biodegradable alloys reported in literature. MgB_2-based samples have lower electro-corrosion rates than Mg (Fig. 2).

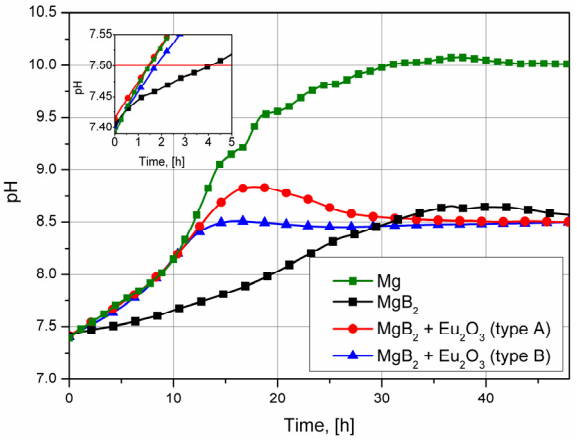

***Fig. 1** Evolution of pH vs. time, for PBS solutions incubated with samples.*

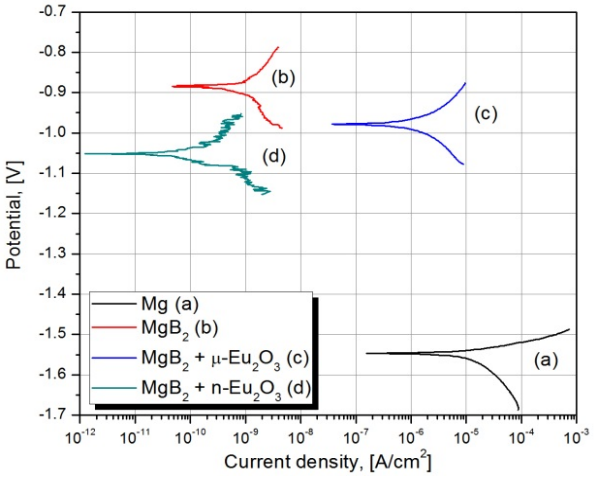

***Fig. 2** Potentiodynamic polarization curves of samples tested in PBS at room temperature.*

Their Vickers hardness is 6.8-10.2 GPa and these values are higher than for biodegradable Mg-based alloys. The MgB_2 has a low *in vitro* biocompatibility (Fig. 3) and a good antibacterial activity (Fig. 4) against *Escherichia coli* and a mild one against *Staphylococcus aureus*.

Our results suggest that MgB_2-based materials deserve attention in establishing their potential

for biomedical applications such as e.g. implants or sterile medical instruments.

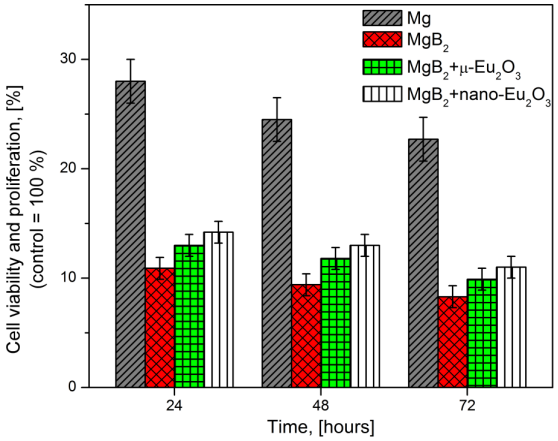

Fig. 3 *Effect of tested samples on rat osteoblasts viability after 24, 48 and 72 hrs of cultivation evaluated by MTT (3-(4,5-dimethylthiazol–2–yl)-2,5-diphenyl tetra-zolium bromide test) assay.*

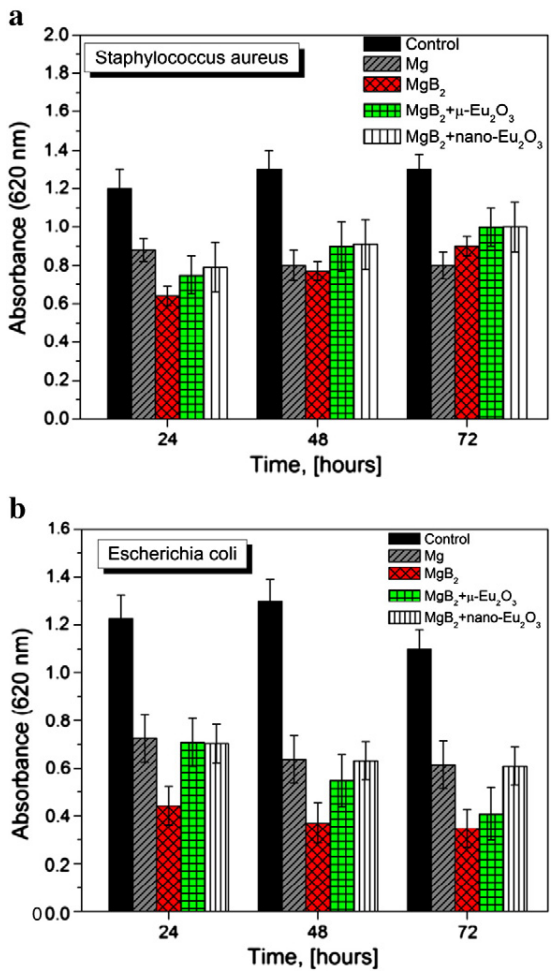

Fig. 4 *The quantitative assay results show the antibacterial activity of the samples: a. S. aureus and b. E. coli cellular dynamics.*

References

[1] A. Lambotte, L'utilisation du magnesium comme materiel perdu dans l'osteosynthese, Bull. Mem. Soc. Nat. Chir. 28 (1932) 1325-1334.

[2] E.D. McBride, Absorbable metal in bone surgery, J. Amer. Med. Assoc. 111 (1938) 2464-2467.

[3] M.P. Staiger, A.M. Pietak, J. Huadmai, G. Dias, Magnesium and its alloys as orthopedic biomaterials: A review, Biomaterials 27(2006) 1728-1734.

[4] B. Denkena, A. Lucas, Biocompatible Magnesium Alloys as Absorbable Implant Implant-Materials Adjusted and Subsurface Properties by Machining Processes, CIRP Ann. 56 (2007) 113-116.

[5] J. Yang, F. Cui, I.S. Lee, X. Wang, Plasma surface modification of magnesium alloy for biomedical application, Surf. Coat. Tech. 205 (2010) S182-S187.

[6] G. Song, Control of biodegradation of biocompatible magnesium alloys, Corros. Sci. 49 (2007) 1696-1701.

[7] F. Wu, J. Wei, H. Guo, F. Chen, H. Hong, C. Liu, Self-setting bioactive calcium-magnesium phosphate cement with high strength and degradability for bone regeneration, Acta Biomat. 4 (2008) 1873-1884.

[8] M.D. Pereda, C. Alonso, L. Burgos-Asperilla, J.A. del Valle, O.A. Ruano, P. Perez, M.A. Fernandez Lorenzo de Mele, Corrosion inhibition of powder metallurgy Mg by fluoride treatments, Acta Biomat. 6 (2010) 1772-1782.

[9] M.B. Kannan, Influence of microstructure on the in-vitro degradation behaviour of magnesium alloys, Mater. Lett. 64 (2010) 739-742.

[10] D. Batalu, A.M. Stanciuc, L. Moldovan, G. Aldica, P. Badica, Evaluation of pristine and Eu_2O_3-added MgB_2 ceramics for medical applications: hardness, corrosion resistance, cytotoxicity and antibacterial activity, Mat. Sci. & Eng. C, 42 (2014) 350-361

Pt-$(Bi,Sb)_2Te_3$ nanocomposite for thermoelectric applications

Marian Sima and Mariana Sima

Thermoelectric devices have potential applications in waste-heat recovery, air conditioning, refrigeration and as sensing devices, such as infrared thermal detectors. They generate an electric potential gradient from a thermal gradient, or vice versa, without any actuating parts.

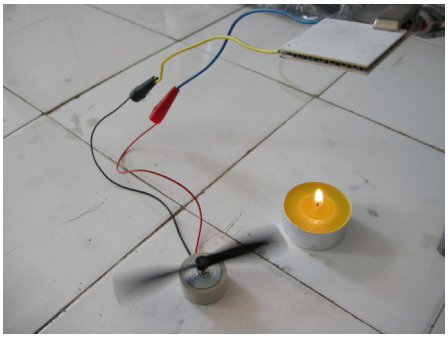

The improvement of thermoelectric devices efficiency is connected with the increase of thermoelectric performance of the materials used to their fabrication. A good thermoelectric material should possess large Seebeck coefficient, low thermal conductivity and high electrical conductivity. Experimental results showed that the thermal conductivity κ was lowered in one and two dimensional nanostructures where the roughness of phase boundaries is large enough to incoherently scatter phonons. At the same time, such surfaces may reflect electrons, preserving their electrical conductivity σ and their Seebeck coefficient S. Nanostructures may also be used to increase the material power factor P ($S^2\sigma$) by a mechanism named energy filtering. This enhancement can be achieved by introducing nanoscaled metal/semimetals into a semiconducting matrix. The interfacial barrier between semimetal and semiconductor is able to filter out cold carriers to enhance Seebeck coefficient without losing mobility. $Bi_{0.5}Sb_{1.5}Te_3$ is the state-of-the-art bulk material that exhibits the best thermoelectric properties at room temperature. Electrodeposition has been successfully applied to preparation of $Bi_{0.5}Sb_{1.5}Te_3$ films and nanowires. We investigated the electrochemical preparation of Pt-$(Bi,Sb)_2Te_3$ nanocomposites. In an approach, the electrochemical reduction process of Bi^{3+}, $HTeO_2^+$ and Sb^{3+} mixture was accompanied by the incorporation of Pt nanoparticles (Fig.1) suspended in the deposition bath. In a second approach, $[PtCl_6]^{2-}$ ions have been electrochemical reduced simultaneously with Bi^{3+}, $HTeO_2^+$ and Sb^{3+} mixture in an acid solution[1].

Pt-$(Bi,Sb)_2Te_3$ *nanocomposite film*

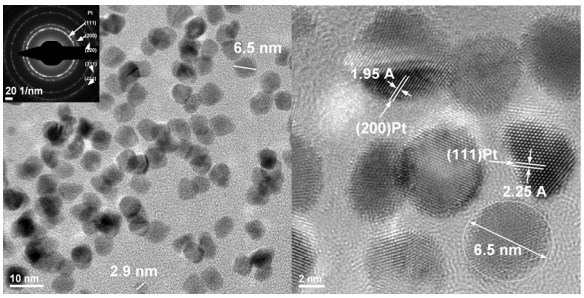

Fig.1:*TEM and HRTEM images of Pt nanoparticles synthesized by polyol method*

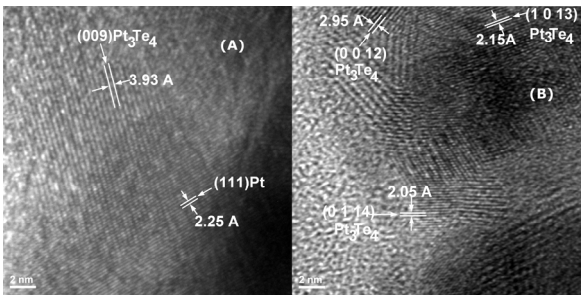

Fig.2. *HRTEM images which present Pt and Pt_3Te_4 nanoparticles embedded in A and B films prepared in the baths 1 and 2 (Table 1), respectively.*

We gave the following plausible mechanism for the incorporation of Pt-Te nanostructures in the film *A* (Fig.2):

- adsorption of tellurium from solution on Pt nanoparticles as TeO_2^+ monolayer
- capturing of Pt…TeO_2^+ nanoparticles on the surface of the electrodeposited film during the cathodic process
- reduction of TeO_2^+ layer to Te, resulting Pt nanoparticles covered with a Te layer. Reduction process could continue with the following step: $3Pt + 4Te \rightarrow Pt_3Te_4$ [2]. Indeed, phase diagram of

Pt/Te system suggested that the dominant phase is Pt_3Te_4 at all temperatures in the range where the platinum and tellurium concentrations are equal [3].

- embedding of Pt-Te nanostructures in the film *A* during the electrodeposition process

The proposed mechanism for incorporating of Pt-Te and Pt nanoparticles in the film *B* (Fig.2) includes the following stages:

- reduction of $[PtCl_6]^{2-}$ and $HTeO_2^+$ ions to Pt and Te, respectively on the surface of the electrode. The reduction process may continue further with the solid-state reaction: 3Pt + 4Te→Pt_3Te_4. Part of platinum remained as a separate phase in Pt-$(Bi,Sb)_2Te_3$ film (diffraction measurements).

- incorporating of Pt and Pt-Te nanoparticles in the $(Bi,Sb)_2Te_3$ film.

Table 1 *Chemical composition of the solutions used for electrodeposition of Pt-$(Bi,Sb)_2Te_3$ films and wires.*

Bath	Composition
1	12.4mM $HTeO_2^+$, 1.5mM $Bi(NO_3)_3$ 7.2mM SbO^+, 0.67M tartaric acid, 1M nitric acid [2]
2	12.4mM $HTeO_2^+$, 1.5mM $Bi(NO_3)_3$, 7.2mM SbO^+, 0.67M tartaric acid, 1M nitric acid + 0.8mg/ml Pt nanoparticles in suspension
3	12.4mM $HTeO_2^+$, 1.5mM $Bi(NO_3)_3$, 7.2mM SbO^+, 0.67M tartaric acid, 2mM H_2PtCl_6, 1M nitric acid

Pt*-$(Bi,Sb)_2Te_3$ *submicrometer wires

Four different deposition potentials (i.e. -0.05, -0.091, -0.17 and -0.25V/Ag-AgCl) were used to deposit by template method $(Bi,Sb)_2Te_3$ submicrometer wires from the solution 1 (Table 1). The wires prepared at -0.17V have the closest composition to that of the alloy $Bi_{0.5}Sb_{1.5}Te_3$. Figs.3A and 3B show the SEM images of $(Bi,Sb)_2Te_3$ wires grown at -0.091 and -0.17V, respectively from the solution 1 (Table 1), after removing of the template. The growth of $(Bi,Sb)_2Te_3$ wires at more cathodic potential seems to lead to inhomogeneous structures.

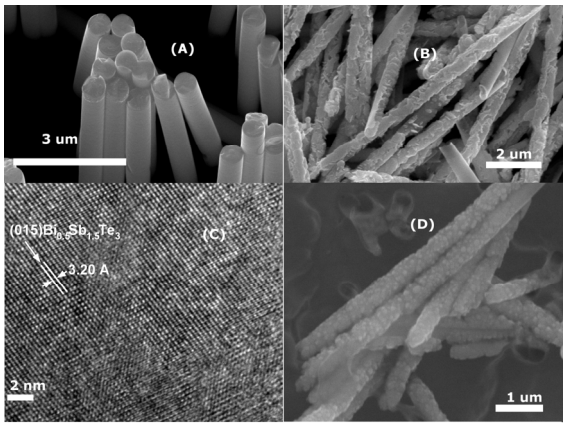

Fig.3. *SEM images of $(Bi,Sb)_2Te_3$ submicrometer wires prepared at -0.091V (A) and -0.17V (B) in the solution 1. C) HRTEM image of a microzone from $Bi_{0.5}Sb_{1.5}Te_3$ submicrometer wire prepared at -0.091V in the solution 1. D) SEM images of Pt-$(Bi,Sb)_2Te_3$ submicrometer wires prepared at -0.17V in the solution 3 (Table 1).*

HRTEM image from Fig.3C shows crystalline ordering on relatively large microzone from $Bi_{0.5}Sb_{1.5}Te_3$ wires prepared at a potential of -0.17V. Somewhat surprisingly, it was found that submicron wires grown at -0.17V from solution 2 does not contain platinum. It is possible most of Pt nanoparticles are retained on the large surface of $Bi_{0.5}Sb_{1.5}Te_3$ submicrometer wires and they are leached during template removing. On the other hand, submicrometer wires (Fig.3D) grown at -0.17V from solution 3 contain an important percent of platinum.

References

[1] Marian Sima, Eugeniu Vasile, Mihai Buda, Mariana Sima, *"Investigation on the electrodeposition of Pt-$(Bi,Sb)_2Te_3$ nanocomposite as film and wires"* Electrochimica Acta 127 (2014) 208

[2] F-H. Li, Q-H. Huang, W. Wang, Electrochim. Acta 54 (2009) 3745.

[3] W.S. Kim, Met. Mater. 2 (1996) 9

Organic materials for photonics and photovoltaics

A. Stanculescu, M. Socol, O. Rasoga, C. Breazu, N. Preda
in cooperation with
F. Stanculescu, I. Ionita
University of Bucharest, Faculty of Physics, Magurele, Romania
M. Grigoras, L. Vacareanu, T. Ivan
"P. Poni" Institute of Macromolecular Chemistry, Iasi, Romania
G. Socol, Ion N. Mihailescu
National Institute for Laser, Plasma and Radiation Physics, Magurele, Romania

Organic materials are promising candidates for a large area of applications from photonics to optoelectronics and photovoltaic conversion. The main challenges are related to optimization of organic materials (small molecules/oligomers/ polymers) and selection of adequate preparation method to assure the target properties. Our interest was focused on new molecular structures based on π-conjugated systems with substituent functional groups for improving the optical (including optical nonlinear/ONL) properties and charge carrier transport. We have investigated the effect of inorganic/organic dopants on the Bridgman-Stockbarger growth conditions and optical properties of bulk small molecule organics like meta-dinitrobenzene (m-DNB) and benzil (Bz), which are characterised by large optical band gap and high nonlinear coefficients [1].

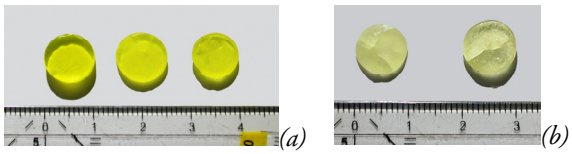

Fig. 1: Typical pictures of Bz (a) and m-DNB (b) slices [1].

The growth interface stability analysed by the stability criterion confirmed the growth of both m-DNB and Bz crystals in the same experimental conditions (Fig. 1) even at high concentration gradient at the interface [1]. The Urbach energy evaluated from the Tauc plots has revealed a more important contribution to disorder of I_2 compared to m-DNB in Bz crystal and a less disordered m-DNB doped with I_2 compared to undoped m-DNB crystal. The ONL phenomenon dominant in m-DNB was the second harmonic generation/ SHG which increased by doping with I_2 and in Bz the two photon absorption fluorescence emission/ TPF which decreased by doping with I_2 (Fig. 2a, b).

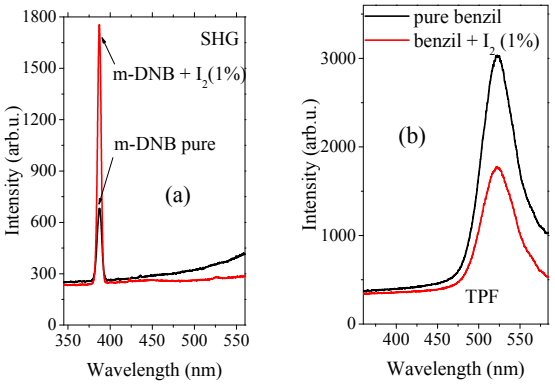

Fig. 2: ONL phenomena in pure and doped m-DNB (a) and Bz (b) slices [1].

We have studied bi-layer heterostructures realized with small molecule organics [zinc phthalocyanine/ZnPc; 1,4,5,8-naphthalene-tetracarboxylic dianhidride/NTCDA; tris-(8-hydroxyquinoline) aluminium salt/Alq3] or arylenevinylene oligomers [3,3'-bis (N-hexylcarbazole)vinylbenzene/P13; 1,4-bis [4(N,N'diphenylamino)phenylvinyl]benzene/P78] and mixed active layer heterostructures realized with star-shaped arylenevinylene compounds (4,4',4"-tris[(4'-diphenylamino) styryl]triphenylamine/IT77) and fullerene derivative ([6,6]-phenyl C61 butyric acid butyl ester /PCBB). The bi-layer and mixed layer heterostructures have been prepared by matrix assisted pulsed laser evaporation (MAPLE) on AZO and ITO transparent conductor electrode [2-4].

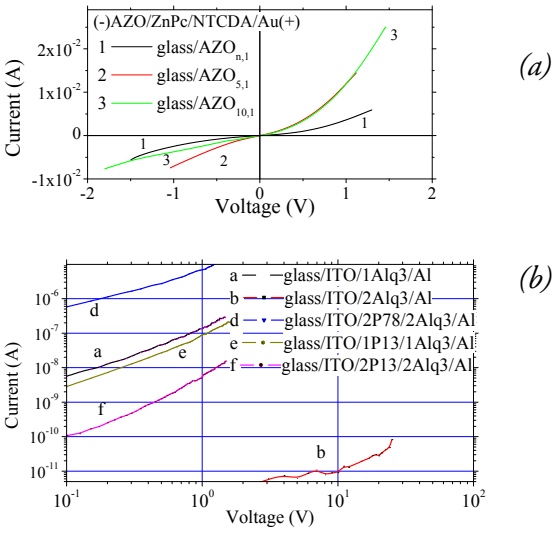

Fig. 3: I-V characteristics of: (a) bi-layer ZnPc/NTCDA heterostructure on AZO: untreated (1); treated in plasma for 5 min (2); treated in plasma for 10 min (3) [2]; (b) Alq3 based heterostructures on ITO [3].

I-V characteristics in dark of ZnPc/NTCDA heterostructures have evidenced an injection contact behavior and the presence of the space charge limited current for voltages > 0.4 V (Fig. 3a). The injection of the charge carrier and increase in current with one order of magnitude at 1 V was favored by the low resistivity of oxygen plasma treated AZO film, determining an increase in the work function of AZO [2]. A good injection contact behavior and symmetric I-V characteristics were also shown by the heterostructures with arylenevinylene oligomers (Fig. 3b), the current increasing in ITO/P78/Alq3/Al with the increase of organic layer thickness [3]. The attention was also focused on the investigation of the heterostructures with mixed active layer of IT77 as donor and PCBB as acceptor in the weight ratio 1:2 using poly(aniline-co-aniline propane sulfonic acid)/An-AnPS as buffer layer, instead of poly(3,4 ethylenedioxythiophene):

poly(styrenesulfonate)/PEDOT-PSS [4].

Most of the heterostructures with mixed active layer have shown an injection contact behaviour, low current and small asymmetry of the I-V curve (Fig. 4a) determining a weak rectifying behavior. Heterostructure P13-glass/ITO/PEDOT-PSS/IT77:PCBB/Al (V_{OC}=-0.34V, I_{SC}=1.98×10^{-9} A, FF=0.29) has presented a typical solar cell behavior (Fig. 4b) [4]. Electrical properties correlated with better charge carriers transport in P13 are determined mostly by the morphology of active layer which is influenced by the buffer layer of PEDOT-PSS [4].

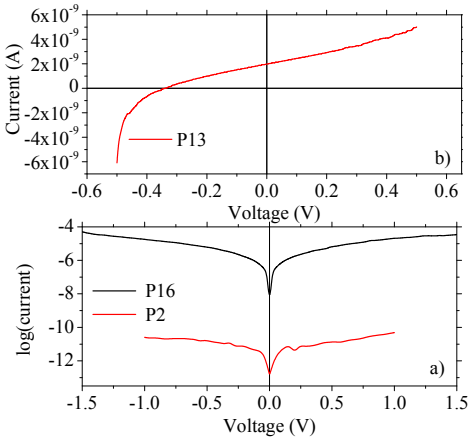

Fig. 4: I-V characteristics for [4]: P2- ITO/An-AnPS/IT77:PCBB/Al; P16- ITO/IT77:PCBB/Al; P13- ITO/PEDOT-PSS/IT77:PCBB/Al.

References

[1] F. Stanculescu, I. Iulian, A. Stanculescu, J. Cryst. Growth 401, 215-220 (2014)

[2] A. Stanculesdcu, M. Socol, O. Rasoga, I.N. Mihailescu, G. Socol, N. Preda, C. Breazu, F. Stanculescu, Appl. Surf. Sci. 302, 169-176 (2014)

[3] M. Socol, N. Preda, L. Vacareanu, M. Grigoras, G. Socol, I.N. Mihailescu, F. Stanculescu, M. Jelinek, A. Stanculescu, M. Stoicanescu, Appl.Surf.Sci. 302, 216-222 (2014)

[4] A. Stanculescu, G. Socol, M. Grigoras, T. Ivan, L. Vacareanu, M. Socol, O. Rasoga, C. Breazu, I.N. Mihailescu, I. Iordache, N. Preda, F. Stanculescu, Appl. Phys. A: Mat. Sci. Proc. 117(1) 261-268 (2014)

Mesopororous $Sn_{0.9-x}In_{0.1}Cu_x^{(I)}O_{2-\delta}$ gas sensors with selectivity to H_2S working under humid air conditions

A. Stănoiu, C.E. Simion
in cooperation with
S. Somăcescu[1], P. Osiceanu[1], J.M. Calderon-Moreno[1], A. Sackmann[2]
[1]"Ilie Murgulescu" Institute of Physical Chemistry, Romania Academy, Bucharest-Romania
[2]"AG Weimar, Institute of Physical Chemistry, University of Tübingen, Germany

In this work mesoporous materials based on $Sn_{0.9-x}In_{0.1}Cu_x^{(I)}O_{2-\delta}$ (with x=0.01-SIC1; 0.03-SIC2 and 0.05-SIC3 mol%) have been prepared via surfactant assisted (CTAB) hydrothermal synthesis route. Prior to explore their gas sensing performance close to real working conditions, structural, morphological and specific surface area investigations were done aiming to harvests insights about their inner properties. As such, analysis of the XRD peak widths indicate a significant reduction of the crystallite sizes for the tetragonal Sn-rich phase with increasing Cu content in SIC2 and SIC3 (Figure 1).

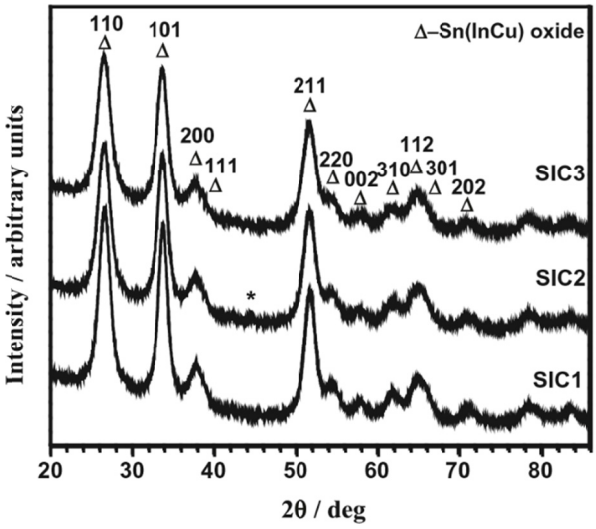

***Fig. 1** XRD patterns of SIC as-prepared materials calcinated at 600°C*

The porosity analysis performed by BET method, proved the existence of mesopores with average pore size around 7nm and specific surface area in the range 88-100m^2/g [1].

In order to acquire the gas sensing performance, the as-prepared materials followed screen-printing deposition technique onto commercial Al_2O_3 substrates provided with interdigitated Pt electrodes on one side and Pt heater on the other side. The final heat treatment was done at 600°C.

Sensitivity and selectivity sensing parameters were analysed regarding four types of target gases: H_2S, NO_2, CO and CH_4 with respect to their chemical interaction potential within a certain operating temperature range. The presence of 50% relative humidity (RH) in the surrounding test gas atmosphere was set as average value during the seasonal changes [2].

In Figure 2 can be seen the sensor signal behaviour towards 20ppm H_2S exposure with respect to the operating temperatures.

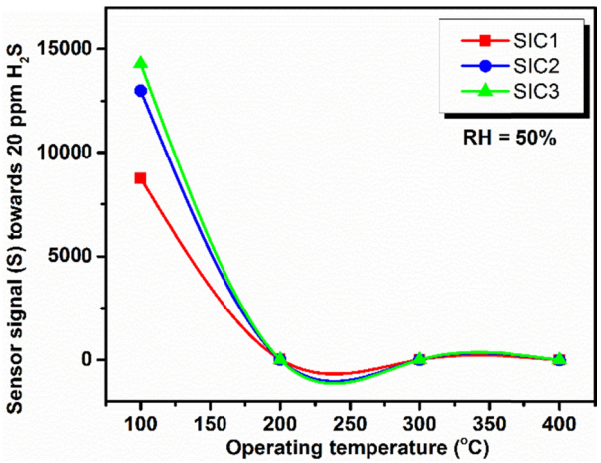

***Fig. 2** Operating temperature influence over the sensor signal for SIC based materials exposed to 20ppm H_2S*

All tested materials show high sensitivity to H_2S when operated at 100°C, yet the sensitivity (sensor signal) increases with the increase in Cu amount from: SIC1<SIC2<SIC3. The sensor signal for the most sensitive material (SIC3) indicate an exponential increase up to four orders of magnitude in the range 0-20ppm H_2S followed by a ceiling trend (Figure 3).

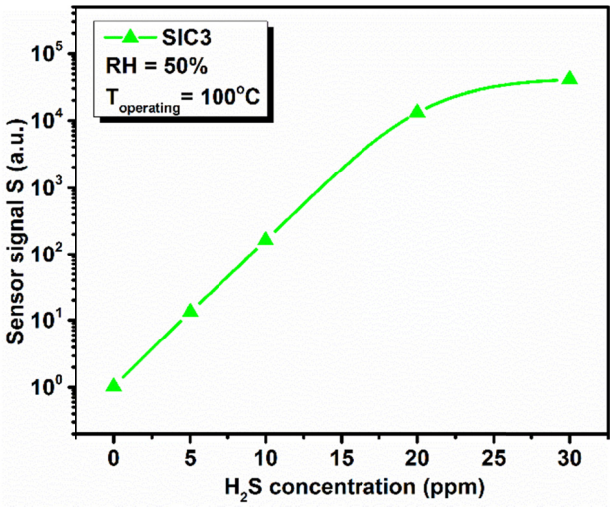

Fig. 3 Sensor signal dependence on the H_2S concentration for SIC3 operated at 100°C under 50%RH

Since the Permissible Exposure Limit (PEL) for H_2S is 20ppm, the test gas concentrations for NO_2, CO and CH_4 were intentionally set above the international recommended values in order to highlight the relative sensitivity (selectivity) towards H_2S detection. The selectivity was investigated within the operating temperature ranges from 100 to 400°C

In Figure 4 can be seen that the sensor signals to 250ppm CO and 7ppm NO_2 exhibit a bell-like behaviour with a maximum value at 300°C. The calculated sensitivities are S~4 for NO_2 whereas S~8 for CO exposure.

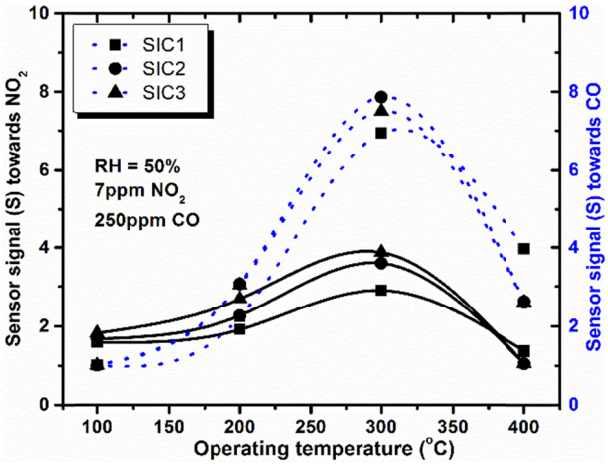

Fig. 4 Operating temperature influence over the sensor signal for SIC based materials exposed to NO_2 an CO

Under the same testing conditions, the highest sensor signal for 2500ppm CH_4 exposure was attained when SIC sensitive materials are operated at the maximum temperature 400°C. As in the case of H_2S detection, one can see that the sensitivity to CH_4 increases with the increase in Cu amount and its magnitude (S) does not exceed a factor of 10 (Figure 5).

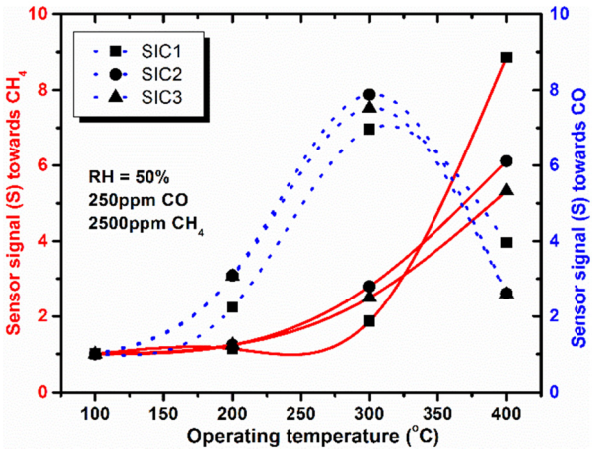

Fig. 5 Operating temperature influence over the sensor signal for SIC based materials exposed to CH_4 an CO

A comprehensive view of all gas-sensing performance investigations lead to the conclusion that, the foremost important operating temperature is 100°C where the SIC materials are showing high response and selectivity to H_2S close to real working conditions (50%RH). The amount of Cu content influences the overall sensing parameters, highlighting that SIC3 is the most sensitive material to H_2S [3].

References

[1] S. Somacescu, P. Osiceanu, J.M. Calderon Moreno, L. Navarrete, J.M. Serra, Microporous Mesoporous Mater. 179, 78-88, (2013).

[2] M. Huebner, N. Barsan, U. Weimar, Sens. Actuators B chem. 171, 172-180, (2012).

[3] S. Somacescu, P. Osiceanu, J.M. Calderon Moreno, A. Sackmann, C.E. Simion, A. Stanoiu, Microporous Mesoporous Mater. 197, 63-71, (2014).

In-situ crystallization of GeTe\GaSb phase change memory stacked films

A. Velea, A. C. Galca, M. Popescu
in cooperation with
G. Socol[1], C. N. Borca[2], D. Grolimund[2], J. A. van Bokhoven[2]
[1]National Institute for Laser, Plasma and Radiation Physics, Bucharest-Magurele, Romania
[2]Paul Scherrer Institute, CH-5232 Villigen-PSI, Switzerland

Due to modern technologies the needs for storage capacity have increased exponentially. The most used nonvolatile memories today are Flash memories which are based on charge storage. Because charge storage memories are facing miniaturization problems, some possible replacements are increasingly investigated. While magnetic and ferroelectric random access memories have problems with scalability, the nonvolatile memories based on resistance change rather than charge storage seem to take the lead. In this class of resistive memories we find phase change memories (PCMs). PCMs store data in a glass containing chalcogens (S, Se or Te) or pnictogens (such as Sb) and use low voltage (or ultra-fast laser pulses) to switch sub-domains of the material between two different states. In one state, the atoms of the glass are arranged in a disordered amorphous lattice (so called 'off' state or digital '0'), while in the other state they have a crystalline distribution ('on' state or digital '1'). The transition from amorphous to crystalline is made using a pulse of intermediate power which locally heats the material above the glass transition temperature and the material switches into the crystalline state. This transition is accompanied by large variations in the electrical conductivity (the electrical resistance is several orders of magnitude higher in the amorphous phase). To switch a PCM memory cell back into the 'off' state, a short intense pulse is used. The material is heated above the melting temperature and by rapid cooling it quenches into a disordered state.

Single and double layer phase change memory structures based on GeTe and GaSb thin films (500 nm\200 nm) were deposited by pulsed laser deposition (PLD) [1]. Their crystallization behavior was studied using in-situ synchrotron techniques. Electrical resistance vs. temperature investigations, using the four points probe method, showed transition temperatures of 138 °C for GeTe single films (Fig. 1). At temperatures below the crystallization threshold, the films were highly resistive due to their amorphous (insulating) phase and the resistivity decreased gradually until exceeding the crystallization/transition temperature. The drop in resistance is of 5 orders of magnitude.

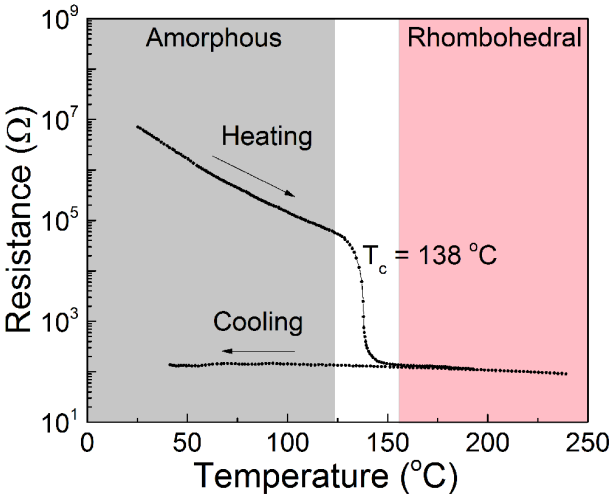

Fig. 1. *Typical resistance – temperature measurements on GeTe thin films.*

For the gallium antimony sample the transition temperature is at 198 °C as shown in Fig. 2 and the electrical contrast is of 4 orders of magnitude. Upon cooling the resistance remains lower than in the amorphous phase.

For the stacked films, it was found that after GeTe crystallization (Fig. 3), Ga atoms from the GaSb layer diffused in the vacancies of the GeTe crystalline structure. Therefore, the crystallization temperature of the Sb-rich GaSb layer is decreased by more than 30 °C to 168 °C. Crystallization temperature was estimated by integrating the area of GaSb (111) and GeTe (202) diffraction peaks as a function of temperature.

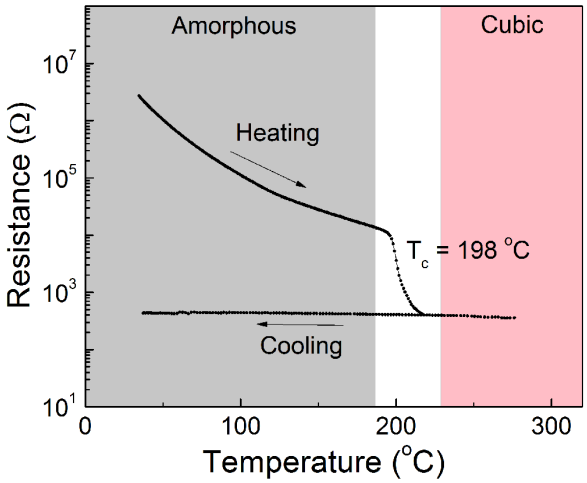

Fig. 2. Electrical resistance – temperature measurements on GaSb thin films.

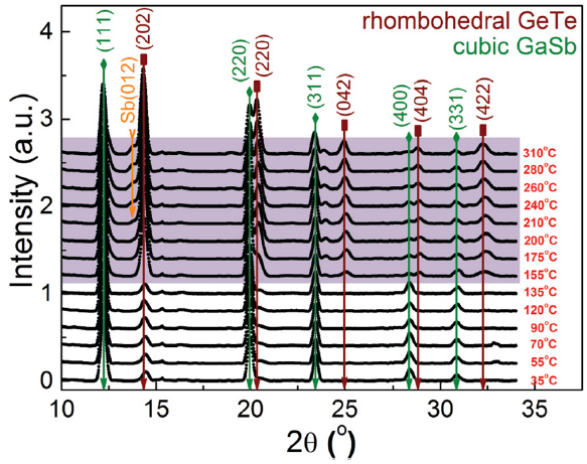

Fig. 3. XRD spectra of GeTe\GaSb stacked films during in-situ annealing between 35 and 310 °C. The crystallization of GeTe film is highlighted.

The crystallization temperatures derived from XRD are usually 10 – 20 °C higher compared to electrical vs. resistance measurements. The reason for this is that XRD peaks require a substantial fraction of the material to be in crystalline state, while the drop in resistivity requires only the existence of a conduction filament between the electrodes. A crystallization temperature of 150 °C was derived for GeTe. Furthermore, at 210 °C, the antimony excess from GaSb films crystallizes as a secondary phase. At higher annealing temperatures, the crystalline Sb phase increased on the expense of GaSb crystalline phase which was reduced.

EXAFS measurements performed on the ex-situ annealed GeTe samples are shown in Fig. 4. A clear change in the local environment of Ge atoms, in samples annealed at 160°C and 250°C compared to as-deposited and 100°C annealed films, is due to GeTe crystallization. The following mechanism has been proposed for phase transition: longer and weaker Ge – Te bonds from the crystalline structure are broken and structural segments with shorter and stronger bonds are formed, thus Ge atoms transition from the less favorable octahedral coordination to the tetrahedral one.

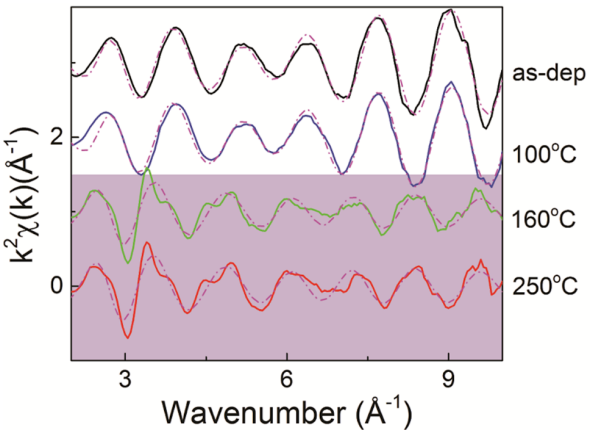

Fig. 4. k^2 – weighted back-Fourier transformed EXAFS oscillations at Ge edge (solid lines) and GeTe structure simulations (dash – dotted lines).

With further improvements in controlling the crystallization of individual layers, the stacked structures could achieve better characteristics than their single films counterparts.

The authors kindly acknowledge the financial support of the Scientific Exchange NMSCH program.

References

[1] A. Velea, C. N. Borca, G. Socol, A. C. Galca, D. Grolimund, M. Popescu, J. A. van Bokhoven, Journal of Applied Physics 116, 234306 (2014).

Patents and Patent Requests

PATENTS

M. Sima, M.Sima, *Cojocaru, A*;
Procedure of preparation of a thermoelectric material
Patent Number RO127531 (30.06.2014)

I. Poeata, A. Chiriac, I.N. Mihailescu, G. Socol, L. Duta, A.C. Popescu, F. Sima, M. Miroiu, ***G. Stan,*** *S. Petrescu, A. Ianculescu*
Method for obtaining of a titanium table covered with hydroxyapatite
Patent Number RO128190 (30.04.2014.)

C. M. Teodorescu
Cuptor cu incalzire rezistiva directa prin doua tuburi conductoare concentrice. Utilizarea acestui cuptor ca sursa de nanoparticule prin destindere adiabatica.
Patent Number RO129723 (29.08.2014)

PATENT REQUESTS

Published

Alexandru Evanghelidis, Cristina Busuioc, Nicoleta Preda, Elena Matei, Monica Enculescu, Camelia Florica, Andreea Costas, Mihaela Oancea, Ionut Enculescu
Procedeu de obtinere a fibrelor de oxid de zinc pure si dopate cu aluminiu, cu diametre submicronice, prin electrospinning folosind solutii de polimetilmetacrilat,
Buletinul Oficial de Proprietate Intelectuala RO-BOPI 4/2014, din 30.04.2014, p. 33

Alexandru Evanghelidis, Cristina Busuioc, Elena Matei, Monica Enculescu, Nicoleta Preda, Camelia Florica, Andreea Costas, Mihaela Oancea, Ionut Enculescu
Procedeu de obtinere a electrozilor bun conductori, transparenti si flexibili prin electrospinning si depunere electrochimica
Buletinul Oficial de Proprietate Intelectuala, RO-BOPI 7/2014, din 30.07.2014, p. 20

Patent Pending

Alexandru Evanghelidis, Cristina Busuioc, Elena Matei , Monica Enculescu, Nicoleta Preda, Camelia Florica, Andreea Costas, Mihaela Oancea**, Ionut Enculescu**
Procedeu de obtinere a electrozilor bun conductori ,transparenti si flexibili prin electrospinning si depunere electrochimica
A/00069, 18.03.2014

Alexandru Evanghelidis, Cristina Busuioc, Monica Enculescu, Nicoleta Preda, Elena Matei, Camelia Florica, Andreea Costas, Mihaela Oancea**, Ionut Enculescu**
Procedeu de obtinere de micro si nanofibre polimerice prin electrospinning folosind materiale textile pentru obtinerea de jeturi multiple
A/00213, 18.03.2014

Nicoleta Preda, Camelia Florica, Monica Enculescu, Irina Zgura, Marcela Socol, Alexandru Evanghelidis, Andreea Costas, Mihaela Oancea, Cristina Busuioc, Elena Matei, Ionut Enculescu
Procedeu de obtinere prin depunere chimica a unor filme nanostructurate tip retele formate din structuri monodisperse de oxid de zinc
A/00561, 24.07.2014

Camelia Florica, Nicoleta Preda, Monica Enculescu, Alexandru Evanghelidis, Andreea Costas, Mihaela Oancea, Cristina Busuioc, Elena Matei, Ionut Enculescu
Procedeu de obtinere prin depunere autocatalitica a unor arii micronice predefinite formate din structuri de oxid de zinc
A/00562, 24.07.2014

G. Stan, A.C.Popa
Metoda de realizare a unui implant dentar de titan cu acoperire de sticla bioactiva
A/00639/21.08.2014.

Piticescu M. R., Rusti C. F., Stoiciu M., ***Stanoiu A., Simion C. E.***
Procedeu hidrotermal pentru sinteza pulberilor nanostructurate de titanat de bariu si strontiu dopat cu lantan pentru aplicatii la senzori de gaze
A00794/27.10.2014

C. Busuioc, A. Evanghelidis, M. Enculescu, E. Matei, N. Preda, C. Florica, A. Costas, *M. Oancea,* ***I. Enculescu***
Dispozitiv Termocromic Bazat pe Electrozi Transparenti Flexibili Obtinuti prin Electrofilare
A/00916, 27.11.2014

E. Matei, C. Busuioc, A. Evanghelidis, M. Enculescu, N. Preda, C. Florica, A. Costas, *M. Oancea,* ***I. Enculescu***
Dispozitiv Electrocromic Bazat pe Electrozi Transparenti Flexibili Obtinuti prin Electrofilare si Electrodepunere de Polianilina
A/00917, 27.11.2014.

Events

CERN-RD50 Workshop

The 24th RD50 Workshop has been held in Bucharest, Romania, on June 11 - 13, 2014 at hotel Novotel. This meeting is the latest of a series of workshops, previous related conferences are listed at: http://rd50.web.cern.ch/rd50/. The 24th RD50 Workshop has been chaired by Michael Moll (CERN) and Ioana Pintilie (National Institute of Materials Physics).

RD50-Radiation hard semiconductor devices for very high luminosity colliders is an international collaboration lead by CERN having as major goal the development of radiation hard semiconductor detectors for very high luminosity colliders, particularly to face the requirements of a possible upgrade scenario of the LHC (Large Hadron Collider) at CEN, Geneva, Switzerland, to a luminosity of $10^{35}cm^{-2}s^{-1}$, corresponding to expected total fluences of fast hadrons above 10^{16} cm^{-2} at a bunch-crossing interval of ~25 ns (see also http://rd50.web.cern.ch/rd50/). The workshop was organized in Romania for the first time and was attended by 50 researchers representing the research institutions involved in RD50. Latest achievements in the field of Si radiation detectors were presented, with a special emphasis on defect engineering to enhance the detection characteristics. The NIMP have a major contribution in detection of those defects with the largest impact on detectors performance and in elaborating dedicated experiments for their structural identification.

ELECTROCERAMICS XIV
conference in Bucharest, Romania, June 16th – 20th, 2014

The fourteenth edition of **ELECTROCERAMICS** conference has been held in Bucharest, Romania, June 16th–20th, 2014, NIMP being awarded as the organizer of this very important international event.

All along the previous **ELECTROCERAMICS** editions the meetings have been proved to be among the most active interdisciplinary forums for promoting and discussing major results in fundamental and applied research in the field, and offered new ideas and solutions, proposed emerging trends and opened new research areas. Electroceramics materials and applications thereof became one of the major research subject in the field of materials science. Important steps in producing particular nano/microstructures by innovative synthesis allowed recent studies on size, shape and interface-driven mesoscale phenomena, whereas new experimental techniques and modeling tools provided a deeper processing-structure-property understanding. The resulted emergent properties opened new application routes and industrial implementation of electroceramic materials. In this spirit, **ELECTROCERAMICS XIV** has provided an interdisciplinary forum for scientists of various theoretical and experimental areas, involved in fundamental as well in applied research or in industrial implementation of such materials in multifunctional devices.

Trough the proposed plenary, invited, oral lectures and poster presentations as well as by the related workshops, the conference has facilitated international exchanges, and discussions about recent progress in various fields of electroceramics. A large participation of young scientists was strongly encouraged, as an important basis to promote the development of electroceramics trough possible new future international co-operations.

The conference program has covered a broad range of scientific interest, such as fundamental, theoretical, modeling & simulation studies, innovative processing, advanced characterisation, properties

and applications in several fields of electroceramics materials like dielectrics, ferroelectrics and multiferroics, as well as ionic, mixed and electronic conduction structures, in the state from bulk to ultrathin films and nanostructures.

Five main sections have been organized:

1. Bulk functional materials (dielectric, fero, piezo, magnetic, multiferroic): synthesis, characterization and applications
2. Thin films and heterostructures for applications in micro and optoelectronic, sensing, energy applications, etc.
3. Nanoscale materials and related investigation techniques
4. Ionic, mixed and electronic conduction and applications
5. Theory and modeling

Two other events satellite have been organized during the same period:

- COST MP0904 Action Showcase "Ferroelectric and multiferroic electroceramics: trends and perspectives"
- Brokerage"From Projects Ideas to Projects Developments" organized in the framework of the NMP TeAM2 project

At this conference have participated over 300 researchers from all the world and 2 plenary contributions, 46 invited lectures, 166 oral contributions and 112 poster presentations.

Among the invited academics which has offerred plenary or invited lectures, an important number of researchers had a world reputation: **Jim Scott** (University of Cambridge, United Kingdom), **Harry Tuller** (MIT Department of Materials Science and Engineering, USA), **Manuel Bibes** (Unité Mixte de Physique CNRS/Thales, France) **, Nava Setter** (EPFL, Switzerland), **Vincenzo Buscaglia** (Institute of Energetics & Interphases IENI-CNR Genoa, Italy), **Dragan Damjanovici** (EPFL, Lausanne, Switzerland), **Dietrich Hesse** (Max Planck Institute for Microstructure Physics, Halle, Germany), **Barbara Malic** (Jozef Stefan Institute, Ljubljana, Slovenia), **Susan Trolier McKinstry** (Penn State University, USA), **Hiromi Nakano** (Toyohashi University of Technology, Japan), **Alain Pignolet** (Institut National de la Recherche Scientifique – Centre Énergie, Matériaux et Télécommunications, Québec, Canada) *et al*.

Advanced workshop in solar energy conversion and nanophysics-Round Table: New opportunities in materials research in NIMP; launching RITECC-research Innovation & Technology Centre-a project financed through POS CCE programme-Magurele-Bucharest, 01-03 September 2014

The workshop is the third scientific event of this kind, organized by the UNESCO Chair at Horia Hulubei Foundation, with the scientific and financiar support of the International Center of Theoretical Physics (ICTP) – Trieste. The workshop has followed two main directions, of vital importance for physics and technology: **solar energy conversion** and **nanophysics**. Besides that, a number of special topics in material physics have been also addressed. In solar energy conversion, several key aspects of this domain are treated, as ab-initio investigation of photocatalysis, nanotechnology and synchrotron radiation techniques for photovoltaics, solar cells on paper substrate, etc. In nanophysics, lectures covered issues like carbon electronics, effective electron materials for Lithium and Sodium ion batteries, electronic materials inspired by nature, superconductivity. The computational approach to materials physics was also well represented. A special session was devoted to very young physicists. The lectures have been presented by active researchers in these fields, mainly from Central European countries. One of the objectives of the workshop was to foster the regional scientific cooperation. The workshop has also included a round table, concerning the new opportumities in materials research in the National Institute for Materials Physics, Magurele-Bucharest.

Nobel prize laureate, Professor Albert Fert, has visited the National Institute of Materials Physics

Professor **Albert FERT, Nobel Prize laureate for Physics in 2007**, has visited the National Institute of Materials Physics (NIMP) between 1st and 3rd of October 2014. Professor FERT has won the Nobel Prize, together with Professor Peter Grunberg, for the discovery of the Giant magnetoresistance. At present he is Scientific Director of a joint laboratory of CNRS and company Thales, Emeritus Professor at University Paris-Sud and member of the French Academy of Sciences.

Professor FERT is the first Nobel Prize laureate to visit a research institution from Romania. This is again a confirmation of the level of excellence in research reached by NIMP which, by infrastructure, quality of the human resources and of the research results, become competitive with top research institutes from Europe and from the world.

The launching conference for the project "Research Innovation and Technology Center for New Materials", RITecC.

On 5th of September 2014, NIMP hosted the launching conference for the project "Research Innovation and Technology Center for New Materials", RITecC.The POS-CCE project is co-financed by the Sectoral Operational Programme "Increase of Economic Competitiveness" "Investments for your future". The event gathered over 30 guests, including officials of the National Ministry of Education and of the Implementation Organism, representatives of firms and of the local authorities, directors and researchers from the same field institutes and universities, as well as mass-media. **NIMP's Scientific director, Dr. Florin Vasiliu**, held a very eloquent general presentation of the institute, in regards to its latest scientific results. **Dr. Andrei Galatanu** presented the technical details of the RITecC project emphasizing the complementarity of the new infrastructure with the existing one, and the scientific and technological motivation of the equipment included in the new project. **NIMP's General Director, Dr. Ionut Enculescu**, presented the development vision of the institution underlining the convergency of the new project with the already named development strategies. As a final part, the guests visited the institute laboratories and relevant facilities.

Sectorial Operational Programme „Increase of Economic Competitiveness

„Investments for Your Future”

Research Innovation and Technology Center for New Materials - RITecC

Project co-financed by the European Regional Development Fund

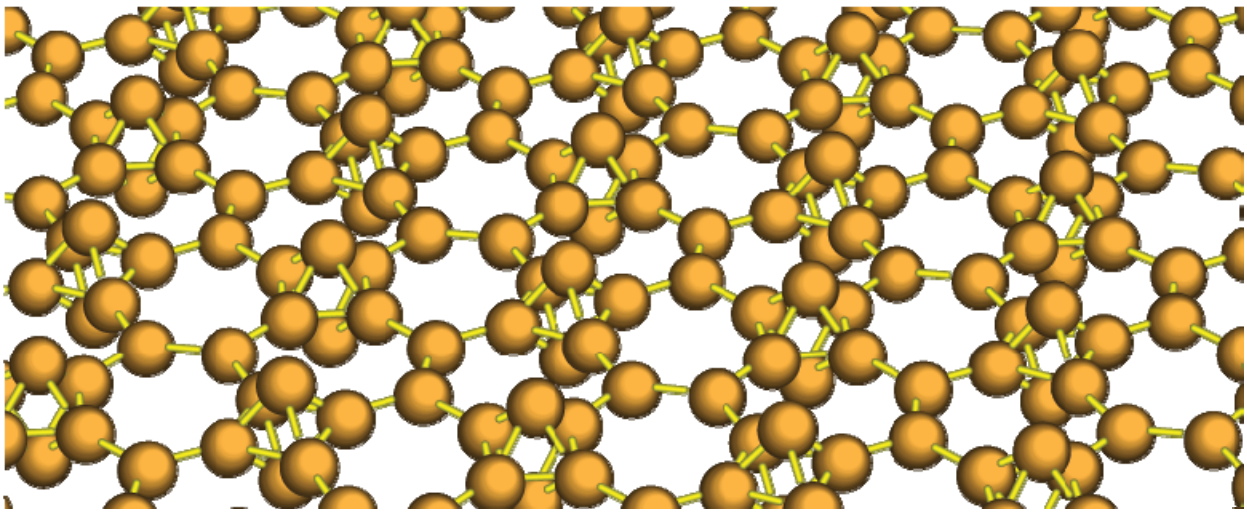

Abstract

The project entitled "Research Innovation and Technology Center for New Materials" RITecC, aims to overcome the barrier between Romanian research and its industrial applications in the field of advanced materials. The project sets as its main goal, the construction of a new building which would host the center and the acquisition of specific equipments required for three new laboratories, complementing NIMP's present infrastructure and enabling capitalization of the know-how already existing at national level. By implementing this project, NIMP aims to develop advanced materials preparation technologies, with a high applicative potential, compatible with modern industrial processes, and also to develop adequate characterization methods for such materials.

L1. Laboratory for production, processing and analyzing of functional materials for high- technology applications

It targets the technological development and innovation in the field of functional and multifunctional materials applications, in key fields such as, informational society, unconventional energies, sensors and devices with applications in agriculture, food industry, biology and medicine, telecommunications, security or environment protection.

L2. Laboratory for production, processing and analyzing materials for increasing life quality

It aims at the development of innovating preparation and characterization methods that can be considered being at the border between biology, chemistry and physics. The applications are numerous, in chemical and petrochemical industry, in cosmetics industry, food or medical industries, as well as archeology or conserving the heritage fields.

L3. Laboratory for production, processing and analyzing materials for extreme conditions

It is devoted to development and delivery of technological solutions, materials and complex composites which are to be used in extreme conditions, especially by modifying their surface properties. The applications are related to energy production industry, transports, and defense or aero-space industries.

OBJECTIVES

Our objectives target the growth of:

- The quality of research by tackling new research themes, in connection with the contemporary technological tendencies;
- The potential of developing income producing applications;
- The technological transfer rate towards the industrial, national and European stakeholders;
- The managerial initiative and the active implications of the personnel, in the operations of marketing new ideas;
- The degree of multidisciplinary training of the institute's human resource;
- The attractiveness of a research career for young graduates, in an environment that salutes personal growth and it is open to new ideas and innovative approaches.

International Cooperation

INTERNATIONAL COOPERATION PROJECTS

Pintilie I

CERN RD50 "Radiation hard semiconductor devices for very high luminosity colliders" (http://rd50.web.cern.ch/rd50/): 48 research institutions from 27 countries around the world

Scientific coordonator of the workpackage "Defect/Material Characterization"

Pintilie I

Project funds SEE (EEA Grants) "Perovskites for Photovoltaic Efficient Conversion Technology" (PERPHECT)

Partners: NIMP (INCDFM), Physics Faculty U. Bocharest, Optoelectronics 2000 SA (Romania); U. Iceland, U. Reykjavík (Iceland); U. Oslo (Norway)

2014-2017

2 FP7 projects

Pintilie L

FP7 project Large-scale integrating project Interfacing Oxides (IFOX) NMP-2009-2.2-1

Coordinator: Theo Rasing (Radboud University, Nijmegen)

Scientific coordinator: Georg Schmidt (Martin-Luther-Universität,Halle-Wittenberg)

Partners: Radboud University Nijmegen (NL), Martin-Luther-Universität Halle Wittenberg (DE), Max Planck Gesellschaft zur Foerderung der Wissenschaften E.V. (MPI-HALLE) (DE), University of Glasgow (UK), Centro Ricerche Fiat SCPA (IT), Universiteit Antwerpen (BE), Paul Scherrer Institut (CH), National Institute of Materials Physics (NIMP) (RO), IBM Research GMBH (CH), Universitat Konstanz (DE), Institute for Nanostructured Materials Bologna (IT), Intel Performance Learning Solutions Limited (IE), Forschungszentrum Jülich GmbH (DE), Twente Solid State Technology (NL), Georg August Universitaet Goettingen (DE),Holy Trinity College Dublin (IE), Organic Spintronics srl (IT), Universiteit Twente (NL)

(http://www.ifox project.eu)

2010-2015

Mercioniu I

Development of a sintering centre and know-how exchange for non-equilibrium sintering methods of advanced ceramic composite materials (SINTERCER)

FP7 EU-Research Potential – Capacities – REGPOT-CT-2013-316232-SINTERCER

Coordinator: The Institute of Advanced Manufacturing Technology, Krakow, Poland

Partners: Politecnico di Torino (POLITO), Torino, Italy, Institute of Ceramics and Glass (ICV-CSIC), Madrid, Spain, University of Rostock (UR), Rostock, Germany, National Institute of Materials Physics (NIMP), Bucharest – Magurele, Romania, Aalto University School of Chemical Technology, Espoo, Finland, RHP-Technology GmbH & Co. KG (RHP), Seibersdorf, Austria, Universidade de Aveiro (UA), Aveiro, Portugal, University of Science and Technology (AGH), Cracow, Poland, Institute of Metallurgy and Materials Science of Polish Academy of Sciences (IMIM), Cracow, Poland

(http://www.ios.krakow.pl/sintercer)

2 Romanian -Swiss Research Program RSRP projects

Baibarac M

Electrochemical functionalization of carbon nanotubes with heteropolyanions and conjugated polymers and the elucidation of interactions at the carbon nanotubes/ heteropolyacid/ conjugated polymer interface

Partners: Ecole Polytechnique Fédérale de Lausanne, Switzerland and Institute for Problems of Materials Science of National Academy of Science of Ukraine

Crisan O

Novel FePt-based hard magnetic materials for sustainable energy applications

Proiect RO-CH RSRP 142256 / 6 / 2012-2015

Partner: Swiss Federal Laboratories for Materials Science and Technology, EMPA Thun, Elvetia

C-ERIC

Teodorescu CM

CERIC Project ID: 20142030 Combined studies on magnetism, electronic structure, morphology and spin configuration in Ge(001) and Si(001) -based diluted magnetic semiconductors

2014-2015

2 IFA-CEA projects

Pintilie L

Pyroelectricity in PZT thin films and multilayers

Partner: Laboratory of components for microactuators, CEA Grenoble, France

2014-2016

Predoi D

New bioceramic nanocomposites with antibacterian activity for biomedical applications

Partner Franta: Laboratory of Chemistry and Biology of Metals (LCBM), Grenoble, France

2014-2016

OTHER EUROPEAN PROJECTS

SCOPES project

Baibarac M

Implementation in East Europe of new methods of synthesis and functionalization of carbon nanotubes for applications in the energy storage and sensors field

Partners: Ecole Polytechniue Federal de Lausanne, Switzerland and Institute for Problems of Materials Science of National Academy of Science of Ukraine

January 2011 - Februarie 2015

Programme Hubert Curien PHC Brancusi: ANCS-CNRS

Crisan O
Hard magnetic nanocrystalline materials obtained from amorphous precursors
Partner: Universite du Maine, Le Mans, Franta
2013-2015

EUROCORE (ESF) Project

Enculescu I
Insect Odorant-Binding Proteins on Conductive Polymer Nanofibers Based Biosensor to Diagnose Crop Disease
2011-2014

PROJECT ANR-ANCS (RO-FR) PN-II-ID-JRP-2011- 2

Teodorescu CM
Service de Physique et Chimie des Surfaces et Interfaces, Institut Rayonnement Matière Saclay, Commissariat à l'Energie Atomique, France
Chemical switching of surface ferroelectric topology
2013-2015

2 COST projects

Banciu MG
COST action VISTA (IC1102) "Versatile, Integrated, and Signal-aware Technologies for Antennas (VISTA)"
(http://www.cost.eu/COST_Actions/ict/Actions/IC1102)
Coordinator action: Dr. Marta Martinez Vazquez, Germania
2011-2015

Pintilie L
COST action MP1308 "Towards Oxide-Based Electronics (TO-BE)"
(http://www.cost.eu/COST_Actions/mpns/Actions/MP1308)
Coordinator action: Dr Fabio Miletto Granozio, Italy
2014-2018

3 EURATOM projects

Galatanu A
Participation of Romania at EUROfusion WPMAT and complementary research
1-EU-8/2014

Galatanu A
Experimental techniques for improved surface properties and non-destructive HHFM investigations
1-EU-8/20149

Kuncser V.
Participation of Romania at EUROfusion WPPFC and complementary research
1-EU-1/20149

ELETTRA (Trieste) Synchrotron projects

Apostol NG
Elettra Project ID: 20145226
Adsorption, desorption and molecular reactions at ferroelectric surfaces
2014-2015

Husanu MA
Elettra Project ID: 20140319
Reactivity and electronic properties of ferroelectric-ferromagnetic interfaces
2014-2015

Pintilie L
Proiect Sincrotron Elettra Trieste proposal No. 20130333
High-speed field effect devices based on graphene on epitaxial ferroelectric oxides: in-situ investigation of ferroelectric-graphene interface formation and properties by XPS and XAS combined with STM.
2013-2015

Teodorescu CM
Elettra Project ID: 20135077
Imaging ferroelectric domains in $BaTiO_3$ and $Pb(Zr,Ti)O_3$ single crystal layers with binding energy contrast. Depth profiling of depolarization charge. Experimental band structure of areas with well defined ferroelectric polarization
2014

Teodorescu CM
Elettra Project ID: 20145462
Photoelectron spectromicroscopic imaging of surface reactions on ferroelectrics with binding energy contrast
2014-2015

Bilateral cooperation projects (Agreements)

Baibarac M
Scientific Cooperation Agreement on **optical and electrical properties of composite nanomaterials based on carbon nanotubes and conjugated polymers** – France, Institut des Materiaux Jean Rouxell

Banciu MG
Collaboration project Romania-Japan JSPS 4903, 13039901-000203, Research Center for Development of Far-Infrared Region, University of Fukui (FIR-UF)
Research on EO sampling devices for ultra-high sensitive detection of THz waves using ferroelectric materials

Cernea M, Dinescu M
Proiect bilateral Romania-Italia
Study and Development of Single-Phase Multiferroic Perovskite Ceramic and Thin Films for Multifunctional Devices
Programul: JOINT RESEARCH PROJECT
Fruth V(coordinator Romania), Galassi C (coordonator Italia)
2014-2016

Stanculescu A
Accord de coopération scientifique dans le domaine des films minces notamment sur les thématiques suivantes: **structures multicouches organiques à basse dimension et composantes organiques et hybrides- France**

Stanculescu A
Scientific Cooperation Agreement on: **polymeric single/multylayer heterostructures for photovoltaic and electronic applications; polymeric field effect transistors for sensing applications; organic and hybrid devices (realisation, characterisation)-South Africa**

Cooperation projects with foreign institutes and universities

Badica P/Sandu.V
Normal University of Beijing
STM/STS studies concerning the local electromagnetic structure of superconducting and nanostructured magnetic materials (STMNANO)
Copbil 629/2013 RO-China

Ciurea ML
Institute of Microelectronics, NCSR "Demokritos", Greece
MOS nanostructures with intermediate layer of Ge nanoparticles and various gate oxides and their application in the area of nonvolatile memories

Ciurea ML
Istituto Nazionale di Fisica Nucleare-Laboratori Nazionali di Frascati (Prof. Stefano Bellucci) Frascati, Italy
Nanostructures based on Ge nanoparticles immersed in oxidic matrices for optical sensors applications

Ciurea ML
Peter Grünberg Institute (Dr. T Stoica), Forschungszentrum Jülich, Germany
Studies of the films formed from Ge nanoparticles immersed in oxidic matrices and of the multilayer Ge/oxide structures

Crisan O
Institut des Materiaux et Molecules du Mans, Universite du Maine, Le Mans, FR
Nanocomposites magnets based on FePt: alternative to rare earth permanent magnets
Capacities, Module III: Bilateral projects Romania-France
Project: NANOMAG-FePt, Contract: 721 / 2013-2014

Diamandescu L
Duquesne University, Physics Department, Pittsburgh, USA
Unconventional synthesis and the investigation of physics and chemistry of iron based oxide structures for applications in sensors and catalysis

Galatanu A
Consortiul EUROfusion
Grant agreement No. 633053
2014-2018.

Ghica C
Institut de Physique et Chimie des Matériaux de Strasbourg, France
Effet de la réduction de taille, de la forme et des caractéristiques des interfaces sur la structure et les propriétes des matériaux nanostructurés
Convention Bilaterale de Cooperation et d' Echange
2012-2016

Maraloiu VA / Teodorescu VS
Institut Lumière Matière – Université Claude Bernard, Lyon, France
Biolocalisation et biotransformation de nanoparticules à coeur d'oxydes magnétiques. Fonctionnalisation des substrats par irradiation laser à faible fluence
Convention Bilatérale de Coopération et d'Echange
2013-2014

Miclea CF
Los Alamos National Laboratory, Los Alamos, NM. USA.
Measurements, co-publication, specimen exchange

Miclea CF
Max Planck Institute for Chemical Physics of Solids, Dresden, Germany
Measurements, co-publication, specimen exchange

Nistor SV
Institutul de Fizica al Academiei Cehe din Praga
Investigation by magnetic electronic resonance techniques and optical spectroscopy of the semiconducting II-VI materials optically activated with transitional ions

Nistor SV
Departamentul de Fizica, Universitatea din Antwerp, Belgium
Development of new advanced multifunctional materials containing defects

Pintilie L, Pintilie I
University of Oulu, Finland
Ferroelectric measurements

Pintilie L
Universitatea Tehnica Darmstadt, Germany
Specimen exchange, co-publication

Pintilie I
Universitatea din Oslo, Norway
Specimen exchange,working stages

Pintilie L
UMP CNRS-Thales, 1 Av. Fresnel, Palaiseau, 91767, France and Université Paris-Sud
Specimen exchange, common measurements

Predoi D
Institut de Chimie de la Matière Condensée de Bordeaux CNRS-UPR 9048 France
Elemental analysis, hydrogen storing

Predoi D
Universite Bordeaux, EA 4592 Géoressources&Environnement, ENSEGID, France
Collaboration project IFA CEA C2-06, TEM, environment tests

Predoi D
Marcoule Institute for Separative Chemistry, France

Predoi D
Institute of Life Sciences Research and Technologies: Laboratory of Chemistry and Biology of Metals (LCBM) Grenoble, France
Collaboration project IFA CEA C4-05- biological tests

Predoi D
Institut des Sciences de la Terre d'Orléans, France
Raman, ICP,magnetic measurements

Predoi D
Université du Havre, France
Ultrasound studies

Predoi D
Horiba Jobin Yvon S.A., France
Zeta potential, DLS, photoluminescence

Predoi D
University of Dayton, Research Institute, USA
Carbon nanotubes

Stan GE
Collaboration Agreement with University of Aveiro, Department of Materials and Ceramic Engineering, CICECO, Aveiro, Portugal
Development of a new generation of highly biocompatible dental titanium implants functionalized by sputtering techniques with novel bioactive glass materials
2012-2014

Funding

NIMP Funding

Core Programme	4.373.435 Euro
Ideas	1.131.584 Euro
Human Ressources	328.857 Euro
Partnerships	981.708 Euro
International Projects	823.997 Euro
ROSA	188.308 Euro
Economic Contracts	47.741 Euro
TOTAL	**7.875.630 Euro**